FREE ELECTRON DENSITY DISTRIBUTION OF THE MILKY WAY

A THESIS SUBMITTED TO
THE GRADUATE SCHOOL OF NATURAL AND APPLIED SCIENCES
OF
MIDDLE EAST TECHNICAL UNIVERSITY

BY

NEZİHE UZUN

IN PARTIAL FULFILLMENT OF THE REQUIREMENTS
FOR
THE DEGREE OF MASTER OF SCIENCE
IN
PHYSICS

JANUARY 2012

Approval of the thesis:

FREE ELECTRON DENSITY DISTRIBUTION OF THE MILKY WAY

submitted by **NEZİHE UZUN** in partial fulfillment of the requirements for the degree of **Master of Science in Physics Department, Middle East Technical University** by,

Prof. Dr. Canan Özgen _____
Dean, Graduate School of **Natural and Applied Sciences**

Prof. Dr. Mehmet T. Zeyrek _____
Head of Department, **Physics**

Assist. Prof. Dr. Sinan Kaan Yerli _____
Supervisor, **Physics Department, METU**

Assoc. Prof. Dr. Aşkın Ankay _____
Co-supervisor, **Physics Department, Boğaziçi University**

Examining Committee Members:

Assoc. Prof. Dr. Sıtkı Çağdaş İnam
Başkent Uni., El. and Elec. Eng. Department _____

Assist. Prof. Dr. Sinan Kaan Yerli
METU, Physics Department _____

Assoc. Prof. Dr. Aşkın Ankay
Boğaziçi Uni., Physics Department _____

Prof. Dr. Altan Baykal
METU, Physics Department _____

Prof. Dr. Ümit Kızıloğlu
METU, Physics Department _____

Date: _____

I hereby declare that all information in this document has been obtained and presented in accordance with academic rules and ethical conduct. I also declare that, as required by these rules and conduct, I have fully cited and referenced all material and results that are not original to this work.

Name, Last Name: NEZİHE UZUN

Signature :

ABSTRACT

FREE ELECTRON DENSITY DISTRIBUTION OF THE MILKY WAY

Uzun, Nezihe
M.Sc., Department of Physics
Supervisor : Assist. Prof. Dr. Sinan Kaan Yerli
Co-Supervisor : Assoc. Prof. Dr. Aşkın Ankay
January 2012, 175 pages

The aim of this study is to determine the free electron density distribution of the Milky Way Galaxy using dispersion measures of pulsars. By making use of 1893 Galactic pulsar, 274 supernova remnant and 543 HII region data, the overall free electron density map of the Galaxy is obtained by using a 3D mesh-like structure of irregular size. The main idea behind the study is to treat each 3D section of the Galaxy privately considering the distance versus dispersion measure graphs of the pulsars that fall into those sections. This sectioning procedure is followed using a trial and error method and results in 348 sections through which free electron densities can be calculated.

Using linear fits of distance versus dispersion measure graphs, pulsars that deviate from the curves are investigated and new distances are adopted to 140 of them that are decided to have wrong distance estimates. By this way both distance values and the free electron densities of the sections are improved.

In the end, by using the free electron density values of 348 sections, a projected and cumulative free electron density map of the Galaxy is plotted in

polar coordinates. This map is compared with three different spiral arm models and it is seen that the best accordance is with Hou et al. (2009) spiral arm model.

Keywords: pulsar, dispersion measure, electron density, Galaxy, spiral arms

ÖZ

SAMANYOLU'NDAKİ SERBEST ELEKTRON YOĞUNLUĞU DAĞILIMI

Uzun, Nezihe
Yüksek Lisans, Fizik Bölümü
Tez Yöneticisi : Yrd. Doç. Dr. Sinan Kaan Yerli
Ortak Tez Yöneticisi : Doç. Dr. Aşkın Ankay

Ocak 2012, 175 sayfa

Bu çalışmanın amacı Samanyolu Galaksisi'nin serbest elektron yoğunluğu dağılımını pulsarların dağılma ölçülerini kullanarak bulmaktır. Galaksinin toplam serbest elektron dağılımının haritasını çıkarmak için büyüklüğü değişken 3 boyutlu bir göze yapısı kullanılmış ve 1893 pulsar, 274 supernova kalıtısı, 543 HII bölgesi verisinden yararlanılmıştır. Bu çalışmanın temelinde, 3 boyutlu gözlere düşen pulsarların uzaklığa karşılık dağılma ölçüsü grafiklerinden yola çıkarak Galaksinin 3 boyutlu her bir gözüne özel işlem uygulamak vardır. Bu 3 boyutlu bölümleme işlemi deneme yanılma yöntemiyle yapılmış ve üzerinden elektron yoğunluğu hesaplanabilecek 348 bölge ile sonuçlanmıştır.

Pulsarların uzaklığa karşılık dağılma ölçüsü grafiklerindeki doğrusal fitler kullanılarak grafiklerden sapan pulsarlar incelenmiş ve uzaklık hatası olduğuna karar verilen 140 pulsar için yeni uzaklıklar hesaplanmıştır. Böylece hem bölgelerin serbest elektron yoğunlukları hem de pulsarların uzaklıkları iyileştirilmiştir.

Sonuç olarak, 348 bölgenin serbest elektron yoğunluğu değerleri kullanılarak

iz düşümlü ve biriktirimli serbest elektron yoğunluğu haritası kutupsal kon düzeninde çizilmiştir. Bu harita 3 farklı Galaktik kol modeliyle kıyaslanmış ve en uyumlu kol modelinin Hou et al. (2009) tarafından verildiği görülmüştür.

Anahtar Kelimeler: pulsar, dağılım ölçütü, elektron yoğunluğu, Galaksi, sarmal kollar

To my parents

ACKNOWLEDGMENTS

I would like to thank to my advisors Assist. Prof. Dr. Sinan Kaan Yerli and Assoc. Prof. Dr. Aşkın Ankay for their support and their time. I would not be doing physics without Sinan Kaan Yerli or would not be able to complete this work without Aşkın Ankay. I would also like to thank to Burak Bülent Güçsav for his contributions to this thesis and for his moral support during the stressful period of thesis writing.

I acknowledge the usage of data set prepared within the project TBAG-109T736 of TÜBİTAK (The Scientific and Technological Research Council of Turkey).

TABLE OF CONTENTS

LIST OF TABLES

TABLES

LIST OF FIGURES

FIGURES

CHAPTER 1

INTRODUCTION

1.1 A General View

The number of astrophysical studies that are conducted in order to understand the structure and the evolution of the Milky Way Galaxy has shown an increase in the last few decades (Altenhoff et al. 1979; Caldwell and Ostriker 1981; Georgelin and Georgelin 1976; Gilmore et al. 1989; Robin et al. 2003). Moreover the astrophysical entities are studied in wide range of physics to understand their compositions, mechanisms or locations. On the other hand, there are only a few astrophysical problems whose solutions provide information both about the structure of the Galaxy and about the properties of the astrophysical entity in question. This thesis presents a study that includes one of the solutions of such type of problem; determination of free electron density distribution of the Milky Way Galaxy using dispersion measures of pulsars.

From the very beginning of pulsar observations it was known that the location of a pulsar gives idea about the free electron content of the interstellar medium (ISM) lying in between the pulsar and the observer (Davidson and Terzian 1969). Following this, in a reverse sense, one can claim that using the information about the free electron content of the ISM, the distance of a pulsar can be estimated. Using such kind of reasoning, both the free electron content and the pulsar distances have been investigated simultaneously in large number of studies.

In early days of the history of this problem, the mathematical models that were built to find the free electron density distribution of the Galaxy were over simplified and the pulsar distances estimated through the models could have distance errors up to 100% (Cordes et al. 1991; Taylor and Cordes 1993). On the other hand, as time went on, the realistic models are constructed considering the free electron sources, over and under densities in the Galaxy and the distance error of pulsars diminished (Cordes and Lazio 2002; Gómez et al. 2001). However, since our Galaxy is way too complex to be modeled by current mathematical models, the idea behind the solution of the problem in this study is purely different since it is purely observational.

In this study, the free electron density distribution of the Galaxy has been studied in 468 lines of sights inspired by the article of Guseinov et al. (2002). Due to the fact that the free electron density is very sensitive to even small changes in line of sight, the Galaxy is divided into as many sections as possible that can be studied on. Following this, using the distance versus dispersion measure graphs of a group of pulsars in each section, free electron density of the path that lies between that group of pulsars and the Sun is calculated. Meanwhile the pulsars deviating from the fitted curves are studied and some of them are adopted new distance values. Using such method, both the densities of sections are improved and the distances of certain pulsars are corrected.

Following the other sections of this chapter, the players and the concepts that take role in this study are presented without directing their actual roles. However, those sections are important in order to have feeling about the overall work. Physics behind the study and the procedure that is followed are presented in "Theory" and "Methodology and Data" chapters so that the links in question can be formed. In the "Sample Work" chapter, an example of actual work and the reasoning behind the decision making procedure are demonstrated so that a guide for future studies is presented. The last chapters are "Results and Discussion" and "Conclusion". In those chapters the final outcome of the work is presented, discussed on and compared with certain studies in literature. In conclusion, suggestions for future studies are

made in order to make a humble contribution to the history of this problem.

1.2 Players

In this section, the astrophysical entities that take part in this study are introduced. Properties of pulsars, H II regions and supernova remnants are briefly summarized so that their roles in the study are made clear.

1.2.1 Pulsars

The simplest definition of a pulsar is a neutron star with misaligned magnetic and rotation axes. A neutron star, hereupon, is a dead star of typical 1.4 solar mass and 10 km radius. The typical central density is about 10^{14}-10^{15} g/cm^3 and the magnetic field strength can go up to 10^{14} Gauss (Lorimer and Kramer 2005). Having such extreme properties, pulsar is considered to be one of the most interesting astrophysical objects in literature and the physics behind its internal structure, emission mechanisms and evolution is still in question. Though, all of these aspects are presented below in short, to have a better understanding of pulsars.

Towards the end of the lifetime of a star, when the nuclear fuel is used up and the radiation pressure becomes inefficient in withstanding the gravitational pressure, collapse of the star becomes inevitable. During the collapse, relativistic degenerate electron gas is produced and the corresponding pressure tries to halt the gravitational collapse. Nevertheless for stars with masses larger than Chandrasekhar limit, degenerate electron pressure is not enough to stop the collapse. On the other hand, as the gravitational potential energy is released and the total energy of the electrons becomes larger than the energy corresponding to mass difference of protons and neutrons, inverse beta decay process ($p + e^- \rightarrow n + \nu_e$) takes place (Longair 2010). After this stage, the energy increases and the inverse beta decay starts to take place in the atomic nuclei, as a result large number of neutrons accumulates at the core of the star. After enough number of neutrons have been created at the core,

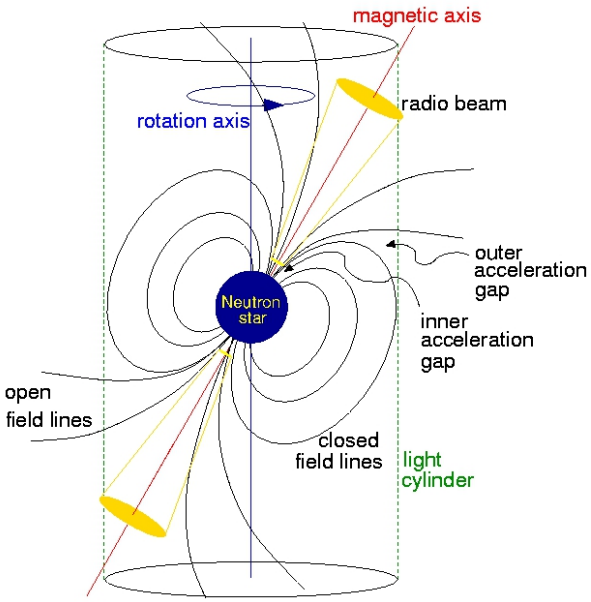

Figure 1.1. A toy model of a neutron star (Lorimer & Kramer, 2005).

degenerate neutron pressure is formed which is strong enough to stop the gravitational collapse of stars less than 2-3 $M_{\odot}$. Now that the collapse is prevented and the resulting star is mostly composed of neutrons, it is called a neutron star.

During the collapse of the star, the core size drops from 10^6 km to 10^1 km. Since the angular momentum is conserved during this procedure, rotation rate of the neutron star increases with about 10^{10} factor. Likewise the magnetic field strength increases with the same amount in order to preserve the magnetic flux. In the end, neutron stars happen to be spinning magnetic dipoles whose periods are in orders of seconds (or even miliseconds).

In the case of pulsars, the magnetic field axis is misaligned with the axis of rotation (see Fig. 1.1). Just like an accelerated particle, or an electric dipole in motion, the rotating magnetic dipole (the pulsar) emits continous radiation. As the pulsar spins around its rotation axis, its magnetic field axis makes a rotating motion around it so that the radiating beam can only be observed when it is aligned with the line of sight of the observer on Earth. As a result the continous emission of the pulsar is observed as pulsed signals and those neutron stars are named as pulsars although the stars themselves show no pulse behaviour.

When it comes to radio emission of pulsars, the reponsible mechanism is still not known very well. One of the first models for radio emission mechanism was bunched curvature emission. According to this model, bunch of particles emit radiation as they flow along the open and curved magnetic field lines of the pulsars, in directions tangent to the field lines. This model has then been laid aside by some of the scientists based on the idea that there can be no mechanism that can create particle bunches in such short times or keep their shape as it is for that long times (Lorimer and Kramer 2005). Most favoured radio emission models of today are called relativistic plasma emission (RPE) models due to the analogy formed with plasma emission in solar radio bursts. In RPE models the emission mechanism is constructed on plasma instability. According to one of the most famous models, plasma in the polar-cap region of the pulsar is considered to be formed in two stages. At the first stage, primary particles are accelerated by the vacuum electric field to high energies so that the particles emit gamma rays. Following this, secondary pairs are created by the decay of gamma rays in a pair production front. In the end, there is free energy creation due to the relative motions of outflowing plasma pairs. This energy is given to waves of the plasma which will eventually be responsible for the radiation that is emitted in radio window (Gedalin et al. 2002). The other physical processes that is observed in pulsars are synchrotron emission, curvature emission and inverse Compton scattering which results in optical, X-ray and gamma ray emissions respectively.

In order to present the dipole radiation of the pulsars, an analogy between an accelerated electric charge and the rotating magnetic dipole is formed. It is known by the Larmor formula that the power associated with the radiation of the electric dipole in motion is:

$$-\left(\frac{d\mathbf{E}}{dt}\right) = \frac{|\ddot{\mathbf{p}}|}{6\pi\epsilon_0 c^3}$$

For a rotating magnetic dipole case the equation becomes:

$$-\left(\frac{d\mathbf{E}}{dt}\right) = \frac{\mu_0\,|\ddot{\mathbf{m}}|}{6\pi c^3} \tag{1.1}$$

Since the magnetic dipole is rotating its time dependence can be given by

$m(t) = m_0 \sin(\Omega t)$. Taking derivative of magnetic dipole moment twice and plugging it into Eq. 1.1 gives:

$$-\left(\frac{d\mathbf{E}}{dt}\right) = \frac{\mu_0 \Omega^4 {m_0}^2}{6\pi c^3} \tag{1.2}$$

Magnetic dipole radiation is in fact an energy loss mechanism and the source of the energy that is derived is the rotational kinetic energy. So change in kinetic energy in time should give the amount of power associated with magnetic dipole radiation. Using this fact one can find the breaking index "n" which is a measure that gives idea about the slowing down of the rotational motion of the pulsar (Longair 2010). So considering;

$$\begin{aligned} -\left(\frac{d\mathbf{E}_{\mathbf{Dipole}}}{dt}\right) &= -\left(\frac{d\mathbf{E}_{\mathbf{Rotation}}}{dt}\right) \\ \frac{\mu_0 \Omega^4 {m_0}^2}{6\pi c^3} &= -\left(\frac{dI\Omega^2/2}{dt}\right) = -I\Omega\dot{\Omega} \end{aligned}$$

Here it is seen that $\dot{\Omega} \sim \Omega^3$. A more general relationship between the rotational velocity and its derivative is given by $\dot{\Omega} = -\kappa\Omega^n$. So the breaking index for a pure magnetic dipole radiation is found to be 3. The exact expression of breaking index is found by taking derivative of $\dot{\Omega}$ and arranging the terms. The result is;

$$n = \frac{\Omega\ddot{\Omega}}{\dot{\Omega}^2}$$

The breaking index is also important in calculation of age estimations of pulsars.

Using $\Omega = 2\pi\nu$ and $\nu = 1/P$ one can find a relation between the period and period derivative of the pulsar as $\dot{P} = -\kappa P^{2-n}$. Now if this equation is integrated assuming a constant breaking index and κ, the result leads to the age of the pulsar:

$$T = \frac{P}{(n-1)\dot{P}}\left[1 - \left(\frac{P_0}{P}\right)^{n-1}\right].$$

Assuming the birth period is much smaller than the present period and plugging $n = 3$ typically, the characteristic age of the pulsar is given by the following expression:

$$\tau_c \equiv \frac{P}{2\dot{P}}.$$

This equation states that period and period derivative give idea about the time evolution of pulsars. Obviously if all of the pulsars had the same conditions at birth, same physical dimensions and mass, same magnetic field strength and same breaking index ($n = 3$ holds only for a hypothetical case of pure magnetic dipole radiation) then all of them would have the same $P - \dot{P}$ relation (Lyne and Graham-Smith 1990). Since this is not the case under real conditions, $P - \dot{P}$ diagrams are used to investigate the evolution of pulsars in literature.

Another important topic about pulsars is pulsar timing. Since pulsars are fastly spinning small objects with directed radiation, their on-pulse durations are very short. Moreover their periodicities are small and definite. Therefore measuring the arrival times of pulsars is not so difficult. On top of that, just by using pulsar timing measurements, one can get idea about the locations of the pulsars and the medium that their signal travels through (Lyne and Graham-Smith 1990). In fact the basis on which this work is constructed is the fact that arrival time of pulsar signals include information about the medium between the pulsars and the observer.

In a most general sense, the arrival time of a pulsar is given by the following (Lorimer and Kramer 2005):

$$t_{\mathrm{SSB}} = t_{\mathrm{topo}} + t_{\mathrm{corr}} + \triangle_{\mathrm{R}_\odot} + \triangle_{\mathrm{S}_\odot} + \triangle_{\mathrm{E}_\odot} - \triangle_{\mathrm{DM}}$$

Here t_{topo} is the time of arrival measured by the clock of the observatory on Earth and t_{SSB} is the time of arrival with respect to center of mass of the Solar System. Since the Earth is not an inertial reference frame, topological arrival time should be converted to the arrival time with respect to an inertial reference frame which is approximated to be the center of mass of the Solar System (SSB). So all other terms on the right hand side of the equation are used to make the necessary conversion. For example t_{corr} term is the clock correction due to time standards. $\triangle_{\mathrm{R}_\odot}$, $\triangle_{S_\odot}$, $\triangle_{\mathrm{E}_\odot}$ are Römer, Shapiro and Einstein delays respectively. They account for corrections due to relative positions of pulsar,SSB and Earth; extra time delay due to space-time curvature created by objects in Solar System and total effect of time delay due

to motion of Earth and gravitational redshift caused by entities in the Solar System. The last term, $\triangle_{DM}$, is the correction due to dispersion measure of the interstellar medium which increases the arrival time of the signal because of the interactions of the free electrons of the plasma with the pulsar signal.

1.2.2 H II Regions

Most of the interstellar gas in the Galaxy is in the form of hydrogen which can be observed in two states; neutral (indicated as HI) and once ionized (indicated as H II). H II Regions are formed when massive O and B type stars' energetic UV photons ionize the HI clouds that surround them. Due to this ionization, the H II regions happen to be composed of ions and free electrons, that come into Maxwellian distribution in a very small amount of time (about 30 s) due to the collisions of photo-electrons (Tielens 2005). Meanwhile those free electrons are observed to create two main physical processes; recombination and thermal Bremsstrahlung, in which the former results in emission of optical photons and the later results in emission of radio photons. To be more precise, when the energies of the free electrons are not enough to recombine with the ionized hydrogen, they scatter under the Coulomb's force of the ions so that a photon with a radio wavelength is emitted (called thermal bremssrahlung) (Longair 2010). Investigating this bremsstrahlung spectrum of the region one can get information about the temperature and electron density of the H II Region.

When it comes to their spatial distribution, it is known that H II Regions are generally found at low latitudes of the Galaxy , near star formation regions (Hou et al. 2009). Although they are considered to be good tracers of the spiral arms they can also be observed at regions between the arms since they extend greatly in the disk region. Likewise most of the pulsars are located at the disk of the Galaxy so that the free electrons that are not recombined in the H II regions can be considered to be one of the main sources of dispersion of the pulsar signals in the Galaxy.

1.2.3 Supernova Remnants - SNRs

When stars come to a point where radiation pressure can not halt the gravitational pressure any longer, supernova explosions take place. Those explosions are considered to be in two types depending on the source of the gravitational pressure in the system. In Type I supernovas, mass accretion from one star to another results in the receiver star to end its life with a supernova explosion. In Type II supernovas, gravitational pressure of the massive star itself is the basic energy source of the explosion. Moreover depending on the mechanism (core collapse or thermonuclear) that derives the explosion, there may or may not be a left over star after the supernova. Nevertheless in either case great amount of mass with energy up to 10^{51} ergs is ejected to interstellar space (Padmanabhan 2001). This ejected material is called supernova remnant and it is mostly studied due to bringing enrichment to its local environment.

The supernova remnants are considered to be in two types. First type has ring-like shape and the second type has an irregular shape with a bright section in the middle. The energy of the first type remnant comes from the explosion itself and the second type supernova remnant has a pulsar at the center so that there is an additional energy source due to the relativistic electrons sent by the pulsar (Karttunen et al. 2003).

The supernova remnants expand in radial direction with such high speeds that the surrounding gas becomes compressed and heated. Due to the high velocity of this compression, the pressure change in the gas is very abrupt and this results in a shock wave in the medium. Those radiative shock waves makes the supernova remnant be visible in optical window.

Moreover with a shell temperature of 10^5 to 10^7 , supernova remnants are considered to be highly ionized mediums. Following this, large numbers of electrons interact with the magnetic fields in the shell so that this synchrotron radiation makes the supernova remnant be observable in radio window (Shiga 2005). Another physical process observed in supernova rem-

nants is thermal Bremsstrahlung and this makes the supernova remnants be observable in X-Ray window.

Due to their rich content of materials and vast emission window at different energy regimes, supernova remnants arouse interest of large number of observers. In this study, on the other hand, their high content of free electrons is the cynosure. Considering 274 supernova remnants in the Galaxy as free electron sources and making use of their spatial distributions which usually correspond to the spiral arms, free electron density distribution of the Galaxy is investigated. To interpret their exact role in the study the "Methodology and Data" chapter should be followed.

1.3 Concepts

In this section, the key concepts of the study are presented. Although these concepts seem to be unrelated at the first glance, they become meaningful after the corresponding links are presented in Chapter 2.

1.3.1 Importance of Determination of Free Electron Density Distribution of the Galaxy

Determination of free electron density distribution of the Galaxy is important in terms of several aspects such as estimation of pulsar distances or determination of the magnetic fields in the Galaxy.

It is known that free electron density distribution is widely used in distance estimation of pulsars. Considering the fact that distances of pulsars can be found through making use of their dispersion measures and the free electron density along the line of sight; estimation of pulsar distances via their dispersion measures is fairly easy, quick and inexpensive when compared to other distance estimation techniques. In order to use this technique to estimate the distances of newly found pulsars, on the other hand, the free electron density along the line of sight of the pulsar should be determined

very accurately. So, determination of pulsar distances via their dispersion measures should be used as an additional technique to cross check estimated distances of the newly found pulsars.

Following this, distance estimations of pulsars become very important for studies that investigate the spatial distribution of pulsars in the Galaxy. Despite their relatively high space velocities, young pulsars are thought to be located close to their birth places, i.e spiral arms of the Galaxy. Thus, investigation of spatial distribution of young pulsars, may give idea about the structure, dynamics and evolution of the Galaxy.

Another crucial role of free electron density distribution is in terms of determination of magnetic fields in the Galaxy. It is known that when polarized emission of a radio source passes near the magnetic fields in the interstellar medium, its plane of polarization is rotated due to two opposite hand polarization modes having different phase velocities (Clarke 2004). This phenomenon is defined as "Faraday Rotation" and the angle of rotation of the signal path that is traversed is given by:

$$\Delta\Psi = RM\lambda^2$$

where RM is the rotation measure and it is given as:

$$RM = \frac{e^3}{2\pi m^2 c^4} \int_0^d n_e B \cos\theta \, \mathrm{d}l.$$

When radio emission of pulsars are considered it is seen that rotation measure is a function of the column density (also called as dipersion measure) of the medium in between the observer and the pulsar, and the magnetic field component along the line of sight. This means that after obtaining the rotation measure of the pulsar and estimating its distance, the only thing left to determine the magnetic field component is the free electron density. Then the magnetic field along the line of sight is given by (Smith 1977):

$$< B\cos\theta > [\mu G] = \frac{\int_0^d n_e B \cos\theta \, \mathrm{d}l}{\int_0^d n_e \, \mathrm{d}l} = \frac{1.232 RM[radm^{-2}]}{DM[pccm^{-3}]}$$

Thus, estimation of free electron density distribution is very important in terms of investigation of magnetic fields in the Galaxy which also leads to answers about the structure and evolution of the Galaxy.

1.3.2 Mathematical Models of Free Electron Density Distribution

Determination of free electron density distribution via optical observations and radio emmission measures is rather difficult considering the fact that they provide information about $< {n_e}^2 T^{-3/2} >$ rather than $< n_e >$ itself (Lyne and Graham-Smith 1990). Therefore the most accurate way of determining the free electron density of the Galaxy is via pulsar measurements.

The mostly used method to obtain free electron density distribution is construction of mathematical models based on dispersion measure data of pulsars. Considering the history of the models, the mathematical model of Lyne et al. (1985) can be given as a good example for early studies of mathematical constructions. In this model, H II regions as being free electron sources are considered to form a single thin disk component of scale hight 70 parsecs. Then, assuming that free electron density decreases with increasing radius (R) and increasing vertical distance (z) from the disk, the model is defined by the equation:

$$n_e = \left[0.025 + 0.015 exp\left(-\frac{|z|}{70}\right)\right]\left[\frac{2}{1+R/10}\right] + 0.28\alpha_{(GN)}$$

Here, $\alpha_{(GN)}$ is 1 for the line of sight of the Gum Nebula and 0 otherwise and the only additional contribution to free electron density distribution is given by this term. This model is obviously an over simplified model of the Galaxy since the actual distribution of free electron sources are not implemented to the model in correct manner. As a result this model and most of the children of it were unsuccessful in mimicing the actual distribution of the free electron density of the Galaxy.

When it comes to recent mathematical models, model of Cordes and Lazio (2002) is considered to be the most succesful model in determining the free electron density distribution of the Galaxy. The basics of this model is no different than the one of Lyne et al. (1985), but its success comes from the integration of spiral arms, voids and certain free electron sources specific to certain line of sights to the model. Nevertheless, even the recent mathematical models are not perfect imitations of the distribution of free electrons in

the Galaxy since each line of sight of the Galaxy is not given special treatment in determining the free electron density distribution. This means that assuming a background density defined by multiplication of two functions and adding contributions in certain line of sights may not be sufficient in mimicing the complex structure of the Galaxy in terms of free electron density distribution.

1.3.3 Dispersion

Dispersion is a resulting concept of a wave packet being separated into group of waves with different wavelengths that the packet is composed of. This fact arises from the interaction of an electromagnetic wave with its surrounding medium and is linked to the phase velocity of any wave being dependent on its frequency. In order for the dispersion to be understood fully, the physical process that triggers the phenomenon should be followed first.

In this study, the "medium" in question is the interstellar medium which is assumed to be in the form of cold plasma and the wave in question is the electromagnetic wave sent by the pulsar. While the pulsar signal travels through the interstellar medium, its electric field disturbs the free electrons of the plasma on the way. This results in a relative displacement between the negative electrons and the positive ions of the medium and an electric field is created in the medium in order to pull the electrons back to their previous positions. Due to the inertia they have, electrons start to oscillate with a frequency called "plasma frequency" (Chen 1974). As the electromagnetic wave of the pulsar passes through such medium, its electric field is superposed with the electric field built up inside the plasma. The resulting wave has the same frequency as its progenitor but its wavelength becomes shortened. As a result the phase velocity of the resulting wave becomes smaller than the one of original wave.

For wave packets including a range of frequencies, the phase velocity of each wave is slowed down with different amount. This is simply because each resulting wave has a characteristic superposition pattern with the electro-

magnetic field built up in the plasma. So basically dispersion is a resulting phenomenon which states that both the phase velocity and the group velocity is frequency dependent.

Due to this fact, when multi frequency observations are conducted on arrival times of signals it is seen that arrival times of the waves with lower frequencies are longer. High frequency waves of the same signal tend to arrive earlier due to dispersion and this difference in arrival times of the waves depends firmly on the free electron content of the medium that the waves travel through. Following the implementation in reverse order, by using the difference between arrival time of the signal in two different frequencies one can get idea about the free electron content about the plasma lying along the pulsar and the Sun.

1.3.4 Distance Estimation Techniques For Pulsars

A visible star's distance can usually be estimated by using the relation between the apparent and the absolute magnitude of the star, in which the former can be obtained through optical measurements and the later can be inferred from its spectral type. On the other hand, this does not hold for the case of pulsars. The absolute magnitude is not a constant in time for a single pulsar while also it may vary from one pulsar to another (Lyne and Graham-Smith 1990). So, since the radiance do not give enough information about the pulsar distance, certain other distance estimation techniques have been used for pulsars which are:

- Annular parallax method
- Timing parallax method
- Association method
- Kinematic method

Here it should be noted that none of those techniques are perfect interms of estimation of pulsar distances. Indeed, the actual hotspot of the difficulty in

determination of free electron density distribution of the Galaxy is based on inaccurate distance estimates of pulsars.

Annular Parallax Method

This method is based on the fact that the apparent position of the pulsar changes as seen from the Earth while it orbits around the Sun. By measuring the angular difference between the observed line of sights that are obtained at two different times of the year and by making use of the radius of the Earth's orbit around the Sun; distance of the pulsar can be found by a simple geometrical relation:

$$d_{\text{pulsar}}(\text{parsec}) = \frac{1}{\text{parallax angle (arcsec)}}$$

Despite its ease, this relation gives accurate results only for nearby pulsars that are located less than 1 kpc. This is simply because as the pulsar distance increases the parallax angle decreases so much that it cannot be determined without much error.

Timing Parallax Method

In this method, wavefront curvature of the pulsar signal is investigated in order to have idea about the distance of the pulsar. As Earth orbits around the Sun, the curvature of the wavefront shows change in apparent direction depending on the position of the Earth. Due to the corresponding change in path of the signal the time of arrival of the signal changes (Deng and Finn 2011; Smits et al. 2011). The timing residual due to the timing parallax is given by (Lorimer and Kramer 2005):

$$\triangle t_{\pi} = -\frac{1}{2cd}(\mathbf{r} \times \hat{s})^2$$

For this method, it is also stated that timing residuals are measureable for pulsars near the ecliptic plane. This is because the amplitude of the variation in the time of arrival of the signal depends on the ecliptic latitude angle (Lorimer and Kramer 2005). Since the distance estimates of timing parallax method are considered to be very succesful for miliseconds pulsars near the ecliptic plane for today, the ways to implement this method for pulsars at higher latitudes are still studied.

Association Method

Considering the origins of the pulsars, they are thought to be located near Population I objects (supernova remnants, open clusters, O-B stars, white dwarfs). Due to that, while estimating distances to pulsars, certain associations with Population I objects with known distances are searched for (Frail and Weisberg 1990). For example, if the progenitor supernova remnant of a pulsar can be found, one can ascribe the distance of the supernova remnant to the pulsar in question. Although distance estimates that are done through association method are considered to be succesful, it is not the mostly favoured technique due to its difficulties in relating the pulsars with associations.

Kinematic Method

Among all of the methods mentioned above, kinematic method is the mostly used one. In this method, 21 cm absorption lines of HI clouds are investigated in order to have idea about the distances of pulsars. Unfortunatelly this method can only give upper or lower limits for pulsar distances so that the error bars of the estimated distances are larger when compared to the ones of other methods. On the other hand, distance estimation is rather easy and it can be applied to great number of pulsars.

The idea behind the technique is very simple. For a given line of sight of a pulsar if there is a HI cloud located infront of it, its signal is absorbed by the HI cloud. Then if the spectra of the cloud is investigated it can be seen that there appears an absorption line specific for the pulsar in question. Considering this, the distance of the HI cloud can be taken as a lower distance limit since the pulsar is certainly located at the back side of the cloud. Same is also true for upper distance limit, but this time absence of an absorption line is what is looked for. In other words, if there is no absorption line at the spectra of the HI cloud, this means that the pulsar is located infront of the HI cloud and its distance can not be larger than the one of the cloud (Frail and Weisberg 1990).

Another aspect of the method is that distances of HI clouds are obtained through Galactic rotation models which cannot be considered to be perfect (Jackson et al. 2002). That is why additional errors come up in lower/upper distance limits of pulsars depending on the Galactic rotation model chosen to estimate the distances of the HI clouds. Nevertheless, estimating the distance limits even with much error is acceptable for the cases where there is no other technique to estimate the distance of the pulsar in question.

CHAPTER 2

THEORY

In this chapter, in order to introduce the theory behind the dispersion phenomenon, a series of mathematical derivations are presented by making use of Chen (1974) and Dawson (1999). Firstly,the medium through which the pulsar signals pass is treated as plasma which is composed of free electrons and positive ions. Following this, using two of the Maxwell's Equations and the equation of motion of electrons, dependence of signal frequency to plasma freqency is derived. Secondly, arrival time of the signal is calculated together with the delay time due to dispersion. Thirdly and finally, mathematical expression of dispersion measure and its link to free electron density is presented. Note that the assumptions are given as "A#" and they have great importance in the derivation process.

2.1 The Relation Between the Signal Frequency and the Plasma Frequency

The initiating equations that are used to determine the dependence of signal frequency to plasma frequency are:

$$\left.\begin{aligned} \boldsymbol{\nabla} \times \mathbf{E} &= -\frac{\partial \mathbf{B}}{\partial t} \\ \boldsymbol{\nabla} \times \mathbf{B} &= \mu_0 \mathbf{j} + \mu_0 \epsilon_0 \frac{\partial \mathbf{E}}{\partial t} \end{aligned}\right\} \quad \text{Two of the Maxwell's Equations} \qquad (2.1)$$

$$\left.\begin{aligned} n_e q_e \mathbf{E} &= n_e m_e \frac{D\mathbf{V_e}}{Dt} \end{aligned}\right\} \quad \text{Equation of Motion of Electrons} \qquad (2.2)$$

(A1) Plasma is treated as fluid and therefore a material derivative is used at

the right hand side of the equation of motion. Then Eq. 2.2 becomes:

$$n_e(-e)\mathbf{E} = n_e m_e \left(\frac{\partial \mathbf{V_e}}{\partial t} + (\mathbf{V_e} \cdot \nabla)\mathbf{V_e} \right)$$

Now, considering each term as the superposition of an equilibrium state and the state due to the perturbation of free electrons in the plasma by the electromagnetic wave:

$$\begin{aligned} n_e &= n_0 + n_1 \\ \mathbf{j} &= \mathbf{j_0} + \mathbf{j_1} \\ \mathbf{V_e} &= \mathbf{V_0} + \mathbf{V_1} \\ \mathbf{E} &= \mathbf{E_0} + \mathbf{E_1} \\ \mathbf{B} &= \mathbf{B_0} + \mathbf{B_1} \end{aligned}$$

(A2) The plasma is assumed to be uniform and neutral before it has been perturbed.

(A3) Initial plasma density is considered to be constant.

Due to the second assumption the equilibrium states are

$$\mathbf{V_0} = \mathbf{E_0} = \mathbf{B_0} = 0.$$

Likewise

$$\frac{\partial n_0}{\partial t} = \frac{\partial \mathbf{V_0}}{\partial t} = \frac{\partial \mathbf{E_0}}{\partial t} = \frac{\partial \mathbf{B_0}}{\partial t} = \frac{\partial \mathbf{j_0}}{\partial t} = 0.$$

Moreover $\nabla \cdot n_0 = 0$ should also hold in order for the third assumption to be true. Next thing to do is to linearize two of the Maxwell's Equations and equation of motion of the electrons. For this, each of the quantities are plugged in as the superposition of equilibrium and perturbed states. Linearizing the first Maxwell's Equaiton gives:

$$\begin{aligned} \boldsymbol{\nabla} \times (\mathbf{E_0} + \mathbf{E_1}) &= -\frac{\partial(\mathbf{B_0} + \mathbf{B_1})}{\partial t} \\ \boldsymbol{\nabla} \times \underbrace{\mathbf{E_0}}_{=0} + \boldsymbol{\nabla} \times \mathbf{E_1} &= -\underbrace{\frac{\partial \mathbf{B_0}}{\partial t}}_{=0} - \frac{\partial \mathbf{B_1}}{\partial t} \\ \boldsymbol{\nabla} \times \mathbf{E_1} &= -\frac{\partial \mathbf{B_1}}{\partial t} \end{aligned} \tag{2.3}$$

Linearizing the second Maxwell's Equation gives:

$$\begin{aligned} c^2[\boldsymbol{\nabla}\times(\underbrace{\mathbf{B_0}}_{=0}+\mathbf{B_1})] &= \frac{1}{\epsilon_0}(\underbrace{\mathbf{j_0}}_{=0}+\mathbf{j_1})+\underbrace{\frac{\partial \mathbf{E_0}}{\partial t}}_{=0}+\frac{\partial \mathbf{E_1}}{\partial t} \\ c^2(\boldsymbol{\nabla}\times\mathbf{B_1}) &= \frac{1}{\epsilon_0}\mathbf{j_1}+\frac{\partial \mathbf{E_1}}{\partial t} \end{aligned} \tag{2.4}$$

Finally linearizing the equaiton of motion gives:

$$\begin{aligned} (-e)(\underbrace{\mathbf{E_0}}_{=0}+\mathbf{E_1}) &= m_e\left[\underbrace{\frac{\partial \mathbf{V_0}}{\partial t}}_{=0}+\frac{\partial \mathbf{V_1}}{\partial t}+[(\underbrace{\mathbf{V_0}}_{=0}+\mathbf{V_1})\cdot\nabla](\underbrace{\mathbf{V_0}}_{=0}+\mathbf{V_1})\right] \\ (-e)\mathbf{E_1} &= m_e\left[\frac{\partial \mathbf{V_1}}{\partial t}+(\mathbf{V_1}\cdot\nabla)\mathbf{V_1}\right] \end{aligned}$$

(A4) This problem can be considered as a small perturbation case. Therefore $(\mathbf{V_1}\cdot\nabla)$ term which results in second order perturbation, can be neglected. So the equation becomes:

$$(-e)\mathbf{E_1} = m_e\frac{\partial \mathbf{V_1}}{\partial t} \tag{2.5}$$

At this point it is beneficial to consider the wave nature of plasma oscillations. For small amplitude oscillations waveform can be taken as sinusoidal so that the states of perturbation can be written as

$$\begin{aligned} \mathbf{V_1} &= V_1 e^{i(\mathbf{kr}-\omega t)}\hat{r} \\ \mathbf{E_1} &= E_1 e^{i(\mathbf{kr}-\omega t)}\hat{r} \\ \mathbf{j_1} &= j_1 e^{i(\mathbf{kr}-\omega t)}\hat{r} \end{aligned}$$

For the next steps, Eq.s 2.3, 2.4 and 2.5 are used together to construct a relation between the signal frequency and the frequency of the medium that the signal passes through. Firstly, curl of Eq. 2.3 and time derivative of Eq. 2.4 are used simultaneously:

$$\boldsymbol{\nabla}\times(\boldsymbol{\nabla}\times\mathbf{E_1}) = \boldsymbol{\nabla}\times\left(-\frac{\partial \mathbf{B_1}}{\partial t}\right) = -\frac{\partial(\boldsymbol{\nabla}\times\mathbf{B_1})}{\partial t} = -\mu_0\frac{\partial \mathbf{j_1}}{\partial t}-\mu_0\epsilon_0\frac{\partial^2 \mathbf{E_1}}{\partial t^2},$$

and since $\boldsymbol{\nabla}\times(\boldsymbol{\nabla}\times\mathbf{E_1}) = \nabla\cdot(\nabla\cdot\mathbf{E_1})-\nabla^2\mathbf{E_1}$,

$$\nabla\cdot(i\mathbf{k}\cdot\mathbf{E_1})+k^2\mathbf{E_1} = -\mu_0(-i\omega)\mathbf{j_1}-\mu_0\epsilon_0(-i\omega)^2\mathbf{E_1}.$$

It is known that for a planar wave, direction of the electric field is perpendicular to the wave vector, so due to the fact that $(\mathbf{k}\cdot\mathbf{E_1}) = 0$ the

first term of the left hand side is zero. Moreover using the equality $\mu_0\epsilon_0 = 1/c^2$, the above equation becomes:

$$k^2\mathbf{E_1} = \frac{i\omega}{c^2\epsilon_0}\mathbf{j_1} + \frac{\omega^2}{c^2} \tag{2.6}$$

(A5) Since the mass difference between the positive ions and the electrons in the plasma is large, the ions are considered to be fixed, hence the only current generators are electrons.

In this case current can be written as:

$$\mathbf{j} = \underbrace{\mathbf{j_0}}_{=0} + \mathbf{j_1} = (n_0 + n_1)(-e)(\underbrace{\mathbf{V_0}}_{=0} + \mathbf{V_1})$$

Neglecting the quadratic terms results in:

$$\mathbf{j_1} = -n_0 e\mathbf{V_1} \tag{2.7}$$

In order to find $\mathbf{j_1}$ term and plug it into Eq. 2.6, $\mathbf{V_1}$ should be determined first. For this, relation given by Eq. 2.5 is used:

$$(-e)E_1 e^{i(\mathbf{kr}-\omega t)} = m_e V_1 (-i\omega) e^{i(\mathbf{kr}-\omega t)}$$

Then,

$$V_1 = \frac{eE_1}{i\omega m_e}$$

Putting V_1 into its place in Eq. 2.7 and substituting this equation into Eq. 2.6 gives:

$$\begin{aligned} \left(k^2 - \frac{\omega^2}{c^2}\right)\mathbf{E_1} &= \frac{i\omega}{c^2\epsilon_0}(-n_0 e)\left(\frac{e\mathbf{E_1}}{i\omega m_e}\right) \\ \frac{\omega^2}{c^2} - k^2 &= \frac{1}{c^2}\frac{n_0 e^2}{m_e\epsilon_0} \end{aligned}$$

When the characteristic oscillation frequency of electrons about the fixed ions in a neutral plasma is derived, it is seen that this frequency is in fact equal to $\sqrt{(n_0 e^2)/(m_e\epsilon_0)}$. This term is mostly named as 'plasma frequency' and it is shown by 'ω_p'. As a result, dependence of the frequency of the signal of the pulsar (ω) on plasma frequency is

$$\omega^2 = {\omega_p}^2 + c^2k^2 \tag{2.8}$$

This final equation states that for a non-dispersive media, phase velocity of the wave is equal to group velocity of the wave packet and they are constant no matter what the frequency of the signal is. On the other hand, for a dispersive media like interstellar medium, both the phase velocity and the group velocity increases with increasing frequency. Moreover it is important to note that it is the electron content of the plasma that causes the velocities being different for each frequency value. The real physical interpretation of this equation is explained in the following section.

2.2 Arrival Time of the Signal

Travel time of the pulsar signal on its way to Sun is simply the distance between the pulsar and the Sun over the group velocity of the signal i.e.

$$t = \frac{L}{V_g}.$$

Using Eq. 2.8 the group velocity can be calculated by:

$$\begin{aligned} V_g &= \frac{\partial \omega}{\partial k} = \frac{\partial \left(c^2k^2 + {\omega_p}^2\right)^{1/2}}{\partial k} \\ V_g &= \frac{c}{\omega}(ck) = \frac{c}{\omega}(\omega^2 - {\omega_p}^2)^{1/2} = c\left(1 - \frac{{\omega_p}^2}{\omega^2}\right)^{1/2} \end{aligned}$$

Here it is seen that for a dispersive media, the speed of light is decreased by an amount that depends on both the plasma frequency and the frequency of the signal. Then the arrival time of the signal can be found as

$$t = \frac{L}{c\left(1 - \frac{{\omega_p}^2}{\omega^2}\right)^{1/2}}$$

(A7) The frequency of the plasma is considered to be very small compared to frequency of the signal. Therefore

$$\frac{1}{\left(1 - \frac{{\omega_p}^2}{\omega^2}\right)^{1/2}} \approx \left(1 + \frac{1}{2}\frac{{\omega_p}^2}{\omega^2}\right) \approx 1 + \frac{{\omega_p}^2}{\omega^2}$$

Then it is seen that the arrival time can be written as addition of two terms;

$$t \cong \frac{L}{c}\left(1+\frac{{\omega_p}^2}{\omega^2}\right) = \underbrace{\frac{L}{c}}_{\text{Travel time in vacuum}} + \underbrace{\frac{L}{c}\frac{{\omega_p}^2}{\omega^2}}_{\text{Delay time due to travel in plasma}}$$

This delay time of the signal is infact the golden key of this work since the whole dispersion phenomenon is constructed on the delay time of the pulsar signals. Plugging the plasma frequency into its place, delay time is found as:

$$\Delta t = \frac{e^2}{m_e \epsilon_0}\frac{L}{c}\frac{< n_e >}{\omega^2} \tag{2.9}$$

where $< n_e >$ is the mean free electron number density and $(L < n_e >)$ is the column density of free electrons along the given line of sight of the pulsar.

2.3 Dispersion Measure And Free Electron Density

As it is explained above, column density includes the information about the distance of the pulsar and the free electron density that lies along the signal path. In Chapter 1 it is stated that the signal of a pulsar gets dispersed due to its interaction with the electric field built up in the interstellar medium which tries to pull the perturbed electrons back to their original positions. The more free electrons that the signal encounters the stronger dispersions occur. As a result, dispersion of the signal depends on the integral effect of the distance traveled and the number density of electrons encountered by the signal. This brings one a to conclusion that column density is in fact a measure of dispersion and just beacuse of that it is also called as 'Dispersion Measure (DM)' in the literature.

In the previous section it is shown that the column density i.e. dispersion measure is responsible for the delay time of the signal. So in a reverse sense if the delay time of the pulsar signal for certain frequency can be measured by some means, the dispersion measure can be calculated. But unfortunately this is not possible since the exact time that the signal is sent by the

pulsar can not be determined. To overcome this obstacle multi frequency observations are used. Since signal have different velocities for different frequencies, measuring the arrival times of the signal in two different frequencies give idea about the delay time of the signal. This becomes more clear when the corresponding equations are studied. Difference in arrival times of the same signal in two different frequencies is found by:

$$t(\nu_2) - t(\nu_1) = \frac{L}{c}\left(1 + \frac{{\omega_p}^2}{{\omega_2}^2}\right) - \frac{L}{c}\left(1 + \frac{{\omega_p}^2}{{\omega_1}^2}\right)$$

The right hand side of the equation, after canceling L/c terms, gives the difference of signal delay times of the signal in two different frequencies such that:

$$t(\nu_2) - t(\nu_1) = \Delta t(\nu_2) - \Delta t(\nu_1) \tag{2.10}$$

So left hand side can be obtained by observational means and unknowns of the right hand side can be calculated by using the equation of the signal delay time (Eq. 2.9). To be more precise:

$$\Delta t(\nu_2) - \Delta t(\nu_1) = \frac{L}{c}\frac{{\omega_p}^2}{2\pi^2}\left(\frac{1}{{\nu_2}^2} - \frac{1}{{\nu_1}^2}\right) = \frac{e^2}{cm_e\epsilon_0 2\pi^2} DM \left(\frac{1}{{\nu_2}^2} - \frac{1}{{\nu_1}^2}\right)$$

Driving DM from here:

$$DM = \underbrace{\left(\frac{cm_e\epsilon_0 2\pi^2}{e^2}\right)}_{2.410 \times 10^{-16}\,\frac{parsec}{cm^3}} \left[\frac{\Delta t(\nu_2) - \Delta t(\nu_1)}{\left(\frac{1}{{\nu_2}^2} - \frac{1}{{\nu_1}^2}\right)}\right]$$

Making use of Eq. 2.10 gives:

$$DM = 2.410 \times 10^{-16} \left[\frac{t(\nu_2) - t(\nu_1)}{\left(\frac{1}{{\nu_2}^2} - \frac{1}{{\nu_1}^2}\right)}\right] \tag{2.11}$$

So if the difference of arrival time of the signal is measured in two known frequencies, DM can be calculated very accurately. Moreover considering the fact that the dispersion measure is in fact the column density itself, the mean free electron density in a given line of sight of a pulsar at known distance can be calculated by:

$$< n_e >= \frac{DM}{L} \tag{2.12}$$

One can use this equation both in forward direction and in backward direction. The basic methodology of this work is to use the equation in forward

direction. Making use of the measured DM values and distances of known pulsars free electron densities in certain lines of sights are determined. The backward direction application of the equation is also used to estimate new distances to some of the pulsars. Using again the DM values and the calculated free electron densities, distances of some of the pulsars are corrected. The details of the work that is constructed on these two applications are presented in the next chapter.

CHAPTER 3

METHODOLOGY AND DATA

3.1 Overall View

The methodology that is used in this study is simply based on radio pulsar and free electron source data of the Milky Way Galaxy. The idea is to use radio pulsars as the signal generators and, Supernova Remnants or H II Regions as the free electron sources so that the players of the dispersion phenomenon are picked up.

For any hypothetical 3 dimensional (3D) section of the Galaxy, if the dispersion measures and the distance values of the pulsars are known, the free electron density of the interstellar medium between the pulsar and the Sun can easily be calculated through the linear equation $n_e = DM/d$ (see Chapter 2). This equation can also be used for a group of pulsars in close neighbourhood that has a constant free electron density between the region that encloses the pulsars and the Sun. Considering the real data, on the other hand, it is very hard to find a 3D section of the Galaxy which has a constant free electron density in between itself and the Sun. Thus, when dispersion measure versus distance (or distance versus dispersion measure) graphs of the pulsars in close neighbourhood are plotted, the resulting curve may not be a perfect straight line as it is expected to be in an hypothetical case. Nevertheless, the first thing to do is to search for 3D portions with constant-like free electron density that lies on signal paths of pulsars. This is done through a trial-and-error method in which the pulsars in each line of sight

make up straightest possible lines in distance versus dispersion measure (d vs DM) graphs.

Secondly, the free electron sources located in the 3D Galaxy portions are placed on d vs DM graphs of the pulsars so that their effects on signal dispersion can be studied. This step also includes tailoring of supernova remnant and H II region data that are given in the catalogs of today.

Thirdly, considering each 3D section, relationships of free electron sources with pulsars are studied. This is done in order to find the reason behind the deviation of any pulsar from the linear fit of the d vs DM graph. A pulsar either deviates from the linear fit of the graph in positive sense that is parallel to DM axis since its signal is dispersed more than other pulsars in the section or it deviates from the linear fit since its distance value has not been estimated correctly.

Finally, after the reason behind the deviation of the pulsar from the fit is found out, either the data of the pulsar is left as it is or a new distance value is adopted to the pulsar. In the end, with corrected data, the free electron density of each 3D portion is calculated using the inverse slopes of d vs DM graphs. Gathering the free electron density data of those 3D portions, the free electron density map of the Milky Way Galaxy is obtained.

3.2 Stages of the Methodology

3.2.1 Step 1: Retrieving Radio Pulsar Data From Existing Catalogs

The pulsar data that is used in this study is obtained from Australia Telescope National Facility (ATNF) Catalog Version 1.43 (Manchester et al. 2005). ATNF Pulsar Catalog consists of 1984 pulsars (1893 of them are Galactic) to date. Pulsar observations have been done since the first pulsar was detected in 1967, by 64m Parkes Radio Telescope which is located in New South Wales, Australia.

Although the ATNF Pulsar Catalog is considered to be the most extensive catalog today for radio pulsars, the provided data may need certain corrections. As it is explained in Chapter 1, pulsar distance estimation is a real challenge for scientists and distance errors can go up to 30-50%. In order to overcome this obstacle, another catalog is used which contains nearly-corrected pulsar distance data. This catalog database was constructed by Guseinov (2009) and is still located in METU Physics Department's servers.

3.2.2 Step 2: Dividing the Galaxy into 3D pieces

The sole aim of this study is to obtain the free electron density map of the Milky Way Galaxy. The mapping process starts by dividing the Galaxy into 3D pieces so that free electron density that falls in front of each section's line of sight can be calculated. The coordinate system that is chosen for the study is the Galactic coordinate system that is centered by the Sun. To start with, considering the Galaxy as a cylinder, the Galaxy is divided into zones in galactic latitude direction. Here it should be noted that the zones obtained in this dividing process is neither equal in thickness nor symmetric for northern and southern hemispheres of the Galaxy. Since the pulsars are mostly populated on the disk region and their number densities decrease at high latitudes, the zones at low latitudes are thin in order to increase the accuracy and they get thicker as latitude increases in northern hemisphere (or decreases in southern hemisphere).

After the zones are obtained, each zone is divided into pieces in galactic longitude direction so that the resulting 3D pieces are frustums of cones. To be more precise, the cone angle is set by the galactic latitude and longitude ranges and conical frustum's height is dictated by the closest and farthest pulsars that fall into this 3D section. The only consideration in this step is to obtain conical frustums that have constant free electron densities between itself and the Sun. For this, a trial-and-error method is followed. Considering the pulsars in each 3D section, distance versus dispersion measure graphs are plotted and one or two linear lines are fit to these pulsars on

the graphs. Following this, the galactic latitude and longitude ranges are changed until the corresponding pulsars are aligned to create linear fits with high fit quality, i.e until the paths that lie infront of the sections have constant free electron densities. Here it should be noted that resulting graphs have positive slopes that give inverse of the free electron densities. Moreover some of those sections are also divided into two in radial direction since the free electron density varies in a given line of sight, as number of free electron sources change with distance.

3.2.3 Step 3: Determination and Tailoring of Free Electron Source Data

Origins of this step are free electron sources which are supernova remnants and H II regions. In order to make comments on d vs DM graphs of pulsars in conical frustums, the free electron sources that fall into those 3D sections should be placed into the corresponding graphs.

In order to place SNRs and H II regions into d vs DM graphs, their galactic coordinates and distance values should be known. Unfortunately, although the galactic coordinates of the sources are well known, the distances of them can be poorly estimated for most of the cases since there are no standards for their sizes or their luminosities so that the distance estimation cannot be done through traditional standard candle technique.

Occasionally, the distance of free electron sources can be accurately determined if the distance of the star ionizing the H II Region is known or a correlation can be found between an association and the SNR. But most of the time, distances of SNRs and H II regions can be estimated by kinematic method which means by using a Galactic rotation model and observed radial velocities.

Galactic rotation models are simplified versions of the complex rotation structure that is observed in reality. Those models estimate axis-symmetric circular orbits for objects in the Galaxy that cannot mimic their rotation pat-

tern very successfully. Moreover, determination of distances of free electron sources at the inner Galaxy is problematic because the kinematic method gives two different distances for the same source that is close to the Galactic Center. As a result, the distance errors can go up to 30-50% for most of the cases (Guseinov et al. 2003).

In order to overcome the near and far kinematic distance ambiguity of H II regions, HI emission/absorption and HI self absorption observations are used (Roman-Duval et al. 2009). For H II regions inside the molecular clouds, by making use of cold HI inside the cloud and the warm HI region that is found in the background interstellar medium, the location of the H II region can be estimated. For example, if the molecular cloud, hence the H II region, is at near kinematic distance, the radiation emitted by the warm HI on the background is absorbed by the cold HI located inside the molecular cloud. Then, if the 21 cm spectrum is investigated for the corresponding line of sight, an absorption line is observed (Jackson et al. 2002). By this way it can be decided whether the H II region is located in near or far kinematic distance. Similar to this method, H_2CO line observations have been used to overcome distance ambiguity for a few decades.

The most extensive H II region catalog of today has been collected by Paladini et al. (2003, 2004) (hereafter P03) and it consists of 1442 H II regions. Following this, lots of studies have been performed in order to resolve distance ambiguity by the methods mentioned above. Hou et al. (2009) (hereafter HHS09) gathered nearly all of the information about the H II regions in the literature and used three different rotation curves for the H II regions whose distances had not been estimated. In the end, HHS09 catalog provides 815 H II region data.

In this study basically the galactic coordinate, distance and size data of H II regions are used in the calculations. P03 catalog provides angular sizes of H II regions but the distance data is not open to public, on the other hand HHS09 catalog provides distances of H II regions but the angular sizes are not tabulated. So, those catalogs are matched and mixed in order to obtain

both distance and angular size data. In this process, the H II regions that have only distance data or only angular size data are excluded so that it turned out to be 518 H II regions left with effective data.

When it comes to supernova remnants, distance is estimated through the diameter-angular size relation of the source. Making a small angle assumption for the angular size, the distance can be calculated by:

$$\text{Distance} = \frac{\text{Diameter}}{\text{Angular size}} \tag{3.1}$$

Despite the simplicity of this equation, obtaining diameter information is another challenge for the scientists while angular size of the SNR can easily be determined.

Since the diameter of the SNR cannot be estimated directly, a surface brightness-diameter $(\Sigma - D)$ relation is used for this problem. It is known that as diameters of SNRs increase, their surface brightnesses decrease. So inorder to use this relation, all known SNRs are put on a $\Sigma - D$ graph and it is seen that most of the SNRs fall into regions which can be fit into two linear curves. As a result, knowing the surface brightness of any SNR, one can estimate its diameter using the mathematical expressions of the empirical curves. Considering this method, diameters of SNRs are calculated by using the $\Sigma - D$ relations given by Guseinov et al. (2003) where the flux data is obtained from Green (2009) and Simbad Catalog that is up to date. In the end, after the diameters are estimated through the empirical curves, the distances of SNRs are calculated using Eq. 3.1.

At the end of this step, knowing the galactic coordinates and the distances of SNRs and H II regions, the free electron sources that fall into each small 3D section of the Galaxy are placed into corresponding d vs DM graphs.

3.2.4 Step 4: Searching for Reasons of Deviations of Pulsars From d vs DM Curves

Since the 3D sections of the Galaxy are assumed to have constant free electron densities between them and the Sun, pulsars are expected to be on

linear curves of the d vs DM graphs. This is of course true for an idealized model, when real data is used, it is seen that pulsars are not aligned perfectly on linear fits for most of the cases. In this step, the aim is to find pulsars that deviate from the estimated fits of d vs DM graphs and the reasons behind those deviations.

The cornerstone information that is used in this step is that dispersion measures of pulsars are estimated very accurately and hence no doubt is shed on this data, i.e deviation of the pulsars cannot be due to error in dispersion measure data. In this case there should be only two possible reasons for a pulsar that deviates from the linear fit of the d vs DM graph:

1. For a pulsar that deviates towards the region that is under the linear curve; if its distance value is assumed to be correct, this means that the pulsar has extra dispersion measure compared to other pulsars in the same section. This is only possible if the signal sent by this specific pulsar passes through an additional free electron source.

2. For a pulsar that deviates in any direction on the graph different than the one of case (1), the distance value of the pulsar has been estimated wrongly.

For those two possibilities there are two corresponding routes to follow:

1. After the free electron sources that fall into each 3D section are determined, one can check for each pulsar whether its signal passes through any of the free electron sources in the corresponding section on its way to Sun. By using galactic coordinate, distance and angular size data this can be determined by simple geometry.

   At this point there is an important concept to be mentioned. The data in hand shows that angular sizes of SNRs are usually larger than the H II region sizes. So when the calculations are done in order to check whether signals of pulsars pass through free electron source or not, at first glance, it is seen that the signals of pulsars pass through only

SNRs but not the H II regions. Of course this is not the case in real conditions. The problem arises from the fact that the H II region observations are done piece by piece so that even if the H II regions are located very close to each other geometrically, one may think that they are not physically linked. In reality, H II regions extend to great amounts. So, when close H II regions are considered, the space in between them must be full of free electrons. Following this, H II regions that are close to each other are put together to form groups in which size of the corresponding group is dictated by the H II regions on the borders of the group. Using this method 121 H II region groups are obtained with inequal number of H II regions inside. In the end, as expected, it seen that the signals of pulsars do pass through H II regions.

At the end of the calculations, for any section, the pulsars whose signals pass through any source is determined. Following this, if the pulsars deviating from the linear fit in positive sense in DM, parallel to dispersion measure axis, are in fact the ones whose signals pass through an additional free electron source then this means that the data and the physics are in correlation.

This investigation is also helpful in certain 3D sections in which signals of all pulsars pass through some free electron source. In a case like this, pulsars are again expected to be on a linear curve since all of them have additional dispersion measures.

2. After one makes sure that the signal of the deviating pulsars do not pass through any of the free electron sources in the corresponding section, it can be concluded that the distances of those pulsars are estimated wrongly. Because, if the signals of pulsars are sent from the same small 3D section of the Galaxy which have constant free electron density along the signal path, their signals must be dispersed with an amount depending only on their distance values. Moreover since the dispersion measures of pulsars are estimated very accurately, this implication brings one to the result that the distances of those pulsars are not estimated correctly.

3.2.5 Step 5: Corrections on Pulsar Distance Values

In the previous step, the reasons of deviating pulsars on the d vs DM graphs are studied. After pulsars that deviate from the linear curves and the reasons behind these deviations are investigated, one can come into two conclusions: if the data and the physics are in correlation, like the one in the first case of the previous section, the pulsar distance data need not to be corrected and the free electron densities should be calculated through the graphs in hand; but if it turns out that distance of any pulsar has been estimated wrongly, a new distance value should be adopted to this pulsar. In order to adopt a new distance, firstly, the pulsar in question is excluded from the d vs DM graph of the section. Afterwards, a new slope is calculated through the linear fit composed of the remaining pulsars. In the end, assuming that the previously deviating pulsar should be on this new, corrected linear fit, a new distance value is adopted by simply using its dispersion measure value.

3.2.6 Step 6 : Determination of Free Electron Density Distribution of the Galaxy

After overall data is worked on for all of the 3D sections, the only thing left is calculating the free electron density of the signal path that falls in front of each section by making use of d vs DM graphs. Calculating the slope of each linear fit and taking its inverse gives the value of the free electron density in question. Repeating this procedure for 517 sections, the free electron map of the Milky Way Galaxy is obtained.

CHAPTER 4

SAMPLE WORK

In this chapter, the methodology that is explained in Chapter 3 is followed for certain part of the Galaxy in order to provide a sample work for this study. Since (-1.0,1.0] degree galactic latitude range is the richest part of the Galaxy in terms of both free electron sources and the pulsars, it is the one that is chosen as the suitable part of the Galaxy for demonstration of the work. Steps that are followed in the work are presented below.

4.1 Step 1: Retrieving Radio Pulsar Data

(-1.0,1.0] degree range contains 533 Galactic pulsars to date. 498 of the pulsar data have been analyzed and corrected in Guseinov (2009), 35 of the pulsar data is taken directly from ATNF Pulsar Catalog (Manchester et al. 2005) without any investigation has been done on the data.

4.2 Step 2: Dividing the Galaxy into 3D Pieces

As it is explained in the Chapter 3, the Galaxy is divided into 3D sections in which the signal path lying in front of these sections are assumed to have constant free electron densities. At the end of this dividing process it turned out be 14 main zones of the Galaxy in galactic latitude direction. The mostly populated zone is the (-1.0,1.0] degree range in terms of galactic latitude. Division of this zone into sections in galactic longitude is done by a trial-

and-error method until constant-like free electron densities are obtained for signal paths lying infront of the group of pulsars in the conical frustums. In the following pages, the abbreviation of 'a:b/c:d' means that the location of the 3D section of the Galaxy is in between 'a' and 'b' degrees in terms of galactic longitude and is in between 'c' and 'd' degrees in terms galactic latitude. The angle ranges of the sections are given in Table 4.1 together with the distance ranges of the 3D sections.

(-1.0,1.0] degree zone is divided into 72 angle ranges and 96 sections in galactic longitude direction. This is because some of the conical frustums are divided into two parts in radial direction since d vs DM graphs are given by two linear fits.

4.3 Step 3: Free Electron Source Data

(-1.0,1.0] degree zone contains 184 supernova remnants and 377 H II regions. Those H II regions make up 84 H II region groups according to our data. H II region groups are shown as 'AXXX.YY' in this study. 'A' indicates that the source in question is an H II region group, 'XXX' defines the galactic longitude coordinate of the group in degrees and 'YY' is the number index of the group that is used to distinguish the H II region groups that are on the same longitude. Using the methodology that is explained before, distances of SNRs are calculated. Likewise, distances and sizes of H II region groups are determined by plugging the H II region data that constitutes the corresponding group into simple geometrical equations.

4.4 Step 4, 5 6: Investigation of Distance versus Dispersion Measure Graphs and Determination of Free Electron Density

Since those three steps are intercorrelated they are presented simultaneously. Here, for each section, pulsars that deviate from d vs DM graphs are studied. Depending on the case, new distances are adopted to some of the

Table 4.1. d

egree zone.]Sections of the (-1.0,1.0] degree zone. GL_{min} and GL_{max} define the Galactic longitude range of the section in degrees; d_{min} and d_{max} define the distance range in kpc.

GL_{min}	GL_{max}	d_{min}	d_{max}	GL_{min}	GL_{max}	d_{min}	d_{max}
358.0	1.0	1.8	5.2	148.0	150.0	2.0	3.8
358.0	1.0	11.4	14.2	200.0	203.0	3.3	6.6
1.0	3.0	1.3	8.5	231.0	238.0	2.6	4.7
3.0	4.5	3.5	11.4	259.0	264.0	3.3	13.5
4.5	6.5	2.5	5.1	264.0	277.0	2.9	6.6
4.5	6.5	11.0	13.1	277.0	282.0	3.5	11.1
6.5	8.0	3.4	5.4	282.0	287.0	2.4	7.9
6.5	8.0	10.0	13.6	282.0	287.0	14.2	16.2
8.0	9.5	3.4	9.3	287.0	289.0	2.3	11.2
9.5	11.5	3.1	3.5	289.0	291.0	2.2	7.2
9.5	11.5	9.5	11.3	291.0	293.0	1.7	6.8
11.5	13.0	5.5	11.6	291.0	293.0	9.1	12.6
13.0	15.5	4.0	9.6	293.0	297.0	1.9	9.2
15.5	16.5	3.0	12	297.0	304.0	8.3	9.6
16.5	17.5	1.4	7.8	297.0	304.0	10.2	13.6
16.5	17.5	10.0	12.6	304.0	306.0	2.3	9.8
17.5	20.0	3.4	11.1	304.0	306.0	13.8	17.3
20.0	21.0	3.0	7.3	306.0	308.0	5.7	16.3
21.0	22.5	3.8	4.7	308.0	312.0	5.1	8.6
21.0	22.5	7.6	8	308.0	312.0	9.2	12.1
22.5	25.0	4.5	10.4	312.0	317.0	0.8	6.2
25.0	27.0	2.1	9.1	312.0	317.0	8.2	10.6
27.0	28.0	4.4	8.3	317.0	321.0	3.3	5.1
28.0	30.0	2.4	4.8	317.0	321.0	7.1	10.5
28.0	30.0	5.9	10.6	321.0	324.0	2.6	6.2
30.0	32.0	3.8	9.1	321.0	324.0	9.2	13.3
32.0	34.0	1.0	4.6	324.0	327.0	3.5	5.2
32.0	34.0	6.4	12.1	324.0	327.0	6.8	9.8
34.0	35.0	2.4	8.6	327.0	332.0	1.1	7.1
35.0	37.0	3.8	13.1	327.0	332.0	8.4	9.8
37.0	39.0	4.0	17.1	332.0	335.0	3.7	9.2
39.0	41.0	2.0	5.9	335.0	338.0	5.5	7.3
39.0	41.0	7.0	12.1	335.0	338.0	8.5	12.0
41.0	44.0	0.4	6.1	338.0	342.0	3.6	6.3
41.0	44.0	7.5	9.5	338.0	342.0	6.8	10.0
44.0	50.0	3.1	5.7	342.0	345.0	4.8	9.7
44.0	50.0	7.0	7.8	345.0	348.0	4.3	6.4
50.0	54.0	3.3	8.3	345.0	348.0	8.6	12.0
54.0	61.0	2.9	7.9	348.0	351.0	2.2	6.6
61.0	66.0	0.3	7.2	348.0	351.0	9.2	10.6
66.0	75.0	5.1	12.5	351.0	354.0	6.3	12.1
75.0	77.0	6.5	12.1	354.0	356.0	3.8	9.6
97.0	107.0	3.0	14.9	356.0	358.0	4.4	8.5
107.0	117.0	2.4	5.6				

pulsars if they are decided to have wrong distance estimates. On the other hand, if the deviation is due to an intervening free electron source, the data is left as it is. Finally the free electron density of the signal path that falls in front of each section is calculated. Here it is important to note that the free electron densities are calculated only through certain distance intervals in given line of sights. Since the density is calculated through a group of pulsar data, it is important to present the distance range of the 3D section that encloses the pulsars because density value is viable for the path that falls in front of the specified distance range only. The following is a sample work of investigation of d vs DM graphs of the (-1.0,1.0] degree zone of the Galaxy. Note that the corresponding graphs are presented in Appendix A, like the other d vs DM graphs of the rest of the zones. Moreover the adopted distances of some of (-1.0,1.0] degree zone pulsars that are mentioned here are also tabulated in Chapter 5.

4.4.1 Range: 358.0:1.0/-1.0:1.0

This section is divided into two distance intervals: 1.8-5.2 kpc and 11.4-14.2 kpc since free electron densities of the paths that fall in front of the intervals seem to be different. This difference may be result of 7 SNRs (G359.1-0.5, G0.3+0.0, G1.0-0.1, G358.5-0.9, G0.0+0.0, G0.9+0.1, G359.1+0.9) that are located in between these 3D sections.

Considering the second interval, J1746-2849 is excluded from the graph since its distance value is far from being realistic. Moreover a new distance value is adopted to J1745-2910 pulsar as 13.5 kpc and J1747-2809 pulsar as 13.8 kpc in order for them to agree with the linear fit of the second interval. Here it should be noted that the signal of J1747-2809 pulsar passes through G0.9+0.1SNR so its adopted distance should be the upper limit for this pulsar since otherwise it would contradict to concept of the effect of intervening free electron sources on the signal arrival times of pulsars. As a result free electron density calculated through 1.8-5.2 kpc interval is 0.091 cm^{-3} which includes certain sections of Sagittarius, Scutum-Centaurus and

Norma Arms. The free electron density calculated through 11.4-14.2 kpc interval is 0.135 cm^{-3} which includes certain sections of Sagittarius, Scutum-Centaurus, Norma, Near 3 kpc, Far 3 kpc and Perseus Arms plus the Galactic Bar Region.

4.4.2 Range: 1.0:3.0/-1.0:1.0

The free electron density calculated through 1.3-8.5 kpc interval is 0.074 cm^{-3} which includes sections of Sagittarius, Scutum-Centaurus, Norma and Near 3 kpc Arms plus the Galactic Bar Region.

4.4.3 Range: 3.0:4.5/-1.0:1.0

A new distance value is adopted to J1755-2534 pulsar as 8.3 kpc in order for it to agree with the linear fit of the interval. The free electron density calculated through 3.5-11.4 kpc interval is 0.075 cm^{-3} which includes sections of Sagittarius, Scutum-Centaurus, Norma, Near 3 kpc and Far 3 kpc Arms plus the Galactic Bar Region.

4.4.4 Range: 4.5:6.5/-1.0:1.0

This section is divided into two distance intervals: 2.5-5.1 kpc and 11.0-13.1 kpc free electron densities of the paths that fall in front of the intervals seem to be different. The free electron density of the 2.5-5.1 kpc interval is 0.100 cm^{-3} which includes sections of Sagittarius, Scutum-Centaurus, Norma and Near 3 kpc Arms; and 11.0-13.1 kpc interval has electron density 0.037 cm^{-3} which includes certain sections of Sagittarius, Scutum-Centaurus, Norma, Near 3 kpc, Far 3 kpc and Perseus Arms plus the Galactic Bar Region.

4.4.5 Range: 6.5:8.0/-1.0:1.0

This section is divided into two distance intervals: 3.4-5.4 kpc and 10.0-13.6 kpc in order to have better fit statistics. Since both of the intervals are affected by same number of free electron sources their electron densities are expected to be the same. Moreover when specific pulsars are considered it is seen that the signal of J1804-2228 pulsar in the first distance interval passes through the A007-01 H II region group and the signal of J1801-2304 pulsar in the second distance interval passes through the G6.4-0.1 SNR. In the end, it is seen that the free electron densities are very close. The free electron density calculated through 3.4-5.4 kpc interval is 0.114 cm^{-3} which includes certain sections of Sagittarius, Scutum-Centaurus and Norma Arms and through 10.0-13.6 kpc interval is 0.113 cm^{-3} which includes certain sections of Sagittarius, Scutum-Centaurus, Norma, Near 3 kpc, Far 3 kpc and Perseus Arms plus the Galactic Bar Region.

4.4.6 Range: 8.0:9.5/-1.0:1.0

A new distance value is adopted to J1801-2115 pulsar as 9.5 kpc in order for it to agree with the linear fit of the interval. Here it should be noted that the signal of J1801-2115 pulsar passes through G8.7-0.1 SNR so its adopted distance should be the upper limit for this pulsar since otherwise it would contradict to concept of the effect of intervening free electron sources on the signal arrival times of pulsars. Moreover it is seen that J1803-2137 calibrator pulsar deviates from the fit in positive sense in DM but since its signal passes through G8.7-0.1 SNR and they are in fact associated couples (Distance between the pulsar and the SNR is 26 parsecs.), this is an expected result. The free electron density calculated through 3.4-9.3 kpc interval is 0.098 cm^{-3} which includes certain sections of Sagittarius, Scutum-Centaurus, Norma and Near 3 kpc Arms plus the Galactic Bar Region.

4.4.7 Range: 9.5:11.5/-1.0:1.0

This section is divided into two distance intervals: 3.1-3.5 kpc and 9.0-11.3 kpc since free electron densities of the paths that fall in front of the intervals seem to be different. In the second distance interval a new distance value is adopted to J1809-1850 pulsar as 9.0 kpc in order for it to agree with the linear fit of the interval. The free electron density calculated through 3.1-3.5 kpc interval is 0.227 cm^{-3} which includes sections of Sagittarius and Scutum-Centaurus Arms and through 9.0-11.2 kpc interval is 0.143 cm^{-3} which includes certain sections of Sagittarius, Scutum-Centaurus, Norma, Near 3 kpc and Far 3 kpc Arms plus the Galactic Bar Region.

4.4.8 Range: 11.5:13.0/-1.0:1.0

The signal of both J1811-1736 and J1812-1733 pulsars pass through A012-01 H II region group. The pulsars in this section seem to be affected by the same group of free electron sources. The free electron density calculated through 5.5-11.6 kpc interval is 0.078 cm^{-3} which includes certain sections of Sagittarius, Scutum-Centaurus, Norma, Near 3 kpc and Far 3 kpc Arms plus the Galactic Bar Region.

4.4.9 Range: 13.0:15.5/-1.0:1.0

Since J1814-1744 is a distant pulsar its distance value might not have been estimated correctly. A new distance value is adopted to this pulsar as 9.4 kpc in order for it to agree with the linear fit of the interval. Moreover the signal of newly found J1818-1556 pulsar passes through A014-01 H II region group, so the estimated distance should be the upper limit for this pulsar since otherwise it would contradict to concept of the effect of intervening free electron sources on the signal arrival times of pulsars. The free electron density calculated through 4.0-9.6 kpc interval is 0.104 cm^{-3} which includes certain sections of Sagittarius, Scutum-Centaurus, Norma, Near 3 kpc and Far 3 kpc Arms plus the Galactic Bar Region.

4.4.10 Range: 15.5:16.5/-1.0:1.0

J1818-1519 has no reason for having such large DM value with this distance value. A new distance value is adopted to this pulsar as 10.6 kpc in order for it to agree with the linear fit of the interval. The free electron density calculated through 3.0-12.0 kpc interval is 0.086 cm^{-3} which includes certain sections of Sagittarius, Scutum-Centaurus, Norma, Near 3 kpc and Far 3 kpc Arms plus the Galactic Bar Region.

4.4.11 Range: 16.5:17.5/-1.0:1.0

This section is divided into two distance intervals: 1.4-7.8 kpc and 10.0-12.6 kpc since free electron densities of the paths that fall in front of the intervals seem to be different. This is obviously seen when individual pulsars are investigated. The signals of both J1819-1408 and J1821-1419 pulsars that are in the second interval pass through A016-02 HII region group so second interval is expected to have larger free electron density. Moreover a new distance value is adopted to J1824-1500 pulsar as 7.1 kpc in order for it to agree with the linear fit of the first interval. The free electron density calculated through 1.4-7.8 kpc interval is 0.098 cm^{-3} which includes certain sections of Sagittarius, Scutum-Centaurus, Norma, Near 3 kpc Arms plus the Galactic Bar Region and through 10.0-12.6 kpc interval is 0.149 cm^{-3} which includes certain sections of Sagittarius, Scutum-Centaurus, Norma, Near 3 kpc, Far 3 kpc and inner Perseus Arms plus the Galactic Bar Region.

4.4.12 Range: 17.5:20.0/-1.0:1.0

The signal of J1824-1159 pulsar passes through G19.1+0.2 SNR (Distance between the SNR and the pulsar is 980 parsecs.) and it deviates from the fit in positive sense in DM. Since this is an expected result, no new distance is adopted to this pulsar. The free electron density calculated through 3.4-11.7 kpc interval is 0.092 cm^{-3} which includes certain sections of Sagittarius, Scutum-Centaurus, Norma, Near 3 kpc and Far 3 kpc Arms plus the Galac-

tic Bar Region.

4.4.13 Range: 20.0:21.0/-1.0:1.0

The free electron density calculated through 3.0-7.3 kpc interval is 0.111 cm^{-3} which includes certain sections of Sagittarius, Scutum-Centaurus, Norma and Near 3 kpc Arms plus the Galactic Bar Region.

4.4.14 Range: 21.0:22.5/-1.0:1.0

This section is divided into two distance intervals: 3.8-4.7 kpc and 7.6-8.0 kpc since their free electron densities seem to be different. The free electron density calculated through 3.8-4.7 kpc interval is 0.150 cm^{-3} which includes certain sections of Sagittarius, Scutum-Centaurus and Norma Arms and through 7.6-8.0 kpc interval is 0.152 cm^{-3} which includes certain sections of Sagittarius, Scutum-Centaurus, Norma, Near 3 kpc and Far 3 kpc Arms plus the Galactic Bar Region.

4.4.15 Range: 22.5:25.0/-1.0:1.0

This section is very rich in terms of free electron sources. Nearly all of the pulsars located in this section have an electron source that causes their signals being delayed.

Signal of J1834-0812 pulsar passes through A023-01, A023-02 and A024-01 H II region groups. Signal of J1834-0742 pulsar passes through A023-01 and A024-01 H II region groups. Signal of J1834-0731 pulsar passes through A024-01 H II region group. Signal of J1833-0827 passes through A023-01 and A024-01 H II region groups. Signal of both J1831-0823 and J1832-0827 pulsars pass through A024-01 H II region group. As a result they are expected to be on the same linear fit. The free electron density calculated through 4.5-10.4 kpc interval is 0.129 cm^{-3} which includes certain sections of Sagittarius, Scutum-Centaurus, Norma, Near 3 kpc and Far 3

kpc Arms plus the Long Bar Region.

4.4.16 Range: 25.0:27.0/-1.0:1.0

The free electron density calculated through 2.1-9.1 kpc interval is 0.096 cm^{-3} which includes certain sections of Sagittarius, Scutum-Centaurus, Norma, Near 3 kpc and Far 3 kpc Arms plus the Long Bar Region.

4.4.17 Range: 27.0:28.0/-1.0:1.0

The free electron density calculated through 4.4-8.3 kpc interval is 0.100 cm^{-3} which includes certain sections of Sagittarius, Scutum-Centaurus, Norma, Near 3 kpc and Far 3 kpc Arms plus the Long Bar Region.

4.4.18 Range: 28.0:30.0/-1.0:1.0

This section is divided into two distance intervals: 2.4-4.8 kpc and 5.9-10.6 kpc since free electron densities of the paths that fall in front of the intervals seem to be different. This is due to the fact that the second interval is richer interms of free electron sources (A029-01 and A029-02 H II region groups and G29.7-0.3 SNR). Moreover a new distance value is adopted to J1844-0310 pulsar as 9.3 kpc in order for it to agree with the linear fit of the second interval. Here it should be noted that the signal of J1844-0310 pulsar passes through A029-01 H II region group so its adopted distance should be the upper limit for this pulsar since otherwise it would contradict to concept of the effect of SNRs on the signal arrival times of pulsars.

The free electron density calculated through 2.4-4.8 kpc interval is 0.059 cm^{-3} which includes certain sections of Sagittarius and Scutum-Centaurus Arms and free electron density calculated through 5.9-10.6 kpc interval is 0.121 cm^{-3} which includes certain sections of Sagittarius, Scutum-Centaurus, Norma, Near 3 kpc and Far 3 kpc Arms plus the Long Bar Region.

4.4.19 Range: 30.0:32.0/-1.0:1.0

Since J1848-0055 is a distant pulsar its distance value might not have been estimated correctly. A new distance value is adopted to this pulsar as 13.9 kpc in order for it to agree with the linear fit of the interval. The free electron density calculated through 3.8-13.9 kpc interval is 0.100 cm^{-3} which includes certain sections of Sagittarius, Scutum-Centaurus and Far 3 kpc Arms plus the Long Bar Region.

4.4.20 Range: 32.0:34.0/-1.0:1.0

This section is divided into two distance intervals: 1.0-4.6 kpc and 6.4-15.7 kpc free electron densities of the paths that fall in front of the intervals seem to be different. This is due to the fact that the second interval is richer in terms of free electron sources (G32.8-0.1, G33.6+0.1, G33.2-0.6 SNRs and A033-01 H II region group). Since J1850-0026 and J1849-0040 are distant pulsars their distance values might not have been estimated correctly. New distance values are adopted to these pulsars as 12.2 kpc and 15.7 kpc respectively in order for them to agree with the linear fit of the second interval. The free electron density calculated through 1.0-4.6 kpc interval is 0.064 cm^{-3} which includes sections of Sagittarius and Scutum-Centaurus Arms and free electron density calculated through 6.4-15.7 kpc interval is 0.084 cm^{-3} which includes Sagittarius Arm, intersection of Scutum-Centaurus Arm with the Long Bar, plus inner section of Perseus Arm.

4.4.21 Range: 34.0:35.0/-1.0:1.0

The free electron density calculated through 2.4-8.6 kpc interval is 0.080 cm^{-3} which includes some section of Sagittarius Arm and intersection of Scutum-Centaurus Arm with the Long Bar.

4.4.22 Range: 35.0:37.0/-1.0:1.0

The free electron density calculated through 3.8-13.1 kpc interval is 0.067 cm^{-3} which includes certain sections of Sagittarius Arm, intersection of Scutum-Centaurus Arm with the Long Bar and some section of Perseus Arm.

4.4.23 Range: 37.0:39.0/-1.0:1.0

J1901+0510 pulsar deviates from the fit in positive sense in DM but since pulsars with small Gz values tend to have extra DM due to effect of expansion of plasma on the disk, this is an expected result. No distance is adopted to J1901+0510 since it has a small Gz value when compared to other pulsars in this interval. The free electron density calculated through 4.0-17.1 kpc interval is 0.066 cm^{-3} which includes certain sections of Sagittarius Arm, intersection of Scutum-Centaurus Arm with the Long Bar plus sections of Perseus and Outer Arms.

4.4.24 Range: 39.0:41.0/-1.0:1.0

This section is divided into two distance intervals: 1.1-5.9 kpc and 7.0-12.1 kpc since free electron densities of the paths that fall in front of the intervals seem to be different. This may be due to difference in number of free electron sources located in each interval (First interval includes only G40.5-0.5 SNR but second interval includes G40.5-0.5 and G39.2-0.3 SNRs.). New distance values are adopted to J1909+06 and J1907+0602 pulsars as 1.1 kpc and 2.0 kpc respectively in order for them to agree with the linear fit of the first interval. In the end, the free electron density calculated through 1.1-5.9 kpc interval is 0.052 cm^{-3} which includes sections of Sagittarius Arm and outer region of Scutum-Centaurus Arm and free electron density calculated through 7.0-12.1 kpc interval is 0.076 cm^{-3} which includes sections of Sagittarius Arm, outer region of Scutum-Centaurus Arm and a section of Perseus Arm.

4.4.25 Range: 41.0:44.0/-1.0:1.0

This section is divided into two distance intervals: 0.4-6.1 kpc and 7.5-9.5 kpc since free electron densities of the paths that fall in front of the intervals seem to be different. When individual pulsars are investigated in the second interval, it seen that there are two pulsars whose signals pass through some electron source(signal of J1908+0909 pulsar passes through G42.8+0.6 SNR and signal of J1907+0740 pulsar passes through A041-02 H II region group.) Hence the free electron density calculated through the linear fit of the second section is greater. Moreover a new distance value is adopted to J1910+0714 pulsar as 2.7 kpc in order for it to agree with the linear fit of the first interval. In the end, the free electron density calculated through 0.4-6.1 kpc interval is 0.052 cm^{-3} which includes sections of Sagittarius Arm and outer region of Scutum-Centaurus Arm and free electron density calculated through 7.5-9.5 kpc interval is 0.116 cm^{-3} which also includes sections of Sagittarius Arm and outer region of Scutum-Centaurus Arm.

4.4.26 Range: 44.0:50.0/-1.0:1.0

This section is divided into two distance intervals: 2.0-5.7 kpc and 7.0-9.5 kpc since free electron densities of the paths that fall in front of the intervals seem to be different. This is an expected result since there are additional free electron sources (G45.7-0.4 and G46.8-0.3 SNRs) affecting the second interval. Moreover new distance values are adopted to J1918+1444, J1914+1122 and J1913+1145 pulsars as 2.0 kpc, 3.2 kpc and 9.4 kpc respectively in order for them to agree with the linear fits of the intervals. In the end, the free electron density calculated through 2.0-5.7 kpc interval is 0.063 cm^{-3} which includes a section of Sagittarius Arm and free electron density calculated through 7.0-9.5 kpc interval is 0.128 cm^{-3} which includes two sections of Sagittarius Arm.

4.4.27 Range: 50.0:54.0/-1.0:1.0

The free electron density calculated through 3.3-8.3 kpc interval is 0.033 cm^{-3} which includes the tangential section of the Sagittarius Arm.

4.4.28 Range: 54.0:61.0/-1.0:1.0

Fit statistics of this interval is rather poor when compared to the other intervals. The free electron density calculated through 2.9-7.9 kpc interval is 0.080 cm^{-3} which includes a section of Orion Spur and inner Perseus Arm.

4.4.29 Range: 61.0:66.0/-1.0:1.0

The signal of J1957+2831 pulsar passes through G65.1+0.6 SNR. This pulsar deviates from the fit in positive sense in DM, which is an expected result. Moreover J1952+2630 pulsar is excluded from the graph since it is a distant pulsar and it would be an overestimation to consider it to have the same electron density as the other pulsars considering the intervening Perseus Arm in between. The free electron density calculated through 0.3-7.2 kpc interval is 0.024 cm^{-3} which includes a section of Orion Spur.

4.4.30 Range: 66.0:75.0/-1.0:1.0

A new distance value is adopted to J2002+30 pulsar as 6.8 kpc. Here it should be noted that since the signal of J2002+30 pulsar passes through A066-01 H II region group, its adopted distance should be the upper limit for this pulsar since otherwise it would contradict to concept of the effect of SNRs on the signal arrival times of pulsars. The free electron density calculated through 5.1-12.5 kpc interval is 0.029 cm^{-3} which includes a section of Orion Spur, Perseus and Outer Arms.

4.4.31 Range: 75.0:77.0/-1.0:1.0

Fit statistics of this interval is rather poor when compared to the other intervals. The free electron density calculated through 6.5-12.1 kpc interval is 0.054 cm^{-3} which includes a section of Orion Spur, Perseus and Outer Arms.

4.4.32 Range: 77.0:97.0/-1.0:1.0

This section is free of known pulsars.

4.4.33 Range: 97.0:107.0/-1.0:1.0

The free electron density calculated through 3.0-14.9 kpc interval is 0.013 cm^{-3} which includes sections of Orion Spur, Perseus and Outer Arms (Only the signal delay of J2208+5500 pulsar may be due to effect of Perseus Arm.).

4.4.34 Range: 107.0:117.0/-1.0:1.0

J2321+6024 pulsar deviates from the fit in positive sense in DM but since pulsars with small Gz values tend to have extra DM due to effect of expansion of plasma on the disk, this is an expected result. So no distance is adopted to J2321+6024 since it has a small Gz value when compared to other pulsars in this interval. Moreover, since the signal of J2257+5909 pulsar passes through A108-01 H II region group and the signal of J2326+6113 pulsar passes through A112-01 H II region group this interval is expected to have greater free electron density. The free electron density calculated through 2.4-5.6 kpc interval is 0.029 cm^{-3} which includes sections of Orion Spur and Perseus Arm.

4.4.35 Range: 117.0:121.0/-1.0:1.0

There is only a single known pulsar in this interval.

4.4.36 Range: 121.0:130.0/-1.0:1.0

This section is free of known pulsars.

4.4.37 Range: 130.0:137.0/-1.0:1.0

There are two known pulsars in this interval. But since distance value of J0248+6021 pulsar is far from being realistic, (The Galaxy do not extend to such distances at anti-center line of sights in terms of baryonic matter) data of J0248+6021 is excluded from this section. So there is only a single known pulsar left in this interval.

4.4.38 Range: 137.0:148.0/-1.0:1.0

This section is free of known pulsars.

4.4.39 Range: 148.0:150.0/-1.0:1.0

There are only two known pulsars in this interval. Although the result is less reliable due to lack of data, the free electron density calculated through 2.0-3.8 kpc interval is 0.027 cm^{-3} which includes sections of Orion Spur and Perseus Arm, moreover this section corresponds to one of the closest sections of the Perseus Arm to Solar System.

4.4.40 Range: 150.0:176.0/-1.0:1.0

This section is free of known pulsars.

4.4.41 Range: 176.0:177.0/-1.0:1.0

There is only a single known pulsar in this interval.

4.4.42 Range: 177.0:200.0/-1.0:1.0

This section is free of known pulsars.

4.4.43 Range: 200.0:203.0/-1.0:1.0

The free electron density calculated through 3.3-6.6 kpc interval is 0.015 cm^{-3} which includes sections of Perseus Arm and Outer Arm.

4.4.44 Range: 203.0:231.0/-1.0:1.0

This section is free of known pulsars.

4.4.45 Range: 231.0:238.0/-1.0:1.0

The existence of A234-01 H II region group located in this section results in relative increase of free electron density. The free electron density calculated through 2.6-4.7 kpc interval is 0.020 cm^{-3} which includes sections of Orion Spur and Perseus Arm.

4.4.46 Range: 238.0:259.0/-1.0:1.0

This section is free of known pulsars.

4.4.47 Range: 259.0:264.0/-1.0:1.0

The free electron density calculated through 3.3-13.5 kpc interval is 0.014 cm^{-3} which basically includes the free electron poor region between the

Perseus Arm and the Sagittarius Arm and some section of Perseus Arm. (Only the signal delay of J0847-4316 pulsar may be due to effect of Perseus Arm.).

4.4.48 Range: 264.0:277.0/-1.0:1.0

The free electron density of this interval is expected to be larger than the previous one because this section is richer in terms of free electron sources (that are A268-01 and A272-01 H II region groups). Moreover the signal of J0922-4949 pulsar passes through A272-01 H II region group showing that those sources are in fact effective in pulsar time delays. On the other hand a new distance value is adopted to J0857-4424 pulsar as 5.2 kpc in order for it to agree with the linear fit of the interval. The free electron density calculated through 2.9-6.6 kpc interval is 0.041 cm^{-3} which includes the region in between Perseus Arm and Sagittarius Arm but closer to the latter.

4.4.49 Range: 277.0:282.0/-1.0:1.0

The free electron density calculated through 3.5-11.1 kpc interval is 0.039 cm^{-3} which includes outer region of the Sagittarius Arm.

4.4.50 Range: 282.0:287.0/-1.0:1.0

This interval is rich in terms of free electron sources. When individual pulsars are investigated, it seen that signal of J1019-5749 pulsar passes through both A284-01 and A285-01 H II region groups and signals of J1032-5911 and J1038-5831 pulsars pass through A285-01 H II region group. Since the two distant pulsars (J1022-5813 and J1019-5749) might have different electron density on the path lying in front of them, this section is divided into two distance intervals: 2.4-7.9 kpc and 14.2-16.2 kpc. A new distance value is adopted to J1021-5601 pulsar as 4.3 kpc in order for it to agree with the linear fit of the first interval. In the end, the free elec-

tron density calculated through 2.4-7.9 kpc interval is 0.070 cm^{-3} which includes a section of the Sagittarius Arm and the free electron density calculated through 14.2-16.2 kpc interval is 0.171 cm^{-3} which includes certain sections of the Sagittarius Arm and Perseus Arm.

4.4.51 Range: 287.0:289.0/-1.0:1.0

Although it seems like this region is very rich in terms of free electron sources, when individual pulsars are investigated it seen that none of the signals of the pulsars pass through the H II region groups. The free electron density calculated through 2.3-11.2 kpc interval is 0.048 cm^{-3} which which includes a section of the Sagittarius Arm.

4.4.52 Range: 289.0:291.0/-1.0:1.0

Since distance value of J1055-6028 pulsar is far from being realistic, (The Galaxy do not extend to such distances at anti-center line of sights in terms of baryonic matter.) data of J1055-6028 is excluded from this section. Moreover a new distance value is adopted to J1055-6022 pulsar as 13.1 kpc in order for it to agree with the linear fit of the interval. Here it should be noted that the signal of J1055-6022 pulsar passes through A289-01 H II region group so its adopted distance should be the upper limit for this pulsar since otherwise it would contradict to concept of the effect of free electron sources on the signal arrival times of pulsars. The free electron density calculated through 2.2-13.1 kpc interval is 0.047 cm^{-3} which includes a section at the inner region of the Sagittarius Arm.

4.4.53 Range: 291.0:293.0/-1.0:1.0

This section is divided into two distance intervals: 1.7-6.8 kpc and 9.1-12.6 kpc since free electron densities of the paths that fall in front of the intervals seem to be different. This is obviously seen when individual pulsars are

investigated in the second interval; for example, the signals of both J1112-6103 and J1114-6100 pulsars pass through A291-01 H II region group. The free electron density calculated through 1.7-6.8 kpc interval is 0.046 cm^{-3} which includes a section of the Sagittarius Arm and free electron density calculated through 9.1-12.6 kpc interval is 0.069 cm^{-3} which includes two sections of Sagittarius Arm.

4.4.54 Range: 293.0:297.0/-1.0:1.0

A new distance value is adopted to J1128-6219 pulsar as 12.3 kpc in order for it to agree with the linear fit of the interval. The free electron density calculated through 1.9-12.3 kpc interval is 0.059 cm^{-3} which includes a section of the Sagittarius Arm and the electron poor region between the of Sagittarius and Scutum-Centaurus Arms.

4.4.55 Range: 297.0:304.0/-1.0:1.0

This section is divided into two distance intervals: 8.3-9.5 kpc and 10.2-13.6 kpc in order to have better fit statistics. Both of the intervals are very rich in terms of free electron sources. In the second interval, the signal of J1220-6318 pulsar passes through A299-01 H II region group and it deviates from the fit in positive sense in DM. Since this is an excepted result, no new distance is adopted for this pulsar. But since J1201-6306 is a distant pulsar its distance value might not have been estimated correctly. New distance value is adopted to this pulsar as 13.1 kpc in order for it to agree with the linear fit of the second interval. The free electron density calculated through 8.3-9.5 kpc interval is 0.154 cm^{-3} which includes a section of Sagittarius Arm and the outer region of the Scutum-Centaurus Arm. The free electron density calculated through 10.2-13.6 kpc interval is 0.148 cm^{-3} which includes two sections of Sagittarius Arm and the outer region of the Scutum-Centaurus Arm.

4.4.56 Range: 304.0:306.0/-1.0:1.0

This section is divided into two distance intervals: 2.3-9.8 kpc and 13.8-17.3 kpc since free electron densities of the paths that fall in front of the intervals seem to be different. Although both are relatively rich intervals in terms of free electron sources, signals of pulsars in the second interval seem to be affected more by the corresponding sources. For example signal of J1316-6232 pulsar in the second interval passes through both A304-01 and A305-01 H II region groups. Moreover a new distance value is adopted to J1303-6305 pulsar as 7.1 kpc in order for it to agree with the linear fit of the first interval. The free electron density calculated through 2.3-9.8 kpc interval is 0.048 cm^{-3} which includes a section of Sagittarius Arm and a tangential section of the Scutum-Centaurus Arm in the given line of sight. The free electron density calculated through 13.8-17.3 kpc interval is 0.104 cm^{-3} which includes two sections of Sagittarius Arm and a tangential section of the Scutum-Centaurus Arm.

4.4.57 Range: 306.0:308.0/-1.0:1.0

J1322-6329 pulsar seems to be problematic. Whichever interval this pulsar is put in, it deviates from the dispersion measure-distance curve of the given section in great amounts. If this pulsar is considered to be in this interval, the adopted distance is 12.4 kpc. The free electron density calculated through 5.7-16.3 kpc interval is 0.052 cm^{-3} which includes two sections of Sagittarius Arm and a section of the Scutum-Centaurus Arm.

4.4.58 Range: 308.0:312.0/-1.0:1.0

This section is divided into two distance intervals: 5.1-8.6 kpc and 9.2-12.1 kpc since free electron densities of the paths that fall in front of the intervals seem to be different. Although both are very rich intervals in terms of free electron sources , signals of the pulsars in the first interval seem to be affected more by the corresponding sources. For example the signal of

J1341-6220 calibrator pulsar passes through G308.8-0.1 SNR and A309-01 H II region group and it deviates from the fit in positive sense in DM. This is an expected result and no new distance is adopted to this pulsar. The free electron density calculated through 5.1-8.6 kpc interval is 0.136 cm^{-3} which includes sections of Sagittarius Arm and Scutum-Centaurus Arm. The free electron density calculated through 9.2-12.1 kpc interval is 0.082 cm^{-3} which includes sections of Sagittarius Arm and Scutum-Centaurus Arm.

4.4.59 Range: 312.0:317.0/-1.0:1.0

This section is divided into two distance intervals: 0.8-6.2 kpc and 8.2-10.8 kpc since free electron densities of the paths that fall in front of the intervals seem to be different. In both of the sections, the signals of the pulsars (J1413-6141, J1420-6048 and J1444-5941) passing through free electron sources (G312.4-0.4 SNR, A312-01 H II region group and A312-01 H II region group) results in pulsars deviating from the linear fits of the intervals in positive sense in DM.This is an expected result. J1410-6132 pulsar is excluded from the graph since its distance value is not realistic. Moreover new distance values are adopted to J1434-6006, J1437-5959 and J1413-6222 pulsars as 6.1 kpc, 9.6 kpc and 10.8 kpc respectively. The free electron density calculated through 0.8-6.2 kpc interval is 0.060 cm^{-3} which includes sections of Sagittarius Arm and Scutum-Centaurus Arm. The free electron density calculated through 8.2-10.8 kpc interval is 0.214 cm^{-3} which includes sections of Sagittarius Arm and Scutum-Centaurus Arm.

4.4.60 Range: 317.0:321.0/-1.0:1.0

This section is divided into two distance intervals: 3.3-5.1 kpc and 7.1-10.5 kpc in order to have better fit statistics. In the first interval, pulsars are aligned perfectly on the fit because the signals of nearly all pulsars pass through the A319-01 H II Region group. Moreover the signal of J1452-5851

pulsar passes through G318.2+0.1 SNR (Distance between SNR and pulsar is 1 kpc.) and it deviates from the fit in positive sense in DM. This is an expected result. On the other hand, a new distance value is adopted to J1509-5850 pulsar as 3.7 kpc in order for it to agree with the linear fit of the first interval. The free electron density calculated through 3.3-5.1 kpc interval is 0.085 cm^{-3} which includes sections of Sagittarius Arm and Scutum-Centaurus Arm. The free electron density calculated through 7.1-10.5 kpc interval is 0.087 cm^{-3} which also includes sections of Sagittarius Arm and Scutum-Centaurus Arm.

4.4.61 Range: 321.0:324.0/-1.0:1.0

This section is divided into two distance intervals: 2.6-6.2 kpc and 9.2-13.3 kpc since free electron densities of the paths that fall in front of the intervals seem to be different. When individual pulsars are investigated it is seen that signals of J1519-5734 and J1524-5706 pulsars in the second interval pass through G321.9-0.3SNR and G322.5-0.1 SNR respectively so it is expected to have larger electron density in this region. Moreover a new distance value is adopted to J1529-5611 pulsar as 3.2 kpc in order for it to agree with the linear fit of the first interval. The free electron density calculated through 2.6-6.2 kpc interval is 0.079 cm^{-3} which includes sections of Sagittarius Arm and Scutum-Centaurus Arm. The free electron density calculated through 9.2-13.3 kpc interval is 0.108 cm^{-3} which includes a section of Sagittarius Arm and two sections of Scutum-Centaurus Arm.

4.4.62 Range: 324.0:327.0/-1.0:1.0

This section is divided into two distance intervals: 3.5-5.2 kpc and 6.8-9.8 kpc free electron densities of the paths that fall in front of the intervals seem to be different. First section seems to be richer interms of free electron sources (A326-01 H II region group) hence it is expected to have greater free electron density. Anew distance value is adopted to J1538-5638 pulsar

in the second interval as 8.7 kpc in order for it to agree with the linear fit of the second interval. J1537-5645 pulsar is excluded from the second interval since it is a distant pulsar and it might have additional free electron density that falls in front of its signal path. The free electron density calculated through 3.5-5.2 kpc interval is 0.132 cm^{-3} which includes sections of Sagittarius Arm and Scutum-Centaurus Arm. The free electron density calculated through 6.8-9.8 kpc interval is 0.090 cm^{-3} which includes sections of Sagittarius,Scutum-Centaurus Arm and outer region of the Norma Arm.

4.4.63 Range: 327.0:332.0/-1.0:1.0

This section is divided into two distance intervals: 1.1-7.1 kpc and 8.4-11.9 kpc since free electron densities of the paths that fall in front of the intervals seem to be different. Since J1609-5158 and J1612-5136 are distant pulsars their distance values might not have been estimated correctly. New distance values are adopted to these pulsars as 11.3 kpc and 11.9 kpc respectively in order for them to agree with the linear fit of the second interval. Here it should be noted that the signal of J1609-5158 pulsar passes through A329-01 HII region group and the signal of J1612-5136 pulsar passes through A330-01 HII region group, so their adopted distances should be the upper limit for these pulsar since otherwise it would contradict to concept of the effect of free electron sources on the signal arrival times of pulsars . The free electron density calculated through 1.1-7.1 kpc interval is 0.088 cm^{-3} which includes certain sections of Sagittarius, Scutum-Centaurus and Norma Arms. The free electron density calculated through 8.4-11.9 kpc interval is 0.177 cm^{-3} which includes certain sections of Sagittarius, Scutum-Centaurus Arms and tangential section of the Norma Arm.

4.4.64 Range: 332.0:335.0/-1.0:1.0

Signal of all of the pulsars except J1623-4949 pulsar passes through A334-01 HII region group, so it can be assumed that they are all affected by

the same electron sources. Since J1616-5109 is a distant pulsar its distance value might not have been estimated correctly. New distance value is adopted to this pulsar as 11.9 kpc in order for it to agree with the linear fit of the interval. The free electron density calculated through 3.7-11.9 kpc interval is 0.123 cm^{-3} which includes certain sections of Sagittarius, Scutum-Centaurus and Norma Arms.

4.4.65 Range: 335.0:338.0/-1.0:1.0

This section is divided into two distance intervals: 5.5-7.3 kpc and 8.5-12.7 kpc since free electron densities of the paths that fall in front of the intervals seem to be different. When free electron sources are investigated it is seen that the second interval includes additional free electron sources so, higher free electron density is expected in this region. New distance values are adopted to J1638-4725 and J1628-4828 pulsars as 6.9 kpc and 12.7 kpc respectively in order for them to agree with the linear fit of the intervals. The free electron density calculated through 5.5-7.3 kpc interval is 0.113 cm^{-3} which includes certain sections of Sagittarius, Scutum-Centaurus and Norma Arms. The free electron density calculated through 8.5-12.7 kpc interval is 0.144 cm^{-3} which includes certain sections of Sagittarius and Scutum-Centaurus Arms and two sections of Norma Arm.

4.4.66 Range: 338.0:342.0/-1.0:1.0

This section is divided into two distance intervals: 3.6-6.3 kpc and 6.8-10.0 kpc since free electron densities of the paths that fall in front of the intervals seem to be different . Both of the intervals are very rich in terms of free electron sources and they are effective on pulsar signal delays. For example signal of J1646-4346 pulsar passes through G341.2+0.9 SNR (Distance between the pulsar and the SNR is 53 parsecs), signal of J1640-4648 pulsar passes through A338-01 H II region group, signal of J1651-4519 pulsar passes through A340-01 H II region group,signals of J1648-4611 and

J1650-4502 pulsars pass through A340-01 H II region group (Hence those three pulsars are expected to be on the same fit.). There is only one pulsar that's distance value needs to be corrected. New distance value is adopted to J1644-4559 pulsar as 6.2 kpc in order for it to agree with the linear fit of the first interval. The free electron density calculated through 3.6-6.3 kpc interval is 0.123 cm^{-3} which includes certain sections of Sagittarius, Scutum-Centaurus and Norma Arms. The free electron density calculated through 6.8-10.0 kpc interval is 0.143 cm^{-3} which includes certain sections of Sagittarius, Scutum-Centaurus and Norma Arms and tangential section of the Near 3 kpc Arm.

4.4.67 Range: 342.0:345.0/-1.0:1.0

New distance values are adopted to J1651-4246 and J1654-4245 pulsars as 6.2 kpc and 10.7 kpc respectively in order for them to agree with the linear fit of the interval. The free electron density calculated through 4.8-10.7 kpc interval is 0.105 cm^{-3} which includes certain sections of Sagittarius, Scutum-Centaurus, Norma and Near 3 kpc Arms.

4.4.68 Range: 345.0:348.0/-1.0:1.0

This section is divided into two distance intervals: 4.3-6.4 kpc and 8.6-12.0 kpc since their free electron densities seem to be different. Both of the intervals are very rich in terms of free electron sources and they are effective on pulsar signal delays. For example signals of J1712-39-1 and J1712-39-2 pulsars pass through G347.3-0.5 SNR (Distance between the J1712-39-1 pulsar and the SNR is 370 kpc) and signal of J1705-4108 pulsar passes through A345-02 H II region group. The free electron density calculated through 4.3-6.4 kpc interval is 0.152 cm^{-3} which includes certain sections of Sagittarius, Scutum-Centaurus, Norma Arms and the outer region of the Near 3 kpc Arm. The free electron density calculated through 8.6-12.0 kpc interval is 0.139 cm^{-3} which includes certain sections of Sagit-

tarius, Scutum-Centaurus, Norma and Near 3 kpc Arms plus the Galactic Bar Region.

4.4.69 Range: 348.0:351.0/-1.0:1.0

This section is divided into two distance intervals: 2.2-6.6 kpc and 9.2-10.6 kpc kpc since free electron densities of the paths that fall in front of the intervals seem to be different. The free electron density calculated through 2.2-6.6 kpc interval is 0.097 cm^{-3} which includes certain sections of Sagittarius, Scutum-Centaurus, Norma and Near 3 kpc Arms. The free electron density calculated through 9.2-10.6 kpc interval is 0.236 cm^{-3} which includes certain sections of Sagittarius, Scutum-Centaurus, Norma and Near 3 kpc Arms plus the Galactic Bar Region.

4.4.70 Range: 351.0:354.0/-1.0:1.0

J1724-35 pulsar deviates from the fit in positive sense in DM but since pulsars with small Gz values tend to have extra DM due to effect of expansion of plasma on the disk, this is an expected result. No distance is adopted to J1724-35 pulsar since it has a small Gz value when compared to other pulsars in this interval . The free electron density calculated through 6.3-12.1 kpc interval is 0.065 cm^{-3} which includes certain sections of Sagittarius, Scutum-Centaurus, Norma and Near 3 kpc Arms, interior of Perseus Arm plus the Galactic Bar Region.

4.4.71 Range: 354.0:356.0/-1.0:1.0

Since J1737-3320 is a distant pulsar its distance value might not have been estimated correctly. New distance value is adopted to this pulsar as 9.8 kpc in order for it to agree with the linear fit of the interval. The free electron density calculated through 3.8-9.8 kpc interval is 0.093 cm^{-3} which includes certain sections of Sagittarius, Scutum-Centaurus, Norma and Near 3 kpc

Arms plus the Galactic Bar Region.

4.4.72 Range: 356.0:358.0/-1.0:1.0

This interval is expected to have greater free electron density since the existence of free electron sources is effective on pulsar signal delays(For example signal of J1739-3049 pulsar passes through G357.7+0.3 SNR). New distance value is adopted to J1738-3211 pulsar as 2.5 kpc in order for it to agree with the linear fit of the interval. The free electron density calculated through 4.4-8.5 kpc interval is 0.120 cm^{-3} which includes certain sections of Sagittarius, Scutum-Centaurus, Norma and Near 3 kpc Arms plus the Galactic Bar Region.

CHAPTER 5

RESULTS AND DISCUSSION

In this study, the free electron density distribution of the Galaxy is obtained through a 3D mesh-like structure in spherical coordinates considering the distribution of pulsars in the Galaxy. In order to understand the results of the work, it is crucial to see that section sizes of this 3D mesh are not equal in galactic latitude, galactic longitude or in radial distance dimensions. The only parameter that dictates the section size is constancy of free electron density of the path that lies in front of the corresponding section. To be more precise, the sizes of the meshes are kept as variables at the beginning and then a trial-and-error method is used to change the borders of each section until a constant free electron density is grasped for the path between the Sun and the 3D section that encloses a group of pulsars.

The trial-and-error method in question is carried on distance versus dispersion measure graphs of pulsars. It is explained in the previous chapters that for a region that has constant free electron density on the path that lies in front of it, when a dispersion measure versus distance graph is plotted for the radio pulsars located in the corresponding region, the resulting plot should be a linear curve and its slope should give the free electron density of the signal path. Note that in this study, distance versus dispersion measure (d vs DM) graphs are used instead of the vice versa, then the free electron densities can be found through taking the inverse of the slopes of d vs DM graphs.

In this chapter, results of the following are presented:

- Mesh structure of the trial-and-error method.

- Accuracy improvements on d vs DM graphs and their side products, i.e adopted distances of pulsars.

- Free electron densities of the sections.

- Projected cumulative free electron density map of the Milky Way Galaxy and comparison of the map with the recent spiral arm models.

- Discussions on success of the free electron density model.

- Discussions on the facts that make this model different from the others and the suggestions for future studies.

5.1 Zones

When the Galaxy is divided into regions in galactic latitude direction, the resulting forms are zones of the Galaxy that look like funnels with different thicknesses and cone angles. The borders of those zones are obtained through a trial-and-error method and the thicknesses of the zones are not equal in magnitude.

At this point, accuracy of creating the zones becomes an important issue since the number of pulsars decrease with increasing latitude. Accuracy of creating the zones and hence the accuracy of the overall work can be increased by either decreasing the thicknesses of zones or increasing the number of pulsars per zone. But since the number of pulsars decrease with increasing latitude those two conditions cannot be satisfied simultaneously, therefore a balance is tired to be founded between the thicknesses of zones and the number of pulsars that falls into each zone. The results can be found in Table 5.1.

5.2 3D Sections

After the zones are obtained, each zone is divided into sections in galactic longitude direction. Considering the galactic latitude and galactic longitude ranges of the regions, the resulting divisions of the Galaxy may seem to be like cones but this is not exactly the case. The galactic latitude and galactic longitude borders of a section, which includes pulsars that fall behind a constant free electron density region, is obtained through the coordinates of the pulsars. Likewise, the radial distance range of the section is obtained through distances of the closest and farthest pulsars in the region. This means that determined free electron densities are calculated through regions in certain distance intervals within specified angle ranges. So the resulting 3D sections are in fact frustums of cones. The free electron densities are calculated by making use of pulsar data that falls into those conical frustums and they are applicable for the signal paths of the corresponding pulsars.

At the end of this process 517 conical frustums are obtained. Here it is important to note that certain d vs DM graphs are given by two fits, meaning that certain cone frustums are divided into two. Especially for the disk region

Table 5.1. Zones that define the Galactic latitude ranges of the Galaxy in degrees. The number of pulsars in each zone is given in the last column.

Zone	**Range**	**Number of Pulsars**
-90.0	-60.0	9
-60.0	-40.0	48
-40.0	-25.0	57
-25.0	-10.0	102
-10.0	-5.0	123
-5.0	-3.0	121
-3.0	-1.0	242
-1.0	$+1.0$	533
$+1.0$	$+3.0$	242
$+3.0$	$+7.0$	168
$+7.0$	$+15.0$	126
$+15.0$	$+30.0$	77
$+30.0$	$+60.0$	55
$+60.0$	$+90.0$	14

and for the upper and lower zones of the disk, free electron densities change with increasing radial distance. This is due to the high number density of free electron sources located in the zones mentioned. Another important point is that out of 517 conical frustums 169 of them either contain only one pulsar or even no pulsar according to current data set. Therefore, only the sections with two or more pulsars are presented here since the electron densities are calculated through d vs DM curves and there should be at least two points to define a linear curve. As a result, the total number of sections is 348.

5.3 Adopted Distances of Pulsars

For the 348 sections that are obtained through the process explained above, the free electron densities of the paths that lie in front of the 3D sections can be determined, yet when d vs DM graphs of those sections are investigated, it is seen that the linear fits that are adjusted for the given graphs do not have perfect fit statistics. As it is mentioned before, dispersion measures of pulsars are estimated very accurately, on the other hand distance errors of pulsars can go up to 30%. This brings one to a conclusion that the fit statistics can be improved by using corrected distance values of pulsars so that more accurate free electron densities can be calculated.

Following the procedure explained in Chapter 3, the pulsars that need corrections on their distances are decided by making enquires about their relations with free electron sources. When it comes to distance adopting step, it is important to note that the graphs through which the pulsar distances are adopted have different reliability ranks. Here, the reliability rank depends on the quality of the fit, number of data used to plot the graph and the proximity of the adopted distance to the distance range of the graph. Reliability rank can be given in 3 levels. If a new pulsar distance is adopted by using the slope of a graph with reliability rank 1 for example, this means that the newly estimated distance value can be trusted more than another pulsar's adopted distance with a corresponding graph of reliability rank 2 (and of

course rank 3).

The followings are the 140 pulsars with their adopted distances. Their original distance data are also provided with the 3D sections that they fall into and the reliability ranks of the graphs through which the distances are adopted in Table 5.2.

At this point there is an important discussion to be made. It is known that pulsar space velocities are larger when compared to main sequence stars. This is usually linked to the fact that the supernova explosions are asymmetric and the explosions give additional pushes to the isolated neutron stars. As a result space velocities of pulsars can go up to 450 km/s at birth and drop to a mean of 300 km/s throughout their life times (Lyne and Lorimer 1995). On the other hand despite the high velocities, young pulsars cannot escape from their birth places considering the limited life time they have to spend on the run. That is why young pulsars, especially at the disk region, are expected to be on the spiral arms of the Galaxy. Here the (-1.0,1.0] degree galactic latitude range pulsars that have been presented with their adopted distances at Table 5.2 are again tabulated with their locations according to original pulsar data and corresponding adopted locations. Investigating Table 5.3, it is concluded that adopted locations of young pulsars at the (-1.0,1.0] degree range fall onto spiral arms of the Galaxy.

5.4 Free Electron Densities of 3D Sections

After certain corrections are brought to pulsars with wrong distance estimates, the free electron density of each 3D section is calculated more accurately. The densities of sections are presented in Appendix A and in Appendix B. Appendix A provides d vs DM graphs of each section through which the free electron densities are calculated and Appendix B presents the tabulated version of the free electron density distribution.

When d vs DM graphs are investigated it is seen that

- Neither the quality of the fits nor the number of pulsars are constant for sections. This prevents the method from having constant error bars in estimating pulsar distances.

Table 5.2. Pulsars with adopted distances. Column definitions are as follows. JNAME: pulsar name; DM: dispersion measure; d: distance value in database; d_a: adopted distance calculated by the model; section: angular ranges in Galactic coordinates that the pulsar falls into; Q^2: quality of the fit; RR: reliability rank of the fit. The suffix ':N' in pulsar names indicates that this pulsar data has not been investigated by Guseinov (2009). The prefix 'u' in distance values indicates an upper limit for that pulsar.

JNAME	DM	d	d_a	section	Q^2	RR
J1747-2809:N	1133	17.6	13.8	358.0:1.0/-1.0:1.0	0.94	1
J1745-2910:N	1088	15.2	13.5	358.0:1.0/-1.0:1.0	0.94	1
J1755-2534	590	6.7	8.3	3.0:4.5/-1.0:1.0	0.98	1
J1801-2115	779	11.2	(u)9.5	8.0:9.5/-1.0:1.0	0.99	1
J1809-1850	598	7.6	8.9	9.5:11.5/-1.0:1.0	0.99	1
J1814-1744	792	10.2	9.4	13.0:15.5/-1.0:1.0	0.99	1
J1818-1519	845	8.2	10.6	15.5:16.5/-1.0:1.0	0.99	1
J1824-1500	571	8.0	7.1	16.5:17.5/-1.0:1.0	0.99	1
J1844-0310	836	9.9	(u)9.3	28.0:30.0/-1.0:1.0	0.99	1
J1848-0055	1166	15.0	13.9	30.0:32.0/-1.0:1.0	0.99	1
J1850-0026:N	947	10.7	12.2	32.0:34.0/-1.0:1.0	0.96	1
J1849-0040	1235	16.0	15.7	32.0:34.0/-1.0:1.0	0.96	1
J1909+06:N	35	1.8	1.1	39.0:41.0/-1.0:1.0	0.97	1
J1907+0602:N	82	3.0	2.0	39.0:41.0/-1.0:1.0	0.97	1
J1910+0714	124	3.6	2.7	41.0:44.0/-1.0:1.0	0.99	1
J1918+1444	27	1.2	2.0	44.0:50.0/-1.0:1.0	0.96	1
J1914+1122	100	2.3	3.2	44.0:50.0/-1.0:1.0	0.96	1
J1913+1145	637	13.0	9.4	44.0:50.0/-1.0:1.0	0.97	1
J2002+30	196	7.4	(u)6.8	66.0:75.0/-1.0:1.0	0.95	1
J0857-4424	184	5.8	5.2	264.0:277.0/-1.0:1.0	0.92	1
J1021-5601	212	5.5	4.3	282.0:287.0/-1.0:1.0	0.99	1
J1055-6022	590	14.0	(u)13.1	289.0:291.0/-1.0:1.0	0.95	1
J1128-6219	675	13.6	12.3	293.0:297.0/-1.0:1.0	0.98	1
J1201-6306	683	14.3	13.1	297.0:304.0/-1.0:1.0	0.98	1
J1303-6305	343	10.0	7.1	304.0:306.0/-1.0:1.0	0.97	1
J1322-6329	659	6.7	12.4	306.0:308.0/-1.0:1.0	0.97	1
J1434-6006	332	4.7	6.1	312.0:317.0/-1.0:1.0	0.95	1
J1437-5959:N	550	11.1	9.6	312.0:317.0/-1.0:1.0	0.45	2
J1413-6222	808	16.3	10.8	312.0:317.0/-1.0:1.0	0.45	2
J1509-5850	138	2.5	3.7	317.0:321.0/-1.0:1.0	0.97	1

Table 5.2. – *continued*

JNAME	DM	d	d_a	section	Q^2	RR
J1529-5611	149	2.3	3.2	321.0:324.0/-1.0:1.0	0.99	1
J1538-5638	546	10.2	8.7	324.0:327.0/-1.0:1.0	0.96	1
J1609-5158	1069	12.7	11.3	327.0:332.0/-1.0:1.0	0.89	1
J1612-5136	1173	14.3	11.9	327.0:332.0/-1.0:1.0	0.89	1
J1616-5109	1160	14.2	11.9	332.0:335.0/-1.0:1.0	1.00	1
J1638-4725	552	6.1	6.9	335.0:338.0/-1.0:1.0	0.91	1
J1628-4828	1209	15.2	12.7	335.0:338.0/-1.0:1.0	0.77	2
J1644-4559	479	4.5	6.2	338.0:342.0/-1.0:1.0	0.96	1
J1651-4246	482	7.2	6.2	342.0:345.0/-1.0:1.0	0.98	1
J1654-4245:N	950	11.8	10.7	342.0:345.0/-1.0:1.0	0.98	1
J1737-3320	804	11.5	9.8	354.0:356.0/-1.0:1.0	0.98	1
J1738-3211	50	1.2	2.5	356.0:358.0/-1.0:1.0	0.98	1
J1750-2438	476	7.1	6.0	1.0:5.0/1.0:3.0	0.94	1
J1755-2025:N	364	8.6	5.3	5.0:10.0/1.0:3.0	0.99	1
J1801-1855	484	8.0	6.6	10.0:14.0/1.0:3.0	0.92	1
J1825-0935	19	0.8	2.2	14.0:22.0/1.0:3.0	0.97	1
J1809-1429	411	7.5	6.5	14.0:22.0/1.0:3.0	0.97	1
J1843-0000	102	3.6	2.7	30.0:34.0/1.0:3.0	1.00	1
J1842-0153	434	6.4	7.2	30.0:34.0/1.0:3.0	0.96	1
J1855+0527:N	362	9.7	8.0	38.0:44.0/1.0:3.0	0.94	1
J1926+1928	445	13.5	17.5	54.0:61.0/1.0:3.0	0.94	3
J0627+16:N	113	5.9	4.3	188.0:196.0/1.0:3.0	1.00	2
J0955-5304	157	4.2	3.1	265.0:282.0/1.0:3.0	0.75	2
J0905-4536	117	3.7	2.7	265.0:282.0/1.0:3.0	0.75	2
J1546-5302	287	4.6	5.6	327.0:331.0/1.0:3.0	0.96	1
J1632-4621	563	8.4	7.4	331.0:338.0/1.0:3.0	0.92	1
J1635-4513	416	7.1	6.3	338.0:343.0/1.0:3.0	0.97	1
J1717-3425	588	14.3	9.7	346.0:353.0/1.0:3.0	0.98	1
J1700-3919	354	5.0	7.4	346.0:353.0/1.0:3.0	0.98	1
J1702-3932	530	7.3	9.1	346.0:353.0/1.0:3.0	0.98	1
J1759-1736	206	3.3	6.0	7.0:12.0/3.0:7.0	0.98	1
J1750-2043	239	5.2	7.0	7.0:12.0/3.0:7.0	0.98	1
J1801-0857D:N	175	10.6	6.6	19.0:21.0/3.0:7.0	0.96	1
J1801-0857C:N	182	10.6	6.6	19.0:21.0/3.0:7.0	0.96	1
J1801-0857B:N	182	10.6	6.6	19.0:21.0/3.0:7.0	0.96	1
J1801-0857A:N	183	10.6	6.6	19.0:21.0/3.0:7.0	0.96	1
J1840+0214	182	6.4	4.7	31.0:36.0/3.0:7.0	0.99	1
J1906+1854	157	7.2	5.5	48.0:56.0/3.0:7.0	0.97	1
J1243-5735	271	9.2	6.8	300.0:308.0/3.0:7.0	0.99	1
J1406-5806	229	4.5	7.1	308.0:315.0/3.0:7.0	0.95	1

Table 5.2. – *continued*

JNAME	DM	d	d_a	section	Q^2	RR
J1649-3805	214	7.6	5.0	339.0:347.0/3.0:7.0	0.87	1
J1648-36:N	222	12.4	5.0	347.0:351.0/3.0:7.0	0.91	1
J1647-36:N	224	13.1	5.0	347.0:351.0/3.0:7.0	0.91	1
J1654-23:N	75	3.6	2.4	357.0:4.0/7.0:15.0	0.86	1
J1810-01:N	135	8.8	4.9	17.0:27.0/7.0:15.0	0.95	2
J1822+0705	62	2.1	0.7	35.0:40.0/7.0:15.0	0.85	2
J1844+1454	42	1.5	2.6	45.0:47.0/7.0:15.0	1.00	1
J1843+2024	85	5.7	4.3	47.0:62.0/7.0:15.0	0.99	1
J0932-3217	102	4.5	3.0	256.0:269.0/7.0:15.0	0.95	1
J1129-53:N	77	2.7	3.9	280.0:294.0/7.0:15.0	0.96	1
J1330-52:N	149	10.6	6.3	308.0:320.0/7.0:15.0	0.96	2
J1517-46:N	139	10.9	6.3	325.0:330.0/7.0:15.0	0.95	2
J1535-4415:N	111	5.4	4.1	330.0:335.0/7.0:15.0	0.82	2
J1610-17:N	53	4.3	3.3	355.0:5.0/15.0:30.0	0.93	1
J1810+17:N	40	1.6	3.4	38.0:48.0/15.0:30.0	0.89	1
J1124-36:N	45	1.8	2.9	283.0:287.0/15.0:30.0	0.80	2
J1549-06:N	22	1.1	2.8	0.0:4.0/30.0:60.0	1.00	2
J1518+0204D	29	8.0	7.0	0.0:4.0/30.0:60.0	1.00	1
J1518+0204C	29	8.0	7.0	0.0:4.0/30.0:60.0	1.00	1
J1518+0204E	29	8.0	7.0	0.0:4.0/30.0:60.0	1.00	1
J1518+0204A	30	8.0	7.0	0.0:4.0/30.0:60.0	1.00	1
J0943+1631	20	1.4	2.0	196.0:217.0/30.0:60.0	0.87	1
J1038+0032	27	2.4	1.8	243.0:259.0/30.0:60.0	0.98	1
J1807-2557:N	385	11.2	5.6	4.5:8.0/-3.0:-1.0	0.84	3
J1813-2242	333	5.0	6.3	8.0:14.0/-3.0:-1.0	0.94	1
J1826-1526	530	9.5	7.4	14.0:18.0/-3.0:-1.0	0.87	1
J1830-1313:N	537	10.4	8.0	18.0:22.0/-3.0:-1.0	0.94	1
J1836-1008	317	6.5	5.1	22.0:25.0/-3.0:-1.0	0.84	1
J1845-0743	281	4.2	5.3	25.0:28.0/-3.0:-1.0	0.95	1
J1903+0135	245	4.4	5.6	31.0:37.0/-3.0:-1.0	0.92	1
J1913+0446	109	3.3	2.8	37.0:40.0/-3.0:-1.0	0.98	1
J1915+0838	358	7.2	8.2	43.0:47.0/-3.0:-1.0	0.99	1
J1931+1536	140	4.7	6.2	51.0:53.0/-3.0:-1.0	0.87	1
J0820-3921	179	5.5	4.1	257.0:268.0/-3.0:-1.0	0.97	1
J0855-4658	473	12.2	14.1	257.0:268.0/-3.0:-1.0	0.97	3
J0908-4913	180	4.5	5.3	268.0:283.0/-3.0:-1.0	0.94	1
J1043-6116	449	7.6	9.9	287.0:295.0/-3.0:-1.0	0.77	2
J1056-6258	320	9.2	7.0	287.0:295.0/-3.0:-1.0	0.77	2
J1225-6408	415	16.5	12.8	295.0:302.0/-3.0:-1.0	0.97	1
J1249-6507	215	7.5	5.2	302.0:306.0/-3.0:-1.0	0.98	1

- Even for a single section, error in adopted pulsar distance cannot be determined since the pulsars constituting the corresponding graph do not have the same distance error bars. Anyone who would like to estimate a pulsar distance using this model should make use of the information about the quality of the fits and the number of pulsars given in d vs DM graph of each section, in order to have idea about the accuracy of the result.

Table 5.2. – *continued*

JNAME	DM	d	d_a	section	Q^2	RR
J1513-5946:N	172	4.3	6.7	317.0:320.0/-3.0:-1.0	0.62	2
J1559-5545	213	5.0	4.1	325.0:330.0/-3.0:-1.0	0.98	1
J1701-4533	526	10.3	7.2	339.0:343.0/-3.0:-1.0	0.92	1
J1707-4417:N	380	9.2	6.8	343.0:345.0/-3.0:-1.0	0.97	3
J1717-40433	539	9.3	8.1	345.0:347.5/-3.0:-1.0	1.00	1
J1725-4043	203	4.8	3.8	347.5:352.0/-3.0:-1.0	0.93	1
J1803-3002B:N	193	7.8	4.9	0.0:5.0/-5.0:-3.0	0.99	1
J1803-3002C:N	195	7.8	4.9	0.0:5.0/-5.0:-3.0	0.99	1
J1824-2328	185	5.6	4.2	5.0:10.0/-5.0:-3.0	0.98	1
J1829-1751	217	4.5	5.5	10.0:18.0/-5.0:-3.0	0.89	1
J1904-0150	162	5.4	4.3	31.0:34.0/-5.0:-3.0	0.95	1
J1935+12:N	190	9.8	7.1	45.0:51.0/-5.0:-3.0	0.92	1
J1558-5756	128	2.9	3.7	325.0:331.0/-5.0:-3.0	0.79	1
J1612-58:N	172	6.3	4.2	325.0:331.0/-5.0:-3.0	0.79	2
J1719-4302	298	5.2	6.7	345.0:351.0/-5.0:-3.0	0.76	2
J1824-2537:N	159	5.5	7.9	3.0:10.0/-10.0:-5.0	0.97	1
J1904-1224	118	4.5	3.8	19.0:26.0/-10.0:-5.0	0.98	1
J1926+0431	102	3.2	4.5	37.0:45.0/-10.0:-5.0	1.00	1
J2027+2146	97	6.2	5.0	56.0:65.0/-10.0:-5.0	0.99	1
J1137-6700	228	11.2	7.5	293.0:297.0/-10.0:-5.0	0.99	2
J1423-6953:N	124	6.4	4.6	297.0:316.0/-10.0:-5.0	0.99	1
J1753-38:N	168	7.0	4.9	345.0:354.0/-10.0:-5.0	0.95	1
J1946-2913	44	3.3	2.6	10.5:20.0/-25.0:-10.0	0.98	1
J2033+00:N	45	4.7	2.2	35.0:51.0/-25.0:-10.0	0.82	2
J1950+05	71	4.3	3.2	35.0:51.0/-25.0:-10.0	0.82	2
J2212+2933	75	3.7	4.9	82.0:91.0/-25.0:-10.0	0.99	1
J0340+41:N	50	1.9	3.2	136.0:155.0/-25.0:-10.0	0.99	1
J1717-5800	125	4.4	2.5	330.0:341.0/-25.0:-10.0	0.99	1
J0421-0345	45	2.7	3.6	197.0:218.0/-40.0:-25.0	1.00	1
J1846-7403	97	5.1	7.1	314.0:327.0/-40.0:-25.0	0.88	2

- Number of pulsars in each zone decreases as the zones get farther away from the disk. At high latitude zones angle ranges of the sections are kept larger in order to have enough numbers of pulsars to construct linear fits. This may be the reason of decrease in accuracy of free electron densities with increasing/decreasing latitude in northern/southern hemisphere.

- Anti-center directions are studied less by the pulsar observers and this fact is the same for all of the zones. Certain sections of anti-center direction consist of just a single known pulsar or even no pulsar. As a

Table 5.3. Adopted locations of pulsars. Column definitions are as follows. JNAME: pulsar name; Age: age of pulsar in logarithmic scale; Loc.: location of the pulsar in database; Loc. (Adopted): adopted location of the pulsar from the model. The suffix ':N' in pulsar names indicates that this pulsar data has not been investigated by Guseinov (2009). Note that spiral arm model of Carey (2008) was used in locating the pulsars. Abbreviations used in the table are (A): Arm; (S): Spur; int: intersection; ct: closer to; GB: Galactic Bar; F3: Far 3 kpc; N3: Near 3 kpc; O: Outer; Nor: Norma; Prs: Perseus; Ori: Orion; Sgt: Sagittarius; SctCen: Scutum Centaurus.

JNAME	Age	Loc.	Loc. (Adopted)
J1747-2809:N	3.73	Nor(A)-SctCen(A)	Outer Prs(A)
J1745-2910:N		Nor(A)	Prs(A)
J1755-2534	5.52	GB(R)	GB(R)
J1801-2115	8.64	Sgt(A)	F3(A)
J1809-1850	6.23	GB(R)	Inner F3(A)
J1814-1744	4.93	Sgt-F3(A) ct F3(A)	F3(A)
J1818-1519	6.56	GB(R)	F3(A)
J1824-1500	6.94	GB(R)	Inner Sgt(A)
J1844-0310	5.91	Sgt(A)	Inner Sgr(A)
J1848-0055	6.51	O(A)	Inner O(A)
J1850-0026:N	4.83	Prs(A)-Sgt(A)	Prs(A)
J1849-0040	5.98	SctCen(A)-O(A) ct O(A)	Outer O(A)
J1909+06:N		Sgt(A)	Outer Sgt(A)
J1907+0602:N	4.29	Sgt(A)	Sgt(A)
J1910+0714	6.85	Inner Sgt	Sgt(A)
J1918+1444	4.95	Sgt(A)-Ori(S)	Outer Sgt(A)
J1914+1122	7.16	Sgt(A)	Sgt(A)
J1913+1145	5.99	Inner O(A)	Inner Prs(A)
J2002+30		Prs(A)	Inner Prs(A)
J0857-4424	5.35	Ori(S)-Sgt(A)	Ori(S)-Sgt(A)

result free electron density corresponding to those lines of sights cannot be determined using the slopes of the corresponding sections since no fit can be estimated to those sections.

5.5 Free Electron Density Map of the Milky Way Galaxy

Using the densities of the 348 sections, free electron density distribution of 14 zones are mapped on polar coordinates (see Fig.5.1-Fig. 5.7). Here the color scaling is done according to the highest and lowest free electron densities in each zone, that is why the sections in different zones should not be compared with each other in terms of the free electron densities just by looking at the color scales. On the other hand, comparing the sections within

Table 5.3. – *continued*

JNAME	Age	Loc.	Loc. (Adopted)
J1021-5601	8.30	Sgt(A)	Sgt(A)
J1055-6022	5.21	Sgt(A)-Prs(A)	Sgt(A)-Prs(A)
J1128-6219	8.87	Sgt(A)-Prs(A)	Sgt(A)-Prs(A) ct Sgt(A)
J1201-6306	6.42	Sgt-Prs(A)	Sgt(A)
J1303-6305	7.23	SctCen(A)-Sgt(A)	SctCen(A)
J1322-6329	6.60	SctCen(A)	SctCen(A)
J1434-6006	6.21	SctCen(A)	Inner SctCen(A)
J1437-5959:N	5.06	SctCen(A)	SctCen(A)
J1413-6222	6.32	Outer Sgt(A)	SctCen(A)
J1509-5850	5.19	Sgt(A)-SctCen(A)	SctCen(A)
J1529-5611	6.50	Sgt(A)-SctCen(A)	SctCen(A)
J1538-5638	6.27	SctCen(A)-Nor(A)	Outer Nor(A)
J1609-5158	6.20	SctCen(A)-Nor(A)	Outer Nor(A)
J1612-5136	6.31	Inner SctCen(A)	Outer Nor(A)
J1616-5109	6.00	Inner SctCen(A)	Outer Nor(A)
J1638-4725	6.40	Inner Nor(A)	Inner Nor(A)
J1628-4828	6.57	Inner SctCen(A)	Outer Nor(A)
J1644-4559	5.56	Outer Nor(A)	Inner Nor(A)
J1651-4246	6.44	Outer N3(A)	Nor(A)-N3(A) ct N3(A)
J1654-4245:N	5.53	Prs(A) int N3(A)	Inner N3(A)
J1737-3320	6.76	F3(A)-Sgt(A)	GB(R)
J1738-3211	7.18	Sgt(A)	SctCen(A)

their own zones gives completely correct results. Another important point is that; the graphs that are presented here are plotted using the projected images of the sections on the Galactic plane. So, one should be careful in studying the distance ranges of the sections.

When the sections in zones are investigated separately, it is seen that some of the galactic longitude intervals are divided into two in radial distance direction. This is because d vs DM graphs of such kind of intervals are given by two linear fits. Investigation of those two-piece longitude intervals shows that; the signal path of the farther distance range section of the corresponding interval usually has higher electron density. This is an expected result since number of free electrons increases with increasing distance due to increase in number of intervening free electron sources. However, there are also certain longitude intervals where the farther section's signal path seems to have lower electron density than the signal path of the closer section. This is only possible when increase in number of free electrons is smaller than increase in the volume of the signal path. It is also important to note that most of these intervals with lower free electron densities at the signal path of the farther sections are located between galactic longitude ranges of 308-327 degrees at (-1.0,1.0] degree galactic latitude zone, 296-310 degrees at the northern hemisphere and 283-330 degrees at the southern hemisphere. Since those intervals may include hints about the warp structure of the Galaxy, they should be kept in mind for future studies of Galactic dynamics.

When it comes to investigation of the overall effect of the zones, the graph plotted using the cumulative effect of free electron densities of the projected sections should be studied. In this graph it is more easily seen that anti-center directions are studied less by the observers and most of the pulsars at the anti-center directions are located at close neighborhood of the Sun. Moreover it should be noted that the close neighborhood of the Sun seems to be very rich in terms of free electron content, nevertheless this is only due to 2D plotting of the cumulative effect of the zones (see Fig. 5.8)

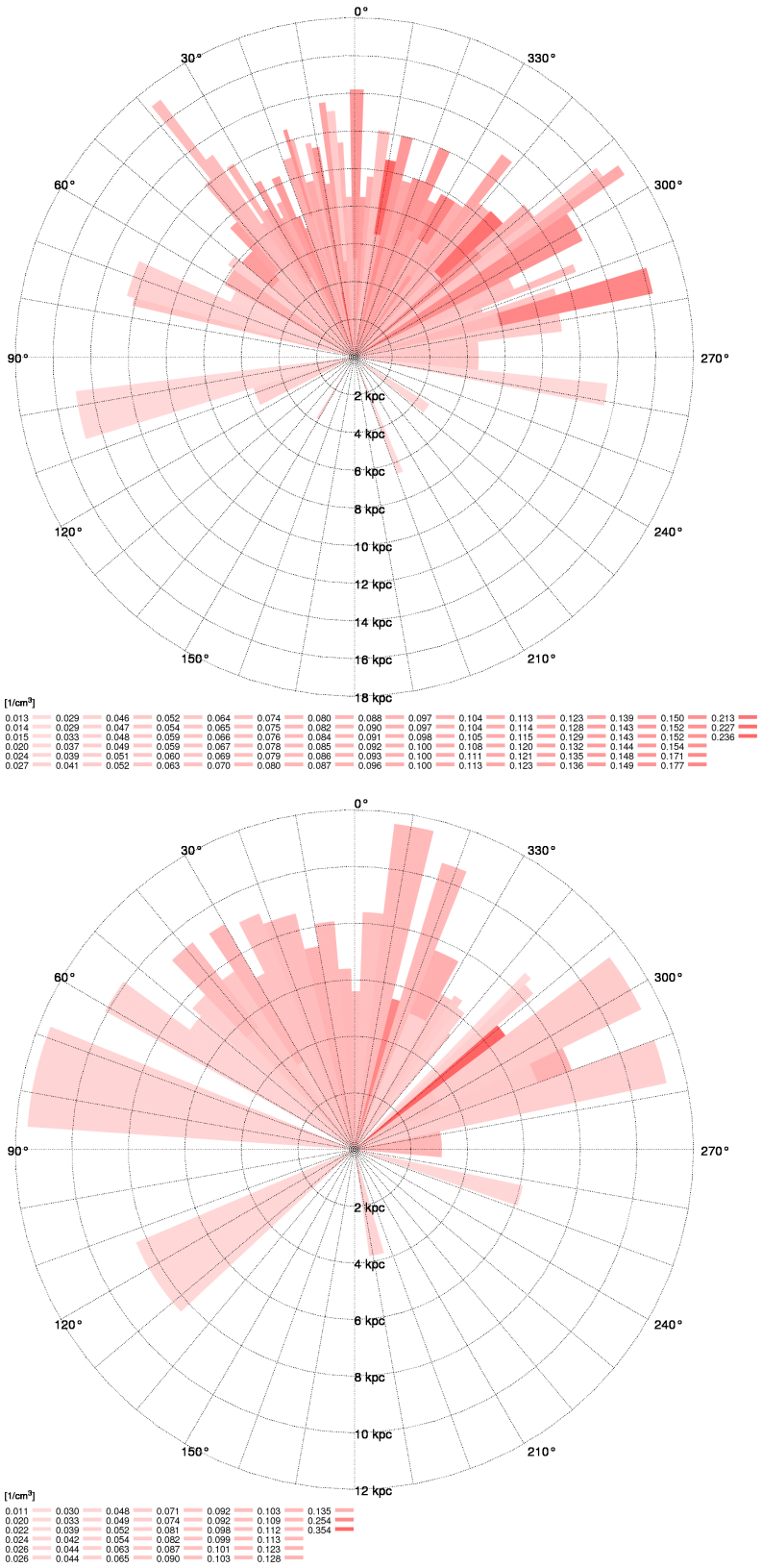

Figure 5.1. Free electron density distribution of galactic latitude ranges: (-1.0),(+1.0) degrees (upper panel) and (+1.0),(+3.0) degrees (lower panel). Image credit: B.B. Gucsav (Ankara Uni., Turkey).

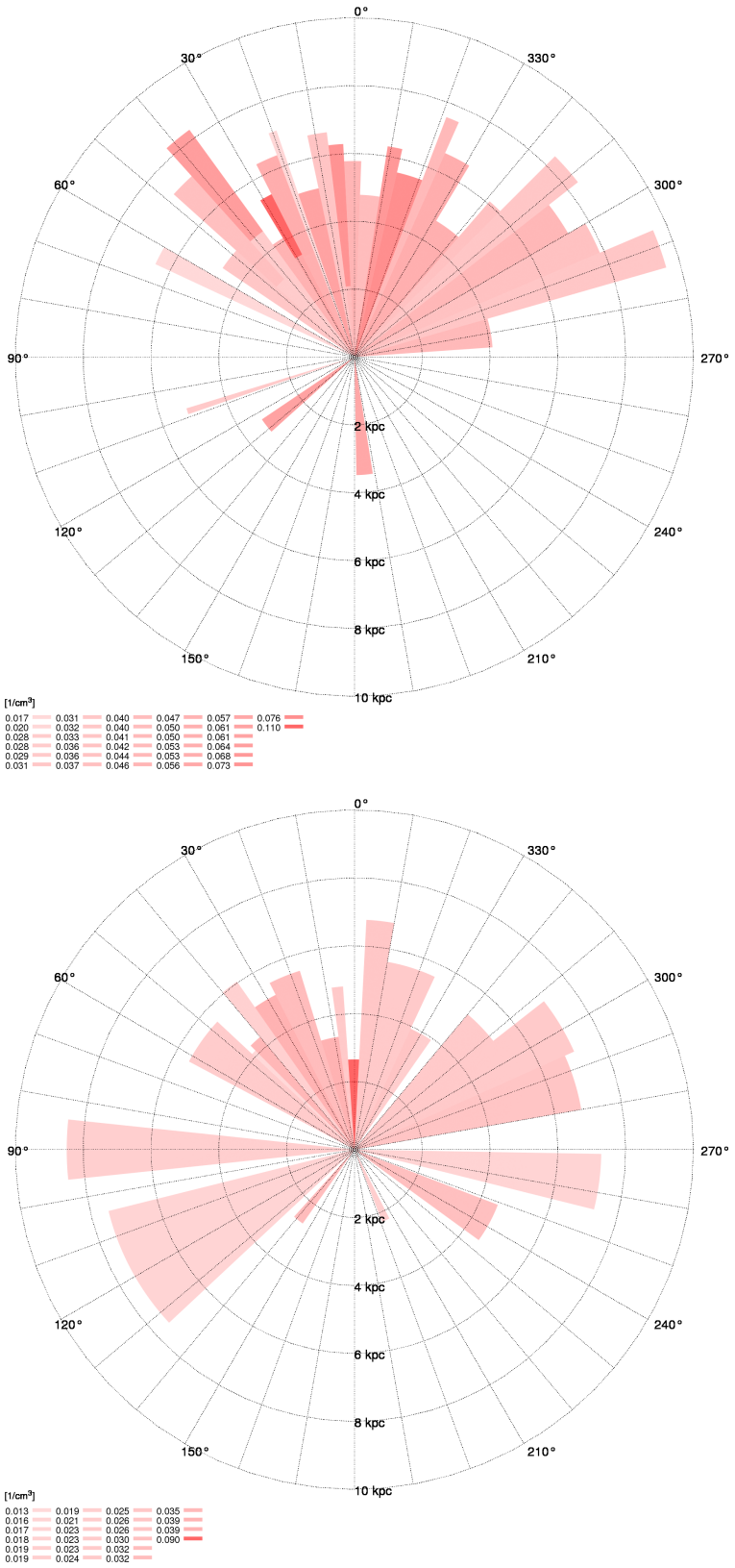

Figure 5.2. Free electron density distribution of galactic latitude ranges: (+3.0),(+7.0) degrees (upper panel) and (+7.0),(+15.0) degrees (lower panel). Image credit: B.B. Gucsav (Ankara Uni., Turkey).

Figure 5.3. Free electron density distribution of galactic latitude ranges: (+15.0),(+30.0) degrees (upper panel) and (+30.0),(+60.0) degrees (lower panel). Image credit: B.B. Gucsav (Ankara Uni., Turkey).

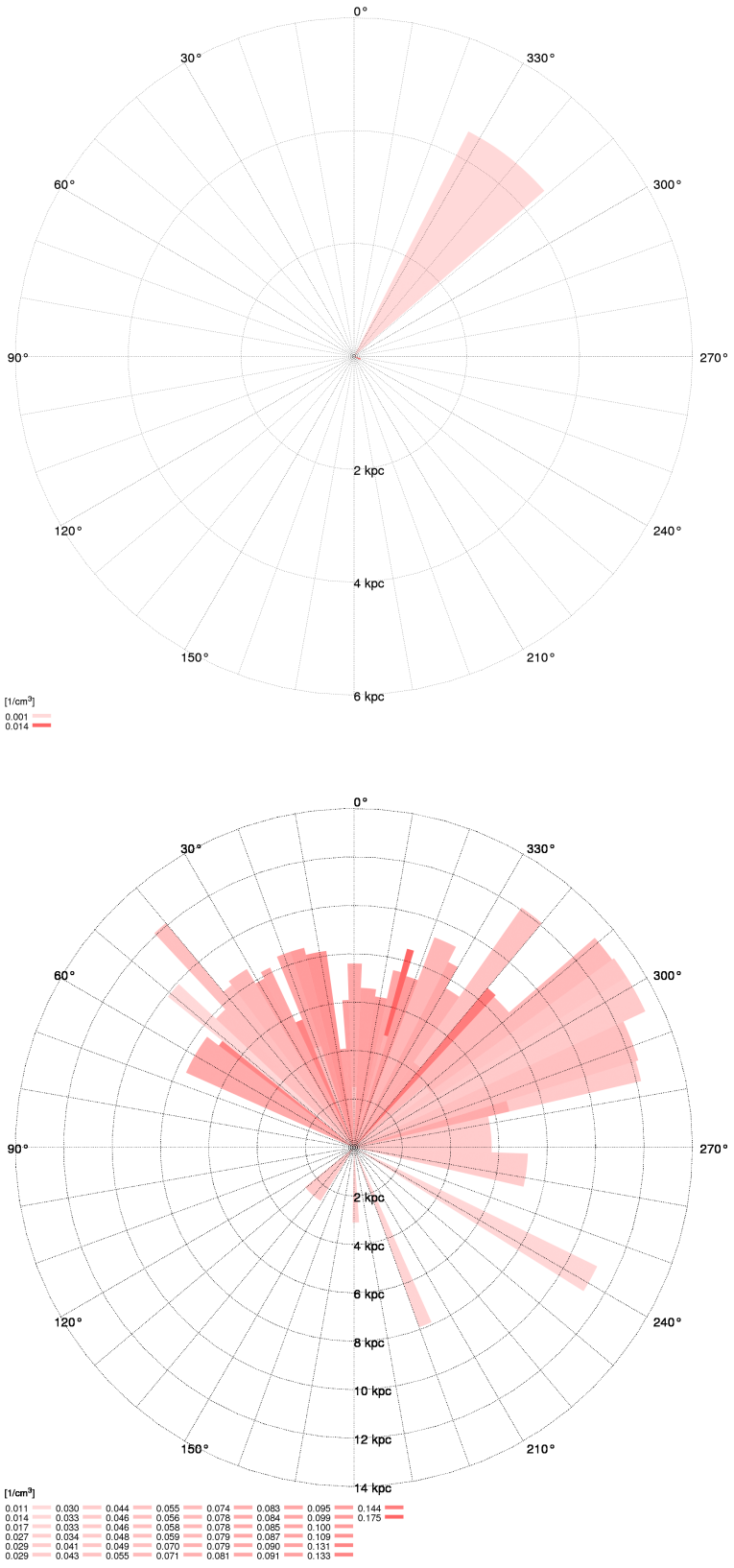

Figure 5.4. Free electron density distribution of galactic latitude ranges: (+60.0),(+90.0) degrees (upper panel) and (-3.0),(-1.0) degrees (lower panel). Image credit: B.B. Gucsav (Ankara Uni., Turkey).

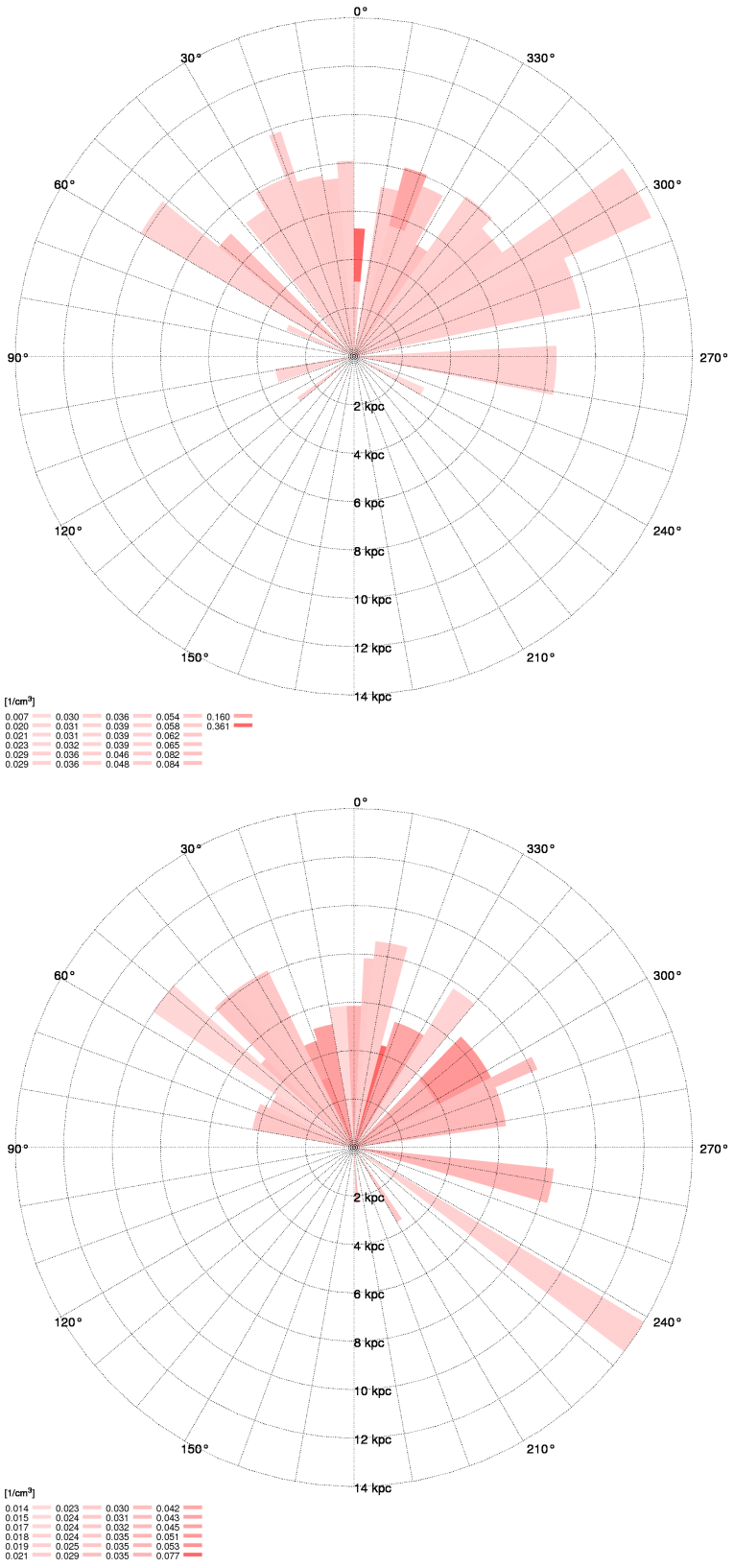

Figure 5.5. Free electron density distribution of galactic latitude ranges: (-5.0),(-3.0) degrees (upper panel) and (-10.0),(-5.0) degrees (lower panel). Image credit: B.B. Gucsav (Ankara Uni., Turkey).

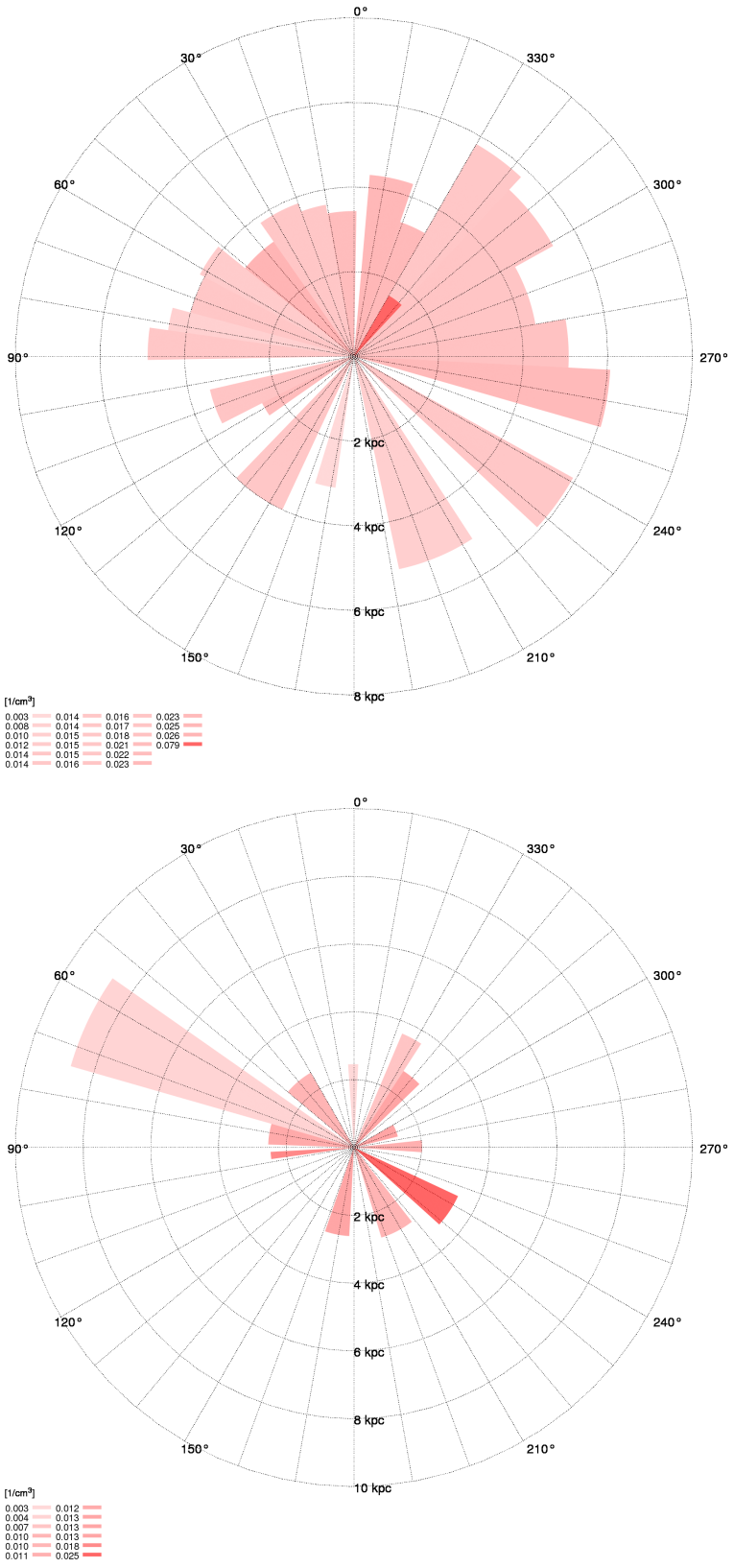

Figure 5.6. Free electron density distribution of galactic latitude ranges: (-25.0),(-10.0) degrees (upper panel) and (-40.0),(-25.0) degrees (lower panel). Image credit: B.B. Gucsav (Ankara Uni., Turkey).

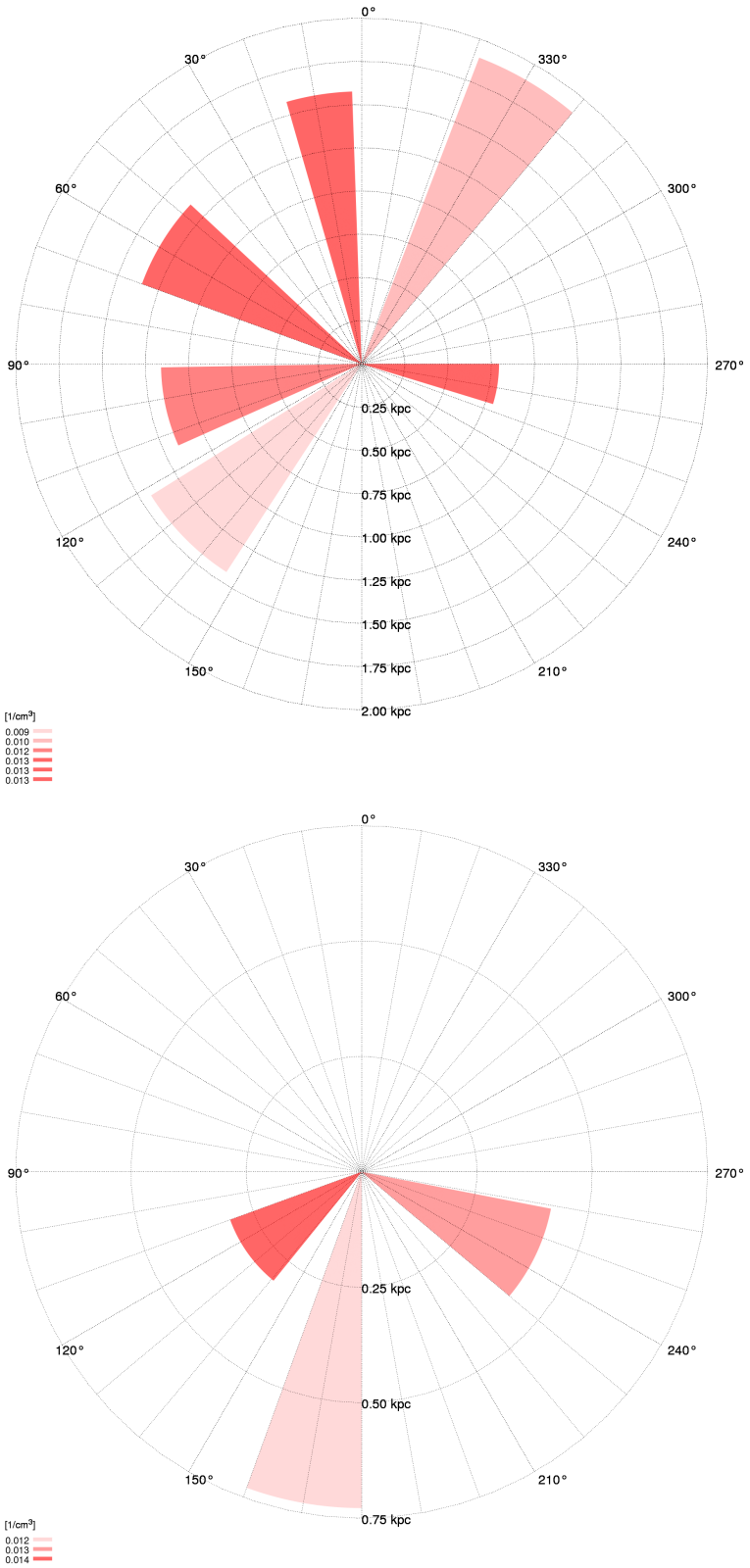

Figure 5.7. Free electron density distribution of galactic latitude ranges: (-60.0),(-40.0) degrees (upper panel) and (-90.0),(-60.0) degrees (lower panel). Image credit: B.B. Gucsav (Ankara Uni., Turkey).

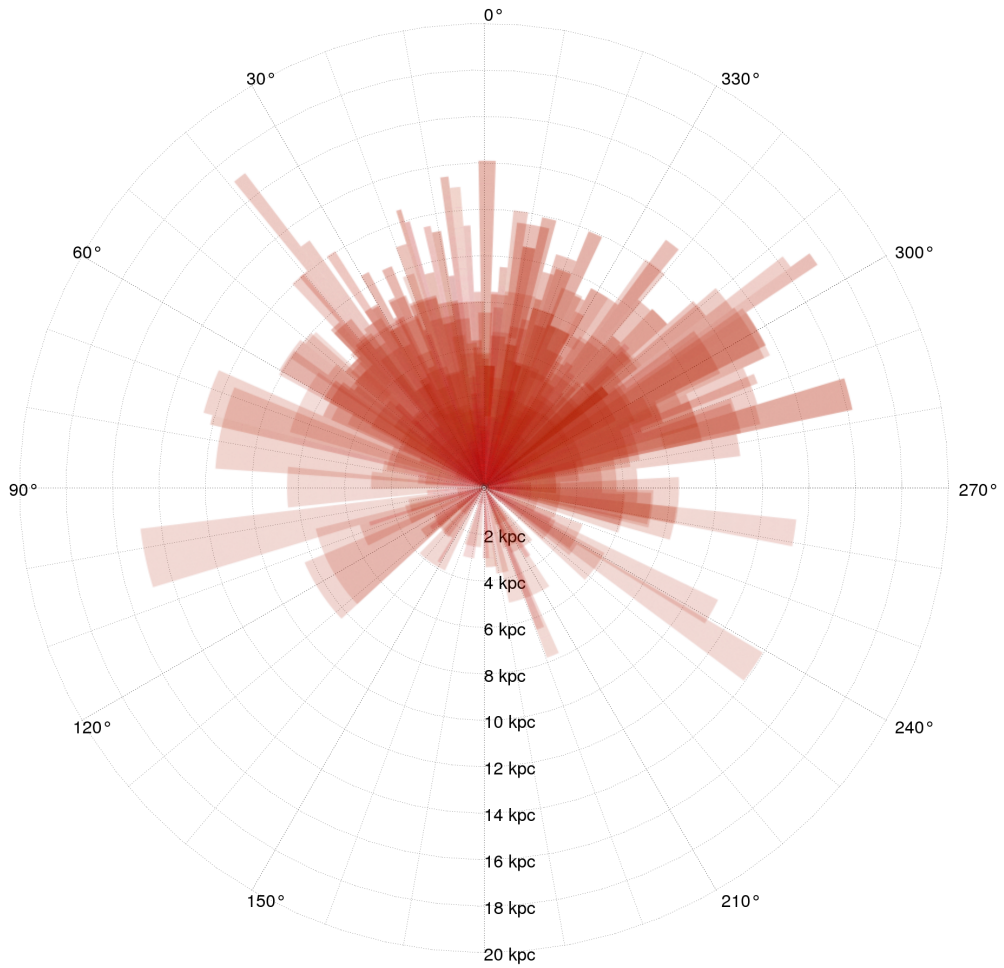

Figure 5.8. Cumulative free electron density distribution of the Milky Way Galaxy. Image credit: B.B. Gucsav (Ankara Uni., Turkey).

In order to see the concordance of the model with the spiral structure of the Galaxy, three different arm models are used.

First spiral arm model in question is given by Vallée (2008). Here, our model complies with the Carina, Sagitarius, Crux and Norma Arms. The tangents of the arms are successfully given by the high electron density regions overlapping each other. Moreover the curvature of the Perseus Arm fits well to our model however our model predicts a thicker Perseus Arm (see Fig. 5.9).

Second spiral arm model in question is simulated by Carey (2008) by using the infrared images of NASA's Spitzer Space telescope. Harmony between

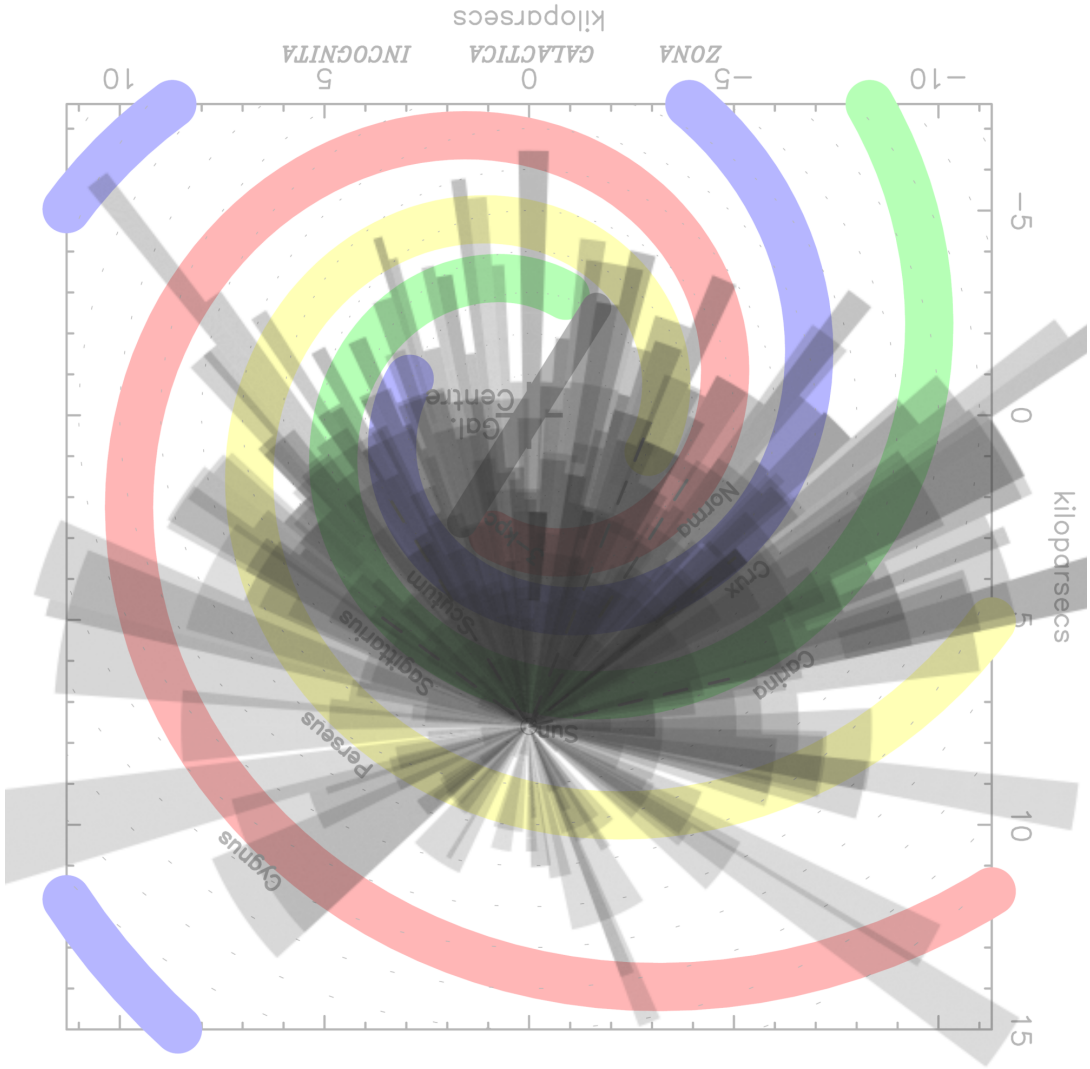

Figure 5.9. Cumulative free electron density distribution of the Milky Way Galaxy displayed on the spiral arm model of Vallée (2008). The original image is rotated 180 degrees for convenience of this work. Image credit: B.B. Gucsav (Ankara Uni., Turkey).

our free electron density model and this model is greater when compared to the one with Vallée (2008) spiral arms. Here the curvature of Near 3 kpc Arm and Sagittarius Arm are perfectly given by corresponding section endings, i.e farthest pulsars in these sections. This means that pulsar distances at those sections can be trusted. Moreover tangents of Scutum-Centaurus Arm and Sagitarius Arm at 290 degrees correspond to high density regions. On top of that, the high density region at 260 degrees fits perfectly with the tangent of the Orion Spur. However the Outer Arm is predicted to be located at a higher distance according to our model (see Fig. 5.10).

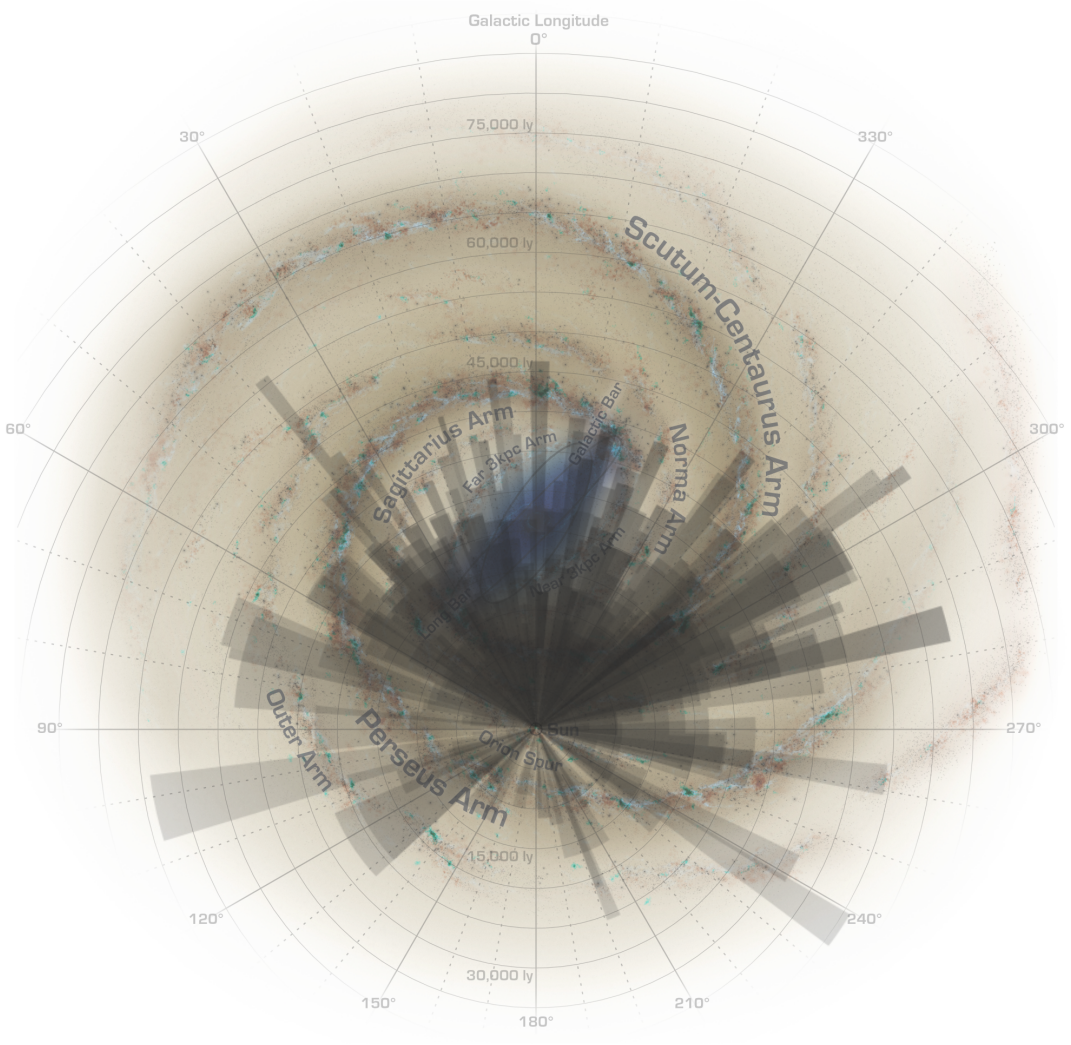

Figure 5.10. Cumulative free electron density distribution of the Milky Way Galaxy displayed on the spiral arm model of Carey (2008). Image credits: Galactic Arm Structure: NASA/JPL-Caltech/R. Hurt (SSC/Caltech); Overlay n_e map graphs: B.B. Gucsav (Ankara Uni., Turkey).

Third spiral arm model used for comparison is given by Hou et al. (2009) (hereafter HH09). The data on which this model is constructed includes H II region data that our model is also made use of. The high density regions of overlapping zones do fit with the line of sights of free electron sources located near the Sun especially between galactic longitude ranges of 15-35 degrees. Moreover the curvature of Arm-2 and Arm-3 fits the model very well. When it comes to high density regions at galactic longitude ranges of 240 and 260 degrees, they are in accordance with the free electron sources given by the HHS09 data. However Arm-1 of HHS09 should have been simulated with

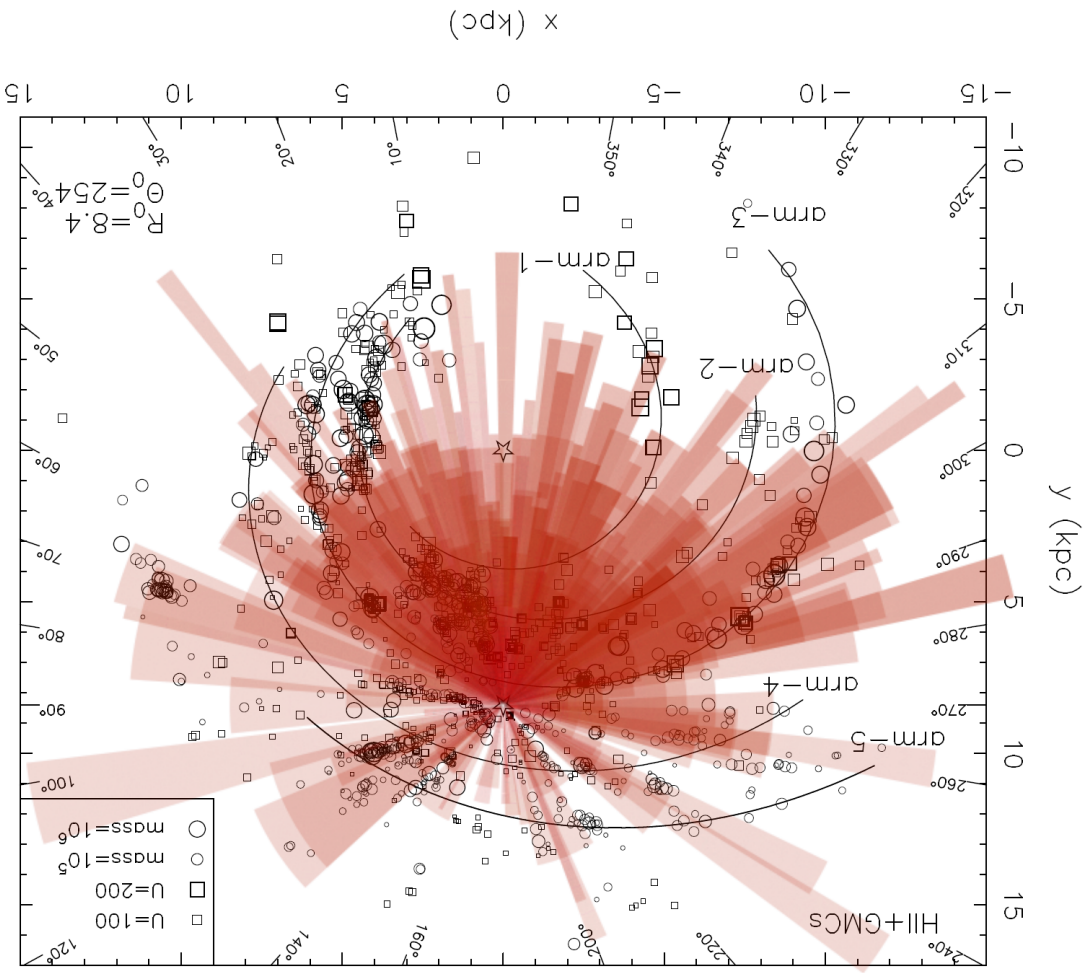

Figure 5.11. Cumulative free electron density distribution of the Milky Way Galaxy displayed on the spiral arm model of Hou et al. (2009). The original image is rotated 180 degrees for convenience of this work. Image credit: B.B. Gucsav (Ankara Uni., Turkey).

smaller radius of curvature according to our model (see Fig. 5.11).

5.6 Success of the Model

In order to test the free electron density model that is introduced here, pulsar data presented in Gómez et al. (2001) (hereafter G01) is used. Table 1 of this article consists of 109 pulsars whose distance information is independently determined from their dispersion measures. Although G01 used the distances of 109 pulsars in order to construct a mathematical model, those

pulsars are used to test the success of this work here. Among 109 pulsars, 3 of them are extragalactic. For the signal paths of 14 of them, the model cannot estimate free electron densities because those pulsars are either excluded from the data set of our model (since they do not fit to any of the sections in any sense) or because they construct single pulsar sections in which no linear curves can be estimated. As a result there are 92 pulsars that are used as testers in which 20 of them have only upper distance limits and 9 of them have only lower distance limits.

Dispersion measures of 92 pulsars and the free electron densities of sections that they fall into are used to calculate model distances. When they are compared with the data set given by G01 it is seen that 58 model distances are in between given error bars (see Fig. 5.12).

34 pulsar distances that are not in agreement with the data given by G01 are compared with the data that is used to construct our model as well. It

Table 5.4. Sequential pulsar names used in Figure 5.12. Pulsar names are taken from G01.

N	Name	N	Name	N	Name	N	Name
1	0138+59	24	1323-62	47	1749-28	70	1904+06
2	0329+54	25	1338-62b	48	1757-24b	71	1907+10
3	0355+54	26	1356-60	49	1758-23b	72	1908+00c
4	0435-47b	27	1358-63b	50	1800-21	73	1910-59b
5	0531+21	28	1449-64b	51	1802-07c	74	1913+10
6	0656+14b	29	1509-58	52	1804-08	75	1914+13
7	0736-40c	30	1516+02Bc	53	1807-24b	76	1915+13
8	0740-28c	31	1534+12b	54	1818-04	77	1919+21
9	0833-45c	32	1556-44b	55	1821+05	78	1920+21
10	0835-41c	33	1557-50c	56	1821-19b	79	1929+20
11	0905-51b	34	1558-50c	57	1829-08	80	1930+22
12	0906-49b	35	1641-45	58	1830-08b	81	1933+16
13	0919+06b	36	1648-42b	59	1845-01	82	1937+21
14	0940-55b	37	1701-30b	60	1849+00	83	1944+17
15	0950+08c	38	1703-40b	61	1853+01	84	1951+32
16	0959-54c	39	1706-44b	62	1855+02	85	2002+31
17	1046-58b	40	1711+07b	63	1855+09c	86	2016+28
18	1054-62c	41	1718-35b	64	1857-26b	87	2020+28
19	1154-62b	42	1737-30b	65	1859+03	88	2021+51b
20	1221-63b	43	1740-53b	66	1859+07	89	2127+11Ac
21	1240-64	44	1741-11b	67	1900+01	90	2255+58
22	1259-63b	45	1742-30b	68	1900+05	91	2319+60
23	1323-58b	46	1745-20c	69	1900+06	92	2334+61b

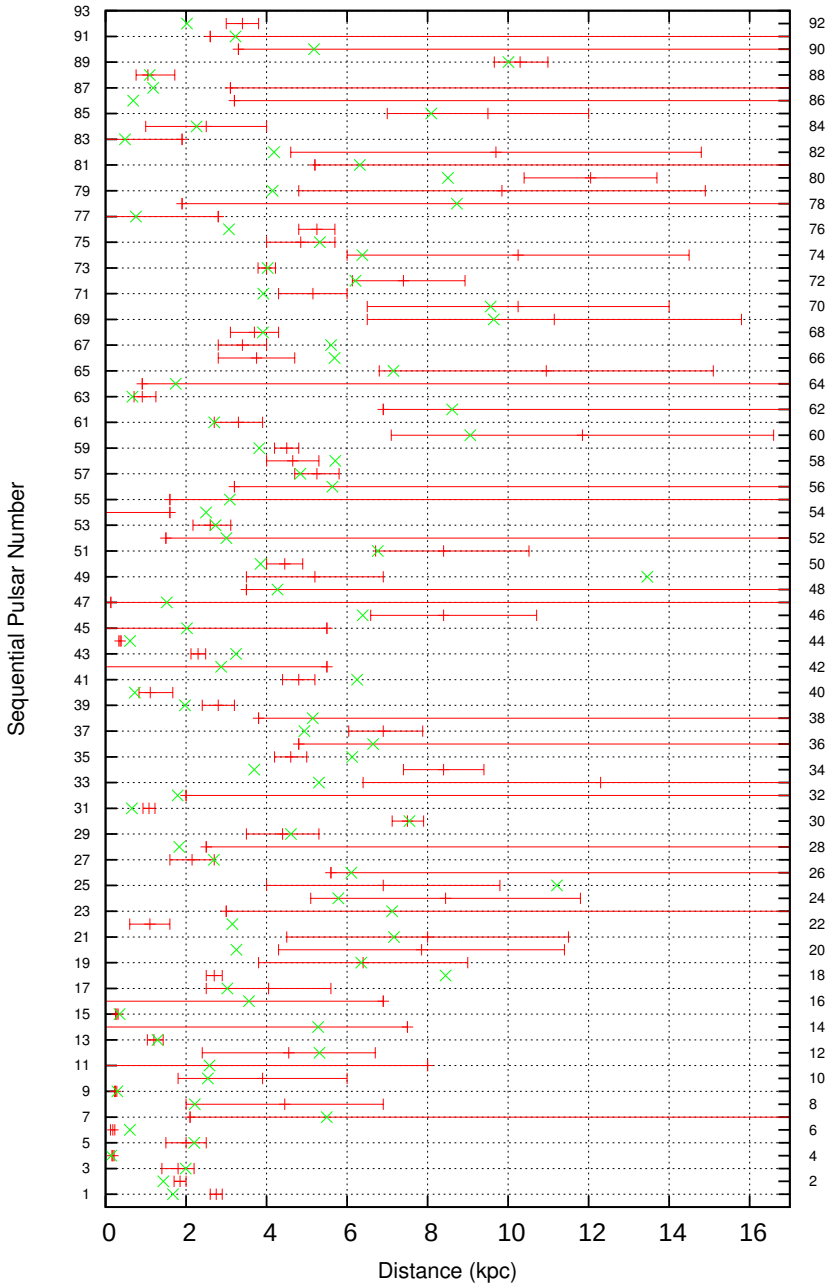

Figure 5.12. Comparison of 92 pulsar distance data given by G01 with distances calculated using the model. Vertical axis gives the sequencial pulsar number (corresponding pulsar names are given in Table 5.4) and the horizantal axis gives distance in kpc. Red lines define the distance range given by G01 data and green crosses represents the model distances.

is seen that 30 of them are in fact in good agreement with the data that have been corrected by Guseinov (2009) (hereafter GPDC). In the end, there are only 4 pulsars with model distances different than the ones presented in both G01 and GPDC (see Table 5.5).

Three of these 4 pulsars (J1644-4559, J1341-6220, J1939+2134) are also on the list of outlier pulsars of the G01 mathematical model, so there might be a basic distance estimation fault in determining the distances of the pulsars. When those 4 pulsars are investigated one by one it is seen that model distances of J1939+2134 and J1932+2020 pulsars are determined through the same d vs DM graph with reliability rank 3. Considering the quality of the fit and the number of pulsars on the d vs DM graph, free electron density of 54.0:61:0/-1.0:1.0 section cannot be determined accurately by our model. Model distance of J1341-6220 pulsar is determined through a d vs DM graph of rank 2. Either with given distances by Gómez et al. (2001) or by Guseinov (2009), J1341-6220 seems to have excess dispersion measure. If the estimated model distance is wrong this means that there is an additional free electron source between the pulsar and the Sun so that its signal gets dispersed more than the others in the same 3D section. When it comes to J1644-4559 pulsar, no possible explanation can be found for its inconsistent model distance. The section that J1644-4559 falls into has a d vs DM graph with reliability rank 1 and all other pulsars at the same section have consistent model distances with the data.

Table 5.5. Outlier pulsars of the model. Jname is the name of the pulsar, l and b are the Galactic coordinates of the pulsar in degrees, Age is the logarithmic pulsar age, DM is the dispersion measure of the pulsar in kpc/cm^3, d_{G01} is the data given by Gómez et al. (2001), d_{GPD} is the data prepared by Guseinov (2009) and d_M is the calculated distance of the pulsar by the model.

Jname	l	b	Age	DM	d_{G01}	d_{GPD}	d_M
J1644-4559	339.19	−0.19	5.56	479	4.6	4.5	6.1
J1341-6220	308.73	−0.03	4.08	717	6.9	8.5	11.2
J1939+2134	57.51	−0.29	8.37	71	9.7	2.9	4.2
J1932+2020	55.57	0.64	6.00	211	9.9	7.8	4.1

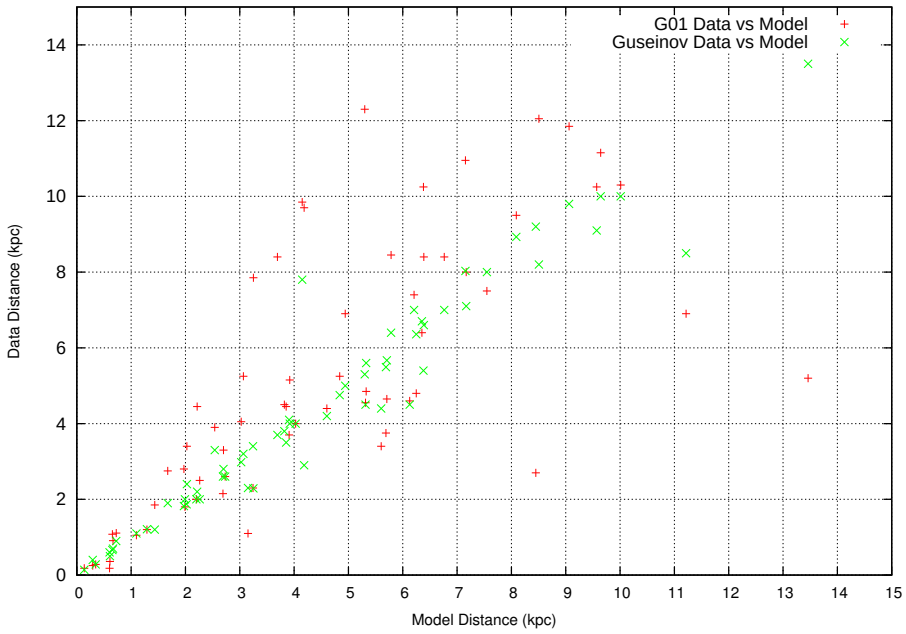

Figure 5.13. Distance versus distance graph of 63 pulsars. Red pluses give the plot of G01 data distances versus model distances. Green crosses give the plot of GPDC distances versus model distances.

Here it is important to note that the origin of the data on which a model is constructed is the main factor in questioning the success of a model. When the 29 pulsars that have either upper or lower distance limits in G01 are excluded from the 92 pulsar group mentioned above, there are 63 pulsars left that can be used in comparison of three different type of data acquisitions. Fig. 5.13 is a graph that includes two plots. The first one is distances given by G01 versus model distances and the second one is distances given by GPDC versus model distances. This graph (Fig. 5.13) shows that the origin of the data of G01 and GPDC is in fact highly different since Guseinov (2009) brought certain corrections to pulsar distances. That is why the success of the model should be examined through comparing the model distances with the distances on which the model is constructed i.e distances given by GPDC.

Looking at the plot of GPDC distances versus model distances, it is seen that nearly all of the pulsars are bunched around the y = x curve. This means

that the model is successful in estimating distances to pulsars and due to that, the free electron density presented by the model is infact reliable. There are only 4 pulsars that deviates from the group that is bunched around the y = x curve. Those pulsars are the ones which are presented in Table 5.5 together with their possible explanations of deviations.

5.7 What Makes This Model Different From the Others?

A literature survey of free electron density models shows that most of them are mathematical constructions. The preliminary mathematical models consider the Galaxy as a disk and give the distribution of the free electron density with multiplication of two functions: a monotonically decreasing function in radial distance and an exponential decay in vertical distance from the Galactic plane. Those preliminary models are built on using limited data of dispersion measures of pulsars with distance estimates found independently of their dispersion measures. Using Eq. 2.12 in forward direction and adding contributions of a few free electron sources like the Gum Nebula, those models can estimate the distances of pulsars up to 100% error (Taylor and Cordes 1993). On the other hand, at the last decade the detailed analysis of interstellar medium brought improvements on mathematical models. Integrating the contributions of free electron sources, voids or over densities to the overall free electron density function, the mathematical models of today give much accurate results for distances of pulsars (Cordes and Lazio 2002, 2003; Gómez et al. 2001).

However, even a glance on the distribution of free electron sources on the Galaxy makes one understand that Galaxy is far from being simple to be modeled by a mathematical model. Each and every line of sight has distinctive free electron sources in different distance ranges. A small change in line of sight may result in a major change in free electron density. So, considering the limited data of pulsars and free electron sources, we are not in a condition to model the distribution of free electron density of the Galaxy today by a mathematical model, especially at high latitudes. For mathe-

matical models, in order to obtain the smooth distribution of free electron density, observations of pulsars and free electron sources should reach to maximum possible value. Moreover the behavior of plasma in ISM should be fully understood. Even in a scenario like that, the mathematical model may not be given in terms of simply multiplication of a monotonically decaying function and an exponential decay. Each section should include additional functional(s) equivalent to the dynamics of the corresponding section.

As a result the only plausible method seems to be a statistical method like the one used in this work. Dealing with each 3D section of the Galaxy separately, the free electron densities are determined through special treatments of relations of pulsar signals with free electron sources. By this way, overestimation of smooth distribution of free electrons is also prevented.

5.8 Suggestions for Future Models

From the very first chapter of this thesis, it is stated that estimating the pulsar distances is a real challenge. Moreover distances of free electron sources cannot be determined with high accuracy as well. Following this, construction of a model that gives the free electron density distribution of the Galaxy is not easy. The process is an iterative method and the success of the model depends both on the number and the quality of the data.

In order to build more successful models it is obvious that the number of data of pulsars and the free electron sources should increase. Nevertheless this criterion on its own is not enough. Methods that are used to estimate pulsar distances should be improved. Moreover better galactic rotation curves should be constructed so that the distances of free electron sources can be estimated more accurately. Considering the fact that no widely accepted Galaxy rotation model has been built after Brand and Blitz (1993), the literature is in need of a more detailed rotation model.

The iterative method that is used here is specifically built on using the data in hand. As the number of pulsar and free electron data increases the it-

eration procedure that is used to form the 3D pieces of the Galaxy should be followed from the very beginning. Considering a certain 3D section for example, addition of a new pulsar or a new free electron source may dictate the section borders to be changed. So, for future studies, the contribution of new pulsars to the density distribution cannot be integrated with ease, rather, the new mesh structure should be constructed specifically to the new data.

In the future, as radio pulsar surveys increase and the number of pulsars reaches a value of 2-3 times of the one of today, the iterative method used here can be done using computer programming. By this way, variable size meshes can be constructed as soon as new data is added on pulsar catalogs.

The last topic that can be argued here is the observational line of sights of pulsar surveys. Since most of the pulsars are located in 270-90 degree ranges in galactic longitude, observers of pulsar surveys choose to investigate the corresponding region of the Galaxy in order to find new pulsars. As a result, the number of pulsars at the anti-center line of sights is kept on a constant value that is not enough to build a free electron density model at anti-center direction. The suggestion for future surveys is to investigate the anti center line of sights more than the one of today so that both the free electron density distribution and the spiral arm structure of that part of the Galaxy can be understood better.

CHAPTER 6

CONCLUSION

The aim of the work that is presented in this thesis is to determine the free electron density map of the Milky Way Galaxy. The methodology that is followed is inspired by Guseinov et al. (2002) article which basically grounds on the dispersion phenomenon of light signals.

In Chapter 1, the players of the dispersion concept are presented. Considering the fact that the group velocity of an electromagnetic wave depends both on its frequency and the frequency of the medium that it travels through, signals of radio pulsars are chosen to be the electromagnetic waves in question and H II Regions and supernova remnants are chosen to be the free electron sources that cause the signals to be slowed down. A brief summary in this chapter states that knowing the delay in arrival time of the signal and the distance of a pulsar, one can calculate the free electron density of the medium that its signal passes through. After that, the importance of determination of free electron density map, mathematicals models of free electron density distribution of the Galaxy, dispersion concept and the distance estimation techniques of pulsars are presented such that the overall picture of the work can be demonstrated.

In Chapter 2, firstly, the relation between the signal frequency and the plasma frequency is derived using two of the Maxwell's Equations and the equation of motion of electrons. Next, the effect of plasma on arrival time of a pulsar signal is derived and it is seen that if the delay time of the signal can be measured, the column density between the pulsar and the observer

can be calculated. This column density is also named as 'dispersion measure' since dispersions of light signals depend on the integral effect of the free electrons that are encountered by the signal. Towards the end of the chapter, it is shown that determination of dispersion measure can only be through observing the arrival time of the same signal in two different frequencies. In the end, it turns out that the free electron density of the signal path of a pulsar can be found by dividing its dispersion measure to the distance travelled by the pulsar signal.

Chapter 3 provides the steps that are followed in estimating the free electron density distribution of the Galaxy. Firstly, the radio pulsar data is gathered from Manchester et al. (2005) and Guseinov (2009) (hereafter GPDC), and it is seen that there are 1893 Galactic radio pulsars that can be studied on. Next, the Galaxy is divided into a 3D mesh structure whose mesh sections are determined through a trial-and-error method. This trial-and-error method is done making use of the distance versus dispersion measure (d vs DM) curves of pulsars. The borders of the mesh sections are kept as variables until the pulsars in a certain galactic latitude, galactic longitude and distance range are on linear fits of the d vs DM graphs; which means the path that lies on the line of sight of pulsars have constant free electron densities. Afterwards, free electron sources are integrated to these d vs DM graphs such that real physical relation between the pulsar signals and the free electron sources could be studied. In the following step, the pulsars that deviate from the d vs DM graphs are investigated. If the deviation of the pulsar cannot be linked to an existence of a free electron source between the pulsar and the Sun, a new distance is adopted to the deviating pulsar. By this way, two important results are obtained; pulsar distances are corrected and more accurate free electron densities are estimated for 3D sections.

Chapter 4 provides an example for the methodology that is explained above. Since the (-1.0,1.0] degree galactic latitude range is the richest zone in terms of number of radio pulsars and free electron sources it is the one that is presented as the archetype. The implications on d vs DM graphs interms of deviating pulsars can be understood more clearly in this chapter.

In Chapter 5, first of all, the 3D mesh structure of the work is presented. This mesh is composed of 14 zones in galactic latitude direction considering the Galaxy as a cylinder and the number of 3D sections is 348 in total. Next, 140 pulsars with adopted distances are tabulated. Considering the fact that young pulsars cannot escape from their birth places, the (-1.0,1.0] degree zone pulsars that have been adopted distances, are presented with their original locations and adopted locations on the Galaxy. This table shows that adopting procedure is in fact successful in locating pulsars since newly estimated locations correspond to regions on the spiral arms of the Galaxy as expected. Afterwards, the free electron density of each 3D section is presented via tables and d vs DM graphs. Following this, free electron density map of the Galaxy is given by 14 graphs corresponding the 14 zones. Finally, those 14 zones are projected on the Galaxy disk and put on top of each other to obtain the cumulative free electron density map of the Galaxy. Then, this overall map is placed on three different spiral arm models in order to present the harmony of the model with the free electron sources.

After the results are presented, the success of the free electron density distribution is investigated. For this, 92 of the pulsar data given by Gómez et al. (2001) (hereafter G01) is plugged into the model. The importance of those pulsars is that their distances are obtained independently of their dispersion measures and that is why they are unbiased testers. In the end, it is seen that 58 pulsar distances are in between given error bars. Of the remaining 34 pulsars, 30 of them are in accordance with GPDC but 4 of them have model distances different both from G01 data and from GPDC data. The possible reasons for this difference is also investigated and presented in the corresponding section.

In the final sections of the last chapter our model is compared with the widely used mathematical models in literature and compatibility of the model with the spiral arm models is discussed. Moreover certain suggestions are made for future studies.

The final comment about this work can be done on the big picture that it

contributes to. Primarily, the free electron density models can be used as an additional method for estimating distances to newly found pulsars. Following this, the overall distribution of pulsars can be used to construct spiral arm models of the Galaxy. Since the young pulsars are expected to be close to their birth places, i.e on the spiral arms, investigating the distribution of young pulsars can give idea about the arm structure on the disk and the warp dynamics in the vertical direction to the disk. Moreover, free electron density distribution is required to model the rotation measures which are used to bring the magnetic field structure of the Galaxy in to light. As a result, it is either for understanding the overall distribution of pulsars in the Galaxy, for modeling the spiral arms or for determining the magnetic field structure; the free electron density distribution serves as an important tool in exploring the overall structure and the evolution of the Milky Way Galaxy.

BIBLIOGRAPHY

W. J. Altenhoff, D. Downes, T. Pauls, and J. Schraml. Survey of the galactic plane at 4.875 GHz. *A&AS*, 35:23–54, January 1979.

J. Brand and L. Blitz. The Velocity Field of the Outer Galaxy. *A&A*, 275:67, August 1993.

J. A. R. Caldwell and J. P. Ostriker. The mass distribution within our Galaxy - A three component model. *ApJ*, 251:61–87, December 1981. doi: 10.1086/159441.

S. J. Carey. MIPSGAL: A View of the Cold and Dusty in the Inner Galactic Plane with the Spitzer Space Telescope. In *American Astronomical Society Meeting Abstracts #212*, volume 40 of *Bulletin of the American Astronomical Society*, page 255, May 2008.

F. F. Chen. *Introduction to plasma physics*. New York: Plenum Press, 1974, 1974.

T. E. Clarke. Faraday Rotation Observations of Magnetic Fields in Galaxy Clusters. *Journal of Korean Astronomical Society*, 37:337–342, December 2004.

J. M. Cordes and T. J. W. Lazio. NE2001.I. A New Model for the Galactic Distribution of Free Electrons and its Fluctuations. *ArXiv Astrophysics e-prints*, July 2002.

J. M. Cordes and T. J. W. Lazio. NE2001. II. Using Radio Propagation Data to Construct a Model for the Galactic Distribution of Free Electrons. *ArXiv Astrophysics e-prints*, January 2003.

J. M. Cordes, J. M. Weisberg, D. A. Frail, S. R. Spangler, and M. Ryan. The Galactic distribution of free electrons. *Nat*, 354:121–124, November 1991. doi: 10.1038/354121a0.

K. Davidson and Y. Terzian. Dispersion Measures of Pulsars. *AJ*, 74:849, September 1969. doi: 10.1086/110872.

S. Dawson. Mapping the electron density in the interstellar medium with the pulsar dispersion measure. Department of Astronomy, Berkeley, 1999.

X. Deng and L. S. Finn. Pulsar timing array observations of gravitational wave source timing parallax. *MNRAS*, 414:50–58, June 2011. doi: 10.1111/j.1365-2966.2010.17913.x.

D. A. Frail and J. M. Weisberg. A critical evaluation of pulsar distance measurements. *AJ*, 100:743–757, September 1990. doi: 10.1086/115556.

M. Gedalin, E. Gruman, and D. B. Melrose. Mechanism of pulsar radio emission. *MNRAS*, 337:422–430, December 2002. doi: 10.1046/j.1365-8711.2002.05922.x.

Y. M. Georgelin and Y. P. Georgelin. The spiral structure of our Galaxy determined from H II regions. *A&A*, 49:57–79, May 1976.

G. Gilmore, R. F. G. Wyse, and K. Kuijken. Kinematics, chemistry, and structure of the Galaxy. *ARA&A*, 27:555–627, 1989. doi: 10.1146/annurev.aa.27.090189.003011.

G. C. Gómez, R. A. Benjamin, and D. P. Cox. A Reexamination of the Distribution of Galactic Free Electrons. *AJ*, 122:908–920, August 2001. doi: 10.1086/321180.

D. A. Green. A Catalogue of Galactic Supernova Remnants (Green, 2009). *VizieR Online Data Catalog*, 7253:0, June 2009.

O. H. Guseinov, E. Yazgan, S. Tagieva, and A. Kupce Yoldas. A Trustworthy and Simple Method to Determine Pulsar Distances and the Electron Distribution in the Galaxy. *ArXiv Astrophysics e-prints*, July 2002.

O. H. Guseinov, A. Ankay, A. Sezer, and S. O. Tagieva. The relation between the surface brightness and the diameter for galactic supernova remnants. *Astronomical and Astrophysical Transactions*, 22:273, March 2003. doi: 10.1080/1055679021000034160.

O.H. Guseinov. Pulsar distances catalogue. The pulsar distances data have been managed at http://astro-cats.org/pulsar/ upto 2009., 2009.

L. G. Hou, J. L. Han, and W. B. Shi. The spiral structure of our Milky Way Galaxy. *A&A*, 499:473–482, May 2009. doi: 10.1051/0004-6361/200809692.

J. M. Jackson, T. M. Bania, R. Simon, M. Kolpak, D. P. Clemens, and M. Heyer. H I Self-Absorption and the Kinematic Distance Ambiguity: The Case of the Molecular Cloud GRSMC 45.6+0.3. *ApJ*, 566:L81–L84, February 2002. doi: 10.1086/339715.

H. Karttunen, P. Kroeger, H. Oja, M. Poutanen, and K. J. Donner. *Fundamental astronomy*. Berlin: Springer, 2003., 2003.

M. S. Longair. *High Energy Astrophysics*. Cambridge University Press, 2010.

D. R. Lorimer and M. Kramer. *Handbook of Pulsar Astronomy*. Cambridge University Press, 2005.

A. G. Lyne and F. Graham-Smith. *Pulsar astronomy*. Cambridge University Press, 1990.

A. G. Lyne and D. R. Lorimer. Pulsar Velocities. *Journal of Astrophysics and Astronomy*, 16:97, June 1995. doi: 10.1007/BF02714827.

A. G. Lyne, R. N. Manchester, and J. H. Taylor. The galactic population of pulsars. *MNRAS*, 213:613–639, April 1985.

R. N. Manchester, G. B. Hobbs, A. Teoh, and M. Hobbs. The Australia Telescope National Facility Pulsar Catalogue. *AJ*, 129:1993–2006, April 2005. doi: 10.1086/428488.

T. Padmanabhan. *Theoretical Astrophysics - Volume 2, Stars and Stellar Systems*. Cambridge University Press, July 2001. doi: 10.2277/0521562414.

R. Paladini, C. Burigana, R. D. Davies, D. Maino, M. Bersanelli, B. Cappellini, P. Platania, and G. Smoot. A radio catalog of Galactic HII regions for applications from decimeter to millimeter wavelengths. *A&A*, 397:213–226, January 2003. doi: 10.1051/0004-6361:20021466.

R. Paladini, R. D. Davies, and G. De Zotti. Spatial distribution of Galactic HII regions. *MNRAS*, 347:237–245, January 2004. doi: 10.1111/j.1365-2966.2004.07210.x.

A. C. Robin, C. Reylé, S. Derrière, and S. Picaud. A synthetic view on structure and evolution of the Milky Way. *A&A*, 409:523–540, October 2003. doi: 10.1051/0004-6361:20031117.

J. Roman-Duval, J. M. Jackson, M. Heyer, A. Johnson, J. Rathborne, R. Shah, and R. Simon. Kinematic Distances to Molecular Clouds Identified in the Galactic Ring Survey. *ApJ*, 699:1153–1170, July 2009. doi: 10.1088/0004-637X/699/2/1153.

D. Shiga. Book Review: AN INTRODUCTION TO THE SUN AND STARS / Cambridge University Press, 2004. *Sky & Telesc.*, 109:120, 2005.

F. G. Smith. *Pulsars*. 1977.

R. Smits, S. J. Tingay, N. Wex, M. Kramer, and B. Stappers. Prospects for accurate distance measurements of pulsars with the Square Kilometre Array: Enabling fundamental physics. *A&A*, 528:A108, April 2011. doi: 10.1051/0004-6361/201016141.

J. H. Taylor and J. M. Cordes. Pulsar distances and the galactic distribution of free electrons. *ApJ*, 411:674–684, July 1993. doi: 10.1086/172870.

A. G. G. M. Tielens. *The Physics and Chemistry of the Interstellar Medium*. Cambridge University Press, September 2005.

J. P. Vallée. New Velocimetry and Revised Cartography of the Spiral Arms in the Milky WAY-A Consistent Symbiosis. *AJ*, 135:1301–1310, April 2008. doi: 10.1088/0004-6256/135/4/1301.

APPENDIX A

D VS DM GRAPHS

This appendix consists of distance versus dispersion measure graphs of pulsars. Graphs of each zone are given under the name of the corresponding zone and graphs of 3D sections that contain one or less pulsars are not given here. Header of each graph gives idea about the angle ranges of the section in terms of galactic longitude and galactic latitude and they are in degrees. The values under the header are in order; quality of the fit, error in DM, standard deviation, the distance value where the fit intersects with the vertical axis, slope of the fit and free electron density of the section. Red pluses indicate pulsars that have been investigated/corrected by Guseinov (2009). Green pluses indicate calibrator pulsars that have reliable distance data and listed by Guseinov et al. (2002). Red squares are data of pulsars that are derived directly from ATNF Radio Pulsar Catalog without any correction done on the data by Guseinov (2009). Horizontal green lines indicate SNRs and horizontal blue lines indicate HII regions that fall into the corresponding section. Their distance data are also given at the right bottom of the graph.

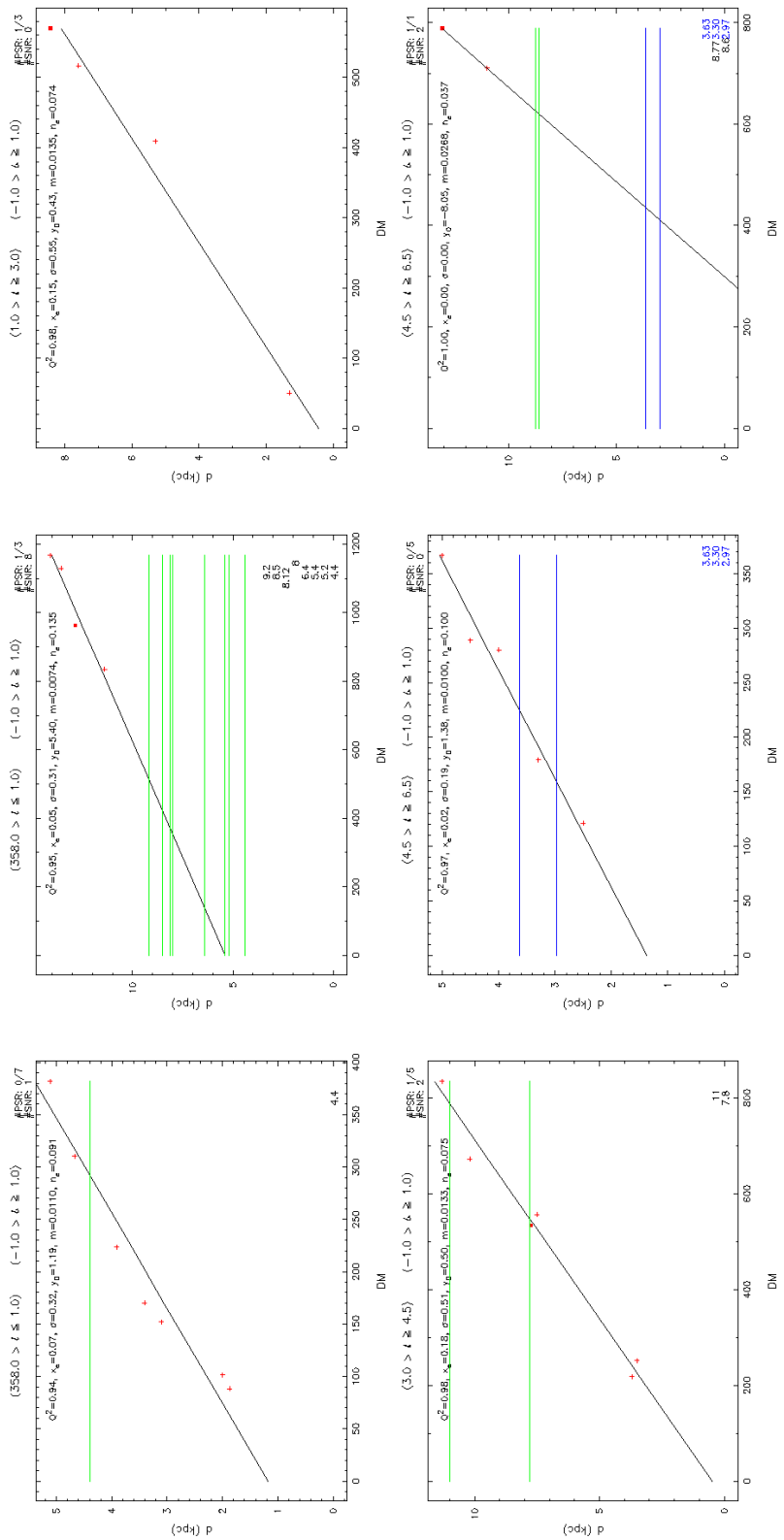

Figure A.1. Latitude Range: (-1.0), (+1.0)

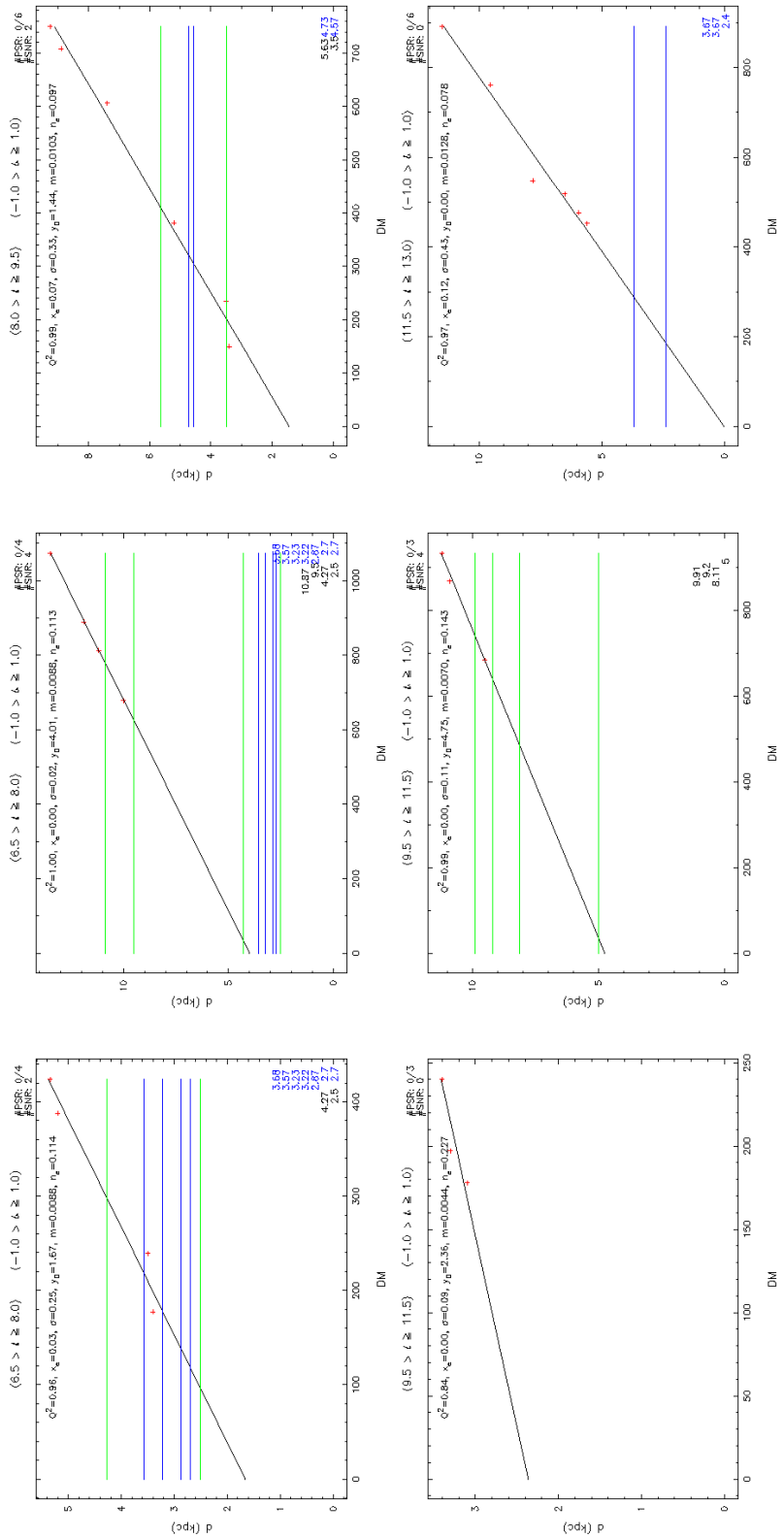

Figure A.2. Latitude Range: (-1.0), (+1.0) – *continued*

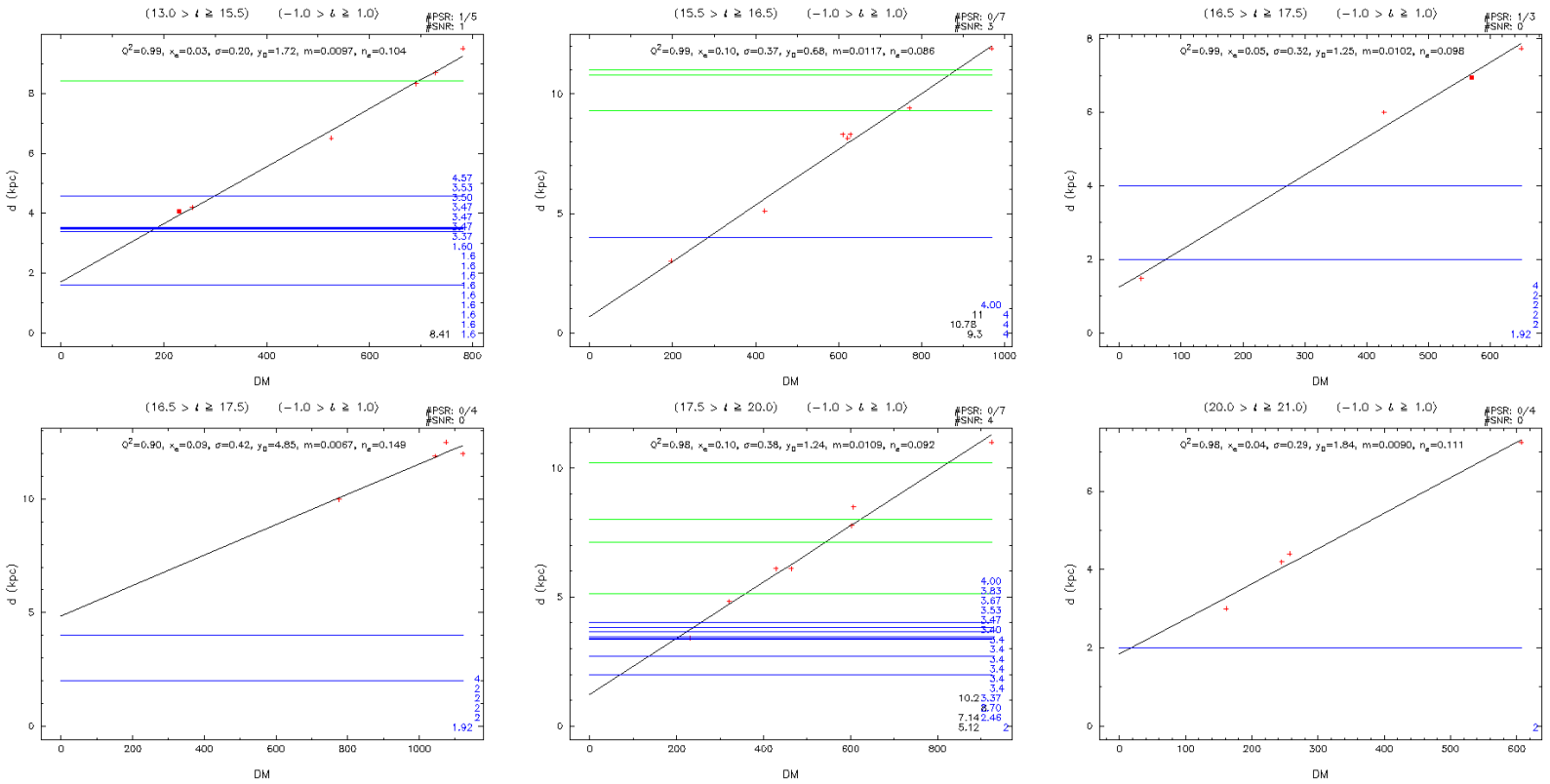

Figure A.3. Latitude Range: (-1.0), (+1.0) – *continued*

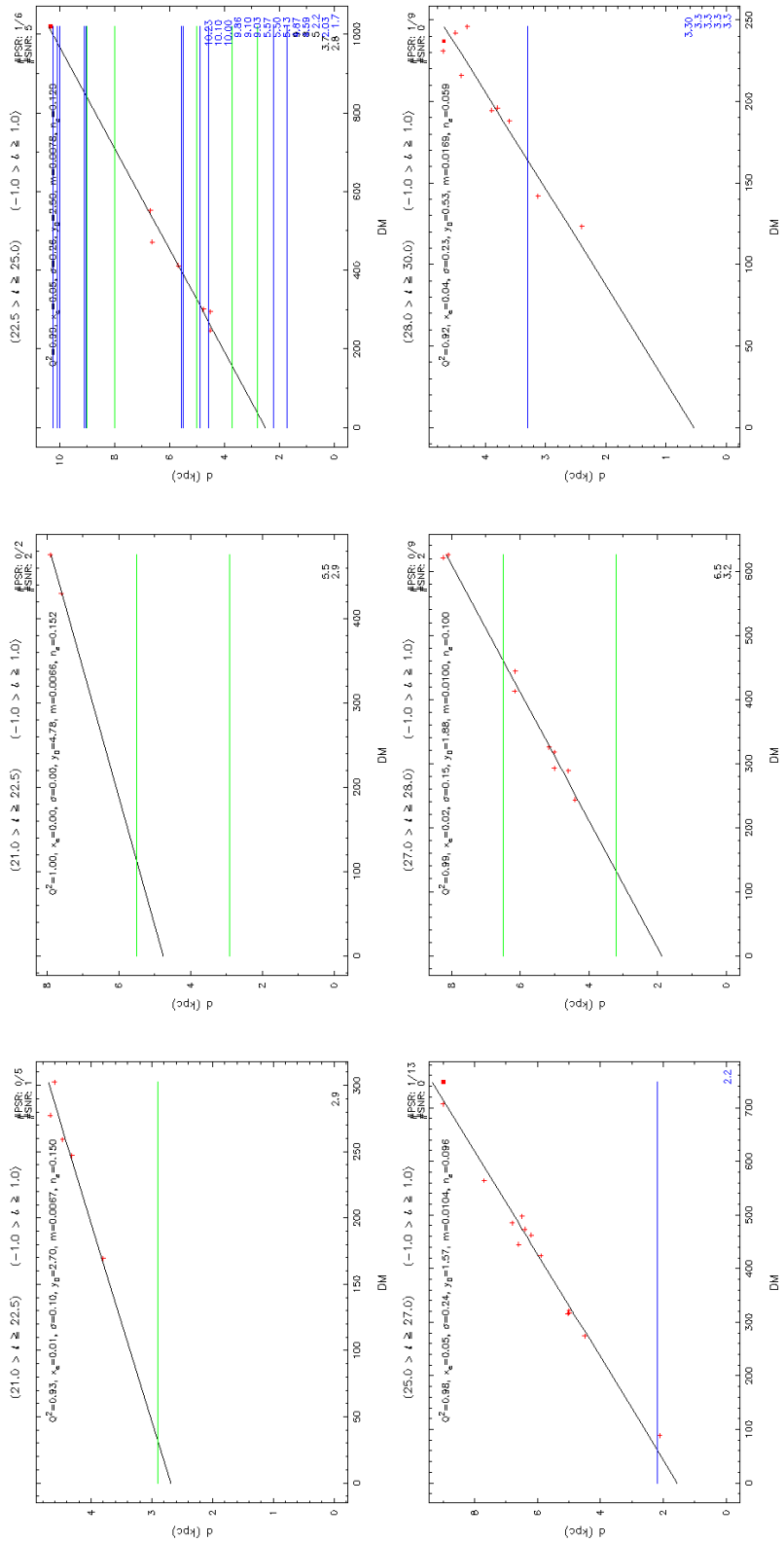

Figure A.4. Latitude Range: (-1.0), (+1.0) – *continued*

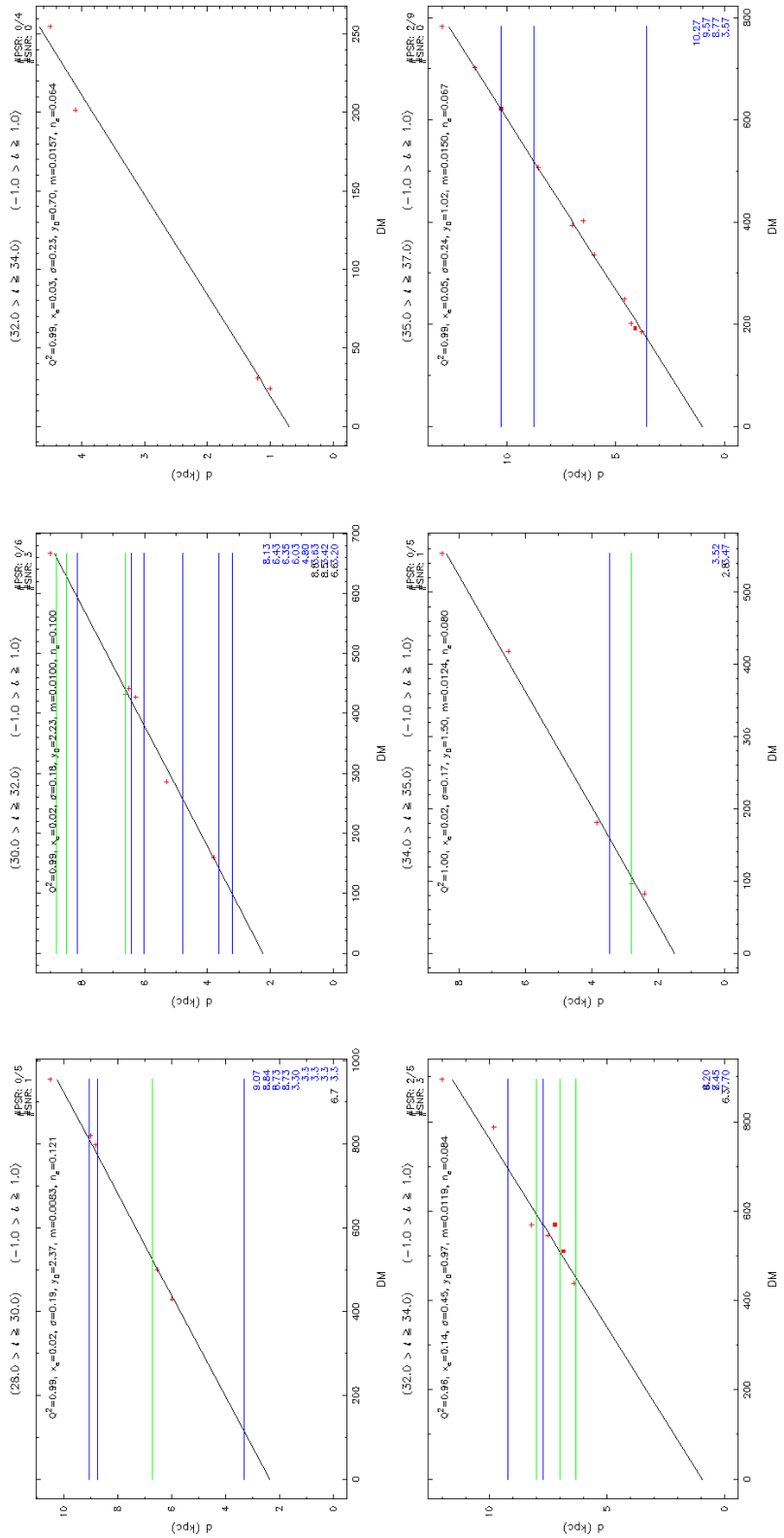

Figure A.5. Latitude Range: (-1.0), (+1.0) – *continued*

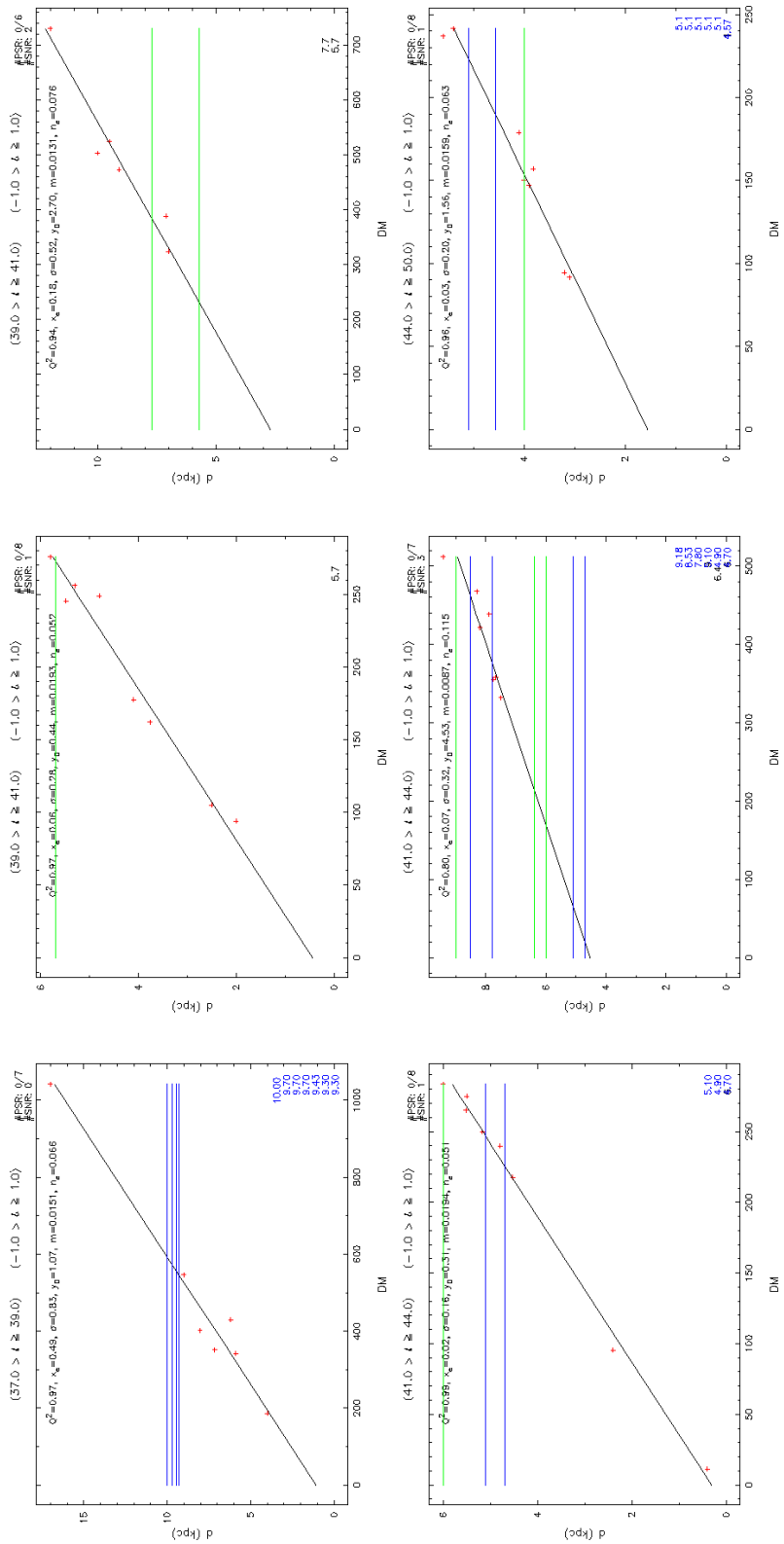

Figure A.6. Latitude Range: (-1.0), (+1.0) – *continued*

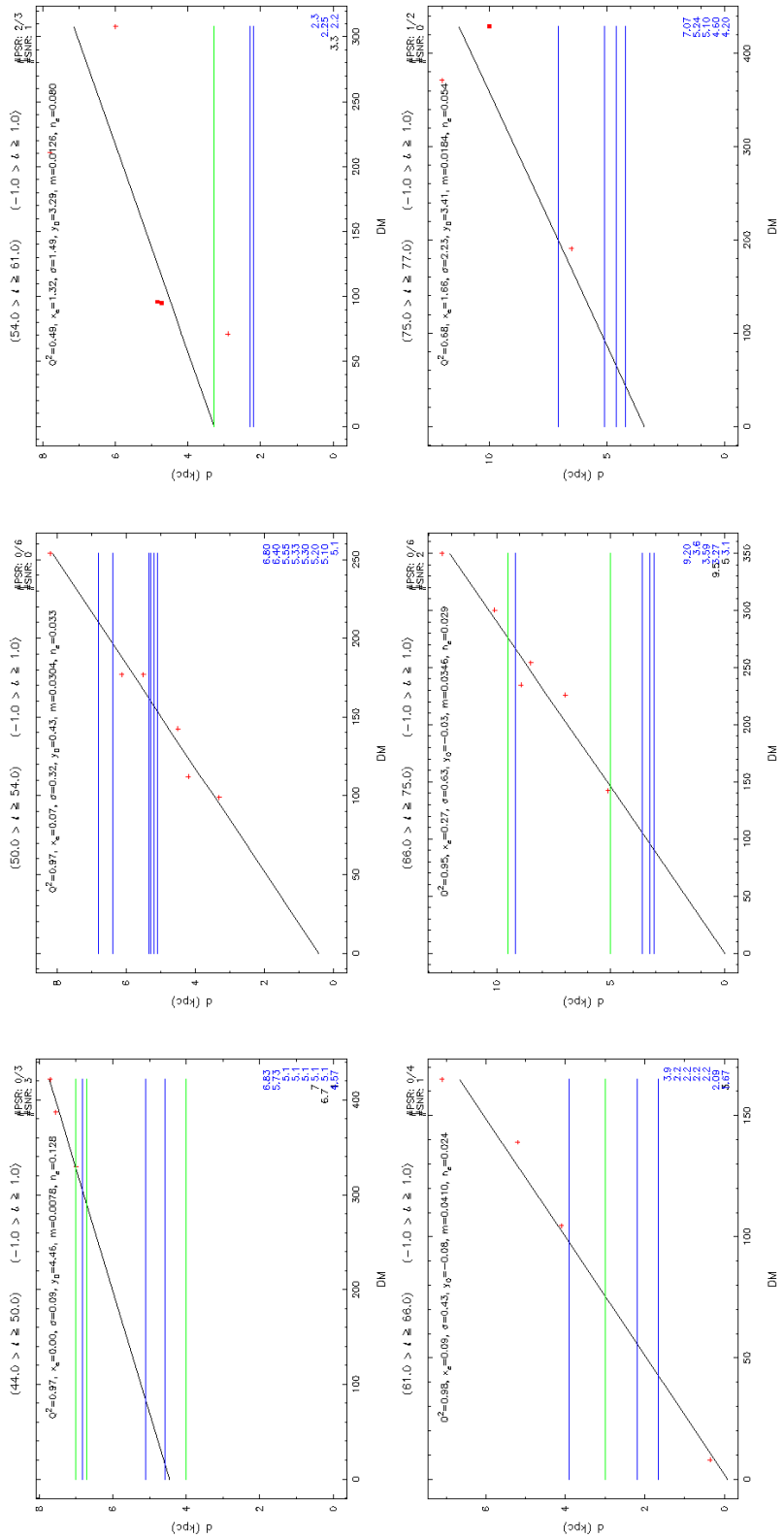

Figure A.7. Latitude Range: (-1.0), (+1.0) – *continued*

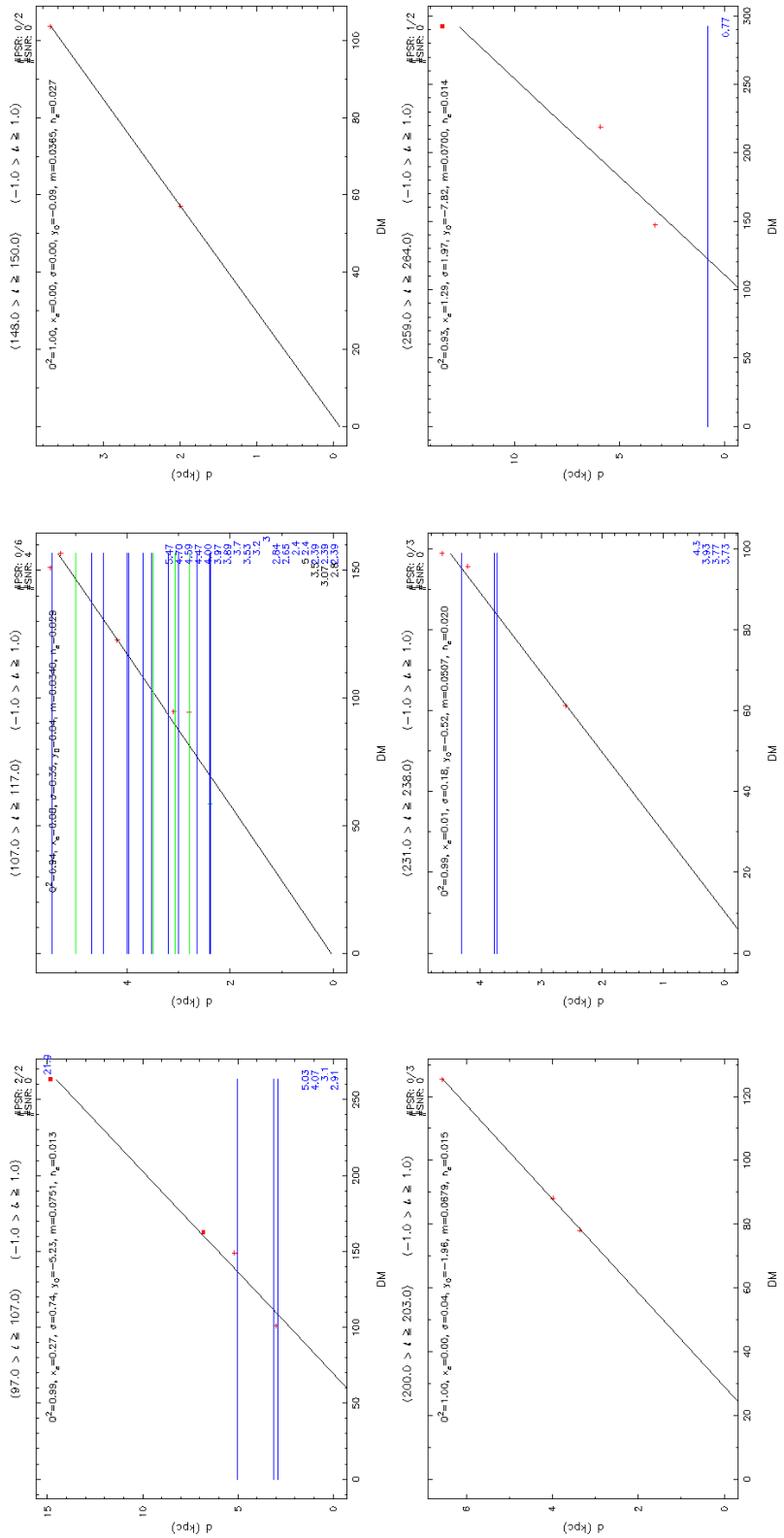

Figure A.8. Latitude Range: (-1.0), (+1.0) – *continued*

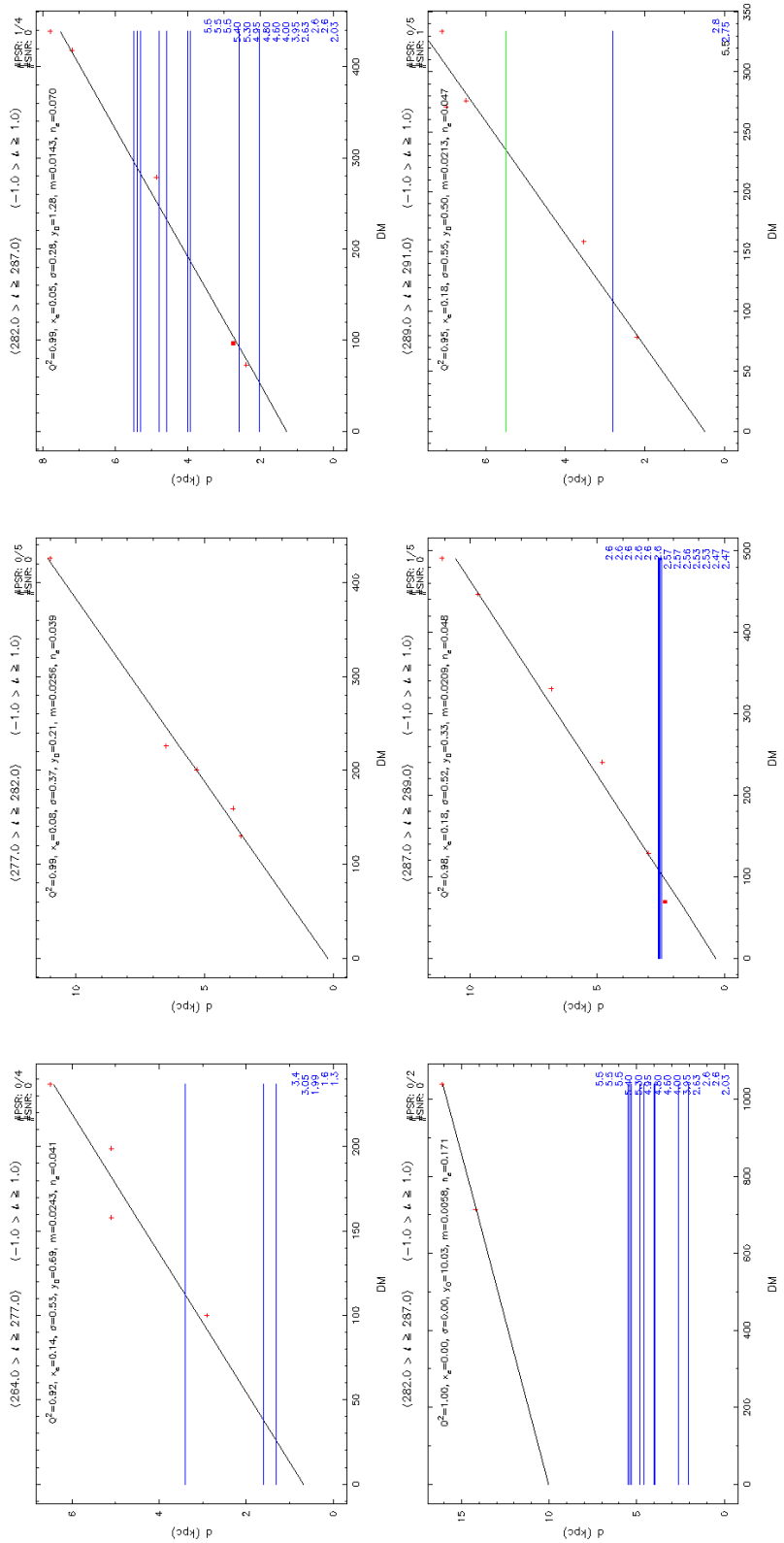

Figure A.9. Latitude Range: (-1.0), (+1.0) – *continued*

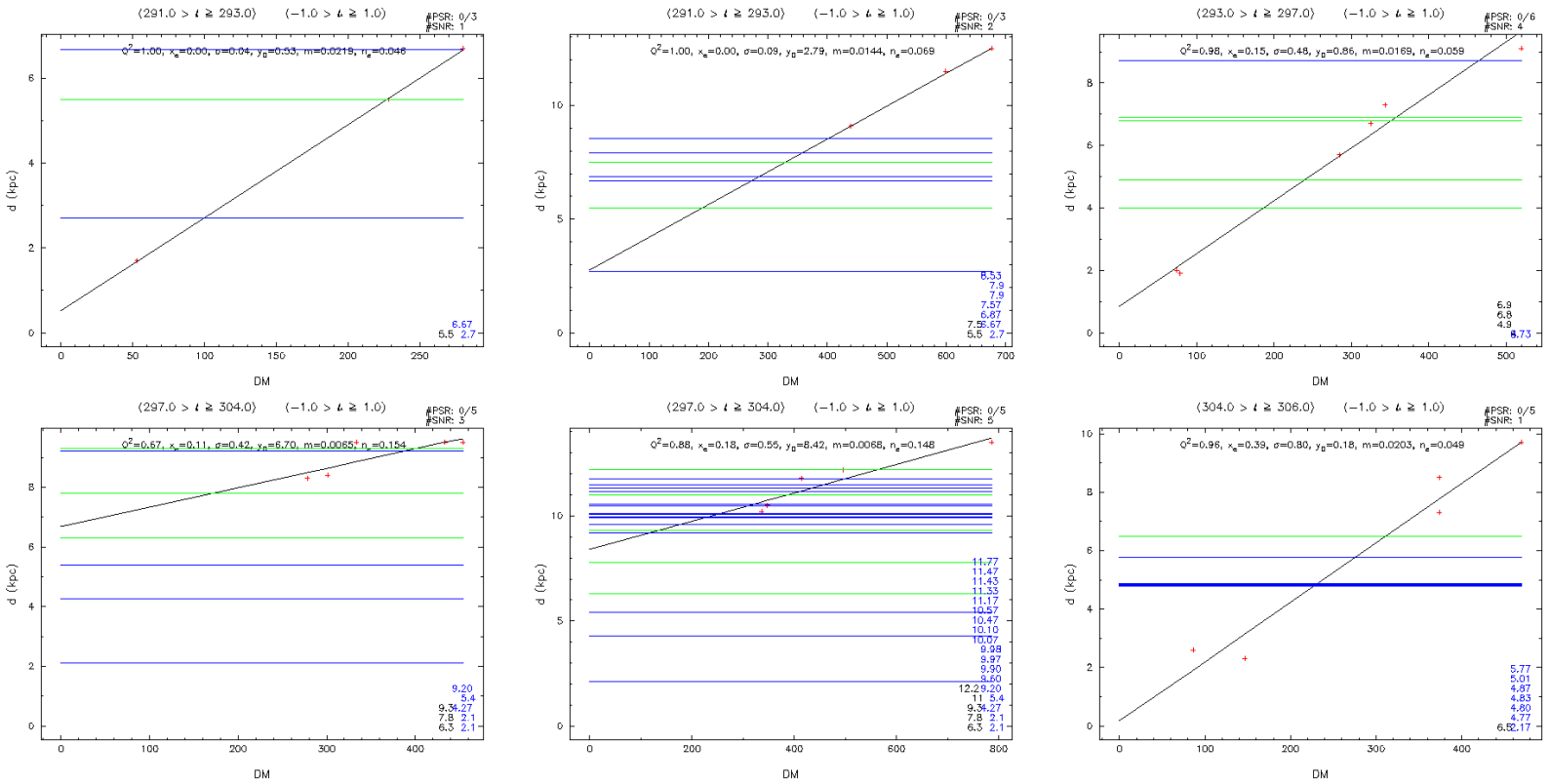

Figure A.10. Latitude Range: (-1.0), (+1.0) – *continued*

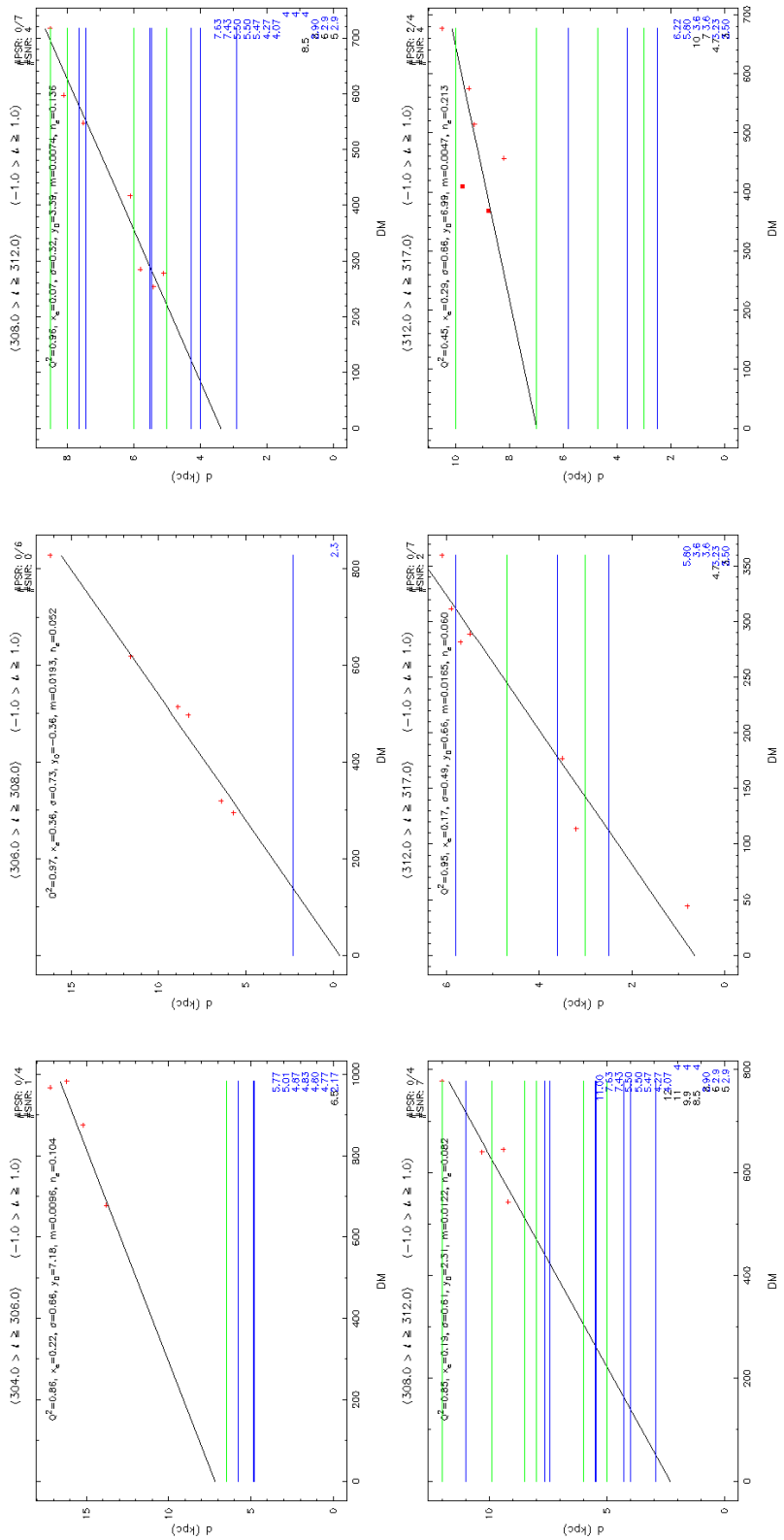

Figure A.11. Latitude Range: (-1.0), (+1.0) – *continued*

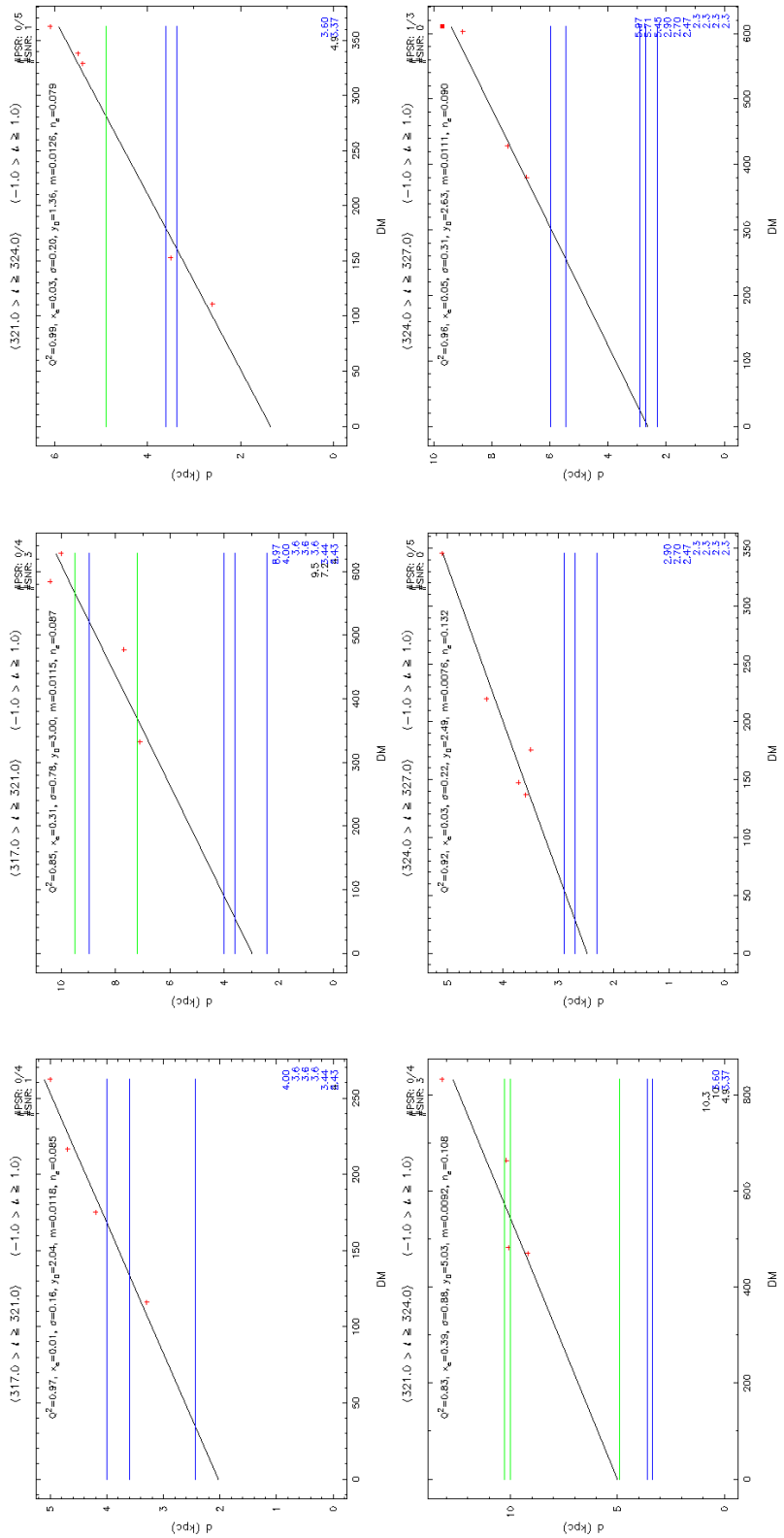

Figure A.12. Latitude Range: (-1.0), (+1.0) – *continued*

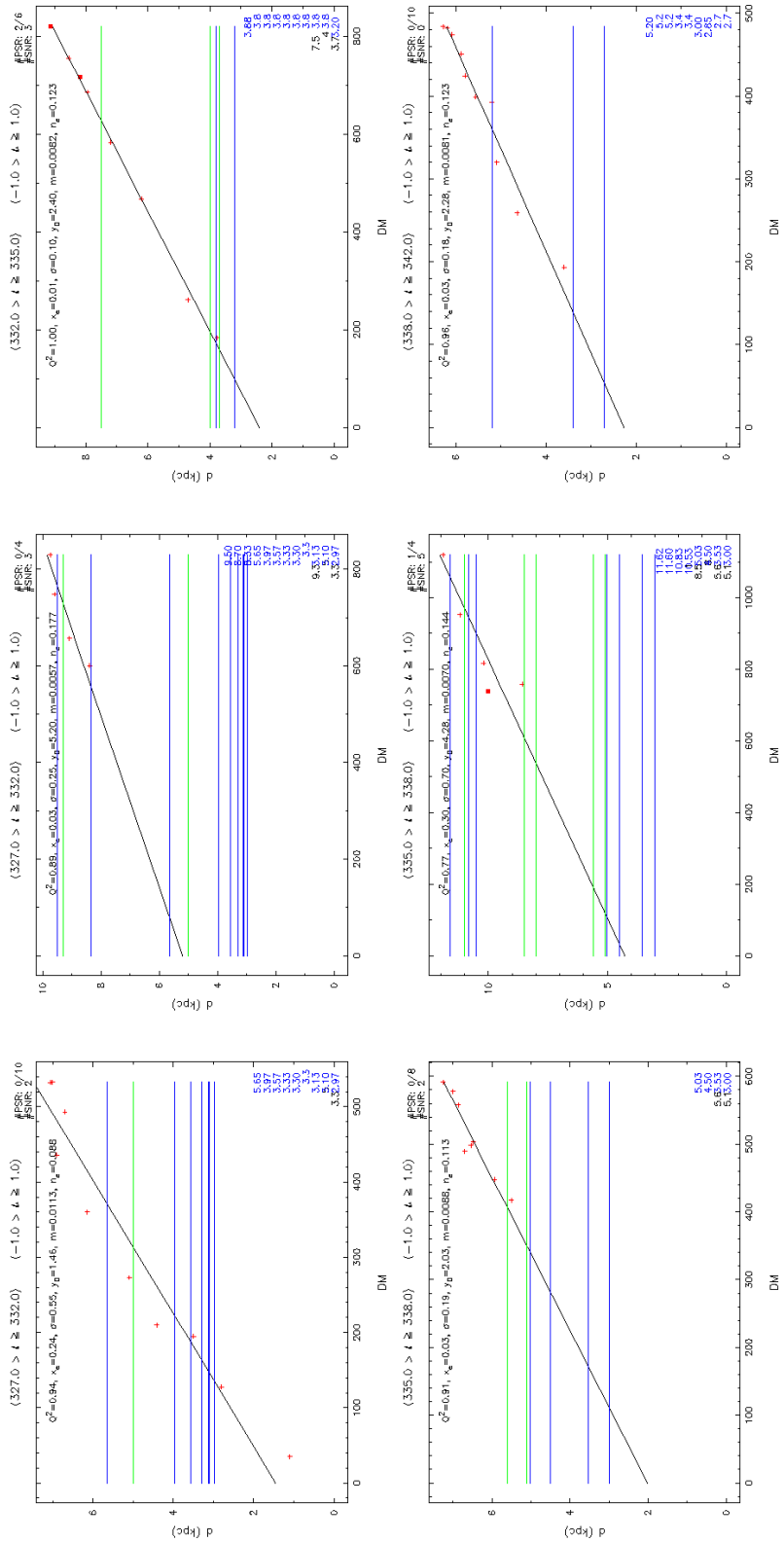

Figure A.13. Latitude Range: (-1.0), (+1.0) – *continued*

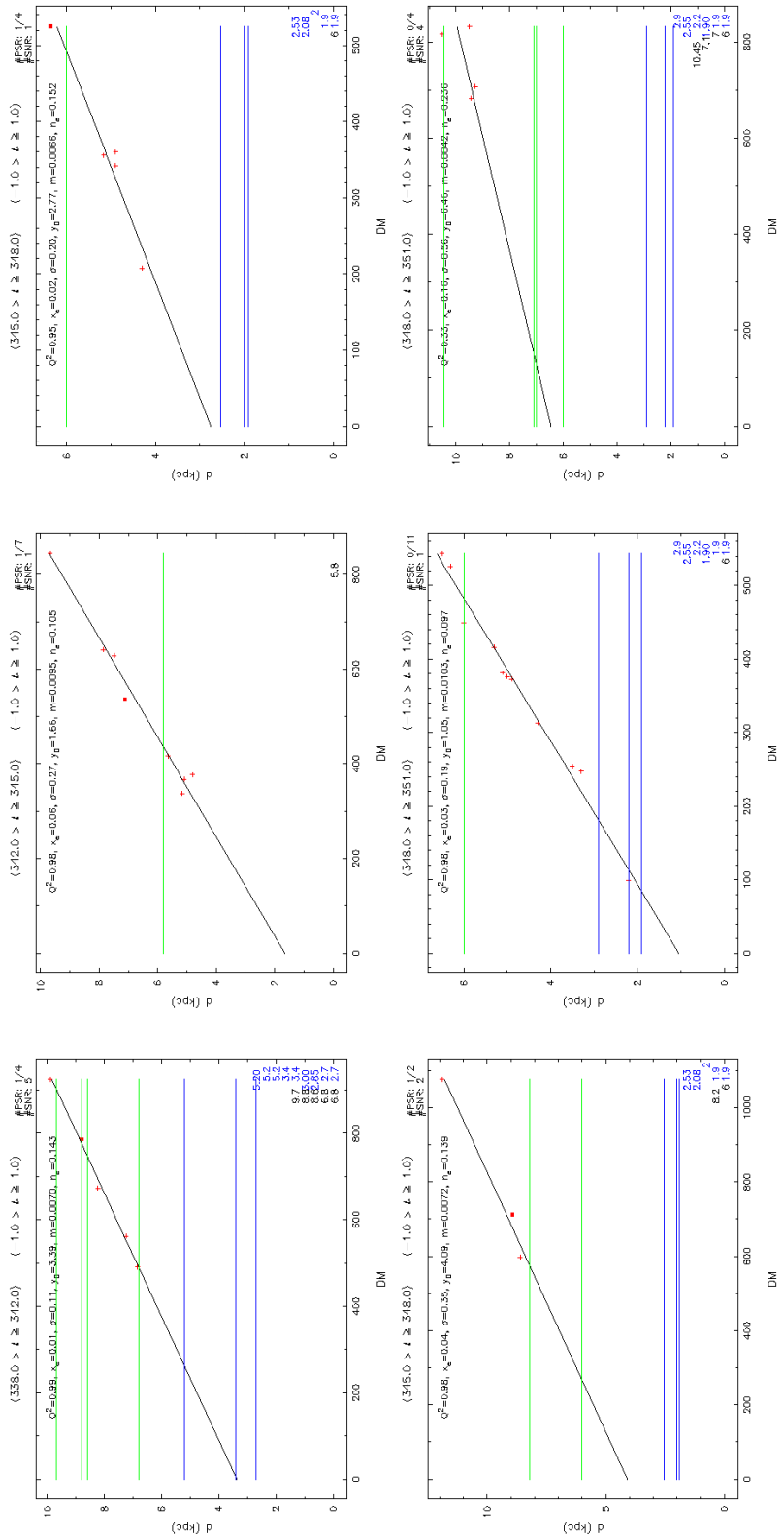

Figure A.14. Latitude Range: (-1.0), (+1.0) – *continued*

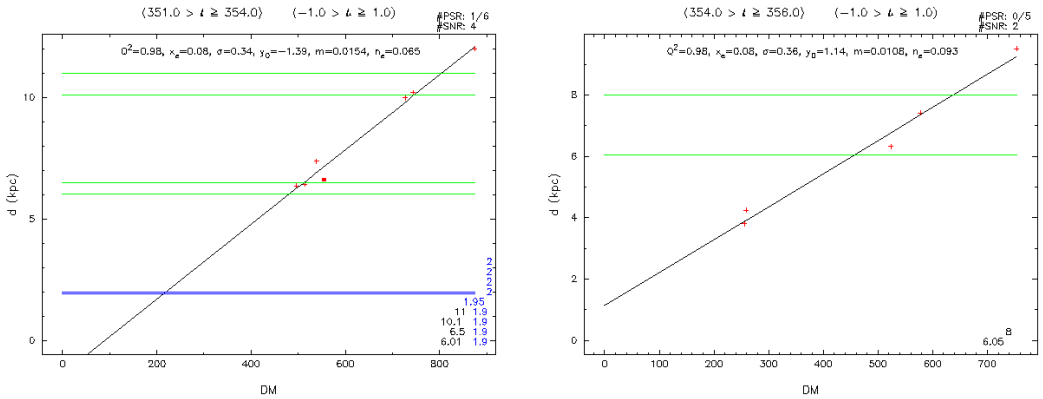

Figure A.15. Latitude Range: (-1.0), (+1.0)

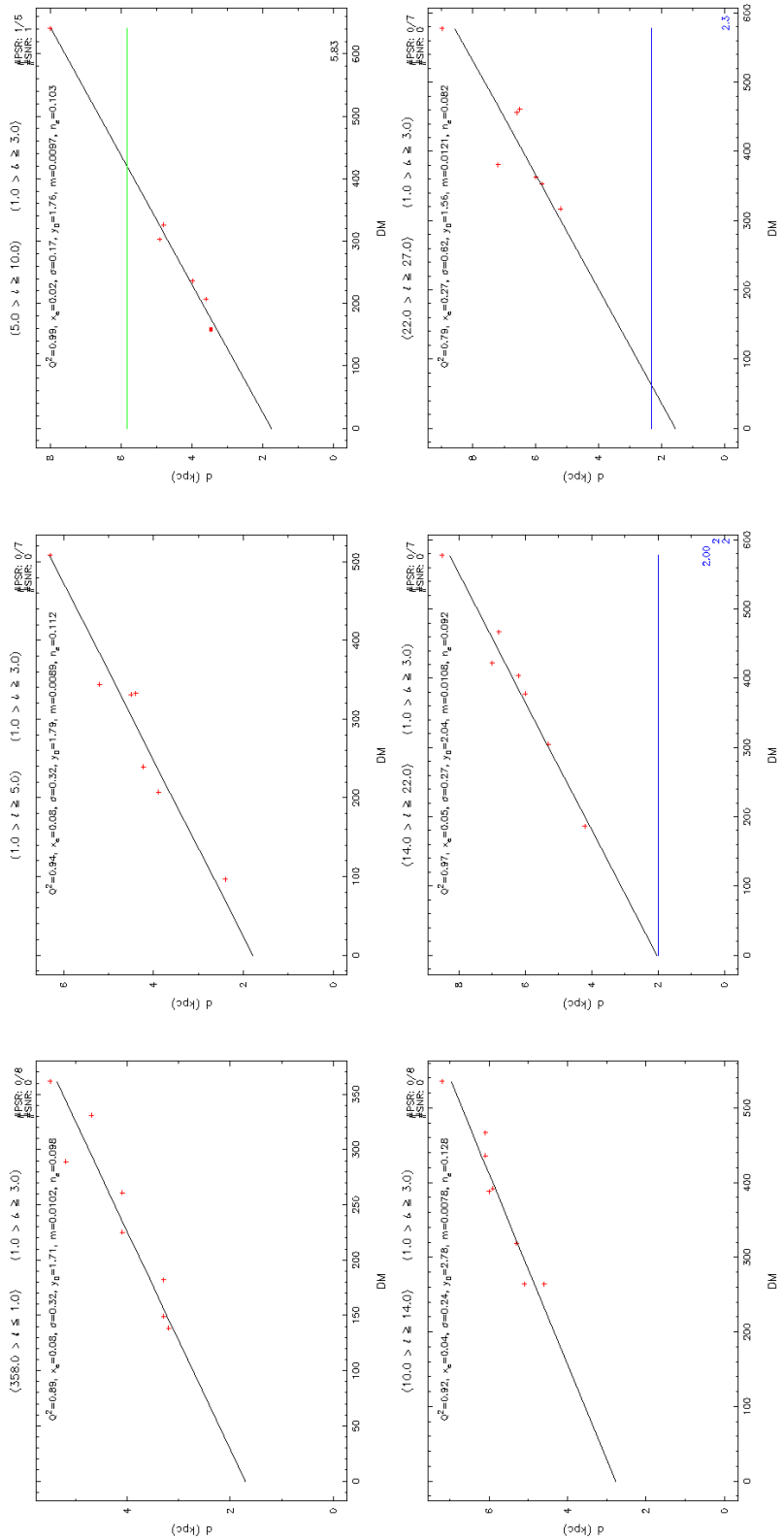

Figure A.16. Latitude Range: (+1.0), (+3.0)

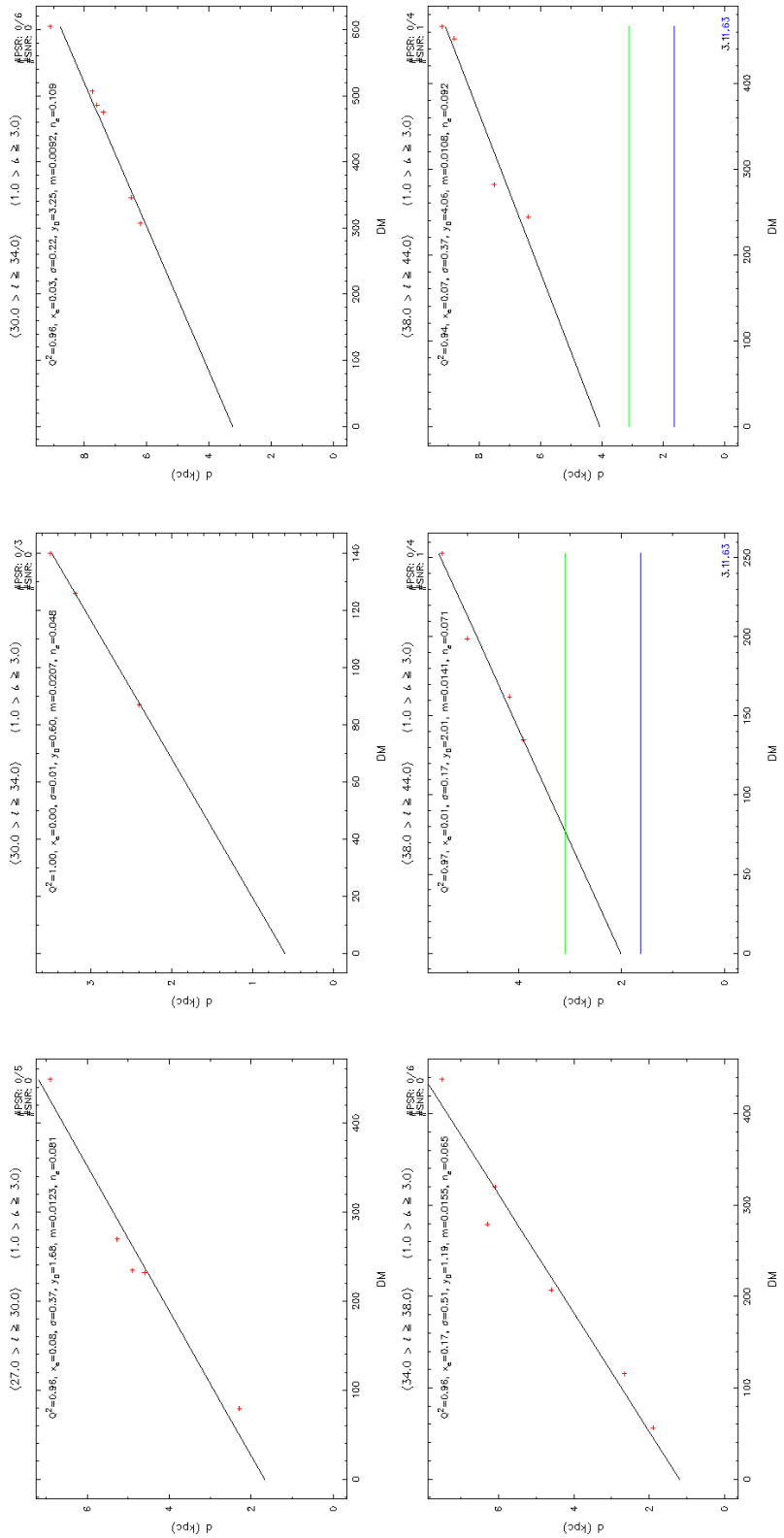

Figure A.17. Latitude Range: (+1.0), (+3.0) – *continued*

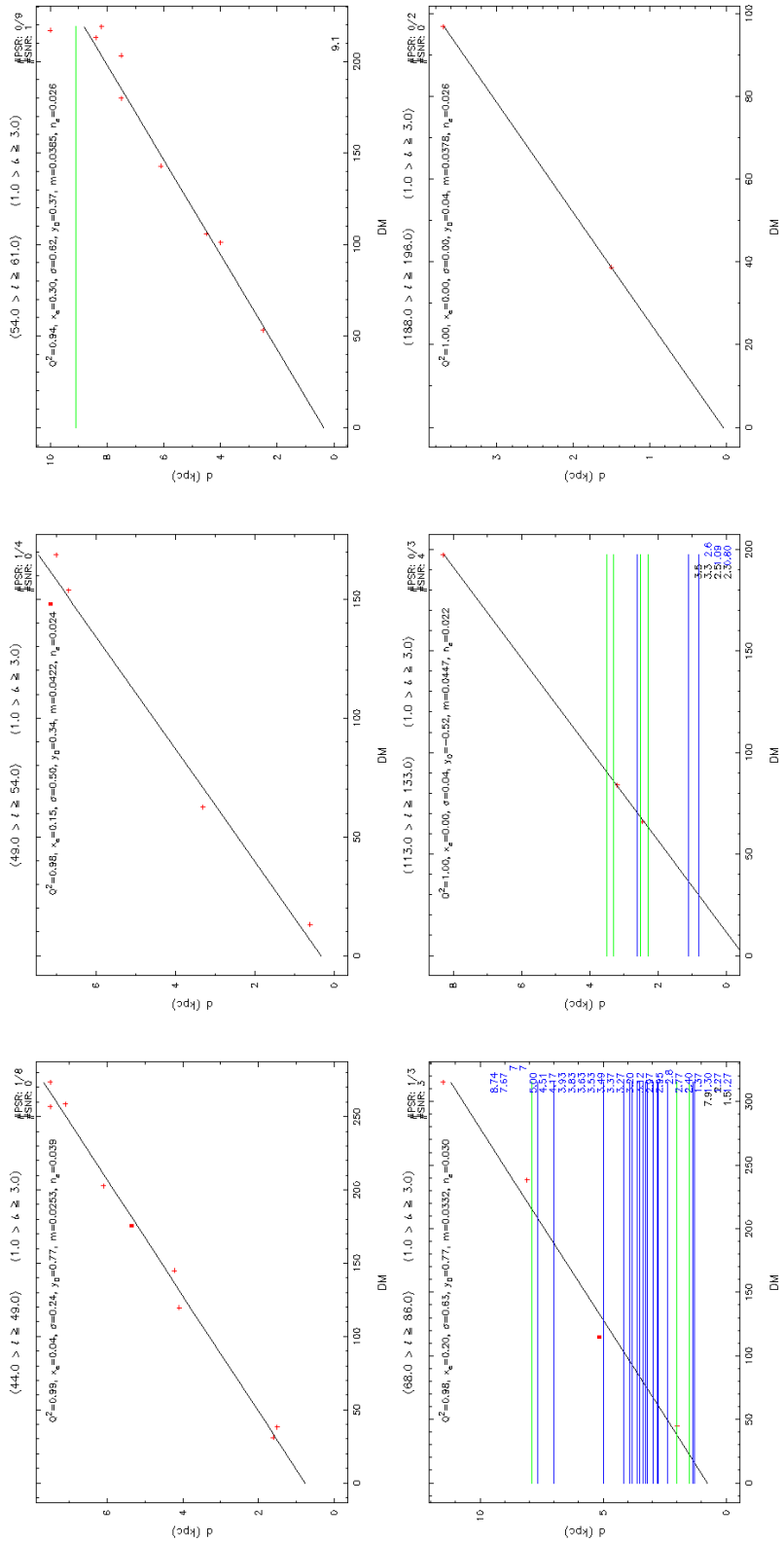

Figure A.18. Latitude Range: (+1.0), (+3.0) – *continued*

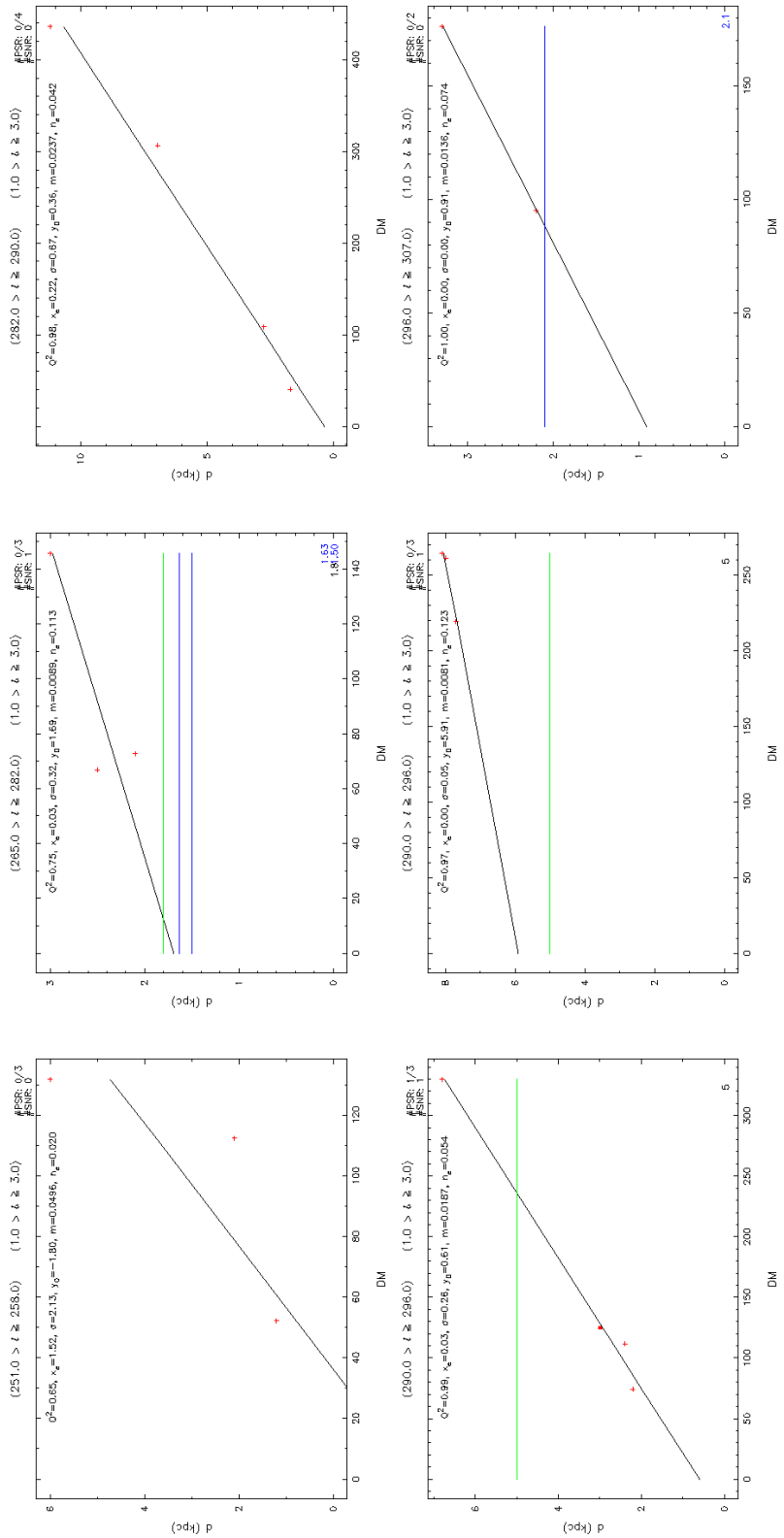

Figure A.19. Latitude Range: (+1.0), (+3.0) – *continued*

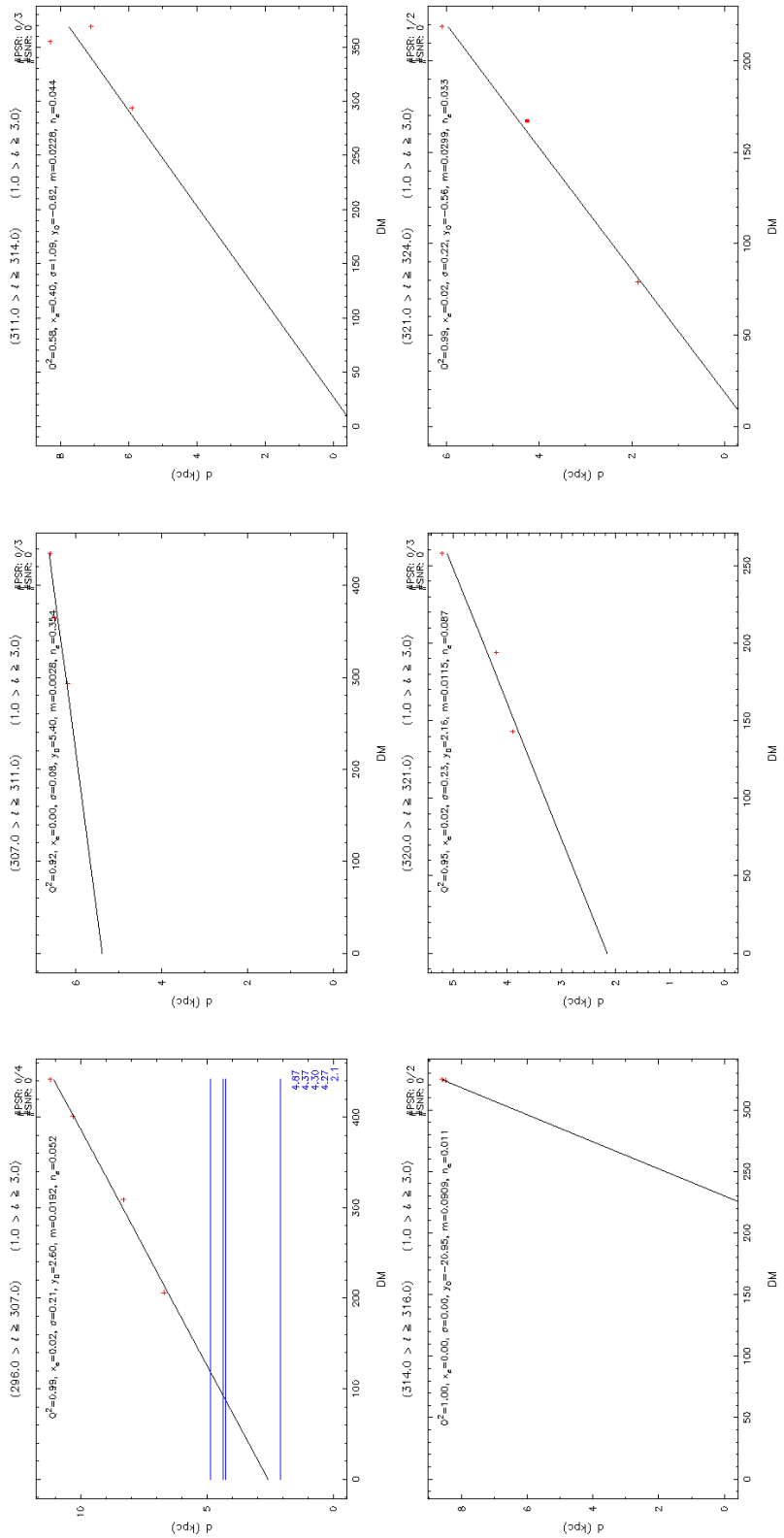

Figure A.20. Latitude Range: (+1.0), (+3.0) – *continued*

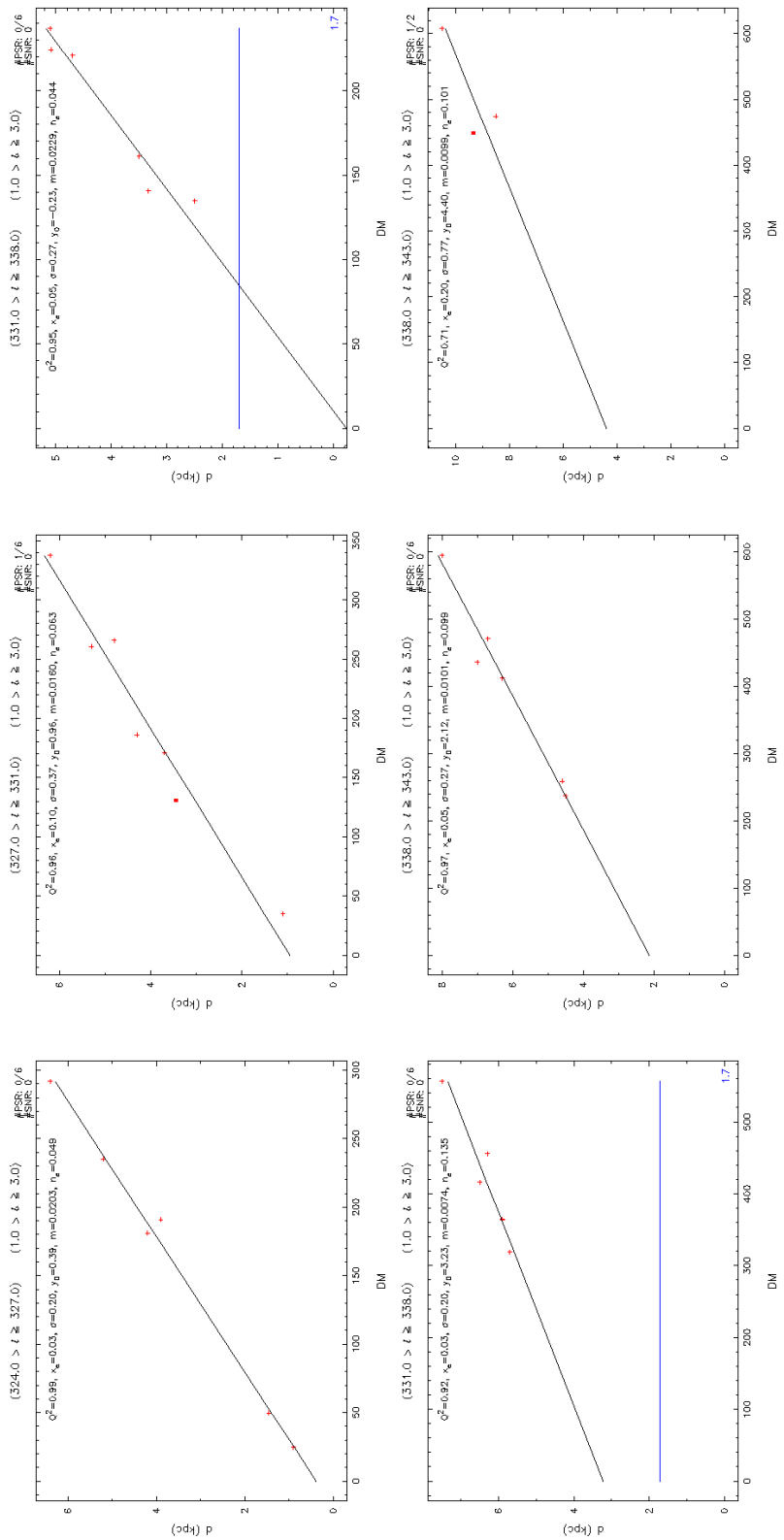

Figure A.21. Latitude Range: (+1.0), (+3.0) – *continued*

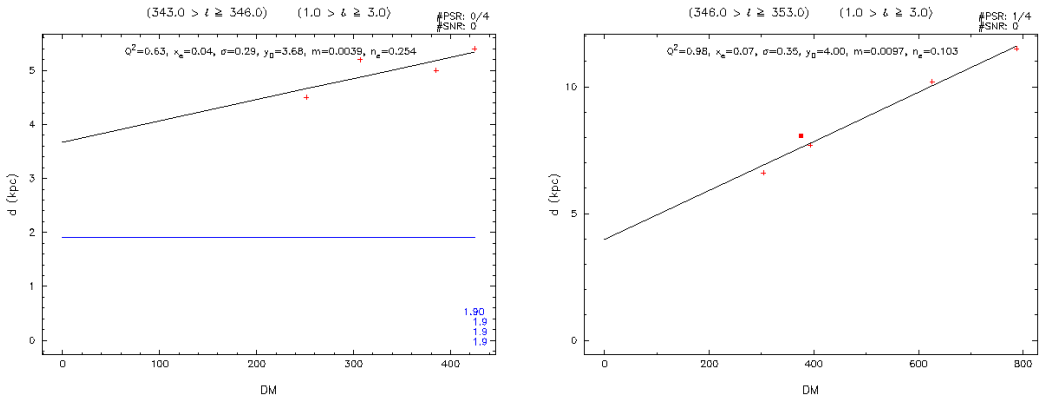

Figure A.22. Latitude Range: (+1.0), (+3.0)

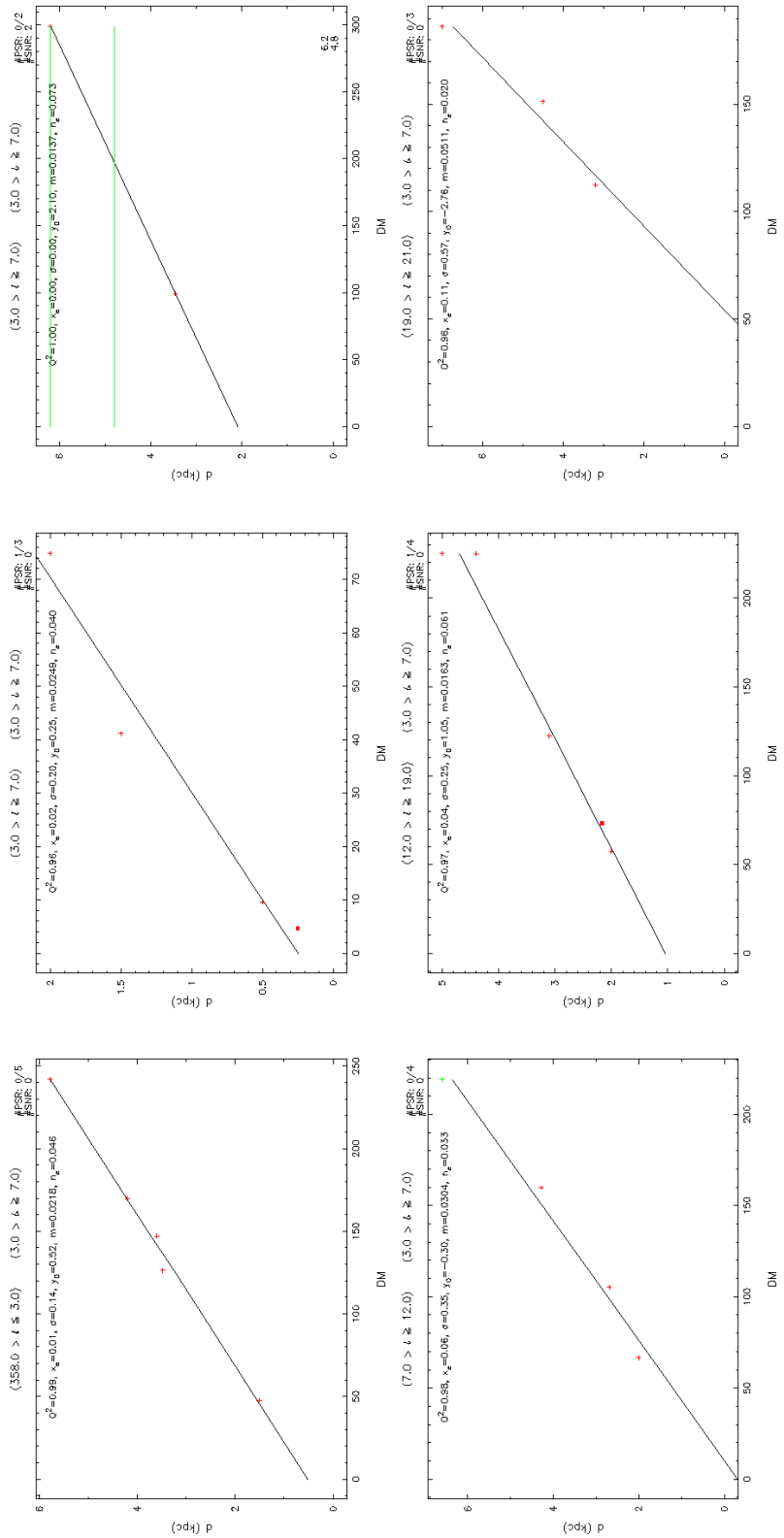

Figure A.23. Latitude Range: (+3.0), (+7.0)

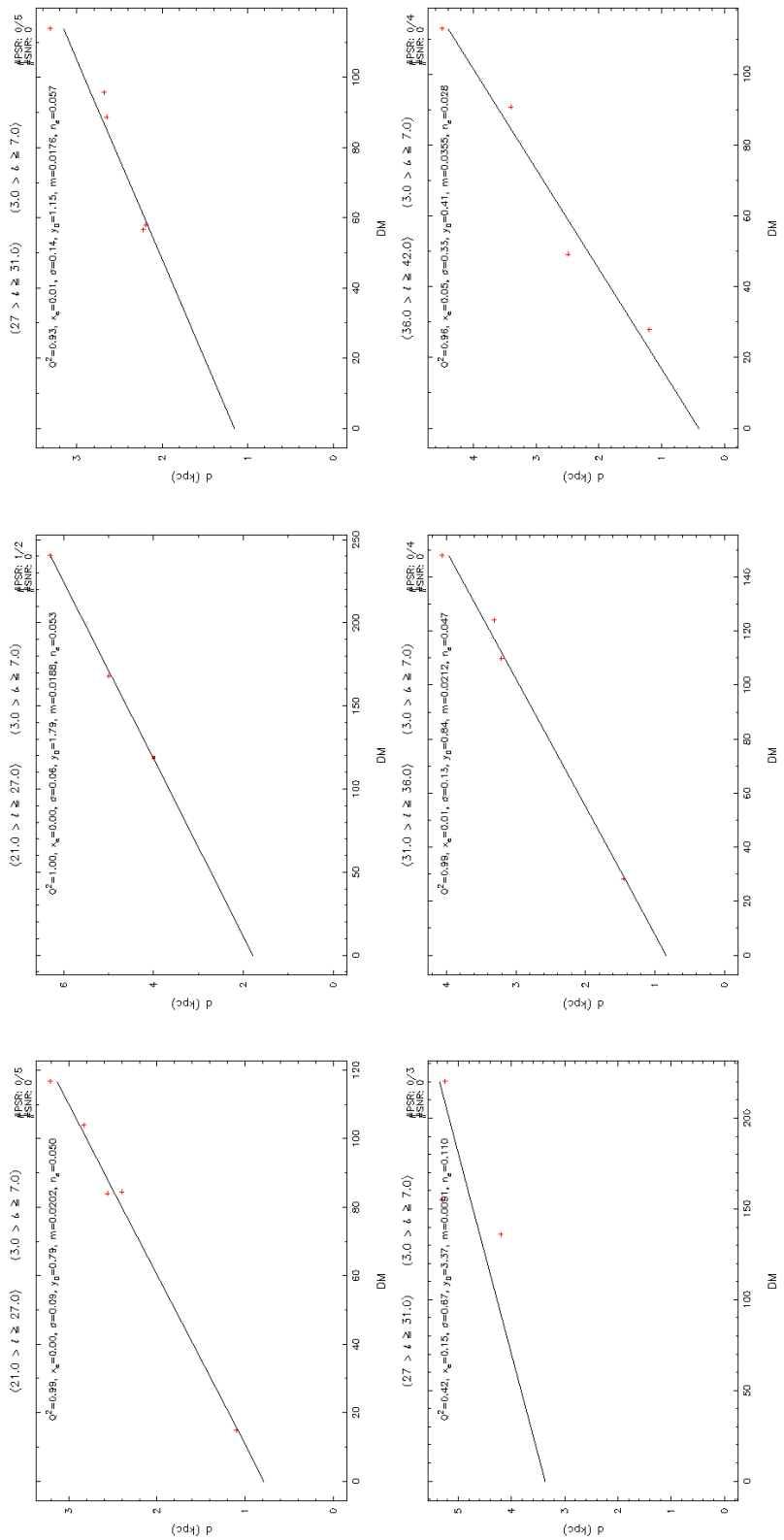

Figure A.24. Latitude Range: (+3.0), (+7.0) – *continued*

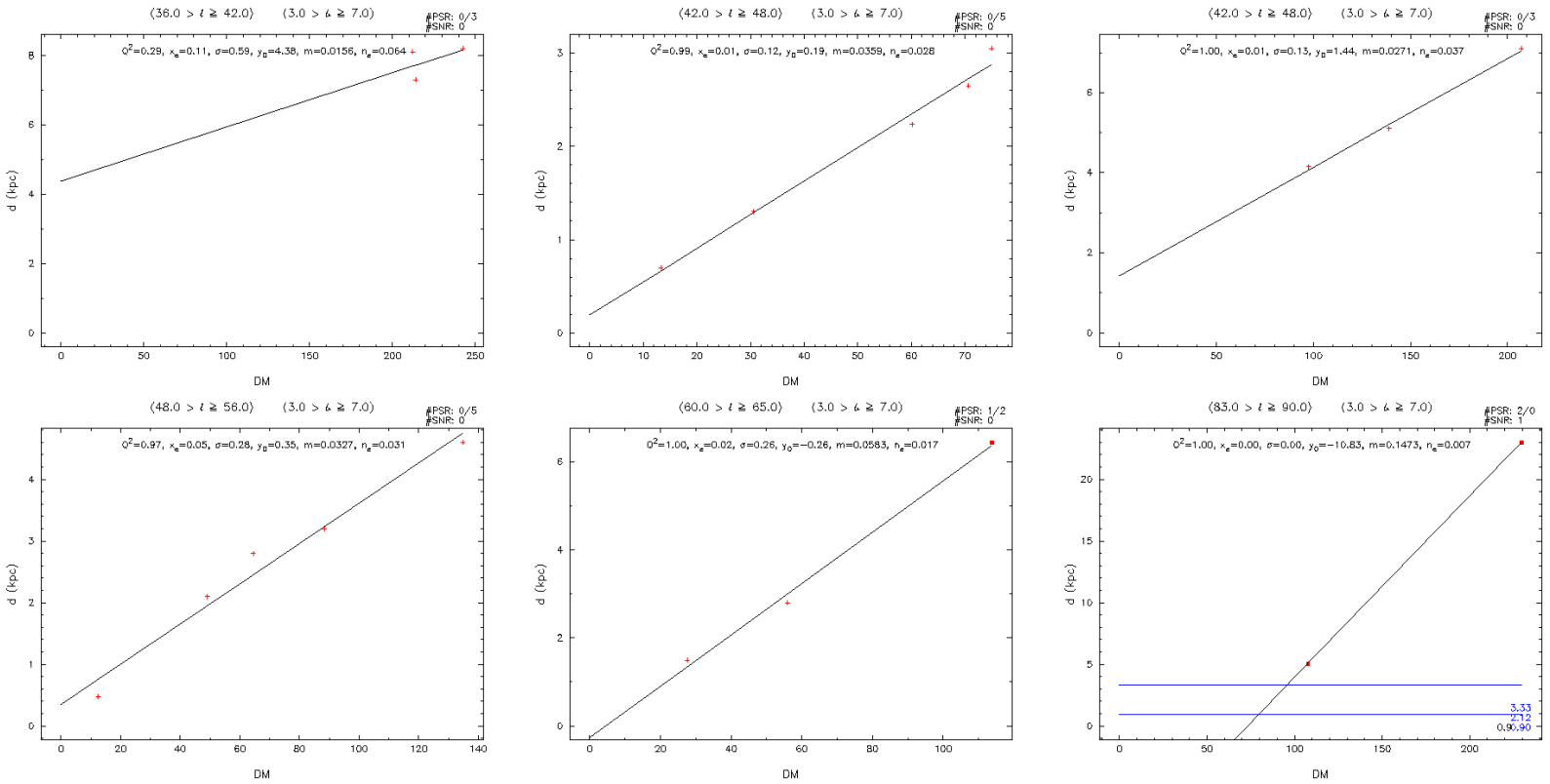

Figure A.25. Latitude Range: (+3.0), (+7.0) – *continued*

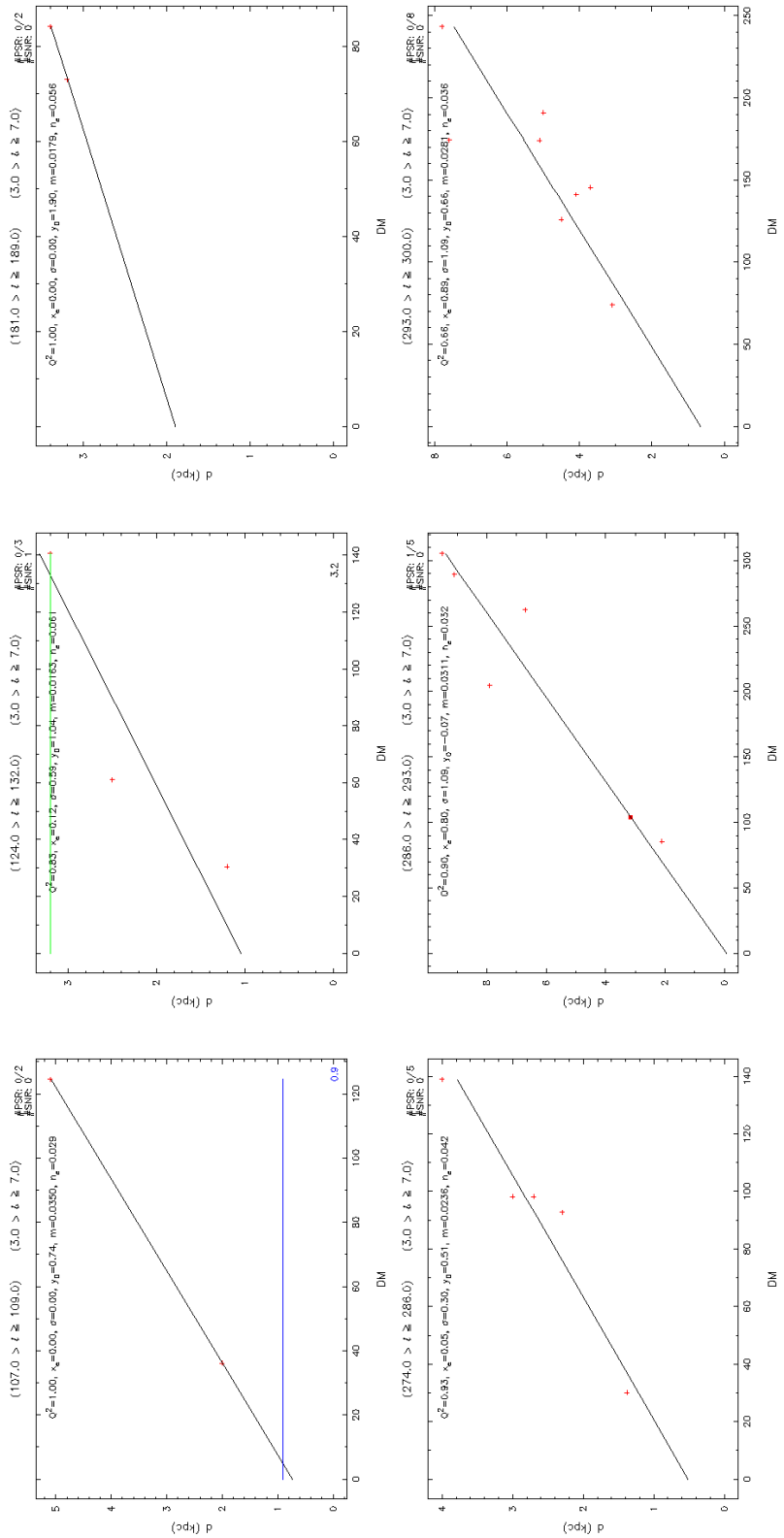

Figure A.26. Latitude Range: (+3.0), (+7.0) – *continued*

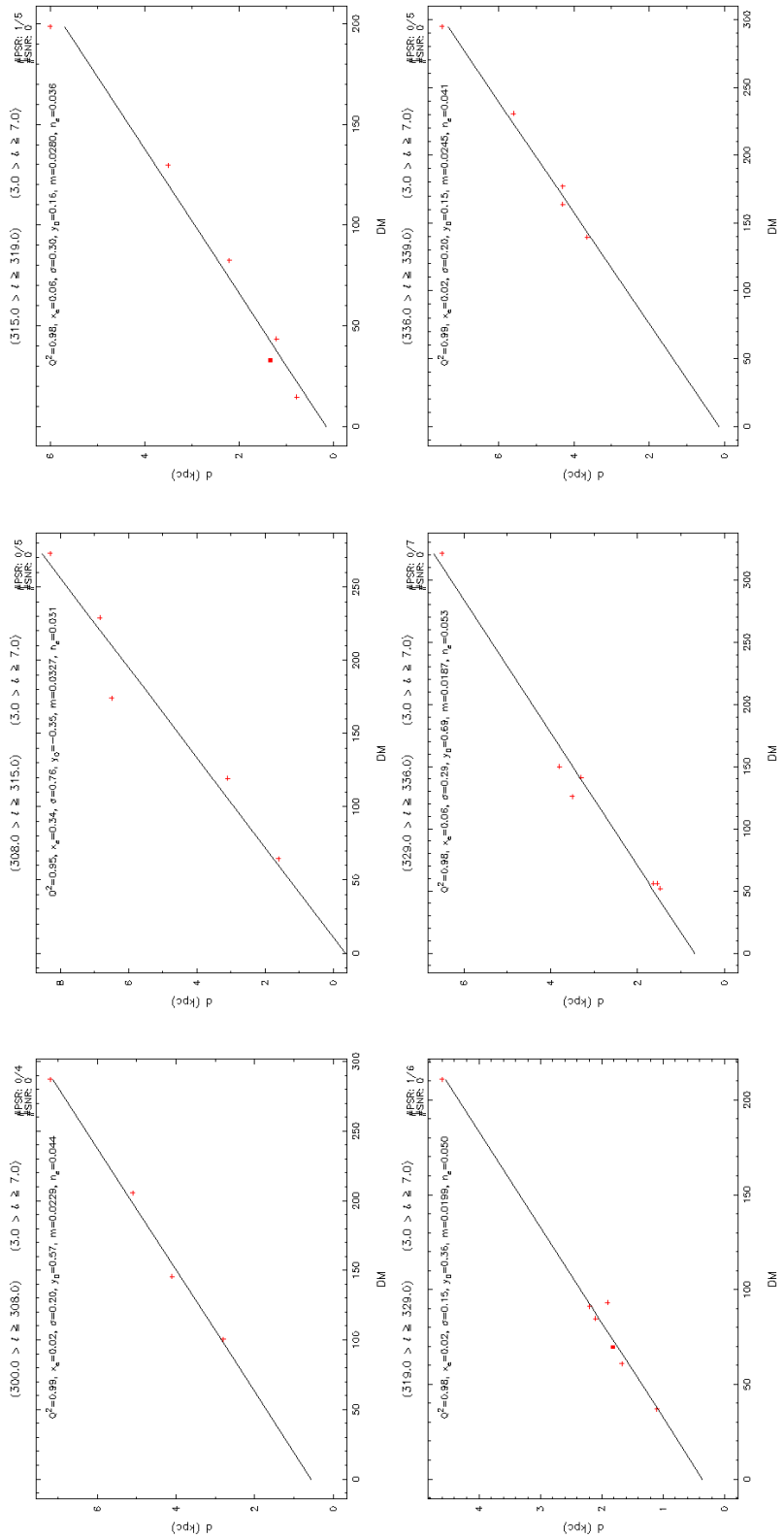

Figure A.27. Latitude Range: (+3.0), (+7.0) – *continued*

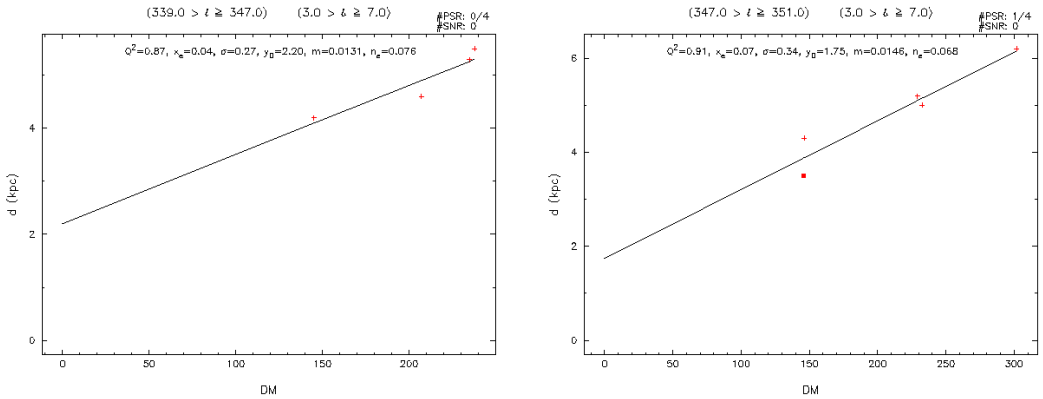

Figure A.28. Latitude Range: (+3.0), (+7.0)

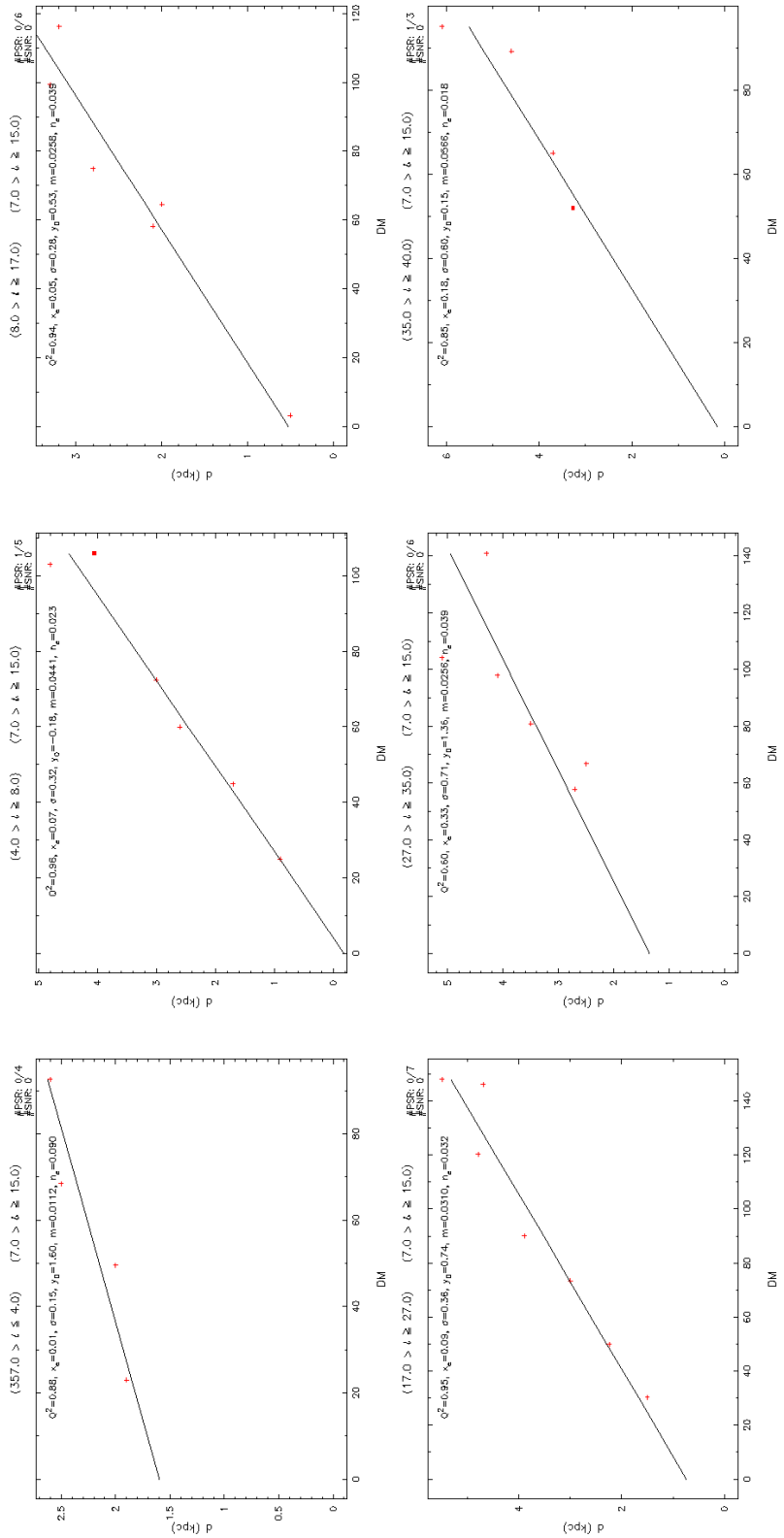

Figure A.29. Latitude Range: (+7.0), (+15.0)

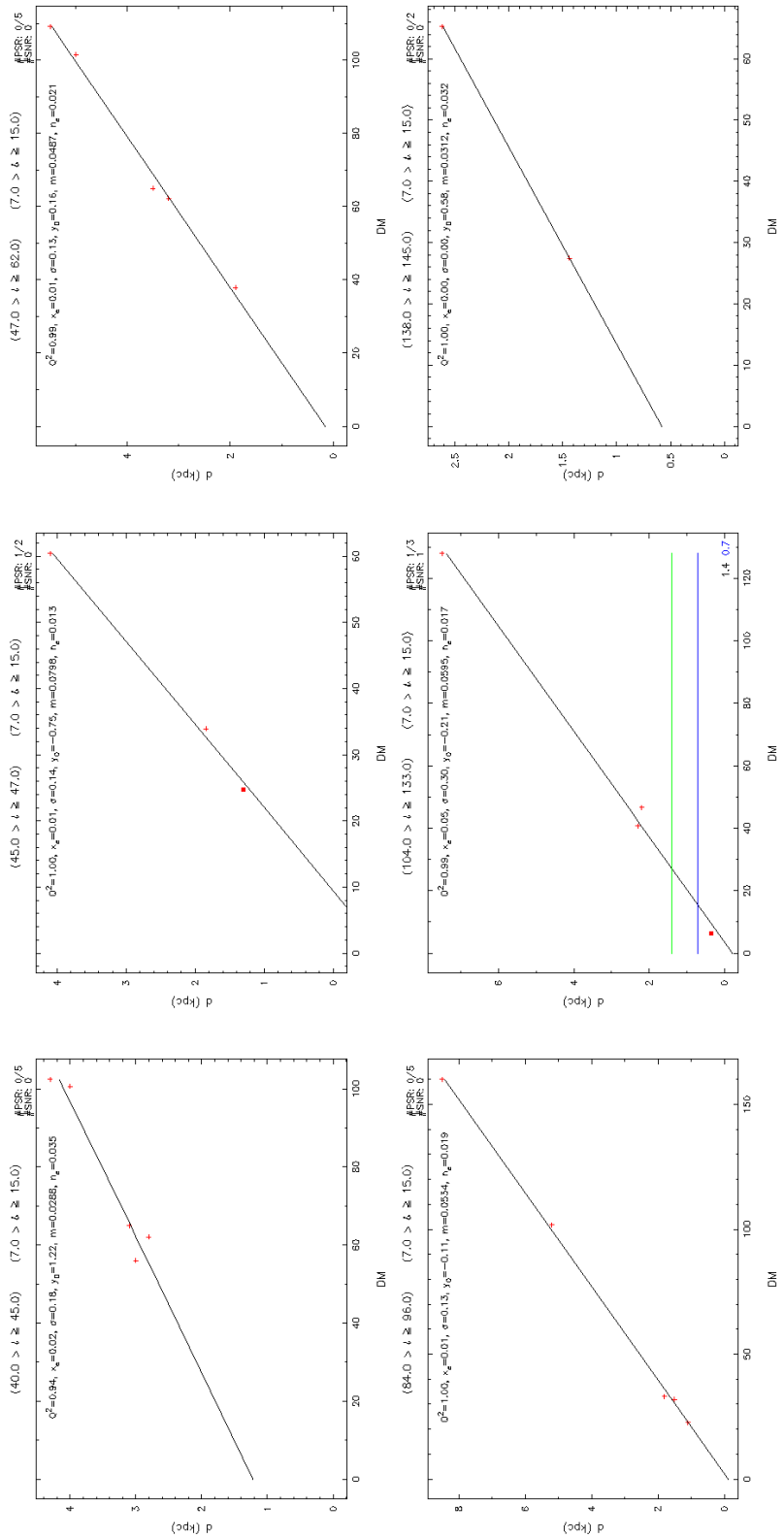

Figure A.30. Latitude Range: (+7.0), (+15.0) – *continued*

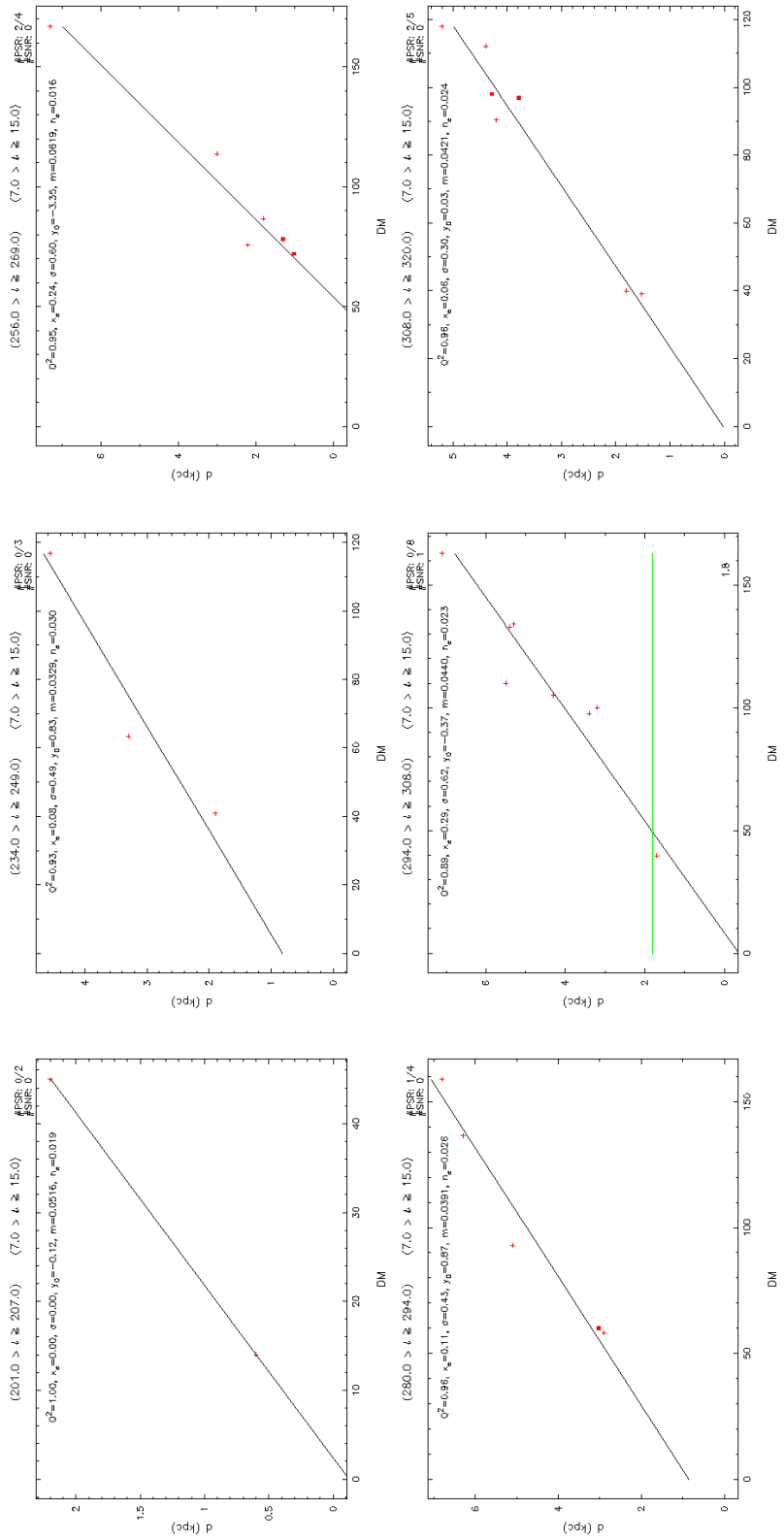

Figure A.31. Latitude Range: (+7.0), (+15.0) – *continued*

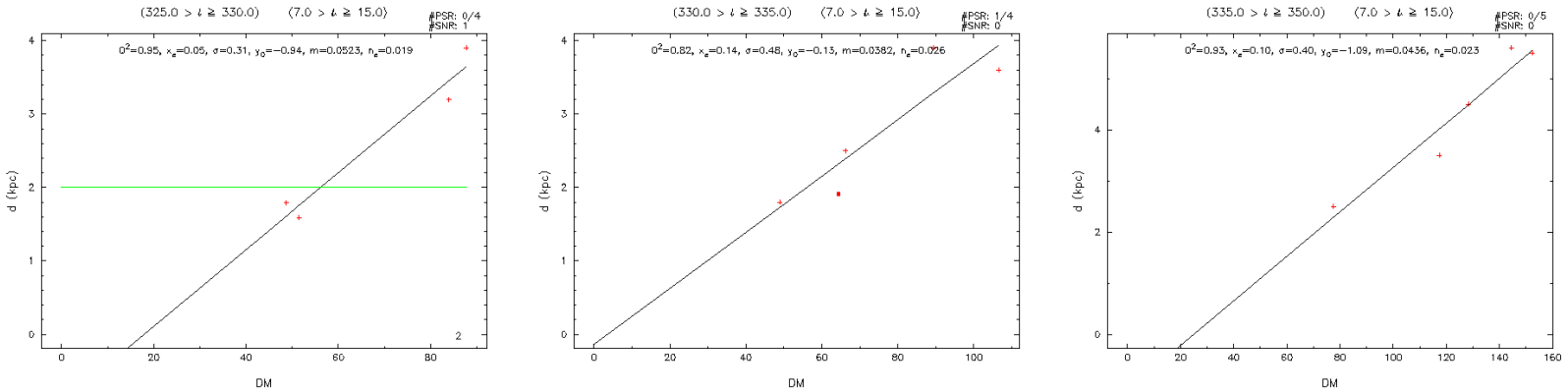

Figure A.32. Latitude Range: (+7.0), (+15.0)

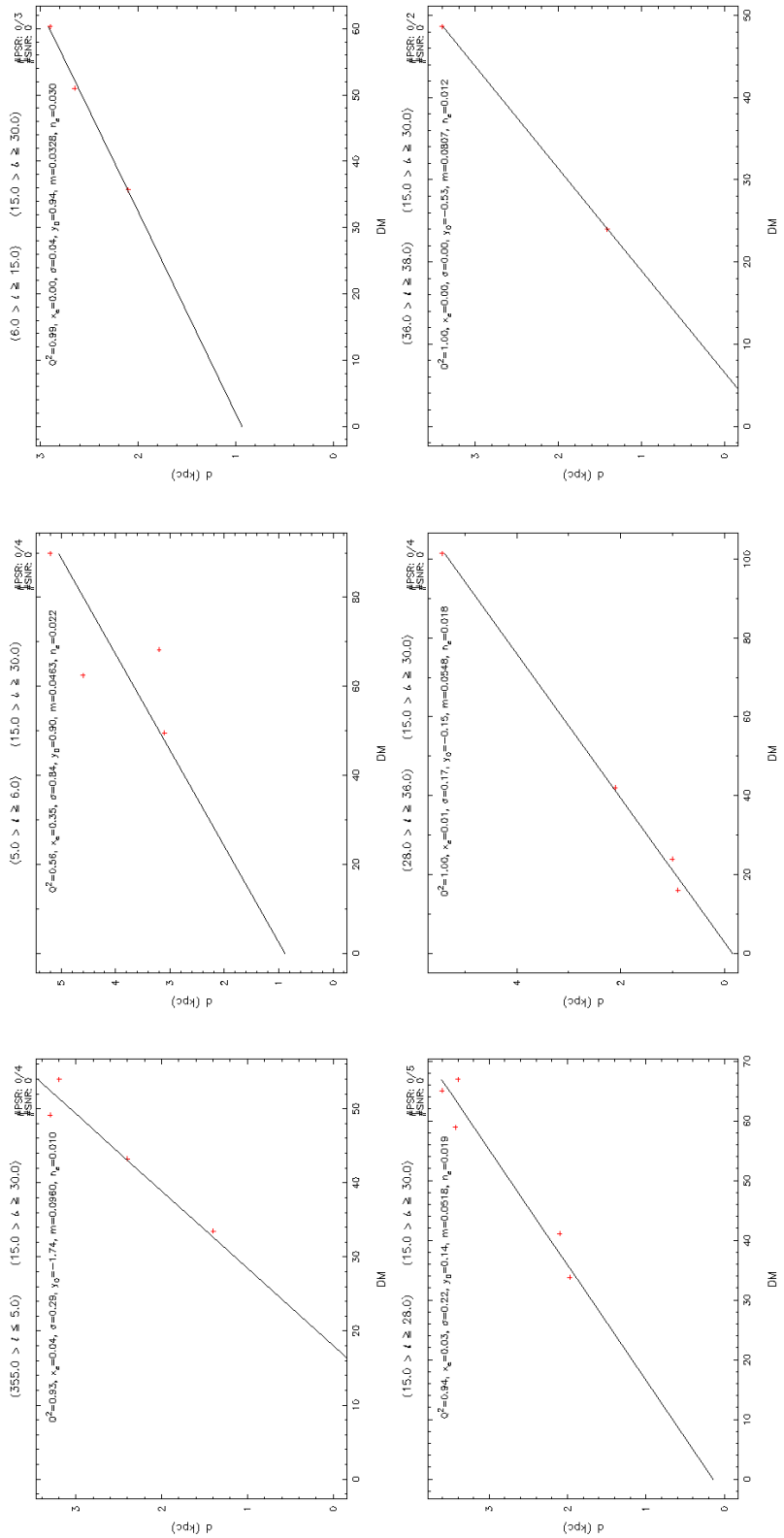

Figure A.33. Latitude Range: (+15.0), (+30.0)

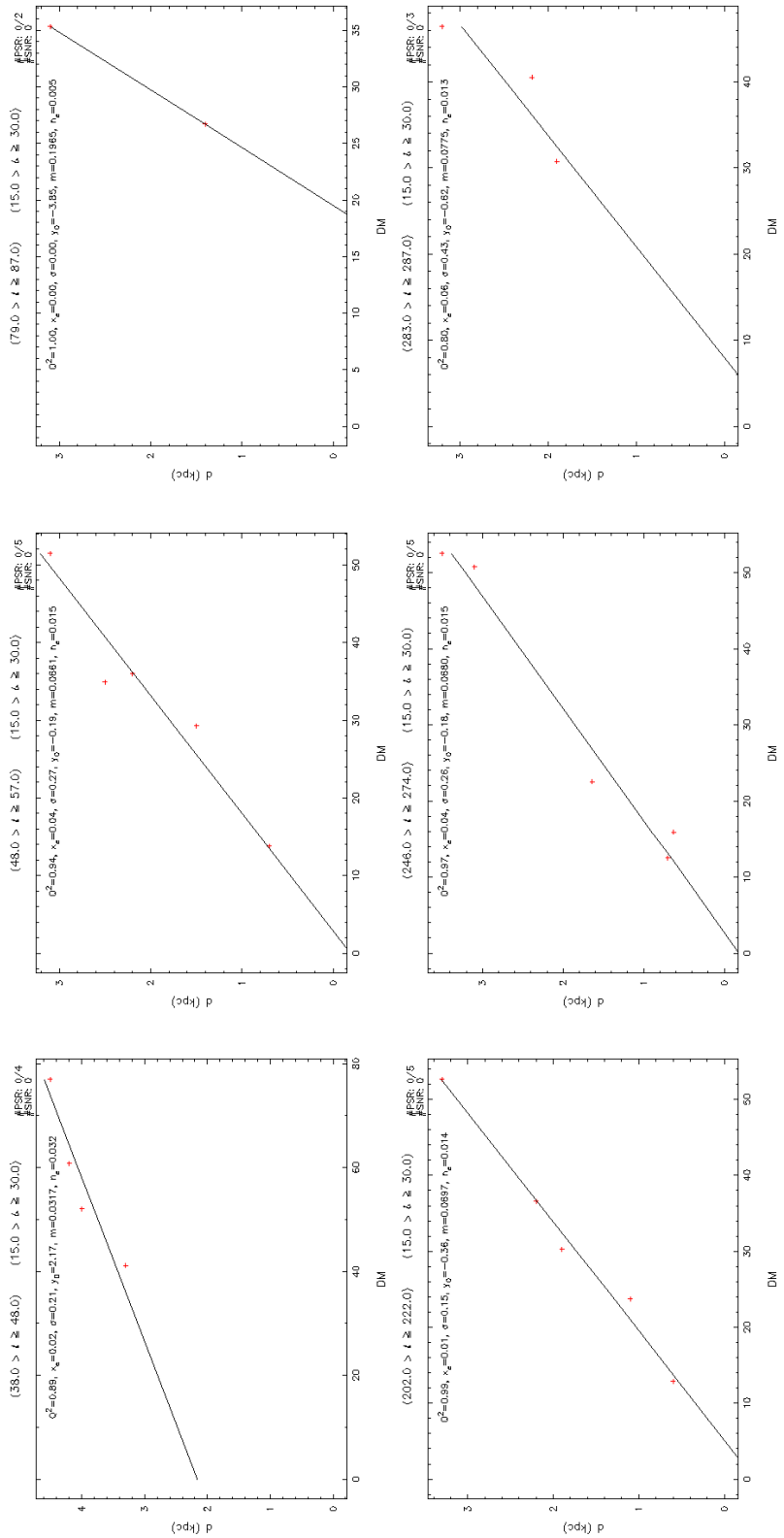

Figure A.34. Latitude Range: (+15.0), (+30.0) – *continued*

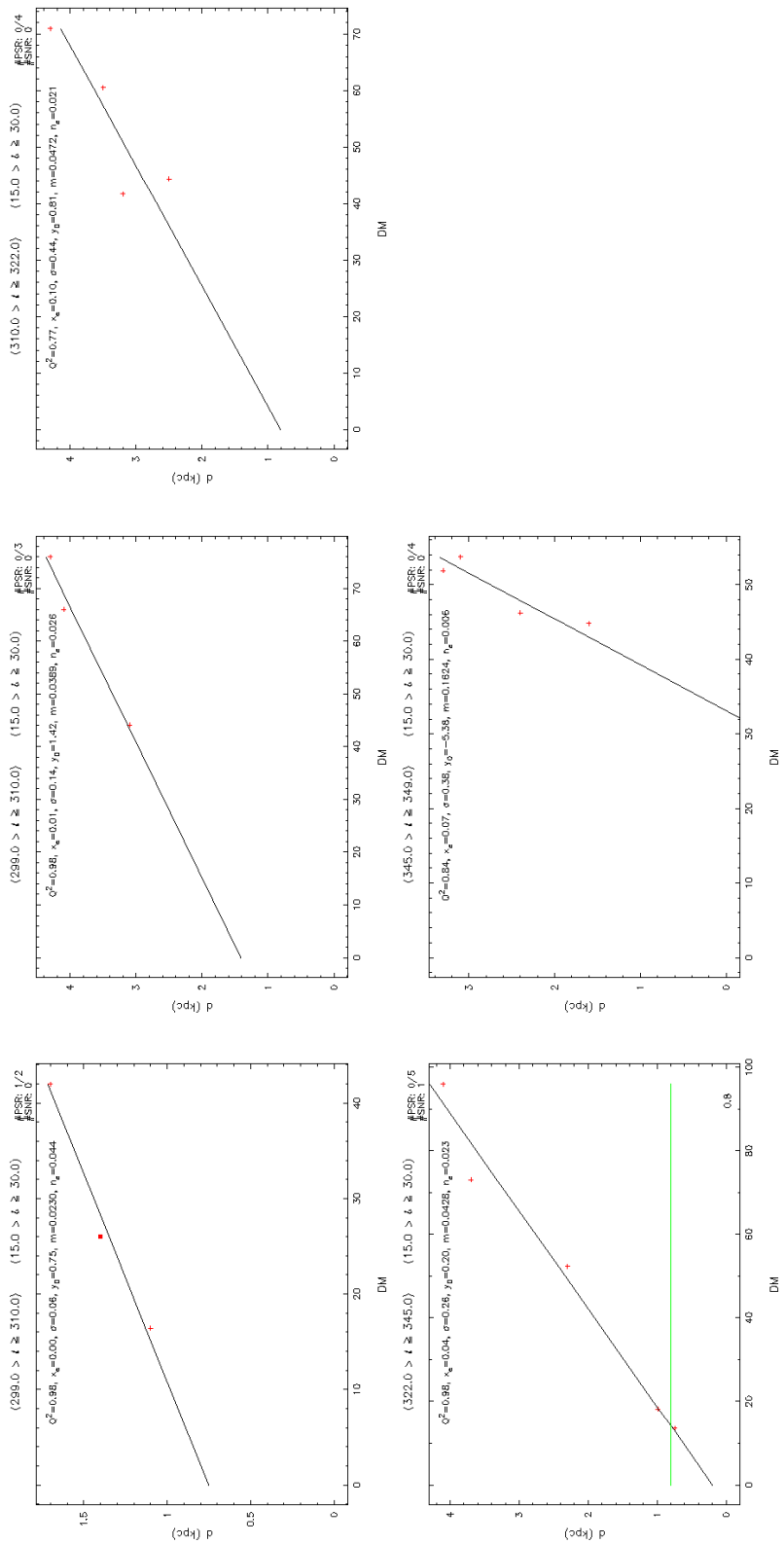

Figure A.35. Latitude Range: (+15.0), (+30.0)

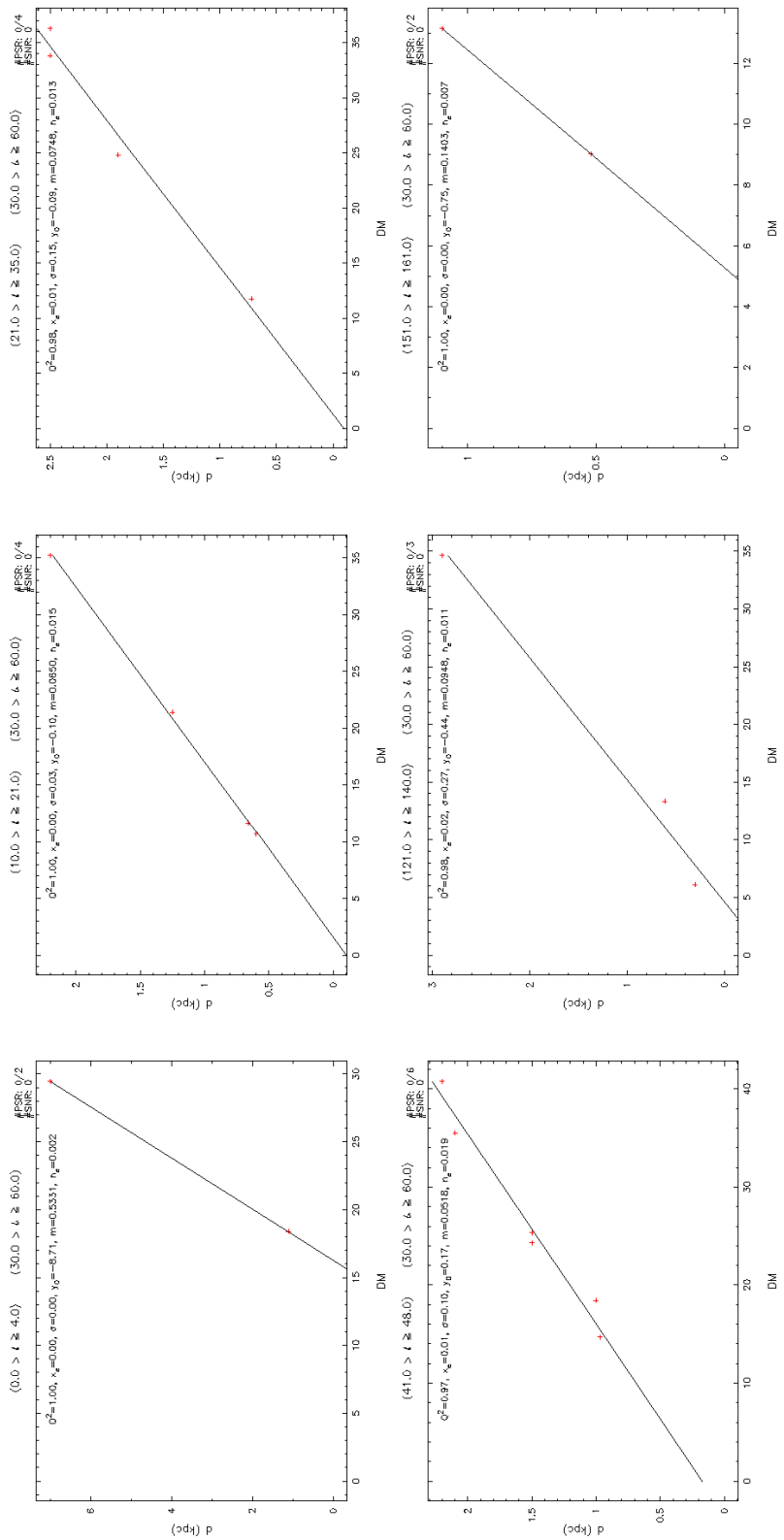

Figure A.36. Latitude Range: (+30.0), (+60.0)

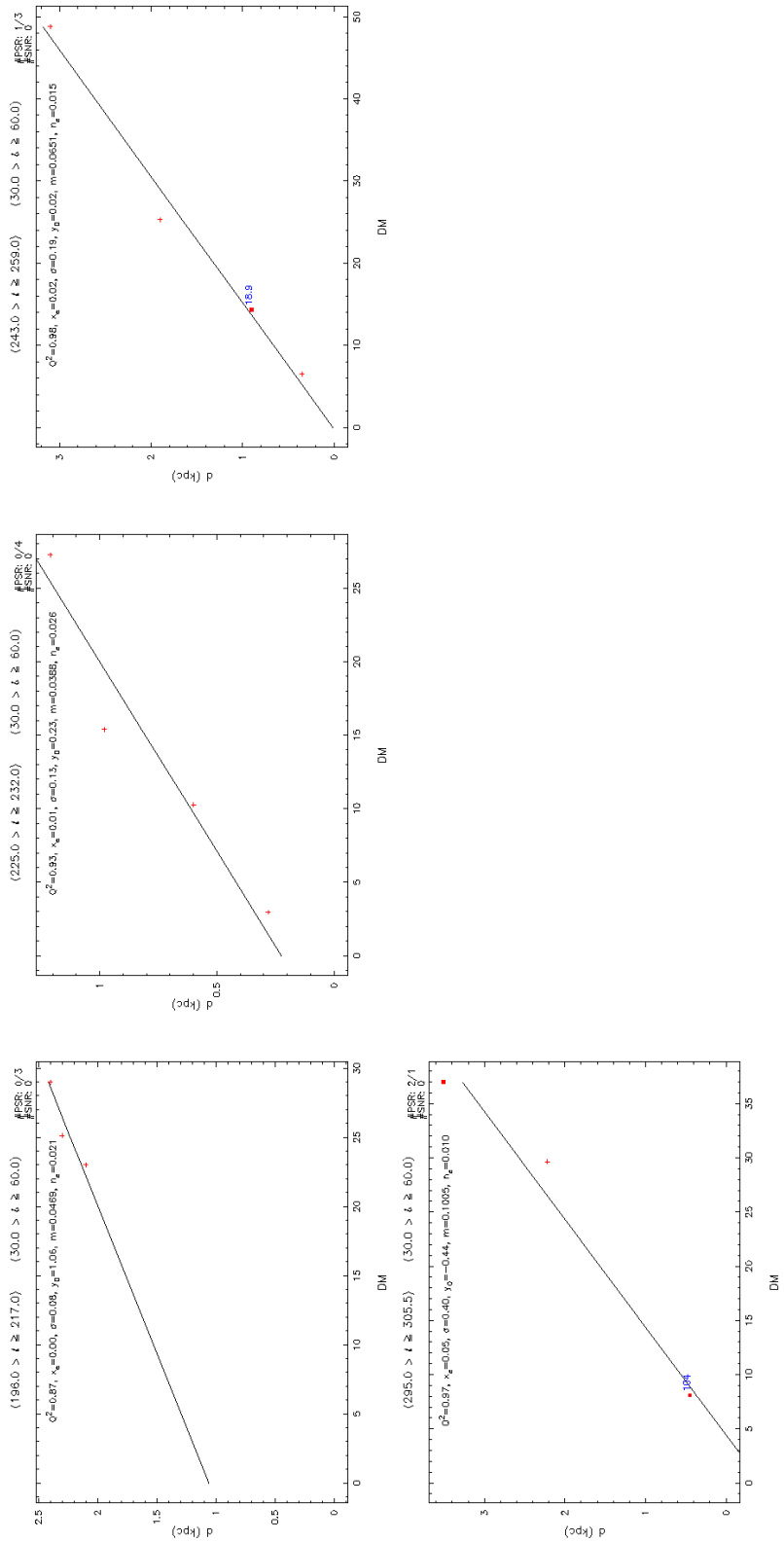

Figure A.37. Latitude Range: (+30.0), (+60.0)

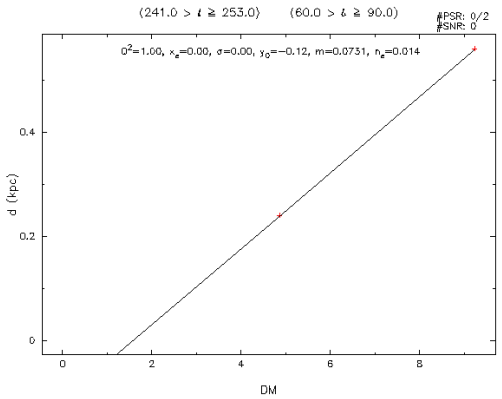

Figure A.38. Latitude Range: (+60.0), (+90.0)

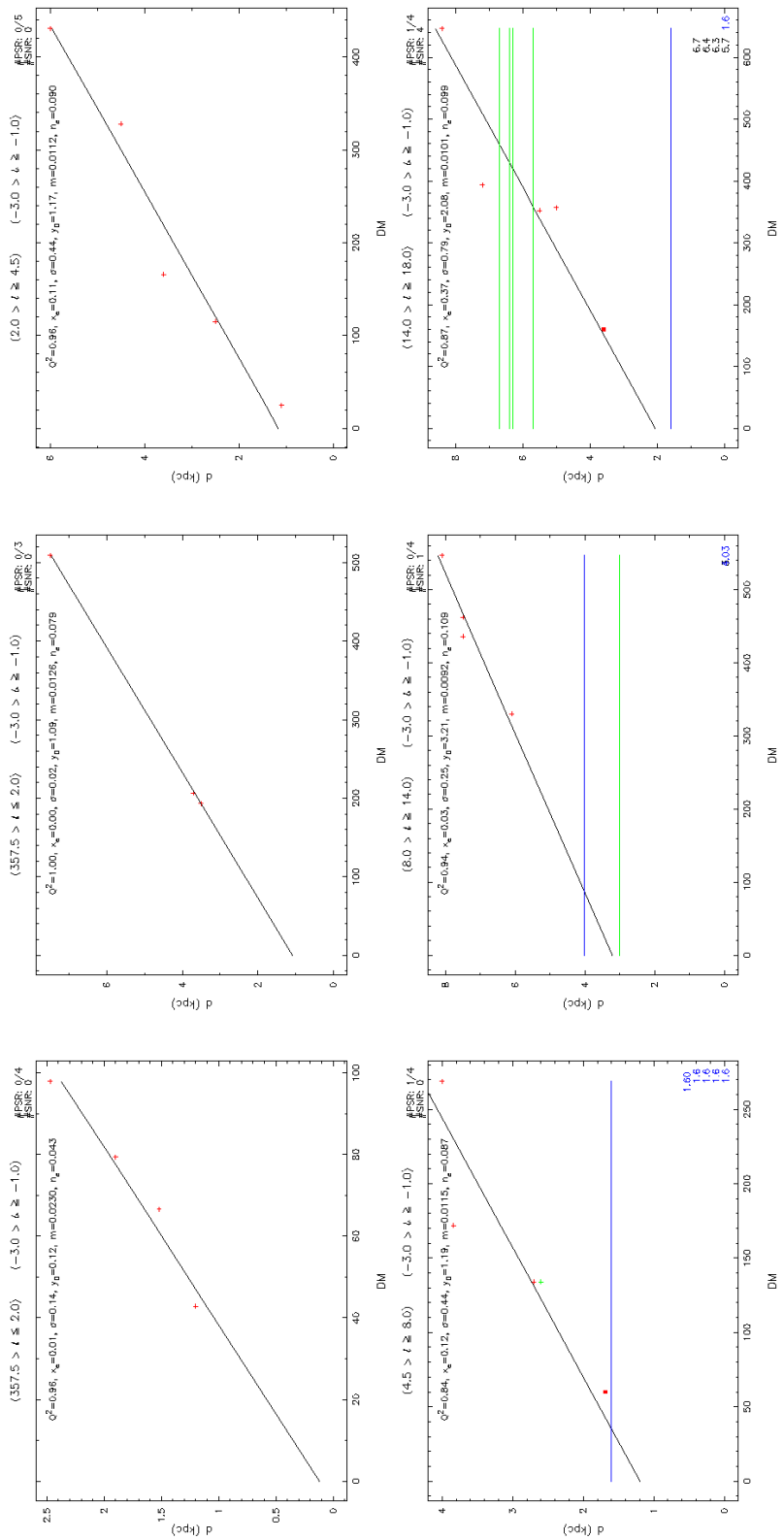

Figure A.39. Latitude Range: (-3.0), (-1.0)

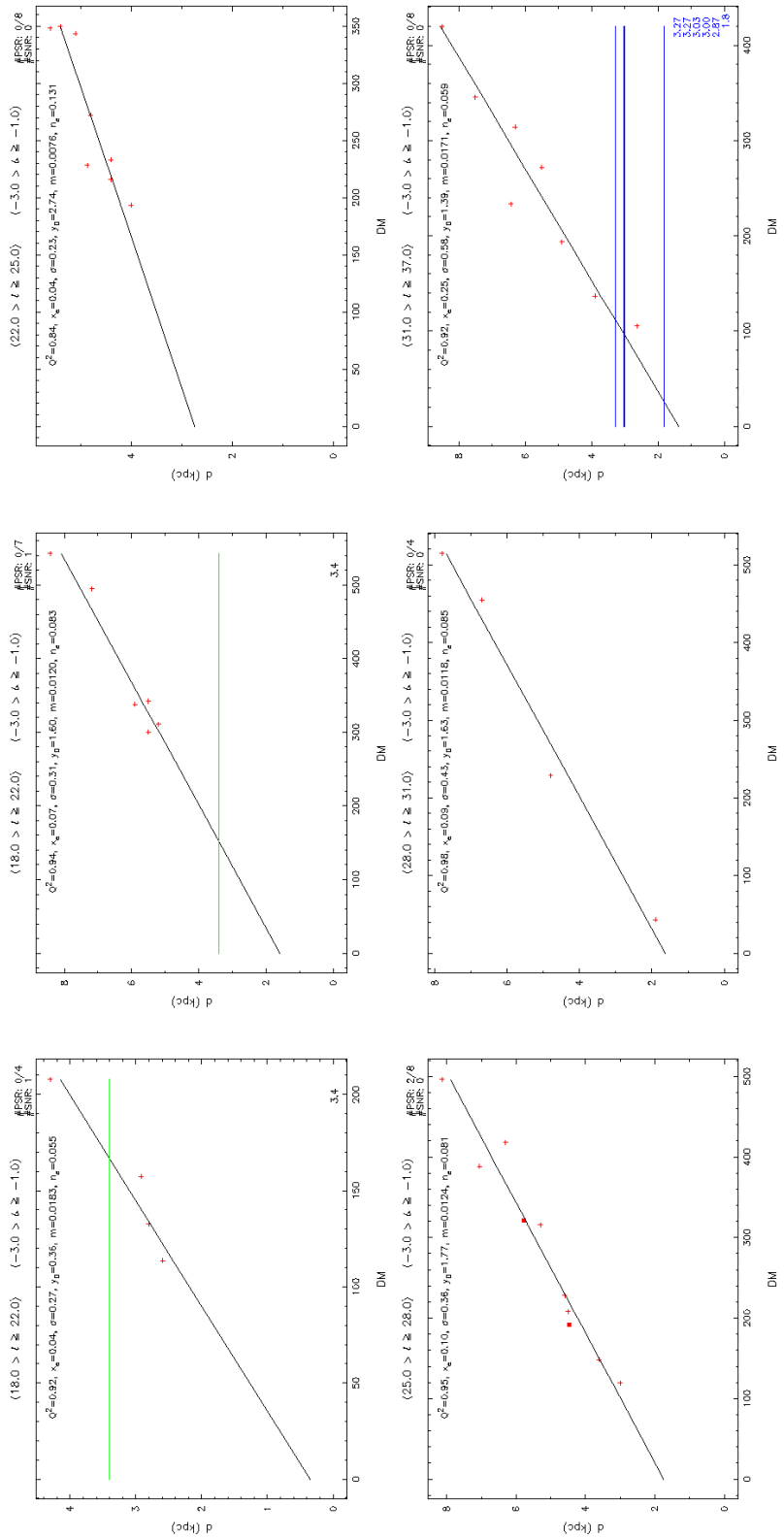

Figure A.40. Latitude Range: (-3.0), (-1.0) – *continued*

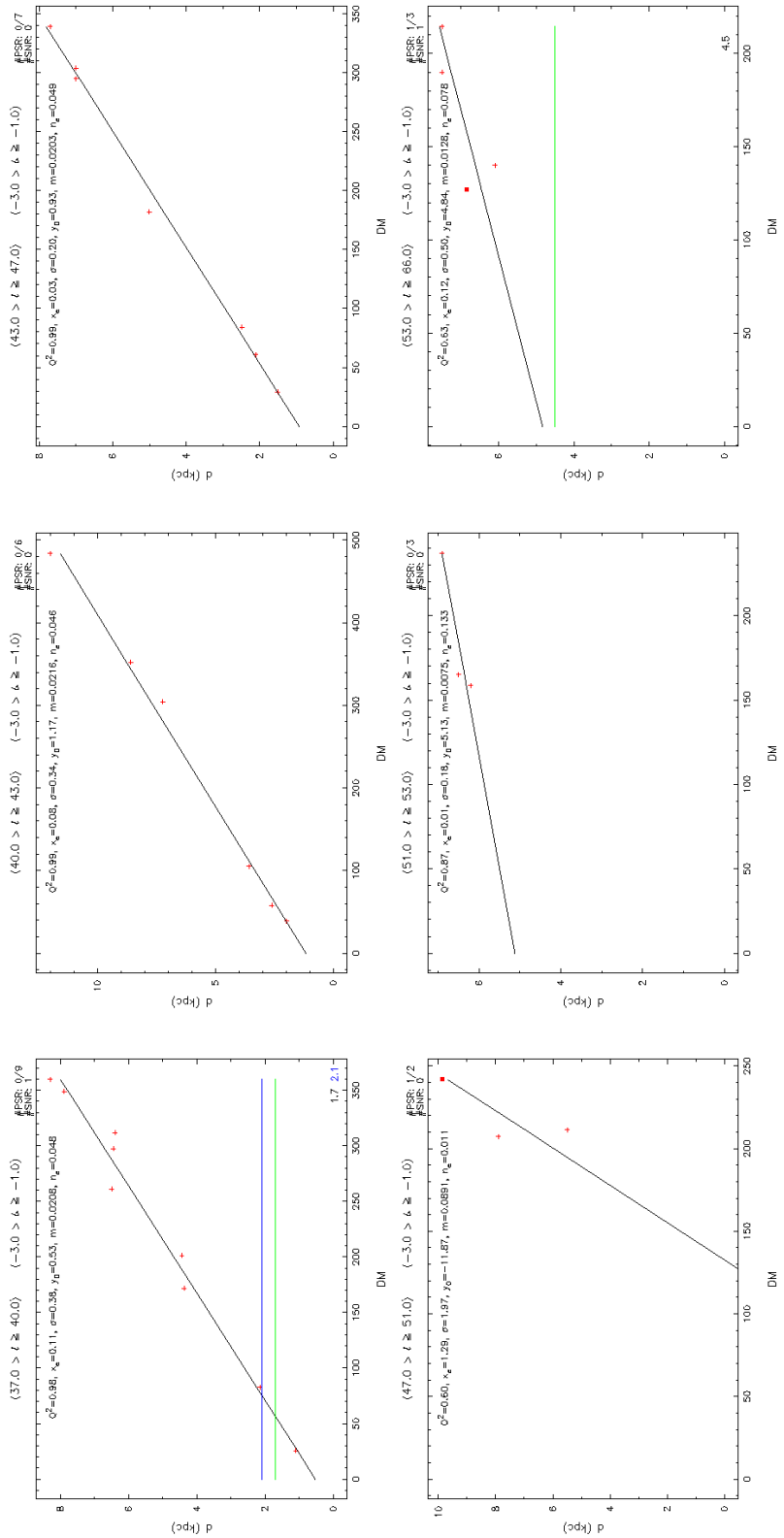

Figure A.41. Latitude Range: (-3.0), (-1.0) – *continued*

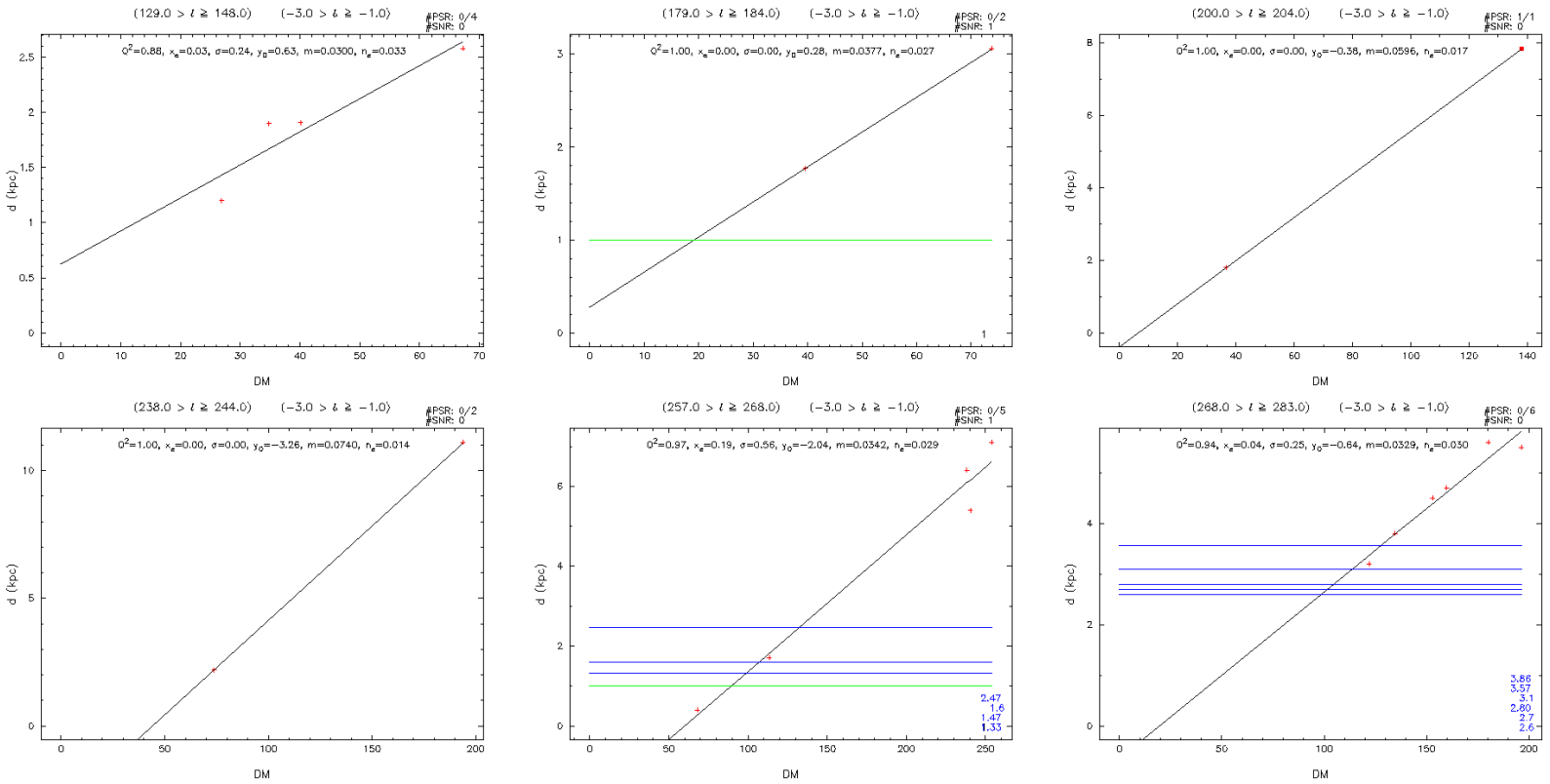

Figure A.42. Latitude Range: (-3.0), (-1.0) – *continued*

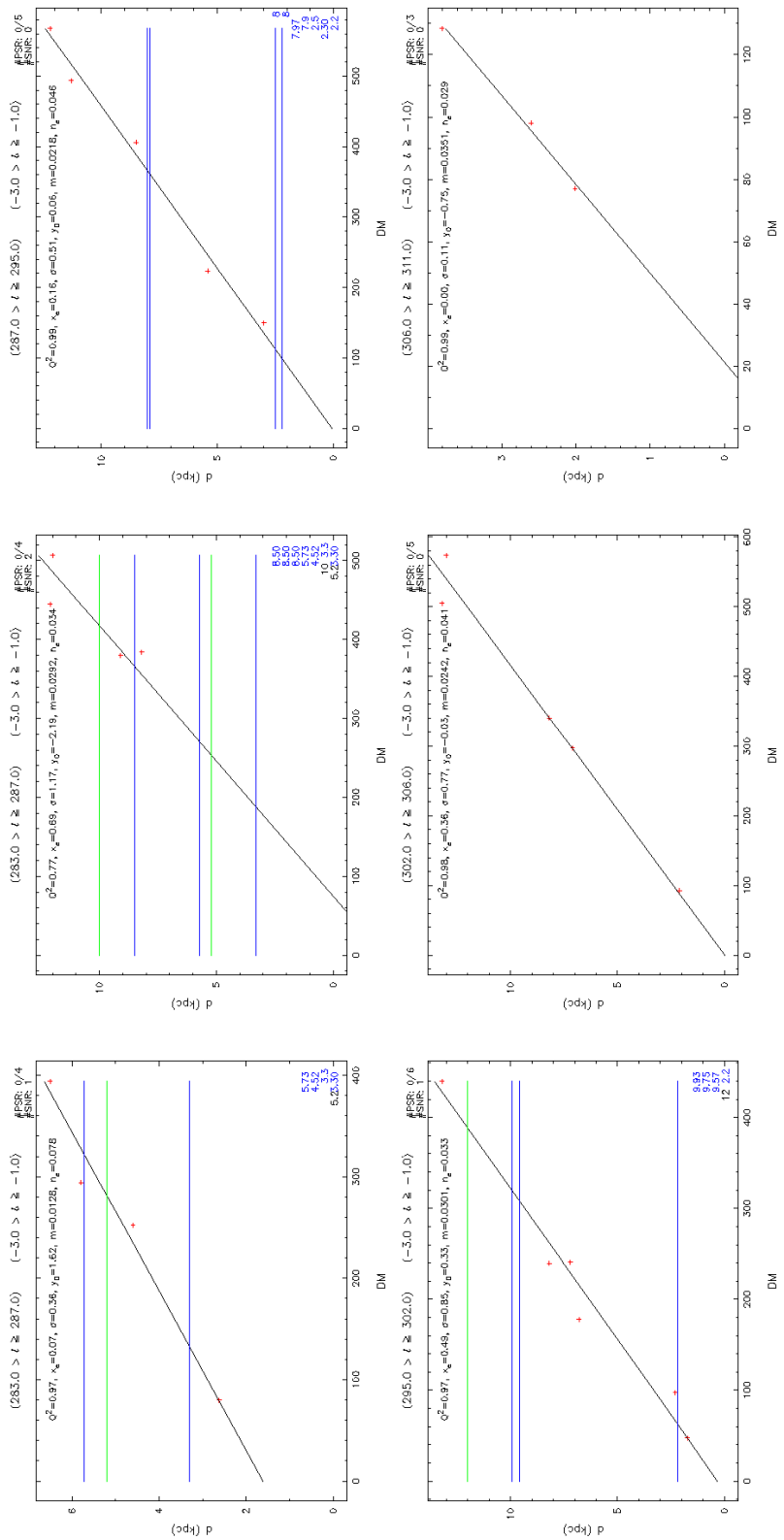

Figure A.43. Latitude Range: (-3.0), (-1.0) – *continued*

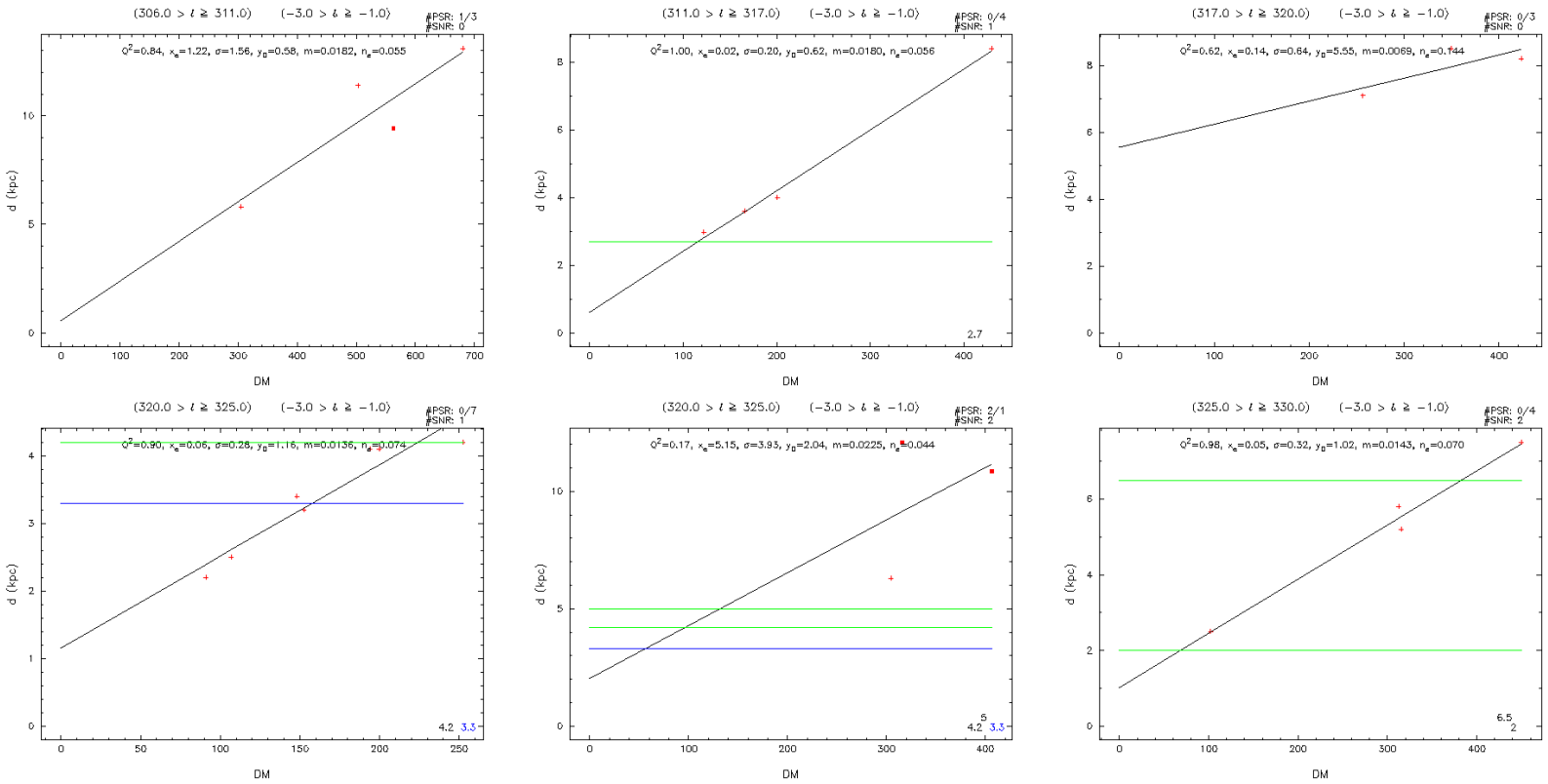

Figure A.44. Latitude Range: (-3.0), (-1.0) – *continued*

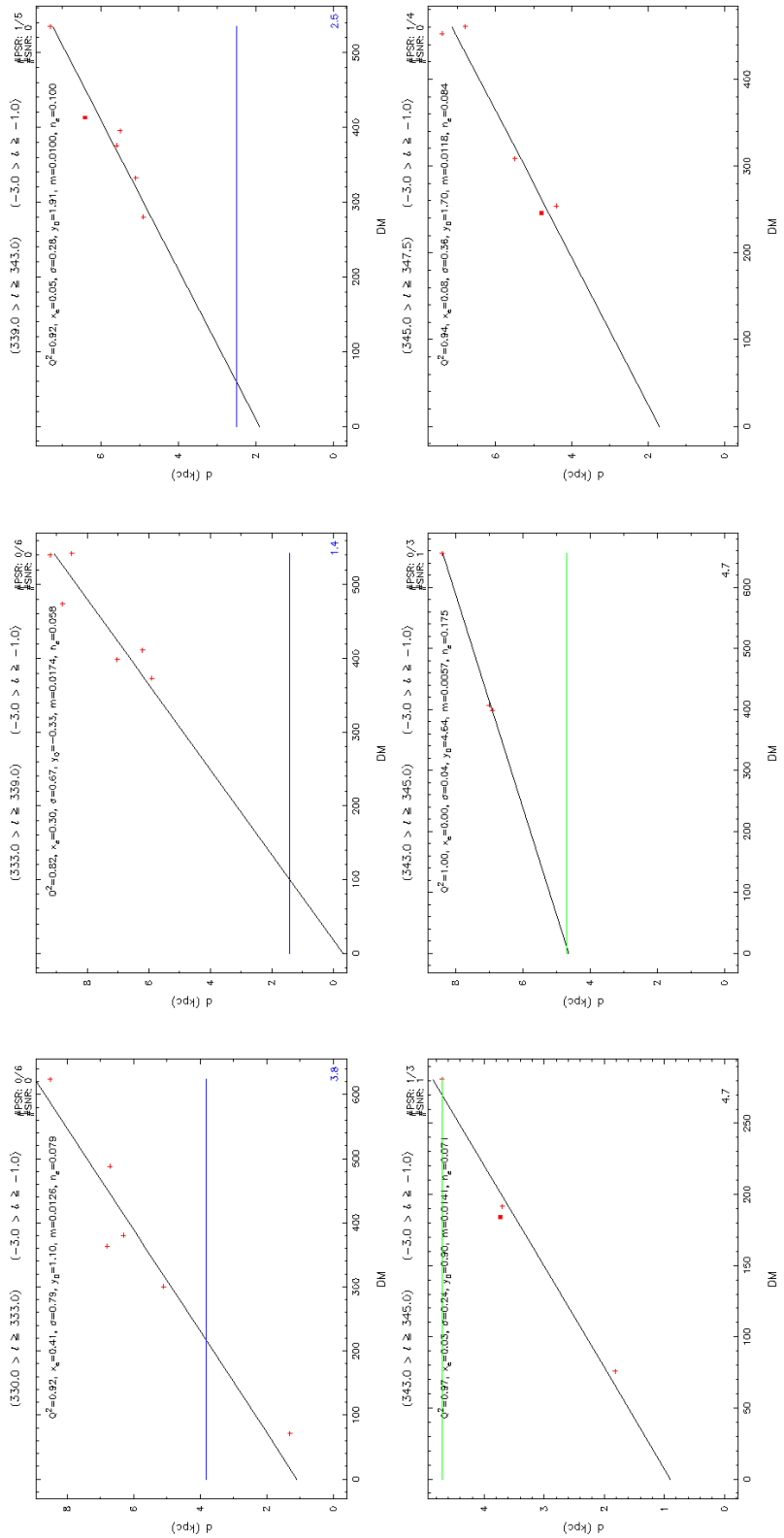

Figure A.45. Latitude Range: (-3.0), (-1.0) – *continued*

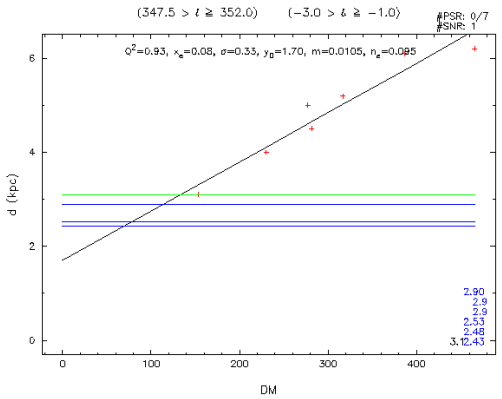

Figure A.46. Latitude Range: (-3.0), (-1.0)

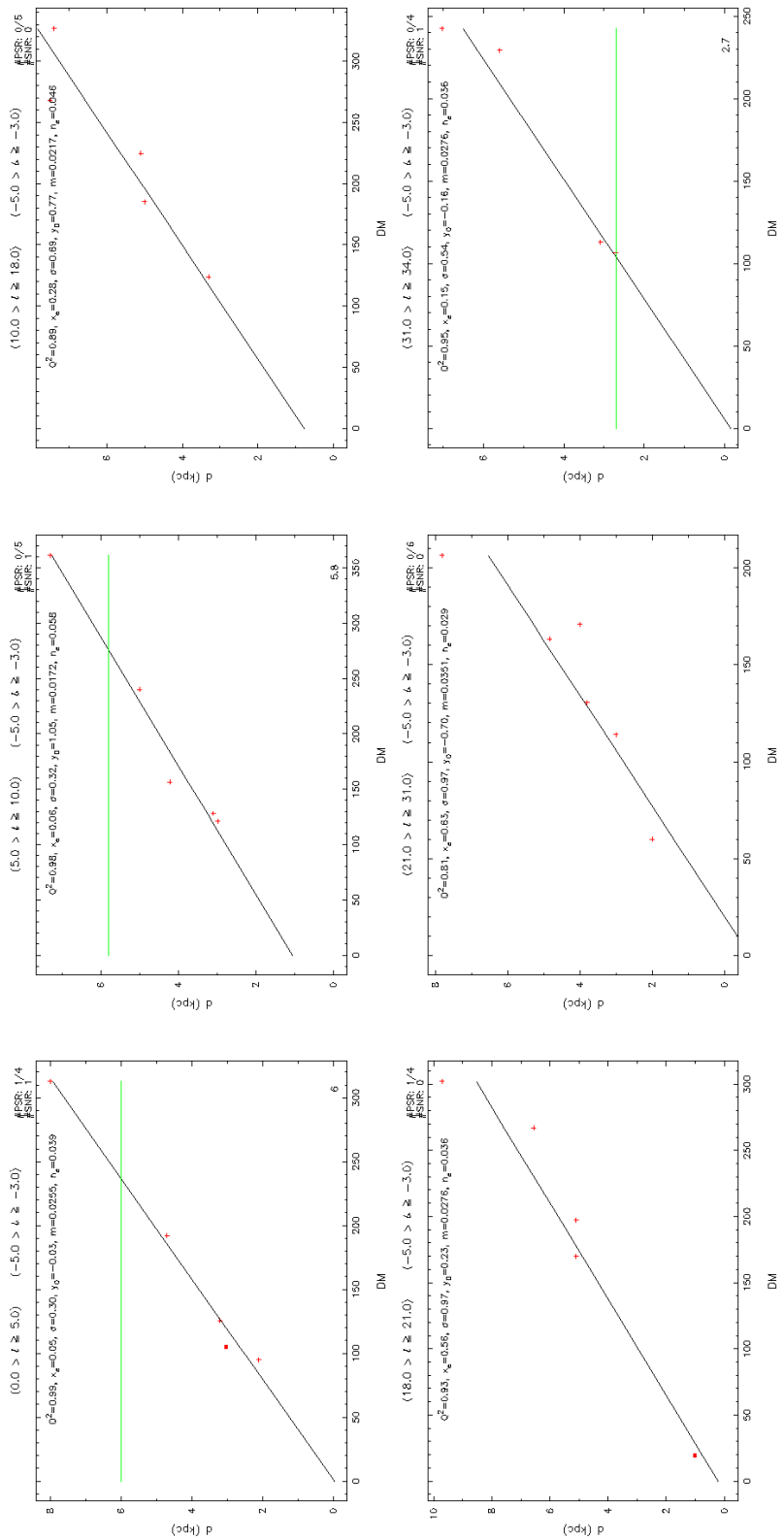

Figure A.47. Latitude Range: (-5.0), (-3.0)

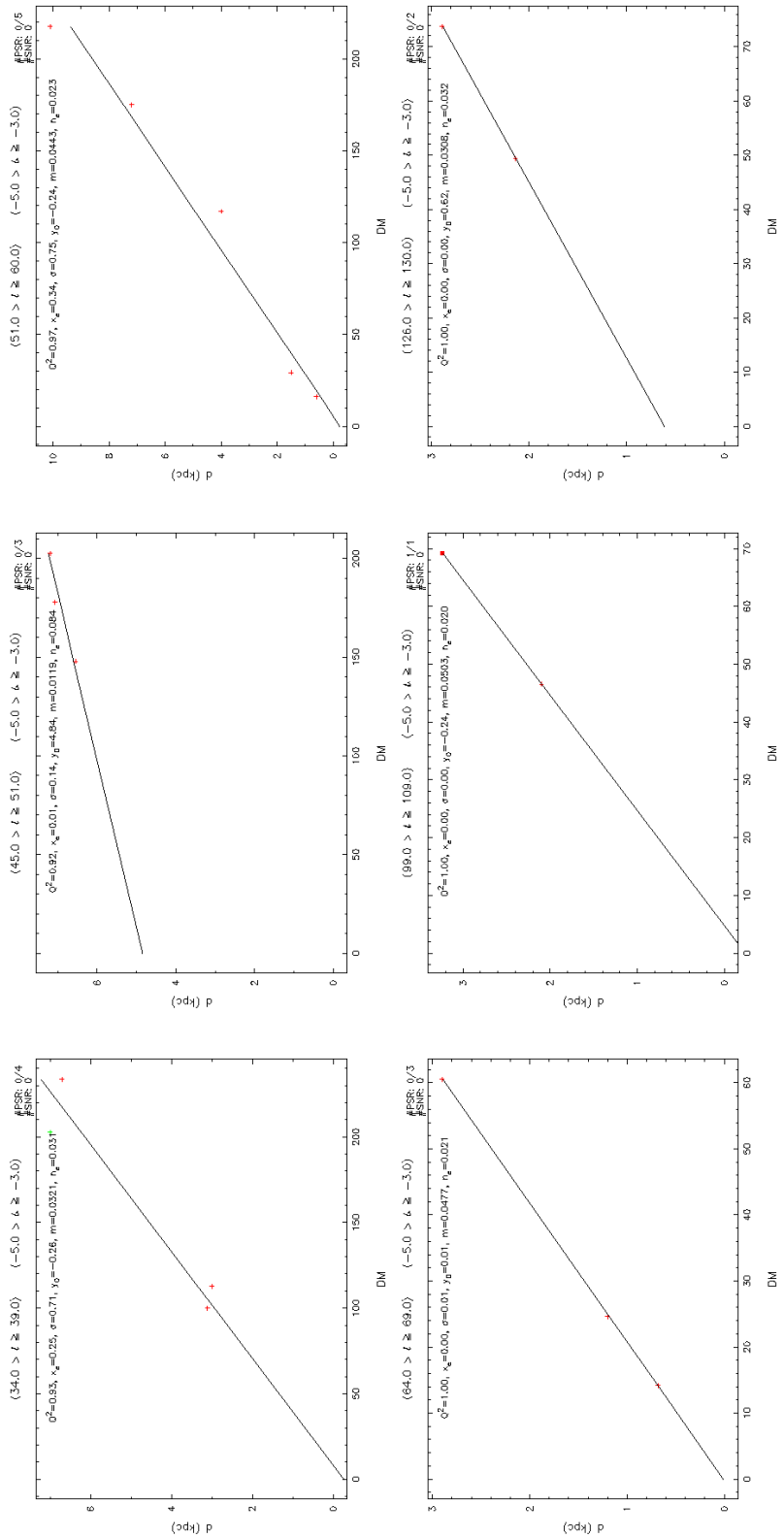

Figure A.48. Latitude Range: (-5.0), (-3.0) – *continued*

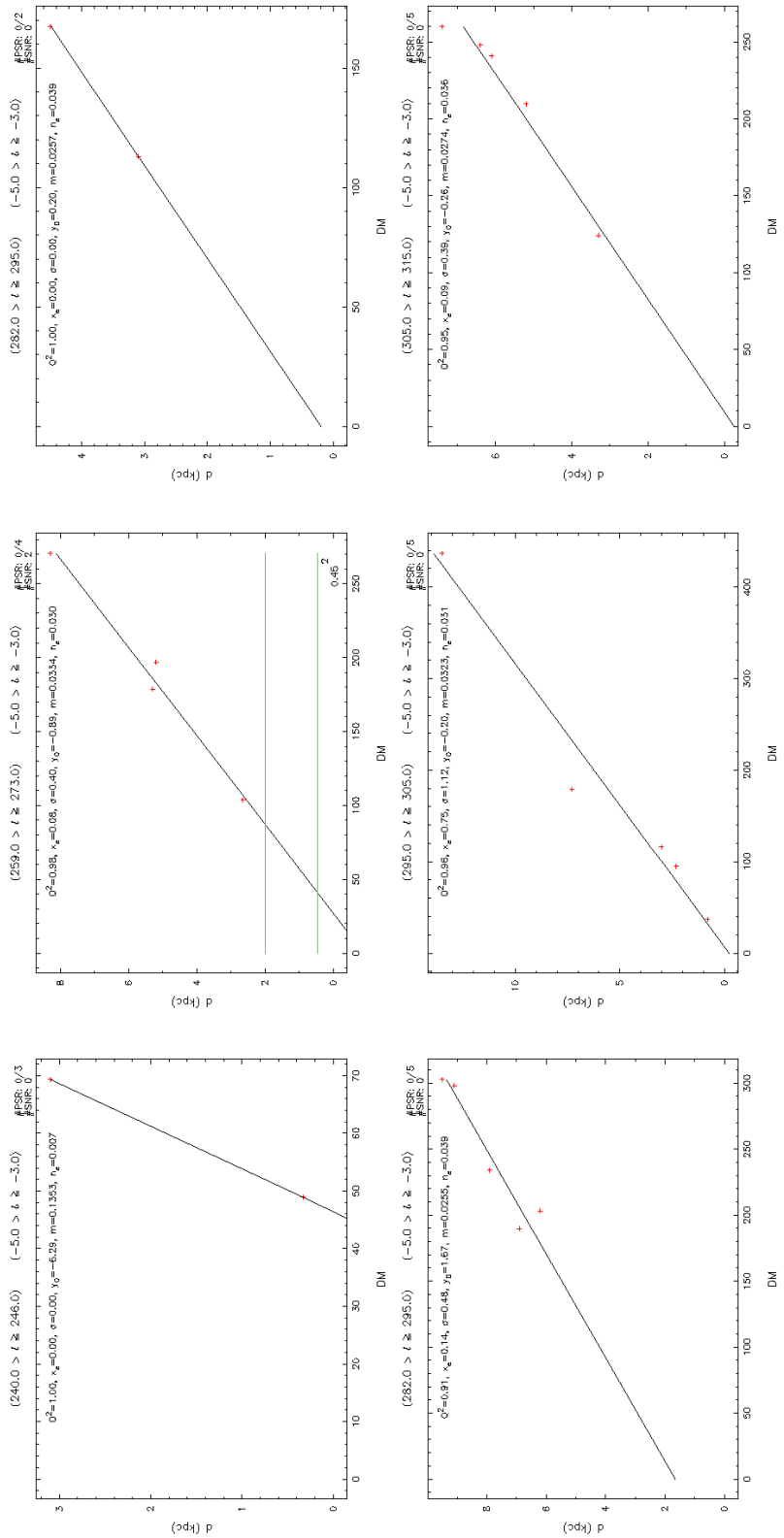

Figure A.49. Latitude Range: (-5.0), (-3.0) – *continued*

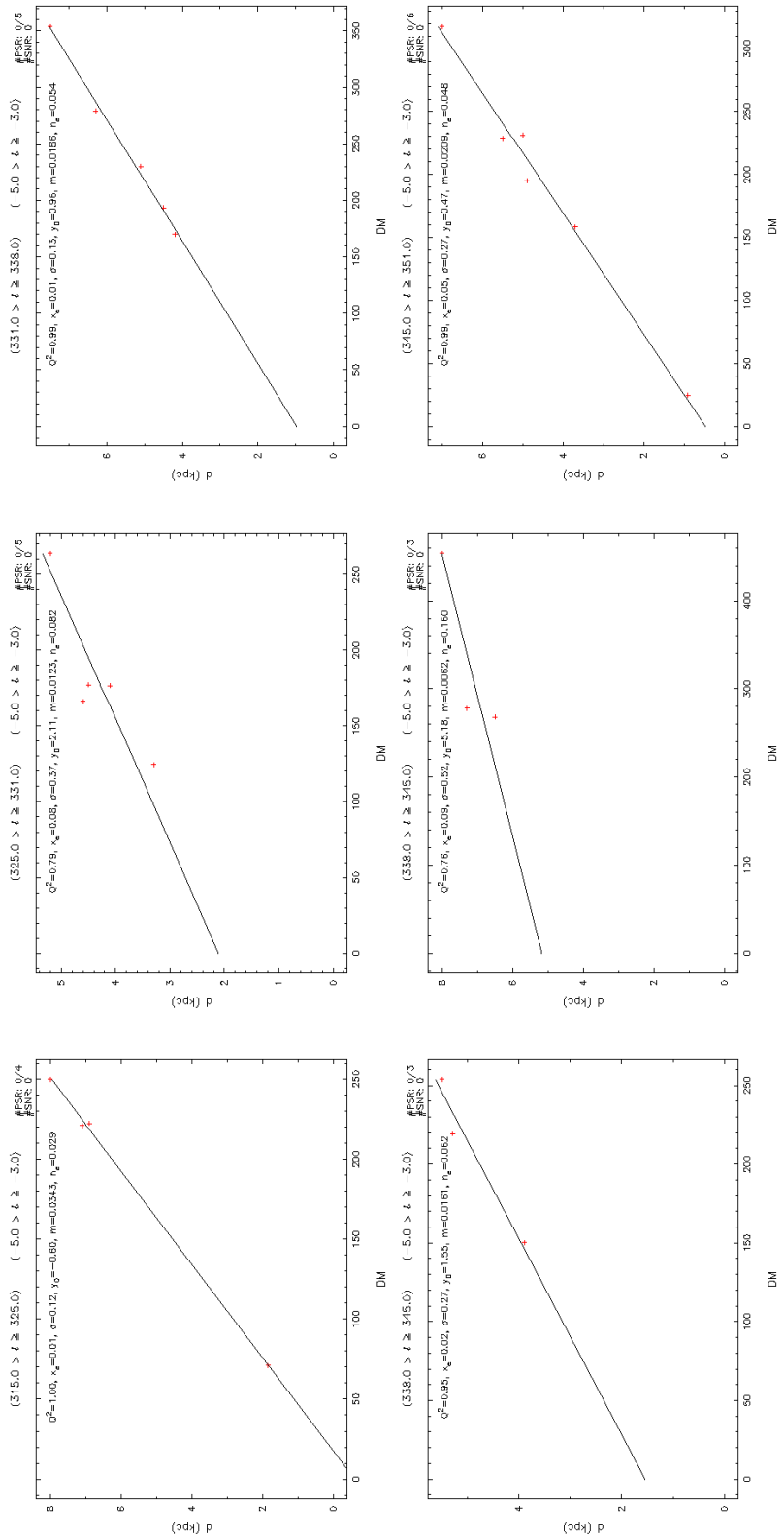

Figure A.50. Latitude Range: (-5.0), (-3.0) – *continued*

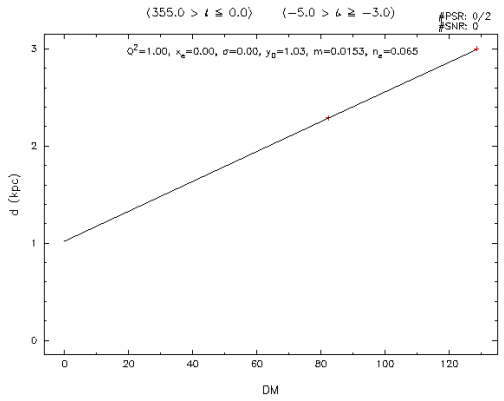

Figure A.51. Latitude Range: (-5.0), (-3.0)

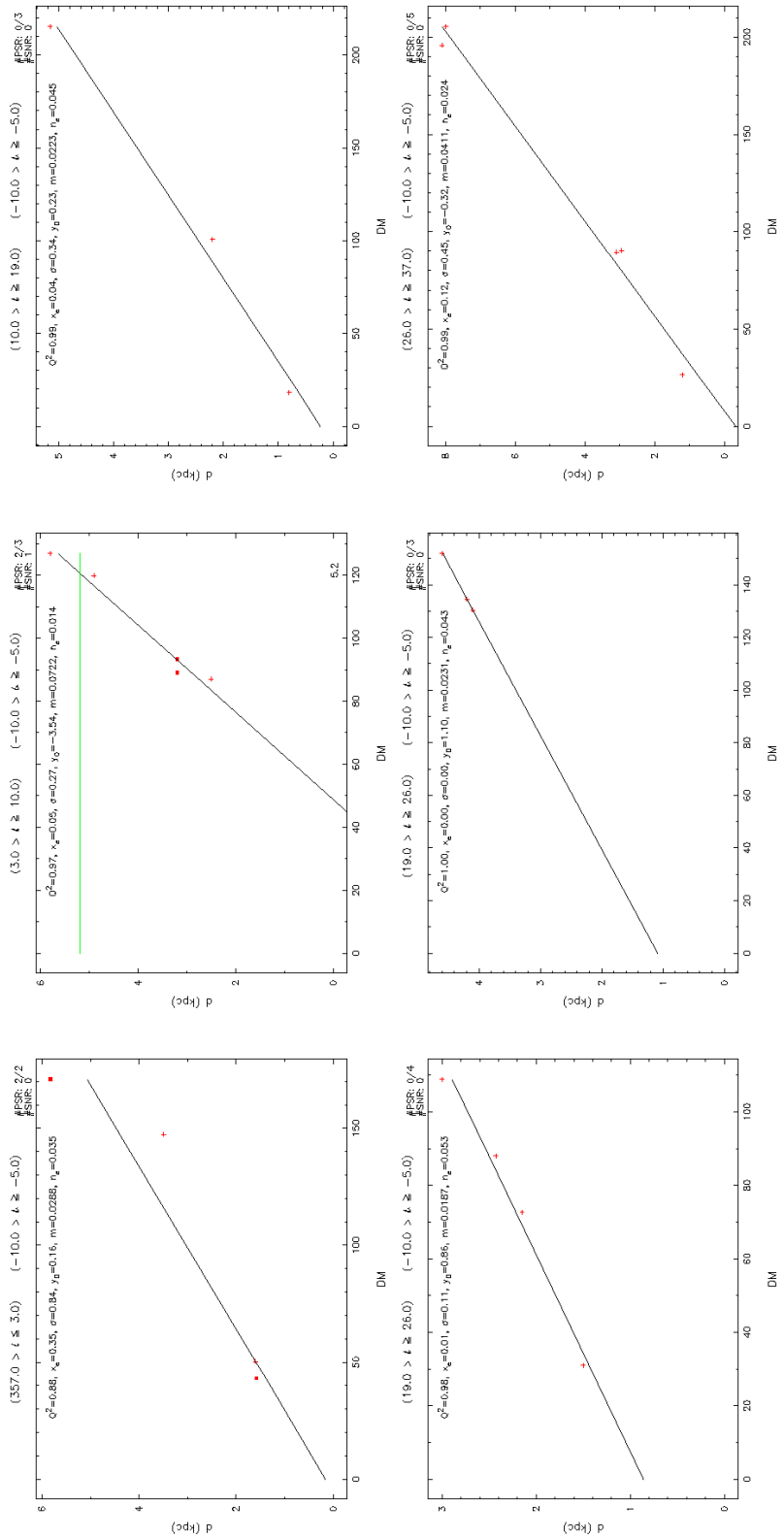

Figure A.52. Latitude Range: (-10.0), (-5.0)

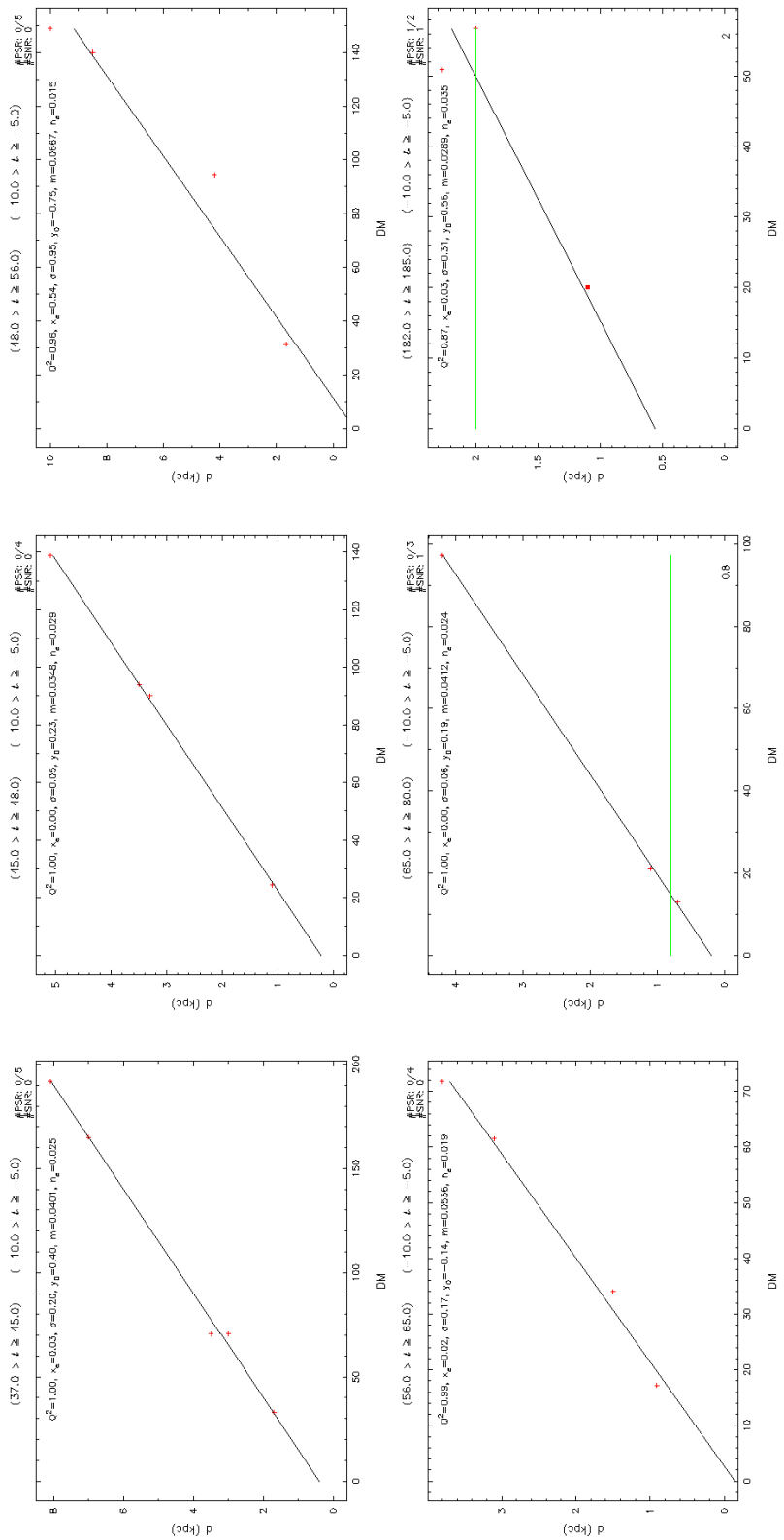

Figure A.53. Latitude Range: (-10.0), (-5.0) – *continued*

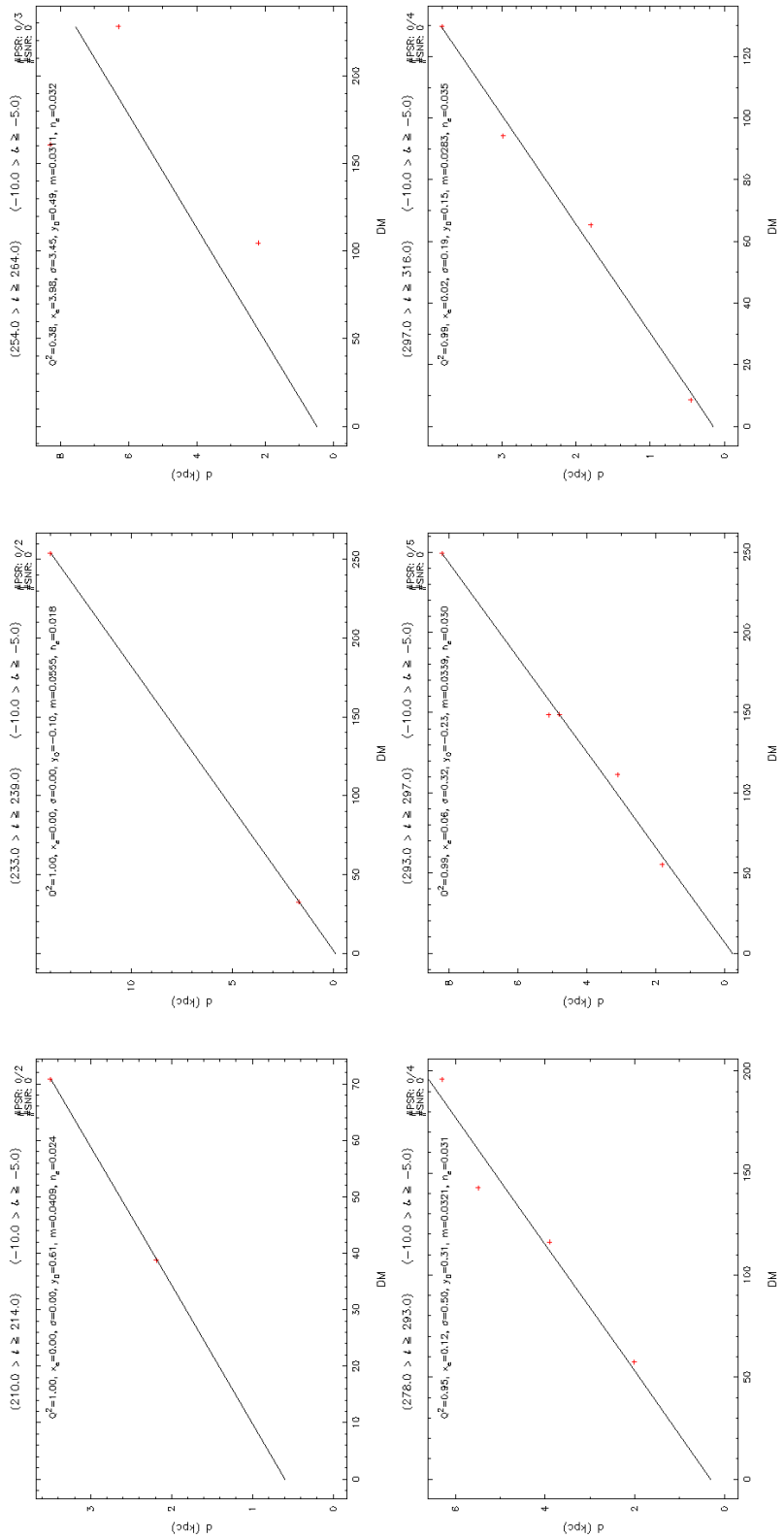

Figure A.54. Latitude Range: (-10.0), (-5.0) – *continued*

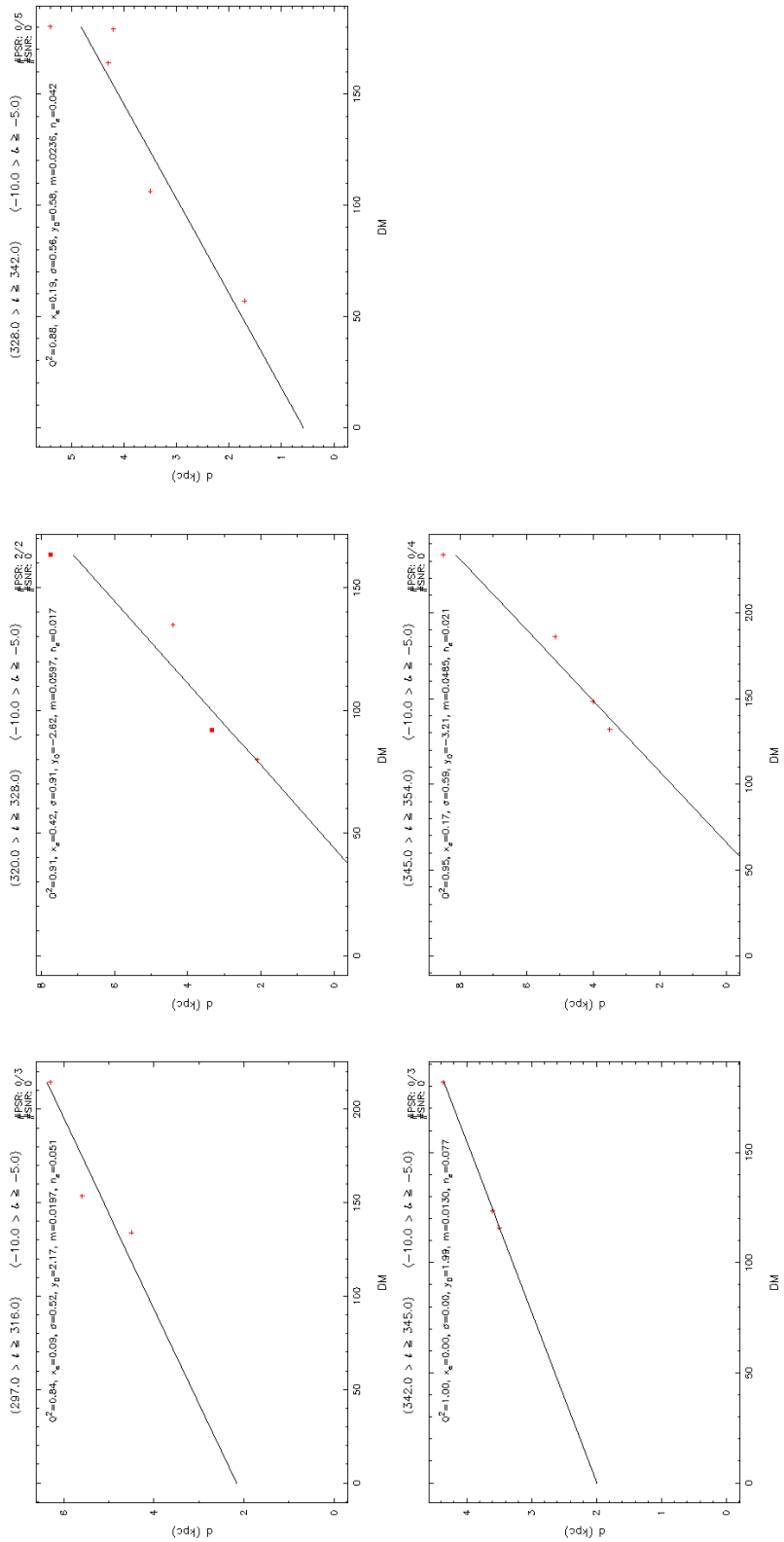

Figure A.55. Latitude Range: (-10.0), (-5.0)

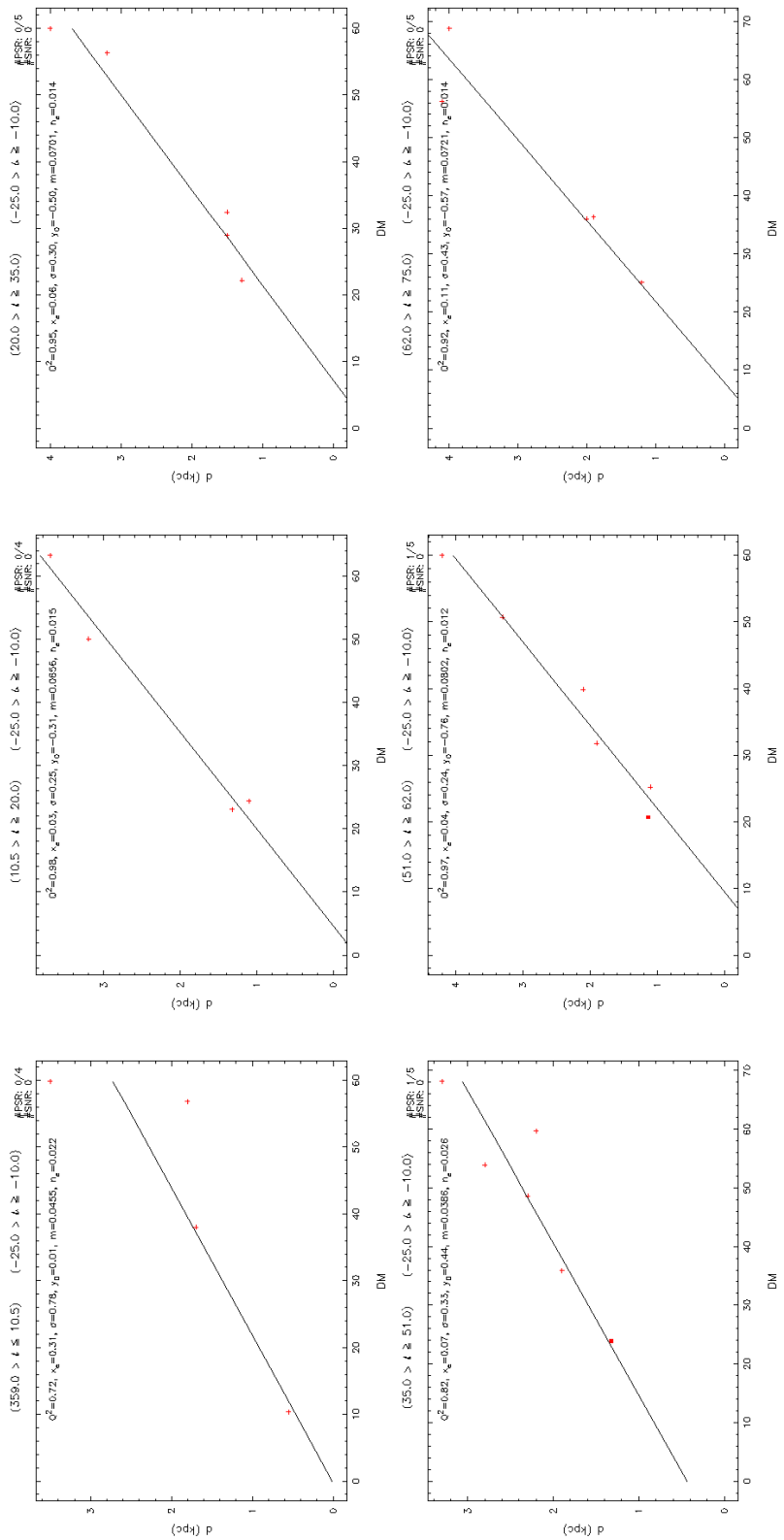

Figure A.56. Latitude Range: (-25.0), (-10.0)

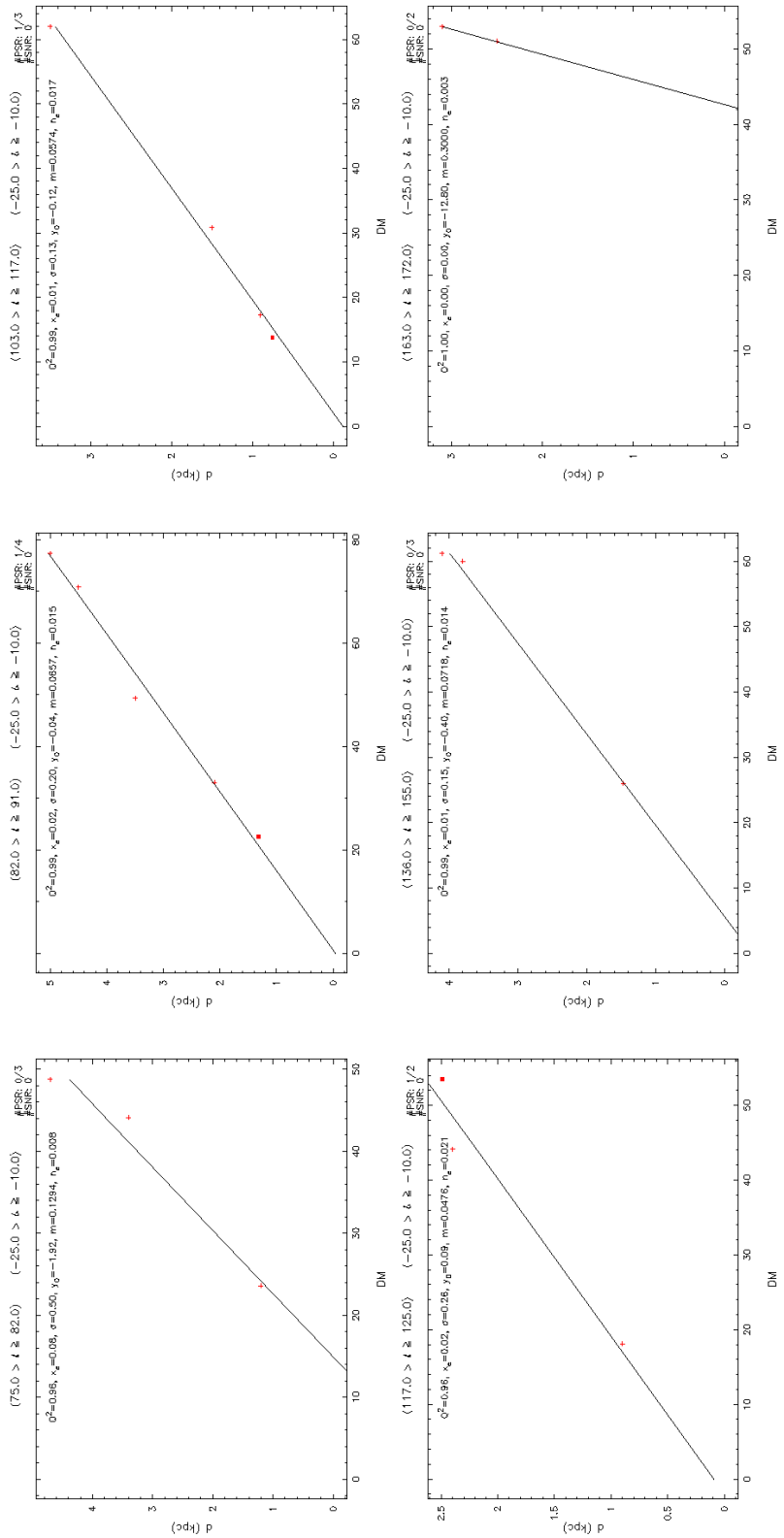

Figure A.57. Latitude Range: (-25.0), (-10.0) – *continued*

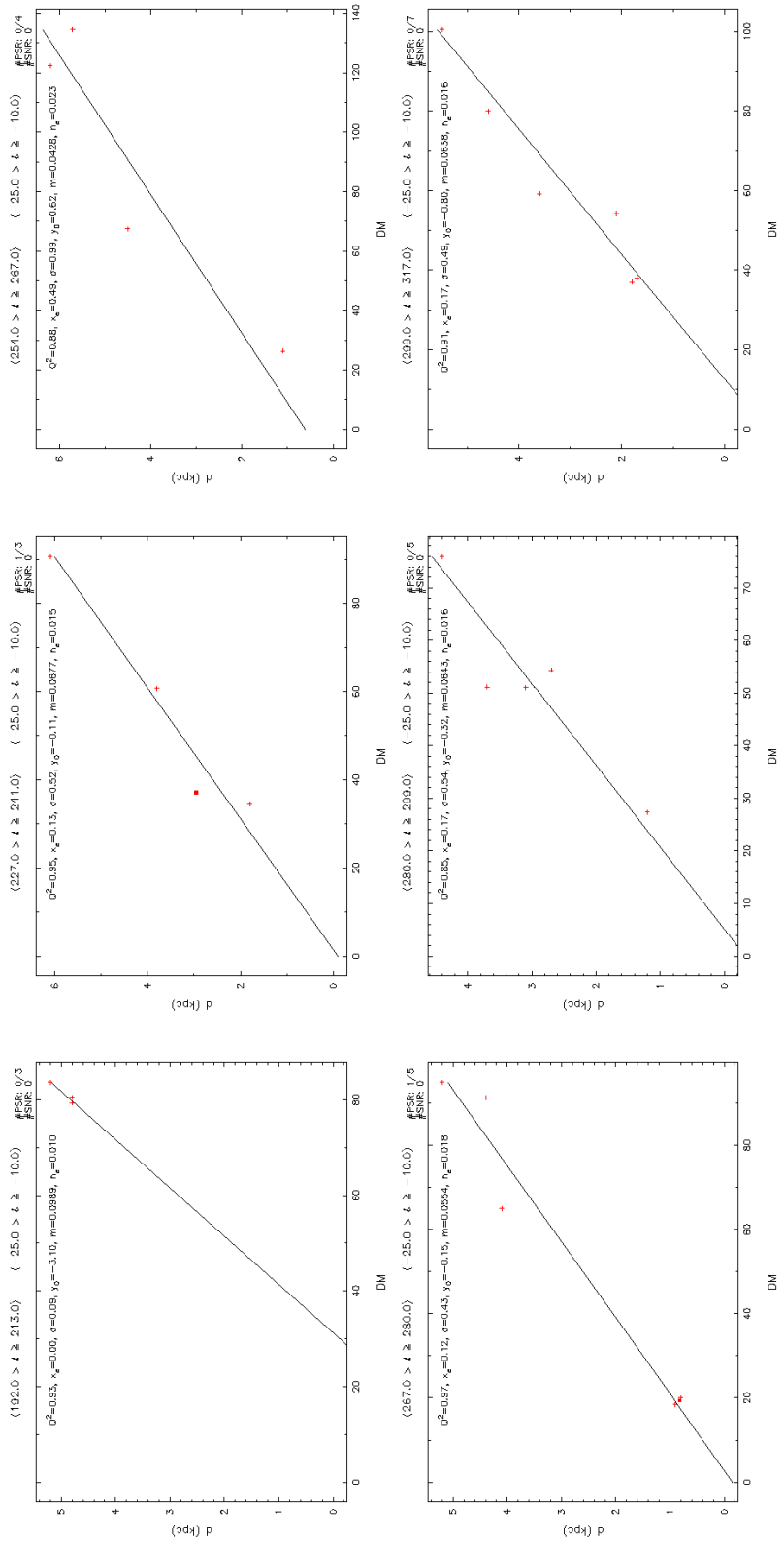

Figure A.58. Latitude Range: (-25.0), (-10.0) – *continued*

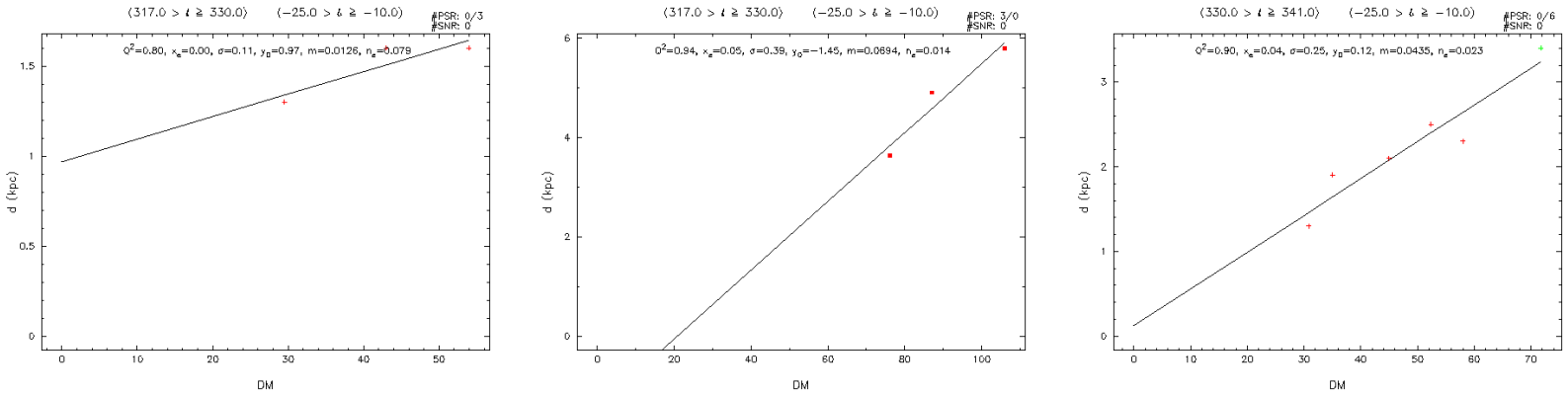

Figure A.59. Latitude Range: (-25.0), (-10.0)

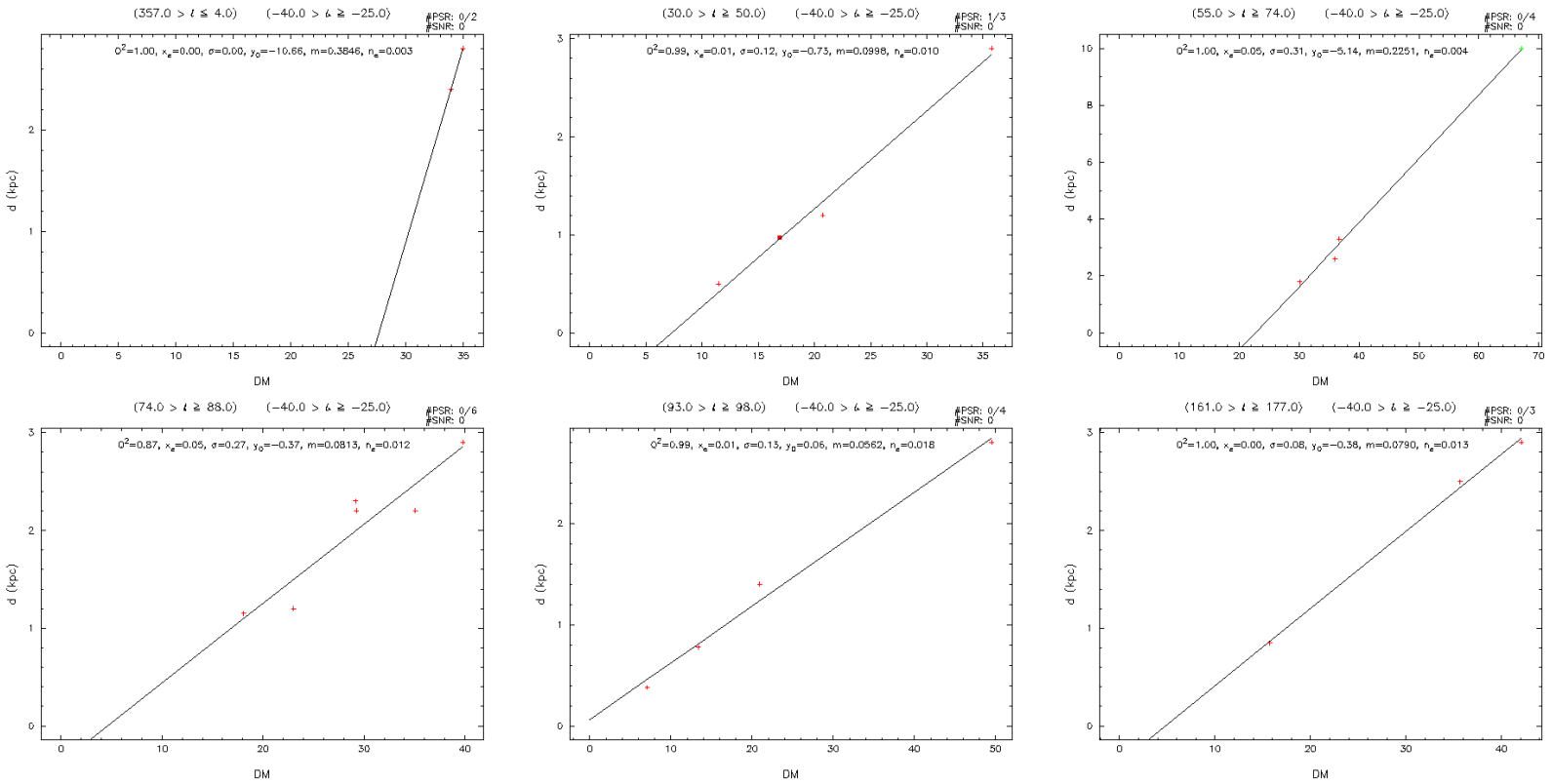

Figure A.60. Latitude Range: (-40.0), (-25.0)

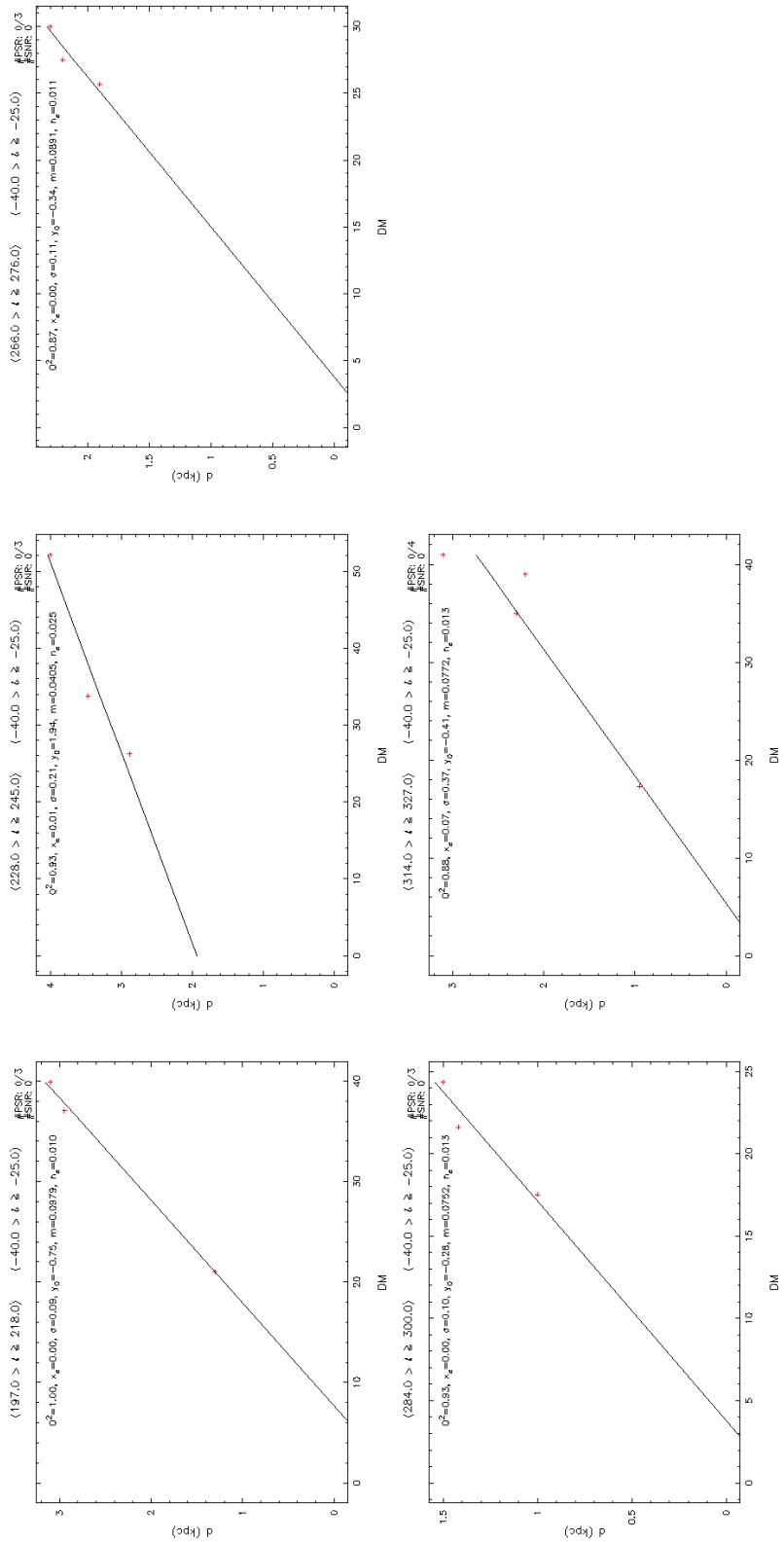

Figure A.61. Latitude Range: (-40.0), (-25.0)

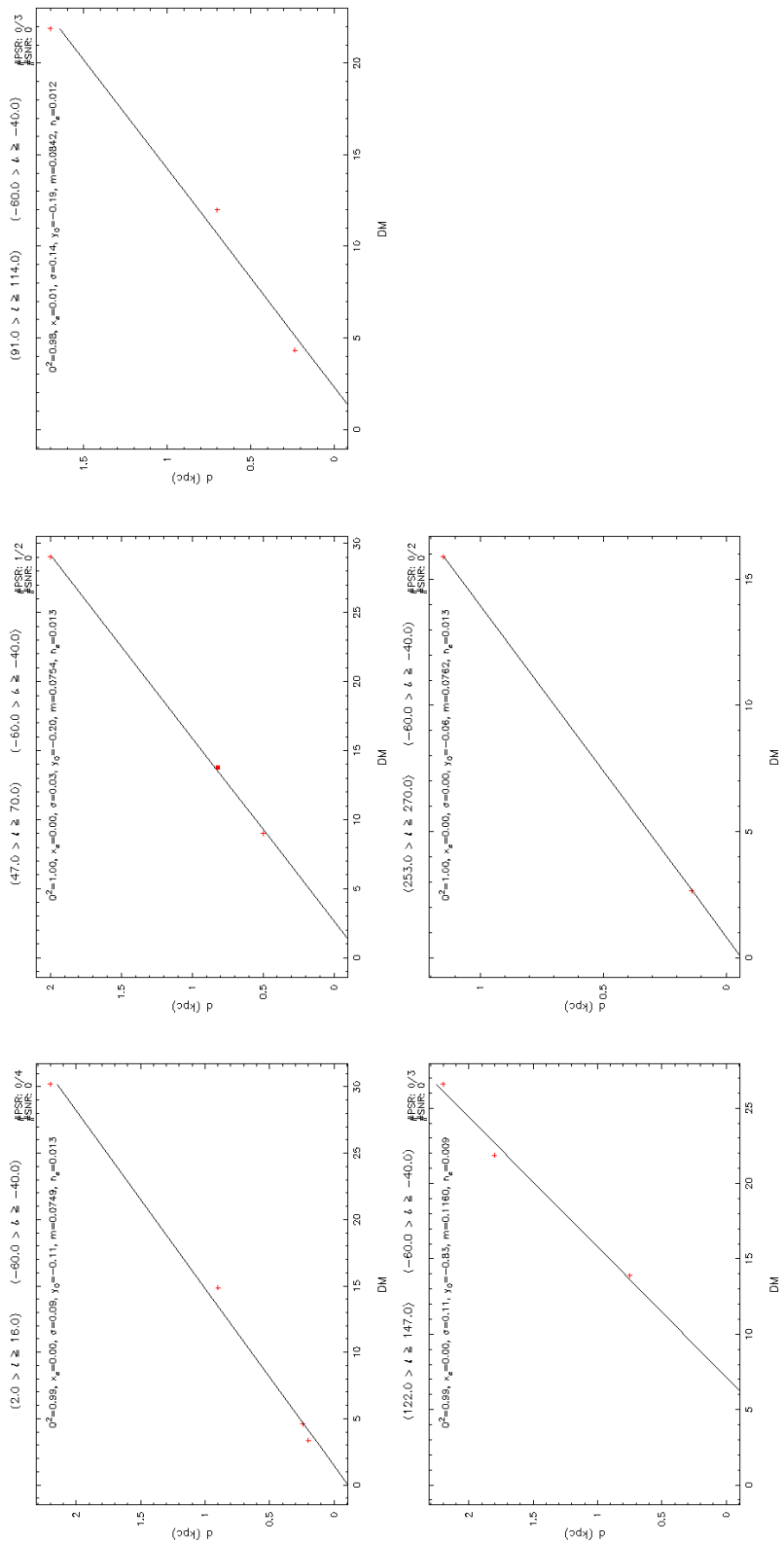

Figure A.62. Latitude Range: (-60.0), (-40.0)

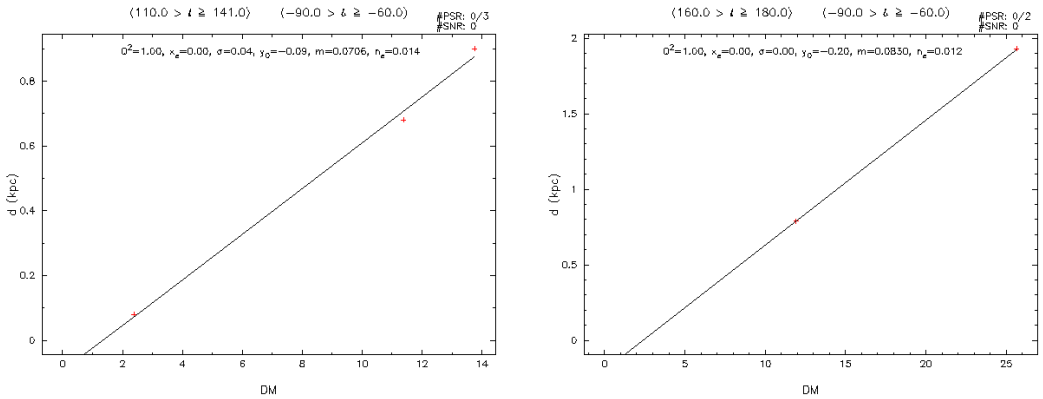

Figure A.63. Latitude Range: (-90.0), (-60.0)

APPENDIX B

D VS DM TABLES

This appendix presents tabulated versions of distance versus dispersion measure graphs of pulsars given in Appendix A. Sections of each zone are given under the name of the corresponding zone and data of 3D sections containing one or less pulsars are excluded.

Columns for all the tables are defined in order as follows: l_{min}, l_{max} (degrees): Galactic longitude ranges of the section; d_{min}, d_{max} (kpc): distance ranges of the section; Q^2: quality of the fit of the d vs Dm graph from which the free electron density is calculated; d_0 (kpc): the distance value where the linear curve instersects with the y-axis; m (cm^3): the slope of the linear fit; n_e (cm^{-3}): the free electron density of the section.

Table B.1. Galactic latitude range (-1.0), (+1.0).

l_{min}	l_{max}	d_{min}	d_{max}	Q^2	d_0	m	$\mathrm{n_e}$
358.0	1.0	1.8	5.2	0.94	1.19	0.011	0.091
358.0	1.0	11.4	14.2	0.95	5.40	0.007	0.135
1.0	3.0	1.3	8.5	0.98	0.43	0.014	0.074
3.0	4.5	3.5	11.4	0.98	0.50	0.013	0.075
4.5	6.5	2.5	5.1	0.97	1.38	0.010	0.100
4.5	6.5	11.0	13.1	1.00	−8.05	0.027	0.037
6.5	8.0	3.4	5.4	0.96	1.67	0.009	0.114
6.5	8.0	10.0	13.6	1.00	4.01	0.009	0.113
8.0	9.5	3.4	9.3	0.99	1.44	0.010	0.097
9.5	11.5	3.1	3.5	0.84	2.36	0.004	0.227
9.5	11.5	9.5	11.3	0.99	4.75	0.007	0.143
11.5	13.0	5.5	11.6	0.97	0.00	0.013	0.078
13.0	15.5	4.0	9.6	0.99	1.72	0.010	0.104
15.5	16.5	3.0	12.0	0.99	0.68	0.012	0.086
16.5	17.5	1.4	7.8	0.99	1.25	0.010	0.098
16.5	17.5	10.0	12.6	0.90	4.85	0.007	0.149
17.5	20.0	3.4	11.1	0.98	1.24	0.011	0.092
20.0	21.0	3.0	7.3	0.98	1.84	0.009	0.111
21.0	22.5	3.8	4.7	0.93	2.70	0.007	0.150
21.0	22.5	7.6	8.0	1.00	4.78	0.007	0.152
22.5	25.0	4.5	10.4	0.99	2.50	0.008	0.129
25.0	27.0	2.1	9.1	0.98	1.57	0.010	0.096
27.0	28.0	4.4	8.3	0.99	1.88	0.010	0.100
28.0	30.0	2.4	4.8	0.92	0.53	0.017	0.059
28.0	30.0	5.9	10.6	0.99	2.37	0.008	0.121
30.0	32.0	3.8	9.1	0.99	2.23	0.010	0.100
32.0	34.0	1.0	4.6	0.99	0.70	0.016	0.064
32.0	34.0	6.4	12.1	0.96	0.97	0.012	0.084
34.0	35.0	2.4	8.6	1.00	1.50	0.012	0.080
35.0	37.0	3.8	13.1	0.99	1.02	0.015	0.067
37.0	39.0	4.0	17.1	0.97	1.07	0.015	0.066
39.0	41.0	2.0	5.9	0.97	0.44	0.019	0.052
39.0	41.0	7.0	12.1	0.94	2.70	0.013	0.076
41.0	44.0	0.4	6.1	0.99	0.31	0.019	0.051
41.0	44.0	7.5	9.5	0.80	4.53	0.009	0.115
44.0	50.0	3.1	5.7	0.96	1.56	0.016	0.063
44.0	50.0	7.0	7.8	0.97	4.46	0.008	0.128
50.0	54.0	3.3	8.3	0.97	0.43	0.030	0.033
54.0	61.0	2.9	7.9	0.49	3.29	0.013	0.080
61.0	66.0	0.3	7.2	0.98	−0.08	0.041	0.024
66.0	75.0	5.1	12.5	0.95	−0.03	0.035	0.029
75.0	77.0	6.5	12.1	0.68	3.41	0.018	0.054
97.0	107.0	3.0	14.9	0.99	−5.23	0.075	0.013
107.0	117.0	2.4	5.6	0.94	0.04	0.034	0.029
148.0	150.0	2.0	3.8	1.00	−0.09	0.037	0.027
200.0	203.0	3.3	6.6	1.00	−1.96	0.068	0.015

Table B.1. *– continued*

$l_{\min}$	$l_{\max}$	$d_{\min}$	$d_{\max}$	Q^2	d_0	m	$\mathrm{n_e}$
231.0	238.0	2.6	4.7	0.99	−0.52	0.051	0.020
259.0	264.0	3.3	13.5	0.93	−7.82	0.070	0.014
264.0	277.0	2.9	6.6	0.92	0.69	0.024	0.041
277.0	282.0	3.5	11.1	0.99	0.21	0.026	0.039
282.0	287.0	2.4	7.9	0.99	1.28	0.014	0.070
282.0	287.0	14.2	16.2	1.00	10.03	0.006	0.171
287.0	289.0	2.3	11.2	0.98	0.33	0.021	0.048
289.0	291.0	2.2	7.2	0.95	0.50	0.021	0.047
291.0	293.0	1.7	6.8	1.00	0.53	0.022	0.046
291.0	293.0	9.1	12.6	1.00	2.79	0.014	0.069
293.0	297.0	1.9	9.2	0.98	0.86	0.017	0.059
297.0	304.0	8.3	9.6	0.67	6.70	0.007	0.154
297.0	304.0	10.2	13.6	0.88	8.42	0.007	0.148
304.0	306.0	2.3	9.8	0.96	0.18	0.020	0.049
304.0	306.0	13.8	17.3	0.86	7.18	0.010	0.104
306.0	308.0	5.7	16.3	0.97	−0.36	0.019	0.052
308.0	312.0	5.1	8.6	0.96	3.39	0.007	0.136
308.0	312.0	9.2	12.1	0.85	2.31	0.012	0.082
312.0	317.0	0.8	6.2	0.95	0.66	0.017	0.060
312.0	317.0	8.2	10.6	0.45	6.99	0.005	0.213
317.0	321.0	3.3	5.1	0.97	2.04	0.012	0.085
317.0	321.0	7.1	10.5	0.85	3.00	0.012	0.087
321.0	324.0	2.6	6.2	0.99	1.36	0.013	0.079
321.0	324.0	9.2	13.3	0.83	5.03	0.009	0.108
324.0	327.0	3.5	5.2	0.92	2.49	0.008	0.132
324.0	327.0	6.8	9.8	0.96	2.63	0.011	0.090
327.0	332.0	1.1	7.1	0.94	1.46	0.011	0.088
327.0	332.0	8.4	9.8	0.89	5.20	0.006	0.177
332.0	335.0	3.7	9.2	1.00	2.40	0.008	0.123
335.0	338.0	5.5	7.3	0.91	2.03	0.009	0.113
335.0	338.0	8.5	12.0	0.77	4.28	0.007	0.144
338.0	342.0	3.6	6.3	0.96	2.28	0.008	0.123
338.0	342.0	6.8	10.0	0.99	3.39	0.007	0.143
342.0	345.0	4.8	9.7	0.98	1.66	0.010	0.105
345.0	348.0	4.3	6.4	0.95	2.77	0.007	0.152
345.0	348.0	8.6	12.0	0.98	4.09	0.007	0.139
348.0	351.0	2.2	6.6	0.98	1.05	0.010	0.097
348.0	351.0	9.2	10.6	0.33	6.46	0.004	0.236
351.0	354.0	6.3	12.1	0.98	−1.39	0.015	0.065
354.0	356.0	3.8	9.6	0.98	1.14	0.011	0.093
356.0	358.0	4.4	8.5	0.98	2.09	0.008	0.120

Table B.2. Galactic latitude range (+1.0), (+3.0).

l_{min}	l_{max}	d_{min}	d_{max}	Q^2	d_0	m	$\mathrm{n_e}$
358.0	1.0	3.2	5.6	0.89	1.71	0.010	0.098
1.0	5.0	2.4	6.4	0.94	1.79	0.009	0.112
5.0	10.0	3.4	8.1	0.99	1.76	0.010	0.103
10.0	14.0	4.6	7.3	0.92	2.78	0.008	0.128
14.0	22.0	4.2	8.6	0.97	2.04	0.011	0.092
22.0	27.0	5.2	9.0	0.79	1.56	0.012	0.082
27.0	30.0	2.2	7.0	0.96	1.68	0.012	0.081
30.0	34.0	2.4	3.6	1.00	0.60	0.021	0.048
30.0	34.0	6.2	9.2	0.96	3.25	0.009	0.109
34.0	38.0	1.9	7.6	0.96	1.19	0.016	0.065
38.0	44.0	3.9	5.5	0.97	2.01	0.014	0.071
38.0	44.0	6.4	9.3	0.94	4.06	0.011	0.092
44.0	49.0	1.5	7.6	0.99	0.77	0.025	0.039
49.0	54.0	0.6	7.2	0.98	0.34	0.042	0.024
54.0	61.0	2.5	10.1	0.94	0.37	0.039	0.026
68.0	86.0	2.0	11.6	0.98	0.77	0.033	0.030
113.0	133.0	2.4	8.4	1.00	−0.52	0.045	0.022
188.0	196.0	1.5	3.8	1.00	0.04	0.038	0.026
251.0	258.0	1.2	6.1	0.65	−1.80	0.050	0.020
265.0	282.0	2.1	3.1	0.75	1.69	0.009	0.113
282.0	290.0	1.7	11.3	0.98	0.36	0.024	0.042
290.0	296.0	2.2	6.9	0.99	0.61	0.019	0.054
290.0	296.0	7.7	8.2	0.97	5.91	0.008	0.123
296.0	307.0	2.2	3.4	1.00	0.91	0.014	0.074
296.0	307.0	6.7	11.3	0.99	2.60	0.019	0.052
307.0	311.0	6.2	6.7	0.92	5.40	0.003	0.354
311.0	314.0	5.9	8.4	0.58	−0.62	0.023	0.044
314.0	316.0	8.5	8.7	1.00	−20.95	0.091	0.011
320.0	321.0	3.9	5.3	0.95	2.16	0.012	0.087
321.0	324.0	1.8	6.2	0.99	−0.56	0.030	0.033
324.0	327.0	0.9	6.5	0.99	0.39	0.020	0.049
327.0	331.0	1.1	6.3	0.96	0.96	0.016	0.063
331.0	338.0	2.5	5.2	0.95	−0.23	0.023	0.044
331.0	338.0	5.7	7.6	0.92	3.23	0.007	0.135
338.0	343.0	4.5	8.1	0.97	2.12	0.010	0.099
338.0	343.0	8.5	10.6	0.71	4.40	0.010	0.101
343.0	346.0	4.5	5.5	0.63	3.68	0.004	0.254
346.0	353.0	6.6	11.6	0.98	4.00	0.010	0.103
353.0	358.0	2.3	8.4	0.97	1.49	0.011	0.090

Table B.3. Galactic latitude range (+3.0), (+7.0).

l_{min}	l_{max}	d_{min}	d_{max}	Q^2	d_0	m	$\mathrm{n_e}$
358.0	3.0	1.5	5.8	0.99	0.52	0.022	0.046
3.0	7.0	0.2	2.1	0.96	0.25	0.025	0.040
3.0	7.0	3.4	6.3	1.00	2.10	0.014	0.073
7.0	12.0	2.0	6.7	0.98	−0.30	0.030	0.033
12.0	19.0	2.0	5.1	0.97	1.05	0.016	0.061
19.0	21.0	3.2	7.1	0.96	−2.76	0.051	0.020
21.0	27.0	1.1	3.3	0.99	0.79	0.020	0.050
21.0	27.0	4.0	6.4	1.00	1.79	0.019	0.053
27.0	31.0	2.1	3.4	0.93	1.15	0.018	0.057
27.0	31.0	4.2	5.4	0.42	3.37	0.009	0.110
31.0	36.0	1.4	4.1	0.99	0.84	0.021	0.047
36.0	42.0	1.2	4.6	0.96	0.41	0.036	0.028
36.0	42.0	7.3	8.3	0.29	4.38	0.016	0.064
42.0	48.0	0.7	3.1	0.99	0.19	0.036	0.028
42.0	48.0	4.1	7.2	1.00	1.44	0.027	0.037
48.0	56.0	0.4	4.7	0.97	0.35	0.033	0.031
60.0	65.0	1.4	6.5	1.00	−0.26	0.058	0.017
83.0	90.0	5.0	23.0	1.00	−10.83	0.147	0.007
107.0	109.0	2.0	5.2	1.00	0.74	0.035	0.029
124.0	132.0	1.2	3.3	0.83	1.04	0.016	0.061
181.0	189.0	3.2	3.5	1.00	1.90	0.018	0.056
274.0	286.0	1.3	4.1	0.93	0.51	0.024	0.042
286.0	293.0	2.1	9.6	0.90	−0.07	0.031	0.032
293.0	300.0	3.1	7.9	0.66	0.66	0.028	0.036
300.0	308.0	2.8	7.3	0.99	0.57	0.023	0.044
308.0	315.0	1.6	8.4	0.95	−0.35	0.033	0.031
315.0	319.0	0.7	6.1	0.98	0.16	0.028	0.036
319.0	329.0	1.1	4.7	0.98	0.36	0.020	0.050
329.0	336.0	1.4	6.6	0.98	0.69	0.019	0.053
336.0	339.0	3.6	7.6	0.99	0.15	0.025	0.041
339.0	347.0	4.2	5.6	0.87	2.20	0.013	0.076
347.0	351.0	3.5	6.3	0.91	1.75	0.015	0.068
351.0	358.0	1.1	4.8	0.94	0.10	0.025	0.040

Table B.4. Galactic latitude range (+7.0), (+15.0).

l_{min}	l_{max}	d_{min}	d_{max}	Q^2	d_0	m	$\mathrm{n_e}$
357.0	4.0	1.9	2.7	0.88	1.60	0.011	0.090
4.0	8.0	0.9	4.9	0.96	−0.18	0.044	0.023
8.0	17.0	0.5	3.4	0.94	0.53	0.026	0.039
17.0	27.0	1.5	5.6	0.95	0.74	0.031	0.032
27.0	35.0	2.5	5.2	0.60	1.36	0.026	0.039
35.0	40.0	3.2	6.2	0.85	0.15	0.057	0.018
40.0	45.0	2.8	4.4	0.94	1.22	0.029	0.035
45.0	47.0	1.3	4.2	1.00	−0.75	0.080	0.013
47.0	62.0	1.9	5.6	0.99	0.16	0.049	0.021
84.0	96.0	1.1	8.6	1.00	−0.11	0.053	0.019
104.0	133.0	0.3	7.6	0.99	−0.21	0.060	0.017
138.0	145.0	1.4	2.7	1.00	0.58	0.031	0.032
201.0	207.0	0.6	2.3	1.00	−0.12	0.052	0.019
234.0	249.0	1.9	4.6	0.93	0.83	0.033	0.030
256.0	269.0	1.0	7.4	0.95	−3.35	0.062	0.016
280.0	294.0	2.9	6.9	0.96	0.87	0.039	0.026
294.0	308.0	1.7	7.2	0.89	−0.37	0.044	0.023
308.0	320.0	1.5	5.3	0.96	0.03	0.042	0.024
325.0	330.0	1.5	4.0	0.95	−0.94	0.052	0.019
330.0	335.0	1.8	4.0	0.82	−0.13	0.038	0.026
335.0	350.0	2.5	5.7	0.93	−1.09	0.044	0.023
350.0	357.0	1.7	6.9	0.97	0.33	0.040	0.025

Table B.5. Galactic latitude range (+15.0), (+30.0).

l_{min}	l_{max}	d_{min}	d_{max}	Q^2	d_0	m	$\mathrm{n_e}$
355.0	5.0	1.4	3.4	0.93	−1.74	0.096	0.010
5.0	6.0	3.1	5.3	0.56	0.90	0.046	0.022
6.0	15.0	2.1	3.0	0.99	0.94	0.033	0.030
15.0	28.0	1.9	3.7	0.94	0.14	0.052	0.019
28.0	36.0	0.9	5.5	1.00	−0.15	0.055	0.018
36.0	38.0	1.4	3.5	1.00	−0.53	0.081	0.012
38.0	48.0	3.3	4.6	0.89	2.17	0.032	0.032
48.0	57.0	0.7	3.2	0.94	−0.19	0.066	0.015
79.0	87.0	1.4	3.2	1.00	−3.85	0.197	0.005
202.0	222.0	0.6	3.4	0.99	−0.36	0.070	0.014
246.0	274.0	0.6	3.6	0.97	−0.18	0.068	0.015
283.0	287.0	1.9	3.3	0.80	−0.62	0.078	0.013
299.0	310.0	1.1	1.8	0.98	0.75	0.023	0.044
299.0	310.0	3.1	4.4	0.98	1.42	0.039	0.026
310.0	322.0	2.5	4.4	0.77	0.81	0.047	0.021
322.0	345.0	0.7	4.2	0.98	0.20	0.043	0.023
345.0	349.0	1.6	3.4	0.84	−5.38	0.162	0.006
349.0	355.0	2.0	3.3	0.95	0.03	0.059	0.017

Table B.6. Galactic latitude range (+30.0), (+60.0).

l_{min}	l_{max}	d_{min}	d_{max}	Q^2	d_0	m	$\mathrm{n_e}$
0.0	4.0	1.1	7.1	1.00	−8.71	0.533	0.002
10.0	21.0	0.6	2.3	1.00	−0.10	0.065	0.015
21.0	35.0	0.7	2.6	0.98	−0.09	0.075	0.013
41.0	48.0	0.9	2.3	0.97	0.17	0.052	0.019
121.0	140.0	0.3	3.0	0.98	−0.44	0.095	0.011
151.0	161.0	0.5	1.2	1.00	−0.75	0.140	0.007
196.0	217.0	2.1	2.5	0.87	1.06	0.047	0.021
225.0	232.0	0.2	1.3	0.93	0.23	0.039	0.026
243.0	259.0	0.3	3.2	0.98	0.02	0.065	0.015
295.0	305.5	0.4	3.6	0.97	−0.44	0.101	0.010
305.5	314.0	0.6	2.4	0.98	−0.68	0.080	0.012

Table B.7. Galactic latitude range (+60.0), (+90.0).

l_{min}	l_{max}	d_{min}	d_{max}	Q^2	d_0	m	$\mathrm{n_e}$
241.0	253.0	0.2	0.6	1.00	−0.12	0.073	0.014
311.0	333.0	0.6	18.1	0.98	−14.00	1.326	0.001

Table B.8. Galactic latitude range (-3.0), (-1.0).

l_{min}	l_{max}	d_{min}	d_{max}	Q^2	d_0	m	$\mathrm{n_e}$
357.5	2.0	1.2	2.5	0.96	0.12	0.023	0.043
357.5	2.0	3.5	7.6	1.00	1.09	0.013	0.079
2.0	4.5	1.1	6.1	0.96	1.17	0.011	0.090
4.5	8.0	1.6	4.1	0.84	1.19	0.012	0.087
8.0	14.0	6.1	8.2	0.94	3.21	0.009	0.109
14.0	18.0	3.5	8.5	0.87	2.08	0.010	0.099
18.0	22.0	2.5	4.4	0.92	0.36	0.018	0.055
18.0	22.0	5.2	8.5	0.94	1.60	0.012	0.083
22.0	25.0	4.0	5.7	0.84	2.74	0.008	0.131
25.0	28.0	3.0	8.2	0.95	1.77	0.012	0.081
28.0	31.0	1.9	7.9	0.98	1.63	0.012	0.085
31.0	37.0	2.6	8.6	0.92	1.39	0.017	0.059
37.0	40.0	1.1	8.4	0.98	0.53	0.021	0.048
40.0	43.0	1.9	12.1	0.99	1.17	0.022	0.046
43.0	47.0	1.5	7.8	0.99	0.93	0.020	0.049
47.0	51.0	5.5	9.9	0.60	−11.87	0.089	0.011
51.0	53.0	6.2	7.0	0.87	5.13	0.008	0.133
53.0	66.0	6.1	7.6	0.63	4.84	0.013	0.078
129.0	148.0	1.2	2.6	0.88	0.63	0.030	0.033
179.0	184.0	1.7	3.1	1.00	0.28	0.038	0.027
200.0	204.0	1.8	7.9	1.00	−0.38	0.060	0.017
238.0	244.0	2.2	11.2	1.00	−3.26	0.074	0.014
257.0	268.0	0.4	7.2	0.97	−2.04	0.034	0.029
268.0	283.0	3.2	5.7	0.94	−0.64	0.033	0.030
283.0	287.0	2.6	6.6	0.97	1.62	0.013	0.078
283.0	287.0	8.2	12.2	0.77	−2.19	0.029	0.034
287.0	295.0	3.0	12.3	0.99	0.06	0.022	0.046
295.0	302.0	1.7	13.3	0.97	0.33	0.030	0.033
302.0	306.0	2.1	13.3	0.98	−0.03	0.024	0.041
306.0	311.0	2.0	3.9	0.99	−0.75	0.035	0.029
306.0	311.0	5.8	13.2	0.84	0.58	0.018	0.055
311.0	317.0	2.9	8.5	1.00	0.62	0.018	0.056
317.0	320.0	7.1	8.6	0.62	5.55	0.007	0.144
320.0	325.0	2.2	4.3	0.90	1.16	0.014	0.074
320.0	325.0	6.3	12.1	0.17	2.04	0.023	0.044
325.0	330.0	2.5	7.6	0.98	1.02	0.014	0.070
330.0	333.0	1.3	8.6	0.92	1.10	0.013	0.079
333.0	339.0	5.9	9.3	0.82	−0.33	0.017	0.058
339.0	343.0	4.9	7.4	0.92	1.91	0.010	0.100
343.0	345.0	1.8	4.8	0.97	0.90	0.014	0.071
343.0	345.0	6.9	8.5	1.00	4.64	0.006	0.175
345.0	347.5	4.4	7.5	0.94	1.70	0.012	0.084
347.5	352.0	3.1	6.3	0.93	1.70	0.011	0.095
352.0	357.5	1.4	6.6	0.94	0.96	0.011	0.091

Table B.9. Galactic latitude range (-5.0), (-3.0).

l_{min}	l_{max}	d_{min}	d_{max}	Q^2	d_0	m	$\mathrm{n_e}$
0.0	5.0	2.1	8.1	0.99	−0.03	0.026	0.039
5.0	10.0	2.9	7.4	0.98	1.05	0.017	0.058
10.0	18.0	3.3	7.6	0.89	0.77	0.022	0.046
18.0	21.0	1.0	9.8	0.93	0.23	0.028	0.036
21.0	31.0	2.0	7.9	0.81	−0.70	0.035	0.029
31.0	34.0	2.7	7.1	0.95	−0.16	0.028	0.036
34.0	39.0	3.0	7.1	0.93	−0.26	0.032	0.031
45.0	51.0	6.5	7.2	0.92	4.84	0.012	0.084
51.0	60.0	0.6	10.2	0.97	−0.24	0.044	0.023
64.0	69.0	0.6	3.0	1.00	0.01	0.048	0.021
99.0	109.0	2.1	3.3	1.00	−0.24	0.050	0.020
126.0	130.0	2.1	2.9	1.00	0.62	0.031	0.032
240.0	246.0	0.3	3.2	1.00	−6.29	0.135	0.007
259.0	273.0	2.6	8.4	0.98	−0.89	0.033	0.030
282.0	295.0	3.1	4.6	1.00	0.20	0.026	0.039
282.0	295.0	6.2	9.6	0.91	1.67	0.026	0.039
295.0	305.0	0.8	13.6	0.96	−0.20	0.032	0.031
305.0	315.0	3.3	7.5	0.95	−0.26	0.027	0.036
315.0	325.0	1.8	8.1	1.00	−0.60	0.034	0.029
325.0	331.0	3.3	5.3	0.79	2.11	0.012	0.082
331.0	338.0	4.2	7.6	0.99	0.96	0.019	0.054
338.0	345.0	3.9	5.6	0.95	1.55	0.016	0.062
338.0	345.0	6.5	8.1	0.76	5.18	0.006	0.160
345.0	351.0	0.9	7.1	0.99	0.47	0.021	0.048
355.0	0.0	2.2	3.1	1.00	1.03	0.015	0.065
355.0	0.0	4.7	5.3	0.56	4.36	0.003	0.361

Table B.10. Galactic latitude range (-10.0), (-5.0).

l_{min}	l_{max}	d_{min}	d_{max}	Q^2	d_0	m	$\mathrm{n_e}$
357.0	3.0	1.5	5.9	0.88	0.16	0.029	0.035
3.0	10.0	2.5	5.9	0.97	−3.54	0.072	0.014
10.0	19.0	0.8	5.2	0.99	0.23	0.022	0.045
19.0	26.0	1.5	3.1	0.98	0.86	0.019	0.053
19.0	26.0	4.1	4.7	1.00	1.10	0.023	0.043
26.0	37.0	1.2	8.2	0.99	−0.32	0.041	0.024
37.0	45.0	1.7	8.2	1.00	0.40	0.040	0.025
45.0	48.0	1.1	5.2	1.00	0.23	0.035	0.029
48.0	56.0	1.6	10.1	0.96	−0.75	0.067	0.015
56.0	65.0	0.9	3.9	0.99	−0.14	0.054	0.019
65.0	80.0	0.6	4.3	1.00	0.19	0.041	0.024
182.0	185.0	1.1	2.3	0.87	0.56	0.029	0.035
210.0	214.0	2.1	3.6	1.00	0.61	0.041	0.024
233.0	239.0	1.7	14.1	1.00	−0.10	0.056	0.018
254.0	264.0	2.2	8.4	0.38	0.49	0.031	0.032
278.0	293.0	2.0	6.4	0.95	0.31	0.032	0.031
293.0	297.0	1.8	8.3	0.99	−0.23	0.034	0.030
297.0	316.0	0.4	3.9	0.99	0.15	0.028	0.035
297.0	316.0	4.5	6.4	0.84	2.17	0.020	0.051
320.0	328.0	2.1	7.8	0.91	−2.62	0.060	0.017
328.0	342.0	1.7	5.5	0.88	0.58	0.024	0.042
342.0	345.0	3.5	4.4	1.00	1.99	0.013	0.077
345.0	354.0	3.5	8.6	0.95	−3.21	0.049	0.021
354.0	357.0	3.5	7.9	0.84	−1.06	0.043	0.023

Table B.11. Galactic latitude range (-25.0), (-10.0).

l_{min}	l_{max}	d_{min}	d_{max}	Q^2	d_0	m	$\mathrm{n_e}$
359.0	10.5	0.5	3.6	0.72	0.01	0.046	0.022
10.5	20.0	1.1	3.8	0.98	−0.31	0.066	0.015
20.0	35.0	1.2	4.1	0.95	−0.50	0.070	0.014
35.0	51.0	1.3	3.4	0.82	0.44	0.039	0.026
51.0	62.0	1.1	4.3	0.97	−0.76	0.080	0.012
62.0	75.0	1.2	4.2	0.92	−0.57	0.072	0.014
75.0	82.0	1.2	4.8	0.96	−1.92	0.129	0.008
82.0	91.0	1.3	5.1	0.99	−0.04	0.066	0.015
103.0	117.0	0.7	3.6	0.99	−0.12	0.057	0.017
117.0	125.0	0.9	2.5	0.96	0.09	0.048	0.021
136.0	155.0	1.4	4.2	0.99	−0.40	0.072	0.014
163.0	172.0	2.5	3.2	1.00	−12.80	0.300	0.003
192.0	213.0	4.8	5.3	0.93	−3.10	0.099	0.010
227.0	241.0	1.8	6.2	0.95	−0.11	0.068	0.015
254.0	267.0	1.1	6.3	0.88	0.62	0.043	0.023
267.0	280.0	0.8	5.3	0.97	−0.15	0.055	0.018
280.0	299.0	1.2	4.5	0.85	−0.32	0.064	0.016
299.0	317.0	1.7	5.6	0.91	−0.80	0.064	0.016
317.0	330.0	1.3	1.7	0.80	0.97	0.013	0.079
317.0	330.0	3.6	5.9	0.94	−1.45	0.069	0.014
330.0	341.0	1.3	3.5	0.90	0.12	0.044	0.023
341.0	355.0	0.9	4.4	0.99	0.00	0.040	0.025

Table B.12. Galactic latitude range (-40.0), (-25.0).

l_{min}	l_{max}	d_{min}	d_{max}	Q^2	d_0	m	$\mathrm{n_e}$
357.0	4.0	2.4	2.9	1.00	−10.66	0.385	0.003
30.0	50.0	0.5	3.0	0.99	−0.73	0.100	0.010
55.0	74.0	1.8	10.1	1.00	−5.14	0.225	0.004
74.0	88.0	1.1	3.0	0.87	−0.37	0.081	0.012
93.0	98.0	0.3	2.9	0.99	0.06	0.056	0.018
161.0	177.0	0.8	3.0	1.00	−0.38	0.079	0.013
197.0	218.0	1.3	3.2	1.00	−0.75	0.098	0.010
228.0	245.0	2.8	4.1	0.93	1.94	0.041	0.025
266.0	276.0	1.9	2.4	0.87	−0.34	0.089	0.011
284.0	300.0	1.0	1.6	0.93	−0.28	0.075	0.013
314.0	327.0	0.9	3.2	0.88	−0.41	0.077	0.013
327.0	337.0	0.6	4.1	1.00	−1.12	0.152	0.007

Table B.13. Galactic latitude range (-60.0), (-40.0).

l_{min}	l_{max}	d_{min}	d_{max}	Q^2	d_0	m	$\mathrm{n_e}$
2.0	16.0	0.2	2.3	0.99	−0.11	0.075	0.013
47.0	70.0	0.5	2.1	1.00	−0.20	0.075	0.013
91.0	114.0	0.2	1.8	0.98	−0.19	0.084	0.012
122.0	147.0	0.7	2.3	0.99	−0.83	0.116	0.009
253.0	270.0	0.1	1.2	1.00	−0.06	0.076	0.013
320.0	339.0	0.6	2.9	0.98	−0.49	0.103	0.010

Table B.14. Galactic latitude range (-90.0), (-60.0).

l_{min}	l_{max}	d_{min}	d_{max}	Q^2	d_0	m	$\mathrm{n_e}$
110.0	141.0	0	1	1	−0.1	0.071	0.014
160.0	180.0	0.7	2	1	−0.2	0.083	0.012
230.0	259.0	0.8	1.6	1	−0.2	0.079	0.013